Diagenetic imprints on reservoir quality, provenance perceptions and paleosalinity conditions of the Miocene Agbada Formation, Niger Delta Basin: A petrographic and geochemical investigation

By

© Brume Overare

A Dissertation submitted to the School of Graduate Studies

in partial fulfilment of the requirements for the degree of

Doctor of Philosophy

Department of Earth Sciences

Memorial University

May 2024

St. John's, Newfoundland and Labrador

Abstract

The main exploration targets for hydrocarbons in the Niger Delta Basin are within the Agbada Formation sandstone reservoirs. Most studies in the Agbada Formation are skewed towards understanding the petroleum system, and this has led to a paucity of datasets on several important subjects, which is a motivation for this research. This investigation utilizes a multi-technical (Thin-section, SEM-MLA, XRD, XRF, ICP-MS and LA-ICP-MS) approach to evaluate the petrographic attributes, diagenesis and influence of rare calcite cement on reservoir quality, inorganic geochemical signatures and their significance for unraveling provenance and paleosanity conditions prevalent in the Agbada Formation. Weathering proxies (e.g. CIA, CIX, $\alpha^{Al}E$), paleoclimatic signatures (e.g., Ga/Rb vs. K_2O/Al_2O_3) and elemental ratios (e.g. La/Co, Cr/Th, Th/Co), including REEs signals (LREE/HREE, flat HREE pattern, Eu/Eu*) diagnostic of provenance for the sandstones and interbedded shales suggests moderate to intense weathering, humid paleoclimatic settings and signatures of sediments derived predominantly from felsic sources. Boron-derived paleosalinometric tools (e.g. equivalent boron, Adam's, Landergren and Carvajal's, and Couch's methods), elemental ratios (e.g. B/Ga, Sr/Ba, and S/TOC) and other proxies sensitive to redox (e.g. Cr, Ni/Co, Mo-EF/U-EF) point to mainly low-saline (brackish) settings with considerable signature inputs from both freshwater and marine water (comparatively lesser), and oxic-suboxic conditions for the interbedded shales. The Agbada sandstones ($Q_{88.58}$ $F_{9.99}$ $RF_{2.43}$) are classified as feldspatho-quartzose and quartzose sandstones, with a predominance of quartzose sandstones and their diagenetic signatures reflect low degree of compaction and lack of pervasive cementation, with compaction comparatively posing more influence on porosity, excluding some intervals with considerable cementation (siderite and ferroan calcite) where compactional porosity-loss was minimal. The occurrence of ferroan calcite cement (mainly ferroan) is generally small, probably discontinuous and may generally not pose a substantial barrier to fluid flow, but understanding their localized influence

may still contribute to building good reservoir models. Petrographic evidence in the sandstones suggests that calcite cement is an early event, but the shale normalized REE + Y patterns appear to reflect non-seawater patterns, indicating possible contamination (Y/Ho = 36.30 ± 1.35) from clastic or detrital grains that depict fluvial/estuarine influence and/or incorporation of particulate matter that can preferentially scavenge LREEs from the overlying water column. A potential concern during reservoir production is the anticipated production of fines and formation damage linked to the occurrence of clay mineral matrix (mostly kaolinitic), but this can be reduced with appropriate reservoir management.

General Summary

The Niger Delta province has been a hub for hydrocarbon exploration and production for over six decades. It hosts several great discoveries in both onshore and offshore parts of the deltaic system and has been the focus of many studies aiming at understanding the petroleum system of the basin. However, little has been forthcoming about the origin of diagenetic cements and their impact on reservoir quality, the inorganic geochemical signatures of the component lithostratigraphic units and their relevance in reconstructing the source of the sediments, source area weathering, climate and the salinity conditions that were prevalent during deposition. This research utilizes insights from several methods to evaluate the Agbada Formation, providing acumen on several important subjects with a scarcity of datasets. The insights deciphered for the sandstones and shales suggest they have experienced moderate to intense weathering, and the parental source is mainly from felsic rocks. Moreover, the evidence unraveled from trace elements provides clues that indicate the interbedded shales were deposited in an environment that is not oxygen-depleted (oxic-suboxic) and reflects low saline (brackish settings) conditions with inputs from freshwater and marine water. The sandstones are quartz-rich, poorly consolidated, and lack pervasive cementation, contributing significantly to the general high porosity, but there are some intervals where cementation (mainly siderite and calcite) is appreciable and porosity is minimal. The occurrence of calcite cementation in the investigated sandstone is small and may generally not pose a substantial barrier to fluid flow, but understanding their localized influence may still contribute to building good reservoir models. Although the petrographic observations suggest that the precipitation of calcite occurred early and should reflect seawater signatures, the shale normalized REY patterns do not mimic seawater patterns due to possible contributions from clastic or detrital grains and/or incorporation of particulate matter that can preferentially scavenge LREEs from the overlying water column. A potential concern during reservoir production is the anticipated production of

fines and formation damage due to the occurrence of clay mineral matrix (mostly kaolinitic), but this can be reduced with appropriate reservoir management.

Acknowledgements

The immense task of completing this research was not limited to my efforts because of the support from several individuals and organizations. I wish to place on record my deep gratitude to my supervisor, Dr. Karem Azmy, for his valuable contributions, guidance, patience, advice, constructive feedback and general academic support. Without his supervision and constant help, this dissertation would not have been possible. I would also like to thank Dr. Eduardo Garzanti for his dedicated review of several manuscripts, contributions and constructive criticisms.

Several organizations and companies deserve to be acknowledged for their financial support and also for the release of datasets. First, I would like to express my sincere gratitude to the Federal Government of Nigeria for granting a scholarship for this research through the auspices of the Niger Delta Development Commission (NDDC) and also to the Federal University of Petroleum Resources, Nigeria, for financial support and contribution to my educational development over the years. I also want to express my indebtedness to the Nigerian Upstream Petroleum Regulatory Commission (NUPRC), Chevron Nigeria Limited, Shell Petroleum Development Company, Nigeria (SPDC) and Exxon Mobil Nigeria for assistance with datasets.

I express my profound gratitude for the countless assistance (logistics and various laboratory analyses) rendered by the Memorial University of Newfoundland staff (Matt Crocker, Dylan Goudie, Markus Walle, Wanda Aylward, Keir Hiscock, Jane O'Neil, and Michelle Miskell) and Dr. Bleuenn Guégen at Pôle de Spectrométrie Océan, IUEM, Brest, France. The support, collaborative efforts and contributions of Dr. Juliet Edafiwogho Emudianughe, Dr. Jerry Osokpor, Dr. Ovie Benjamin Ogbe, Dr. Enivwenaye Oghenero Avwenagha, and Dr. Godwin Okumagbe Aigbadon are highly appreciated.

I am grateful to my wife and best friend, Areghehefe Elfreda Overare, for her encouragement, patience, prayers and unstinting support (in various ways too numerous to mention). You believed in me, and I did not fail you. I thank my kids, Tonero, Gabriela and Splendor Overare,

for being my biggest motivation and source of joy, which kept me going, even in challenging times.

Table of Contents

List of Figures

List of Tables

List of Appendices

Chapter I

Introduction

1.1 General introduction

The most attractive region for petroleum exploration in Nigeria is the Niger Delta province. It is located on the continental margin of West Africa and has been a hub for hydrocarbon exploration and production for over six decades, hosting several great discoveries in both onshore and offshore parts of the deltaic system. Being the host to some substantial recoverable reserves estimated as one hundred and ninety (~190.4) trillion cubic feet of gas resources and thirty-seven (37) billion barrels of oil (BP, 2020), it is one of the world's most prolific hydrocarbon provinces. Moreover, with an area of about 300,000 km^2 (Kulke, 1995), a sediment volume of 500,000 km^3 (Hospers, 1965), and a sediment thickness of ~12000 m (Reijers, 2011), the Niger Delta is easily considered as one of the largest regressive deltas in the world.

The Niger Delta Basin has attracted much attention from both the academia and stakeholders in the oil and gas industries, which is evidenced in the intensified chain of hydrocarbon exploratory activities in the basin from when oil was first discovered in commercial quantity in 1956 and the numerous publications (e.g., Allen, 1965; Short and Stauble, 1967; Burke, 1972; Weber and Daukoru, 1975; Avbobvo, 1978; Evamy et al., 1978; Ekweozor and Okoye, 1980; Lambert-Aikhionbare and Ibe, 1984; Whiteman, 1982; Ejedawe and Coker 1984; Nwachukwu and Chukwura, 1986; Bustin, 1988; Doust and Omatsola, 1990; Reijers et al., 1997; Tuttle et al., 1999; Corredor et al., 2005; Krueger and Grant, 2011; Reijers, 2011; Nwajide, 2013; Sun et al., 2018; Ekpo et al., 2018; Anomneze et al., 2020; Ogbe et al., 2021; Overare et al., 2021; Obi et al., 2024). Nevertheless, despite the numerous publications that have given birth to a vast amount of geologic datasets, providing a rich platform for discussing and projecting various aspects of the basin's geology, most studies are skewed toward understanding the petroleum system, resulting in a scarcity of datasets on several subjects, providing the needed

motivation for this research. Therefore, this research explores the Agbada Formation, highlighting some important subjects with a paucity of datasets or where little has been forthcoming, including petrographic attributes of the Agbada Formation sandstone units, the significance of diagenetic activities in the control of reservoir quality, and the inorganic geochemical signatures of the component units (sandstones and interbedded shales), providing insights on provenance, weathering intensity, paleoclimate and paleosalinity conditions. The background, utility and insights deciphered from the aforementioned areas and their relevance to the Agbada Formation are the focus of this research. They are discussed contextually in the subsequent chapters where they are utilized.

1.2 Rationale and Scientific Objectives

Sedimentary units have special genetic significance because their diagnostic characteristics can be used as a tool to demystify the evolution of Earth's landscapes and life forms through time. This is systematically achieved by interpreting sediments and sedimentary rocks in terms of transport and depositional processes and how they are distributed in space and time in various sedimentary environments. One technique that can be utilized to understand better the various processes that controlled the attributes of the sediments during and after their deposition is the bulk inorganic chemical composition of sedimentary units. This concept has experienced steady growth in the literature due to the sensitivity of certain trace elements (e.g., Y, Th, Nb, Zr, Hf, and Sc) and their elemental ratios (e.g., Th/Sc, Cr/Th, La/Sc, Th/Sc), including rare earth elements (REE) that are well suited for reconstructing provenance and source rock composition, geodynamic settings, source area weathering, paleoclimate and paleo-depositional conditions of various sedimentary units (e.g., McLennan et al., 1993; Cullers, 2000; von Eynatten et al., 2003; Bauluz, 2000; Hofer et al., 2013; Armstrong-Altrin et al., 2015; Madhavaraju et al., 2020; Overare et al., 2020; Wu et al., 2022; Castro et al., 2023).

Considering the scarcity of datasets on the bulk inorganic geochemical composition and their application for constraining sedimentary processes in the Agbada Formation, the first part of the current research reports the distribution of the major and trace elements, including REEs, of sandstones and interbedded shales of the Agbada Formation, in order to decode the influence of the aforementioned factors on their composition and consequently, to evaluate (i) intensity of weathering (ii) provenance signatures and (iii) paleo-redox conditions associated with the depositional subenvironment. The geochemical data and source area interpretations presented in this investigation will improve the understanding of paleogeographical knowledge, especially with the understanding that the progradation of the siliciclastic system across the pre-existing continental slope into the Atlantic Ocean is still active today. Moreover, the Niger River catchment encompasses a large part of cratonic sub-Saharan western Africa, consisting of metamorphic and igneous rocks that range from Paleoarchean granitoid gneisses of the Man Shield in Guinea to the recent anorogenic lavas of the Cameroon Line, offering an unexcelled opportunity to test the effects of various sedimentary processes on the geochemical signature of the Agbada Formation. In a broader context, although the geochemical provenance of shales is usually more emphasized in siliciclastic studies, being a precious complement to petrographic analysis largely because fine-grained lithologies cannot be adequately investigated using traditional petrographic methods, this study therefore provides an opportunity for a direct comparison between the geochemical composition of sandstones and shales.

The second part of the current study provides a rare insight into the significance of diagenetic activities, including the influence of rare calcite cementation on the reservoir quality of the Agbada Sandstones, which are the main exploration targets for hydrocarbons in the Niger Delta Basin. As the quest for more hydrocarbon reserves increases in the Niger Delta Basin, exploration and production are gradually moving from more easily identifiable reservoirs, which are several well-imaged targets (shallow zones), to deeper targets (poorly imaged zones),

so understanding the temporal and spatial variations of reservoir quality within a diagenetic framework are desired. Moreover, considering the geologic settings of the area and the large siliciclastic influx, calcite cemented intervals are not abundant but do locally occur, requiring a rigorous examination to identify them. There is also a scarcity of datasets on their origin, influence and distribution. Therefore, the second part of this research evaluates the roles of framework composition and diagenetic processes, particularly calcite cementation, on reservoir quality in Miocene intervals of the Agbada Formation sandstone, Niger Delta Basin. The purpose is to support reservoir quality prediction by establishing a relationship or connection between diagenetic minerals and porosity distribution. The main objectives are to (i) investigate the petrographic characteristics of the Agbada sandstones and the diagenetic evolution of cements, (ii) shed light on the paragenetic sequence of the cementation events and highlight their influence on porosity distribution, (iii) determine the diagenetic processes that have been more influential in shaping the reservoir quality, and (iv) elucidate the origin of calcite cements and their influence on porosity development.

The third part of this research is focused on paleosalinity reconstruction in the Agbada Formation. The Agbada Formation (Niger Delta Basin) is a classic example of paralic facies representing unique spatial and temporal variations in sediment characteristics, water chemistry, and hydrodynamic systems. Paralic environments are sometimes complex to understand because their convolution reduces the ability of geologists to effectively decipher geological histories and reconstruct paleoenvironments from the rock record. Hence, the availability of proxies that can reliably decode sensitive changes in water mass salinity in space and time and/or complement other techniques for this type of system is desired. Geochemical evidence for water mass salinity is a tool commonly used as an alternative to complement other techniques or refine intervals, especially where signals from fossil assemblage and/or other methods are inconclusive. Bulk sediment geochemical proxies (e.g., B/Ga, Sr/Ba, S/TOC) for

reconstructing paleosalinity and their general applicability to fine-grained siliciclastic sediments in the Agbada Formation have not been demonstrated. Therefore, this investigation presents the first utility of B/Ga, Sr/Ba, and S/TOC for paleosalinity watermass reconstruction in the Agbada Formation, Niger Delta Basin. The purpose is to utilize several geochemical proxies (B/Ga, Sr/Ba, S/TOC) to establish the salinity conditions prevalent in the paleodepositional environment. Further insight utilizing a quantitative approach (boron-derived paleosalinity proxies) is also considered to complement and provide a robust evaluation of paleosalinity, refining insights and limiting secondary influences on any single proxy, thereby improving confidence in the interpretation. This investigation presents the first utility of B/Ga, Sr/Ba, and S/TOC for paleosalinity watermass reconstruction in the Agbada Formation, providing an inorganic geochemical perspective and valuable contribution to the geology of the Niger Delta Basin.

1.3 Structure of the Thesis

This dissertation is written in manuscript style and consists of five separate chapters. The study areas, geological setting and methodology relevant to each chapter are adequately discussed in the respective sections to provide quick reference to the background information needed to understand the respective chapter. The constituent chapters are either published, under review or ready to be submitted to a scholarly journal. Accordingly, the reference style for each chapter is prepared to conform to the guidelines of its respective journal.

Chapter 1 (this Chapter) provides an introduction and background information for the thesis. Chapters 2 through 4 are individual papers in manuscript form that are either published or under review. Finally, Chapter 5 summarizes the main results and conclusions reported in this research.

Chapter 2 is titled “Decrypting geochemical signatures in subsurface Niger Delta sediments: Implication for provenance, weathering, and paleoenvironmental conditions” by Brume

Overare, Karem Azmy, Eduardo Garzanti, Jerry Osokpor, Ovie B. Ogbe, Enivwenaye O. Avwenagha, and is published in Marine and Petroleum Geology, 126 (2021) 104879. This chapter demonstrates the utility of inorganic geochemical composition for evaluating weathering intensity, parental affinity and paleo-redox conditions.

Chapter 3 is titled "Diagenetic imprints in the reservoirs of Agbada Formation, Niger Delta Basin: Implication for reservoir quality and appraisal of calcite cement" by Brume Overare, Karem Azmy, Eduardo Garzanti, Enivwenaye O. Avwenagha, Juliet E. Emudianughe, and is also published in Marine and Petroleum Geology, 163, 106746. This chapter examines the roles of framework composition and diagenetic processes, particularly calcite cementation, on reservoir quality in Miocene intervals of the Agbada Formation sandstone, Niger Delta Basin.

Chapter 4 is titled "Paleosalinity signals deciphered from parts of the Agbada Formation, Niger Delta Basin: A geochemical approach" by Brume Overare, Karem Azmy, Enivwenaye O. Avwenagha, Godwin O. Aigbadon, and it is currently under review in the Journal of Geosystems and Geoenvironment. This chapter presents the utility of several geochemical proxies to establish the salinity conditions prevalent in the paleodepositional environment of the Agbada Formation, Niger Delta Basin.

1.4 Methodology

The rock samples (ditch cuttings, cores) and well logs utilized for this research were acquired from operating oil companies through the Nigerian Upstream Petroleum Regulatory Commission (NUPRC). This research project consists of a strong laboratory component that utilizes a broad range of different methods, including X-ray Fluorescence (XRF), inductive-coupled-plasma mass-spectrometry (ICP-MS), Laser Ablation – Inductively Coupled Plasma–Mass Spectrometry (LA-ICP-MS), Electron microprobe analysis (EMPA), thin-section analysis, Scanning Electron Microscopy (SEM), Mineral Liberation Analysis (MLA), Scanning Electron Microscopy/Energy Dispersive Spectroscopy (SEM-EDS) and Quantitative X-ray

Diffraction (XRD) analysis. These methods are adequately discussed in the respective chapters, where they were applied to provide quick reference to the background information needed to understand the chapter.

In Chapter Two, ditch cuttings (sandstones and shales) from hydrocarbon-producing zones of the Agbada Formation were selected for inorganic geochemical analyses. The sandstone samples are mainly representative of two reservoirs, whereas the shale samples belong to units that seal both the top and bottom of reservoirs. Major oxides were analyzed by XRF, whereas trace elements, including REE, were analyzed by ICP-MS. The results were used to reconstruct source area weathering, provenance and depositional conditions prevalent in the Agbada Formation.

The multi-technical methods utilized in Chapter Three include thin section analysis, SEM-MLA, SEM-EDS, XRD, EPMA, LA-ICP-MS and XRD. Core samples (sandstones) were analyzed using optical microscopy to identify mineralogy, texture, grain size, secondary alteration/phases, pore space and approximate concentrations. To verify and spatially resolve mineralogy and better estimate void/pore space, polished thin sections were analyzed under SEM to reveal further the fabric of the sandstones, including quantitative evaluation of minerals and maps of mineral distribution using SEM-MLA and SEM-EDS methods. Moreover, the concentration of Calcium (Ca) in calcite cement was predetermined with an electron probe micro-analyzer (EPMA) before analysis for major, trace and rare-earth elements + Yttrium (REY) using LA-ICP-MS. The REY concentrations were normalized using Post Archaean Australian Shales (PAAS; McLennan, 1989) and anomalies were defined using established conventions (e.g., Bau and Dulski, 1996; Webb and Kamber, 2000). Y has been included in this investigation, considering its identical charge and similarity in atomic radii to its neighbors (Bau and Dulski, 1999; Jiang et al., 2015). For convenience, REY is used to denote rare earth

elements and Yttrium throughout this study. The clay mineralogy (< 2 μm) of the samples was determined by quantitative X-ray diffraction analysis and clay speciation. Results from all methods were integrated to unravel the influence of diagenesis, including calcite cementation on the reservoir quality of the sandstones.

In Chapter Four, core samples (shales) were analyzed using High-Resolution Inductively Coupled Plasma Mass Spectrometry (HR-ICP-MS), Elementar Isotope Cube, and XRD. Trace element analyses were conducted with High-Resolution Inductively Coupled Plasma Mass Spectrometry (HR-ICP-MS). The <2 μm fractions of representative shale samples were analyzed for their mineralogical compositions using XRD. The Elementar Isotope Cube was used to determine the N%, C%, H%, and S% of the samples. The paleosalinity of the Agbada Formation was reconstructed from elemental ratios (S/TOC, Sr/Ba, B/Ga) and boron-derived paleosalinity proxies such as Equivalent boron, Adam's, Landergren and Carvajal's and Couch's quantitative approach.

1.5 Co-Authorship Statement

This dissertation consists of materials that are the result of a research project under the supervision of Dr. Karem Azmy. The research was designed by Dr. Karem Azmy, who guided, advised and monitored the progress of the project, including the review of all manuscripts prior to submission. Brume Overare is the primary author and researcher for all manuscripts/chapters, including formulating research questions, experimental design, synthesizing and interpreting data and manuscript preparation.

Chapter 2 has been published in the Journal of Marine and Petroleum Geology. Chapter 3 has also been published in the Marine and Petroleum Geology Journal, and all concerns and suggestions have been considered, and the manuscript has been re-submitted. Chapter 4 is currently under review in the Journal of Geosystems and Geoenvironment. Dr. Karem Azmy is a co-author of all the manuscripts (Chapters 2 - 4) included in this dissertation. He provided

the motivation, insight and direction during the conceptual design stage of each project (article/chapter). Dr. Karem Azmy designed the project and was also involved in reviewing and editing all manuscripts. Dr. Eduardo Garzanti is a co-author for Chapters 2-3 and was involved in some petrographical descriptions and validation, as well as the review and editing of each manuscript. Dr. Juliet Emudianughe (Chapters 3-4), Dr. Ovie B. Ogbe (Chapter 2) and Dr. Jerry Osokpor (Chapter 2) were actively involved in the acquisition, preparation and quality assurance of samples/datasets (well logs, ditch cuttings and cores). Dr. Jerry Osokpor and Dr. Enivwenaye O. Avwenagha (Chapters 2-4) made fruitful observations and suggestions on the final version of the manuscripts. Dr. Enivwenaye O. Avwenagha and Godwin O. Aigbadon (Chapter 4) helped with the separation of clay minerals (< 2 μm fraction) and XRD data acquisition.

References

Allen, J.R.L., 1965. Late Quaternary Niger Delta, and adjacent areas-sedimentary environments and lithofacies. AAPG (Am. Assoc. Pet. Geol.) Bull. 49, 547–600.

Anomneze, D. O., Okoro, A.U., Ajaegwu, N.E., Akpunonu, E.O., Obiadi, I.I., Ahaneku, C.V., Okeke, G.C., 2020. Description and interpretation of fault-related sedimentation and controls on shelf-edge deltas: implication on sand transportation to the basin floor in parts of Eastern Niger Delta. Journal of Petroleum Exploration and Production Technology, 10, 1367–1388.

Armstrong-Altrin, J.S., Nagarajan, R., Balaram, V., Natalhy-Pineda, O., 2015. Petrography and geochemistry of sands from the Chachalacas and Veracruz beach areas, western Gulf of Mexico, Mexico: Constraints on provenance and tectonic setting, Journal of South American Earth Sciences, Volume 64, (1), 106548.

Avbovbo, A.A., 1978. Tertiary lithostratigraphy of Niger Delta. AAPG (Am. Assoc. Pet. Geol.) Bull. 62 (2), 295–300.

Bau, M., Dulski, P., 1996. Distribution of yttrium and rare-earth elements in the Penge and Kuruman iron-formations, Transvaal Supergroup, South Africa. Precambrian Res. 79, 37–55.

Bau, M., Dulski, P., 1999. Comparing Yttrium and rare earths in hydrothermal fluids from the Mid-Atlantic Ridge: implications for Y and REE behaviour during near-vent mixing and for the Y/Ho ratio of Proterozoic seawater. Chem. Geol. 155 (1), 77–90

Bauluz, B., Mayayo, M.J., Fernandez-Nieto, C., Lopez J.M.G., 2000. Geochemistry of Precambrian and Paleozoic siliciclastic rocks from the Iberian Range (NE Spain): implications for source-area weathering, sorting, provenance, and tectonic setting. Chemical Geology, 168, 135–150.

BP, 2020. British Petroleum statistical review of World Energy, 69th edition. 65p. https://www.bp.com/en/global/corporate/energy-economics/statistical-review-of-world-energy.html.

Burke, K., 1972. Longshore drift, submarine canyons and submarine fans in development of Niger Delta. AAPG (Am. Assoc. Pet. Geol.) Bull. 56, 1975–1983.

Castro, A.P. de., Guedes, C.C.F., Vesely, F.F., Silveira, D. M. da., Neves, L.F., 2023. Provenance, diagenesis and reservoir quality of sandstone facies of the Maracangalha Formation, Recôncavo Basin – Northeastern Brazil, Marine and Petroleum Geology,158, Part B, 106548. https://doi.org/10.1016/j.marpetgeo.2023.106548

Corredor, F., Shaw, J.H., Bilotti, F., 2005. Structural styles in the deep-water fold and thrust belts of the Niger Delta. AAPG (Am. Assoc. Pet. Geol.) Bull. 89 (6), 753–780.

Cullers, R.L., Podkovyrov, V.N., 2000. Geochemistry of the Mesoproterozoic Lakhanda shales in south-eastern Yakutia, Russia: implications for mineralogical and provenance control, and recycling Precambrian Research, 104, 77–93.

Ejedawe, J.E., Coker, S.J., Lambert-Aikhionbare, D.O., Alofe, K.O and Adoh, F.O., 1984. Evolution of oil-generative window and oil and gas occurrence in Tertiary Niger Delta basin. American Association of Petroleum Geologists Bulletin 68, .1744–1751.

Ekpo B.O., Essien, N., Neji, P.A., Etsenake., R.O., 2018. Geochemical fingerprinting of western offshore Niger Delta oils. Journal of Petroleum Science and Engineering, 160, 452–464.

Ekweozor, C.M., Okoye, N.V., 1980. Petroleum source-bed evaluation of Tertiary Niger Delta. AAPG Bulletin, 64, 1251-1259.

Evamy, B.D., Haremboure, J., Kamerling, P., Molloy, F.A., Rowlands, P.H., 1978. Hydrocarbon habitat of tertiary Niger delta. AAPG Bulletin 62, 1–39.

Hofer, G., Wagreich, M., Neuhuber, S., 2013. Geochemistry of fine-grained sediments of the upper Cretaceous to Paleogene Gosau Group (Austria, Slovakia): Implications for paleo-environmental and provenance studies. Geoscience Frontiers, 4, 449-468.

Jiang, L., Cai. C., Worden, R.H., Li, K., Xiang, L., Chu, X., Shen, A., Li, W., 2015. Rare earth element and yttrium (REY) geochemistry in carbonate reservoirs during deep burial diagenesis: Implications for REY mobility during thermochemical sulfate reduction. Chemical Geology, 415, 87–101.

Krueger, S.W., Grant, N.T., 2011. The growth history of toe thrusts of the Niger Delta and the role of pore pressure. In: McClay, K., Shaw, J., Suppe, J. (Eds.), Thrust Fault- Related Folding: AAPG Memoir, 94, 357–390.

Kulke, H. (1995): Nigeria. In: Kulke, H. (Eds), Regional Petroleum Geology of the World. Part II: Africa, America, Australia and Antarctica, Gebru Borntraeger, Berlin, 143–172.

Lambert-Aikhionbare, D. O., and Ibe, A.C., 1984. Petroleum source-bed evaluation of the Tertiary Niger Delta: discussion: American Association of Petroleum Geologists Bulletin, 68, 387-394.

Madhavaraju, J., Rajendra, S. P., Lee, Y. I., Montoya, E. R., Ramasamy, S., & SantaCruz, R. L. (2020). Mineralogy and geochemistry of clastic sediments of the Terani Formation, Cauvery Basin, southern India: implications for paleoweathering, provenance and tectonic setting. Geosciences Journal, 24(6), 651–667. doi:10.1007/s12303-019-0047-2

McLennan, S M., 1989. Rare earth elements in sedimentary rocks: Influence of provenance and sedimentary processes. Review of Mineralogy, 21, 169-200.

McLennan, S.M., Hemming, S., McDaniel, D.K., Hanson, G.N., 1993. Geochemical Approaches to Sedimentation, Provenance, and Tectonics. Geological Society of America Special Papers, 284, 21-40.

Nwachukwu, J.I., Chukwura, P.I., 1986. Organic matter of Agbada Formation, Niger Delta, Nigeria. AAPG (Am. Assoc. Pet. Geol.) Bull. 70, 48–55.

Nwajide, C.S., 2013. Geology of Nigeria's Sedimentary Basins. CSS Bookshops Limited, Lagos, p. 565.

Obi, I.S., Onuoha, K.M., Dim, C.I.P., 2024. Highlighting relationships between sand thicknesses, reservoir-seal pairs and paleobathymetry from a sequence stratigraphic perspective: An example from Tortonian Serravallian deposits, onshore Niger Delta Basin. Energy Geoscience, 5, 100215. https://doi.org/10.1016/j.engeos.2023.100215.

Ogbe, O.B., Okoro, A.U., Ogagarue, D.O., Osokpor, J., Overare, B., Ocheli, A., Opatola, A.O., Oluwajana, O.A., 2021. Reservoir hydrocarbon prospectivity and productivity evaluations of sands S-600 and S-700 of Fega field, onshore Niger Delta Basin, Nigeria. Journal of African Earth *Sciences,* 184, 104311.

Overare., B., Azmy, K., Garzanti, E., Osokpor, J., Ogbe, O.B., Avwenagha, E.O., 2021. Decrypting geochemical signatures in subsurface Niger delta sediments: Implication for provenance, weathering, and paleoenvironmental conditions. Marine and Petroleum Geology, 126, 104879.

Reijers, T.J.A., 2011. Stratigraphy and sedimentology of the Niger delta. Geologos,17 (3) 133–162.

Reijers, T.J.A., Petters, S.W., and Nwajide, C.S., 1997. The Niger Delta Basin, in Selley, R.C., ed., African Basins--Sedimentary Basin of the World 3: Amsterdam, Elsevier Science, 151-172. doi.org/10.1016/S1874-5997(97)80010-X

Short, K.C., Stauble, A.J., 1967. Outline of geology of Niger Delta. AAPG (Am. Assoc. Pet. Geol.) Bull. 51, 761–779.

Sun, Y., Liu, L., 2018., Structural evolution of thrust-related folds and associated fault systems in the eastern portion of the deep-water Niger Delta, Marine and Petroleum Geology, 92, 285-307, https://doi.org/10.1016/j.marpetgeo.2017.12.012.

Tuttle, M.L.W., Charpentier, R.R., Brownfield, M.E., 1999. The Niger Delta Petroleum System: Niger Delta Province, Nigeria, Cameroon, and Equatorial Guinea. USGS Open-file, Africa report 99-50-H.

von Eynatten, H., Barcelò-Vidal, C., Pawlowsky-Glahn, V., 2003. Composition and discrimination of sandstones: a statistical evaluation of different analytical methods. Journal of Sedimentary Research 73, 47–57.

Webb, G.E. and Kamber, B.S. (2000) Rare earth elements in Holocene reefal microbialites: a new shallow seawater proxy. Geochim. Cosmochim. Acta, 64, 1557–1565.

Weber, K.J., Daukoru, E.M., 1975. Petroleum Geology of the Niger Delta: Proceedings of the Ninth World Petroleum Congress, vol. 2. Applied Science Publishers, pp. 210–221.

Whiteman, A., 1982. Nigeria: Its Petroleum Geology, Resources and Potential: London, Graham and Trotman, 394 pp.

Wu, Z., He, S., He, Z., Li, X., Zhai, G., Huang, Z., 2022. Petrographical and geochemical characterization of the Upper Permian Longtan formation and Dalong Formation in the Lower Yangtze region, South China: Implications for provenance, paleoclimate, paleoenvironment and organic matter accumulation mechanisms, Marine and Petroleum Geology, 139, 105580.

Chapter II

Decrypting geochemical signatures in subsurface Niger Delta sediments: Implication for provenance, weathering, and paleo-environmental conditions

Overare, B*.[a, b.], Azmy, K.[a], Garzanti, E.[c], Osokpor, J.[b], Ogbe, O.B.[b], Avwenagha, E.O[d]

[a]Department of Earth Sciences, Memorial University of Newfoundland, St. John's, NL, A1B 3X5, Canada.

[b]Department of Earth Sciences, Federal University of Petroleum Resources, P.M.B 1221, Effurun, Delta State, Nigeria

[C]Laboratory for Provenance Studies, Department of Earth and Environmental Sciences, University of Milano-Bicocca, Piazza della Scienza 4, 20126 Milano, Italy.

[d]Department of Earth Sciences, Arthur Jarvis University, Akpabuyo, P.M.B 1404, Calabar, Cross River State, Nigeria

*Corresponding author's email address: boverare@mun.ca.

Published in the Journal of Marine and Petroleum Geology

Overare et al., 2021. Marine and Petroleum Geology, volume 126, 104879

https://doi.org/10.1016/j.marpetgeo.2020.104879

Abstract

Geochemical signatures of siliciclastic rocks constituting the sedimentary fill of a basin can provide useful clues for constraining sedimentary processes. The inorganic geochemical composition of interbedded sandstone and shale in hydrocarbon-producing zones of the Agbada Formation (Niger Delta Basin) were used as proxies to determine the provenance signatures, evaluate weathering intensity in the source area, and reconstruct paleo-redox conditions in the depositional environment. The Al_2O_3-($CaO + Na_2O$)-K_2O relationship, Th/U ratio, CIA versus SiO_2 correlation, and other weathering proxies (e.g., CIA, CIX, $\alpha^{Al}E$ indices) indicate moderate to intense weathering conditions in the source area. Various elemental ratios such as La/Co, Cr/Th, Eu/Eu*, $(La/Lu)_N$, Th/Co, LHREE/HREE (light to heavy rare earth elements), and the Eu anomaly suggest predominantly felsic sources. Other ratios (e.g., V/Cr, Ni/Co, Cu/Zn, Mo-EF/U-EF) sensitive to redox conditions reflect an oxic-suboxic depositional environment. The interbedded sandstones and shales reflect insignificant disparity in terms of their source area weathering and provenance.

2.1. Introduction

The geochemical composition of sedimentary rocks provides relevant information about the geologic evolution of sedimentary basins through time (Taylor and McLennan, 1985). The geochemistry of siliciclastic rocks is controlled by several factors, including source-rock mineralogy, chemical weathering, hydraulic-sorting processes during erosion, transport, deposition, and post-depositional diagenetic reactions (McLennan, 1989; Bauluz, 2000). Many authors have investigated the relationships between the inorganic geochemical composition of clastic sediments and the tectonic setting and geomorphological features of source rocks (e.g., Bahlburg, 1998; Hofer et al., 2013; Garzanti et al., 2014a; Tao et al.; 2014; Zhang et al., 2014; Zaid and Al Gahtani, 2015; Chen et al., 2016; Armstrong-Altrin et al., 2014; Dinis et al., 2016, 2020; Maharana et al., 2018; Pang et al., 2018; Edegbai et al., 2019; Tang et al., 2020). In

sedimentary geology and basin analysis, petrographic techniques have been routinely used for provenance studies. Several discrimination diagrams, which take into consideration the ratio among major siliciclastic framework components (i.e., quartz, feldspar, and rock fragments), were devised based on the knowledge acquired from known geotectonic and sedimentary settings (e.g., Dickinson and Suczek 1979; Dickinson et al., 1983; Dickinson 1985; Zuffa, 1985; Garzanti et al., 2007; Maravelis and Zelilidis, 2009; Garzanti, 2016). Trace elements (e.g., Y, Th, Nb, Zr, Hf, and Sc), including rare earth elements (REE), have also been used widely in complementary approaches to obtain salient information about provenance and geologic processes (McLennan et al., 1993, Bauluz, 2000; Armstrong-Altrin et al., 2004). Several studies (e.g., Garver et al., 1996; Armstrong-Altrin et al., 2004; Gallala et al., 2009; Abd El-Rahman et al., 2010; Akarish and El-Gohary, 2011) have noted their relevance in decrypting issues that are not easily recognised from petrographic analysis alone, including the presence of mafic/ultramafic source rocks and hydrodynamic control (e.g., von Eynatten et al., 2003; Padoan et al., 2011). Geochemical studies are particularly suitable as a precious complement to petrographic analysis, especially for fine-grained siliciclastic rocks that cannot be properly investigated using traditional petrographic methods (McLennan et al., 1993; Hassann et al., 1999; Do Campo and Guevara, 2005).

The Niger Delta Basin, being a prolific hydrocarbon basin, has been the focus of many studies mostly aiming at understanding the petroleum system (e.g., Allen, 1965; Short and Stauble, 1967; Avbovbo, 1978; Lambert-Aikhionbare and Ibe, 1984; Nwachukwu and Chukwura, 1986; Doust and Omatsola, 1990; Corredor et al., 2005; Krueger and Grant, 2011; Osokpor et al., 2016; Obiadi et al., 2019; Dim et al., 2020; Ogbe, 2020). However, little has been forthcoming about the inorganic geochemical signatures of the component lithostratigraphic units and their significance in constraining sedimentary processes in the basin. The current study utilizes the inorganic geochemical composition of sandstone and shale of the Agbada Formation in part of

the Niger Delta Basin to constrain: (i) source-area weathering and paleogeography; (ii) provenance and (iii) paleo-redox conditions associated with the depositional subenvironment.

2.2 Geologic Setting and Stratigraphy

The study area is located in the offshore depobelt of the Cenozoic Niger Delta Basin (Fig. 2.1). The basin is situated in the north-eastern fringe of the Gulf of Guinea along the equatorial Atlantic margin of West Africa. It covers an area of about 300,000 km^2 (Kulke,1995) and has a sediment volume of ~500,000 km^3 (Hospers, 1965), with a thickness of ~12 km (Reijers, 2011). The basin's boundaries are defined by the Benin flank (north), outcrops of Cretaceous strata on the Abakaliki high (northeast), the Calabar flank (east-south-east), the Cameroon volcanic line (east), and the Dahomey Basin (west) (Tuttle et al., 1999).

The origin of the Niger Delta siliciclastic wedge is associated with a failed arm of a triple junction that initially developed during the break-up of Africa from South America in the Late Jurassic to mid-Cretaceous (Burke et al., 1972). The failed arm evolved into the Benue Trough, whereas the other two arms developed into the West African passive continental margin along coastal Cameroon and Nigeria (Doust and Omastsola, 1990). The siliciclastic system of the Niger Delta began its progradation across the pre-existing continental slope into the deep sea in the late Eocene (Bulke et al., 1972) and is still active today. The progradation resulted in the development of depobelts (Fig. 2.1, 2.2), which correspond to discrete periods of the delta's evolutionary history from the oldest Northern depobelt to the youngest Offshore depobelt (Doust and Omatsola, 1990; Ekweozor and Daukoru, 1984). Based on sedimentation, structural deformation, and hydrocarbon generation and accumulation, each depobelt is believed to constitute a largely independent unit delimited by major bounding faults (Evamy et al., 1978).

The Cenozoic Niger Delta displays three diachronous subsurface lithostratigraphic subdivisions representing prograding depositional facies (Fig. 2.3): lower prodelta, middle delta front, and upper delta top (Reijers et al., 1996). These units are distinguished mostly based on the sand/shale ratio (Tuttle et al., 1999) and are, from bottom to top: the Akata Formation, the Agbada Formation, and the Benin Formation. The characteristics of these formations have been discussed in detail by earlier studies (e.g., Short and Stauble, 1967; Avbobvo, 1978; Doust and Omatola, 1990; Kulke, 1995; Nwajide, 2013).

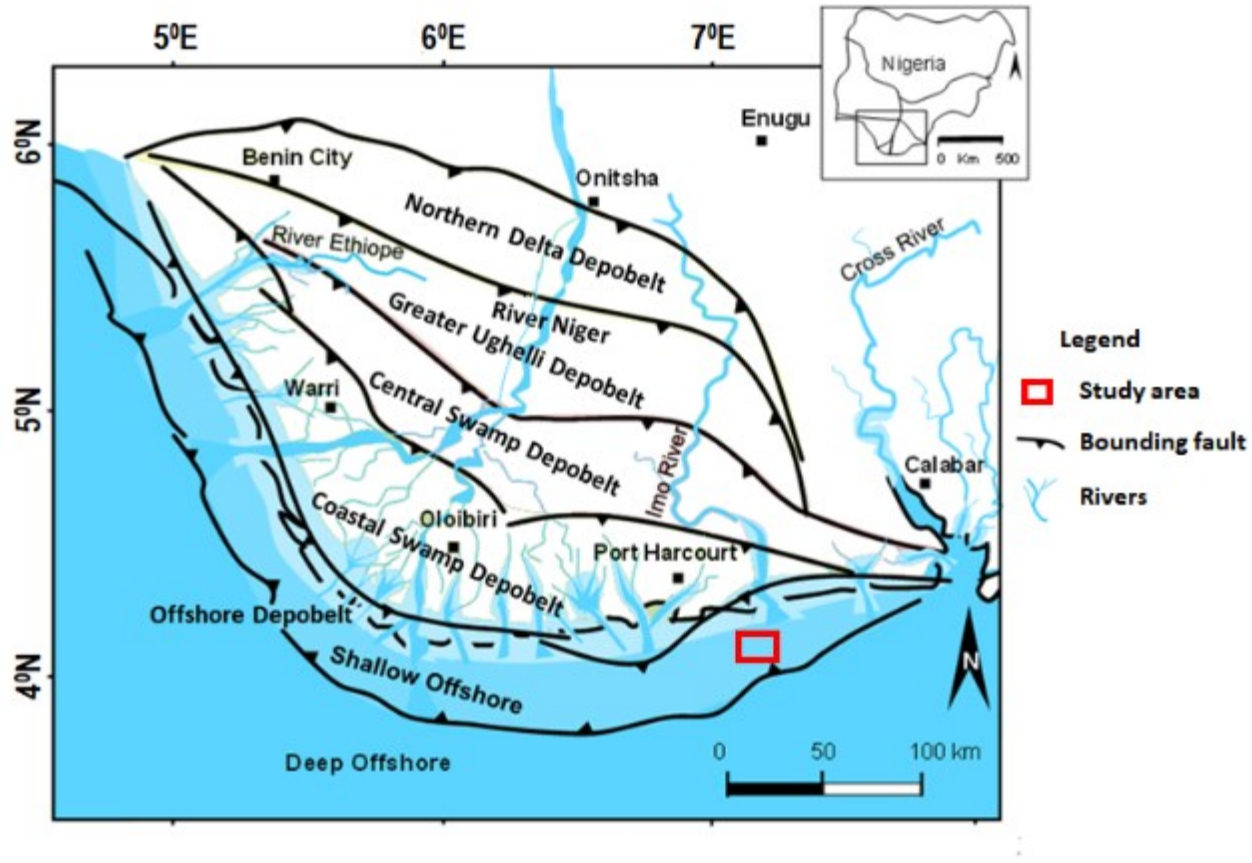

Figure 2.1: Map of the Niger Delta showing the study area (red rectangle) and the diverse depobelts (modified from Ogbe et al., 2020).

2.2.1. Akata Formation

The Akata Formation (Fig. 2.3) is the major transgressive lithological unit of the Niger Delta and consists predominantly of marine shale but also contains silty and sandy turbidite beds and continental-slope channel fills. The shales are generally dark grey, sandy, or locally silty and contain plant remains and some mica, especially in the upper beds. The shales are mostly under-compacted and may contain lenses of abnormally high-pressured siltstone or fine-grained sandstone (Abvobvo,1978). The thickness of the Akata Formation may reach 7000 m in the central part of the delta (Doust and Omatsola, 1990), but it is ~ 5000 m in the deep-water fold and thrust belts (Bilotti et al., 2005; Corredor et al., 2005). In seismic sections, the mid-Akata reflection is a major structural marker defining detachment levels (Corredor et al., 2005). The formation also exhibits low P-wave seismic velocity (~2000 m/s), suggesting regional fluid overpressures (Bilotti and Shaw, 2001). The Akata Shales range from Paleocene to Holocene in age and are currently being deposited on the continental slope and possibly as far as the lower part of the prodelta slope (Nwajide, 2013).

2.2.2. Agbada Formation

The Agbada Formation (Fig. 2.3) is the primary petroleum-bearing unit and mostly consists of interbedded sand/sandstone and shale deposited in a paralic to marine environment. It represents the deltaic portion of the sequence accumulated in delta front, delta top-set, and fluvio-deltaic environments (Doust and Omatsola, 1990). The alternation of sand/sandstone and shale, typically providing reservoir-seal couplets, results from differential subsidence, variation in sediment supply, and shifts of the delta depositional axes associated with transgressions and regressions. The sand/sandstones are very fine to very coarse-grained, predominantly unconsolidated or slightly consolidated, with a calcareous, fairly-clean, glauconitic, and shelly matrix. They are mainly composed of quartz, with subordinate potassium feldspar and minor plagioclase, kaolinite, and illite. Other minor components include mud chips, mica, and rock

fragments. Heavy minerals occur in trace amounts (Nwajide, 2013). Bioclasts and carbonaceous debris are locally abundant. Sorting is generally poor, except in intervals where the sand/sandstone grades into shale. The coarser and less sorted sand/sandstone bodies indicate a fluviatile origin, whereas the better-sorted, finer-grained sand/sandstone beds with glauconite grains and shell fragments represent beach or coastal-barrier deposits.

The shales are usually medium to dark grey, fairly hard, and silty with local glauconite. They predominantly contain kaolinite (~75%) with small amounts of illite-montmorillonite mixed layers (Abvovbo, 1978). Microfauna is best developed at the base of shale units and becomes sparse or absent in the upper part grading into the overlying sand and sandstone bodies, suggesting an increasing deposition rate in front of the advancing delta. Larger foraminifera may occur at the base of shale units, suggesting that marine sedimentation could prevail at the onset of transgression.

The top of the Agbada Formation reflects the shallowest occurrence of shale containing brackish or marine fauna and may appear on seismic profiles as an erosional surface at the base of the overlying unfaulted Benin Sands. In other localities, this boundary is instead transitional. The base of the Agbada Formation is usually marked by the occurrence of the first significant shale body, whereas, on seismic profiles, the demarcation becomes more evident with the occurrence of shale bulges. The thickness of the Agbada Formation varies significantly across the delta between 2926 m and 4267m (Weber and Daukoru, 1975). It is thinnest on the present-day shelf because of well-developed Akata Shale diapirism and thickest in the coastal and central swamp depositional belts, where the Benin Formation is also thickest. The age of the Agbada Formation is Eocene to Holocene, with deposition still taking place on the inner shelf and within the landward limits of the brackish mangrove swamp environment (Nwajide, 2013).

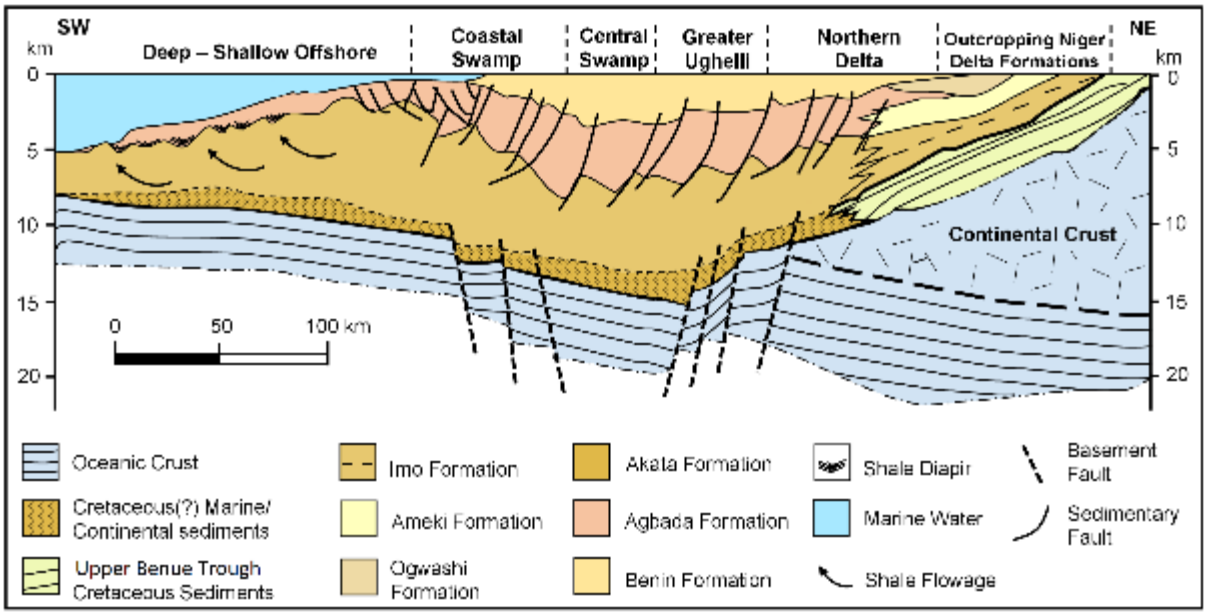

Figure 2.2: A schematic section across the Niger Delta Basin depicting the depobelts, the diachronous lithostratigraphic units, and the associated depositional structures (after Ogbe et al., 2020)

2.2.3. Benin Formation

The Benin Formation (Fig. 2.3) extends across the whole Niger Delta Basin from the Benin-Onitsha area to beyond the present coastline, whereas it is interrupted by the Afam Clay Member towards the east. The Benin Sands were deposited in a braided-river environment and included gravel and back-swamp deposits. The formation is characterised by a high percentage of sand (70–100 %) with only local thin shale interbeds (Abvobvo, 1978) and a lack of a distinctive marine or brackish-water microfauna. The white (yellowish-brown if coated with limonite) sand/sandstones range from fine- to coarse-grained, commonly granular and pebbly, poorly sorted, with subangular to well-rounded clasts. Hematite and feldspar grains are common. The greyish-brown, sandy to silty mudrocks may contain plant remains and lignite occurring as thin streaks or finely dispersed fragments. Sedimentary features reflect an upper deltaic environment, with the sand/sandstones representing point-bar deposits, channel fills, or

natural levees, whereas the shales testify to back-swamp deposits and oxbow fills (Reijers, 2011).

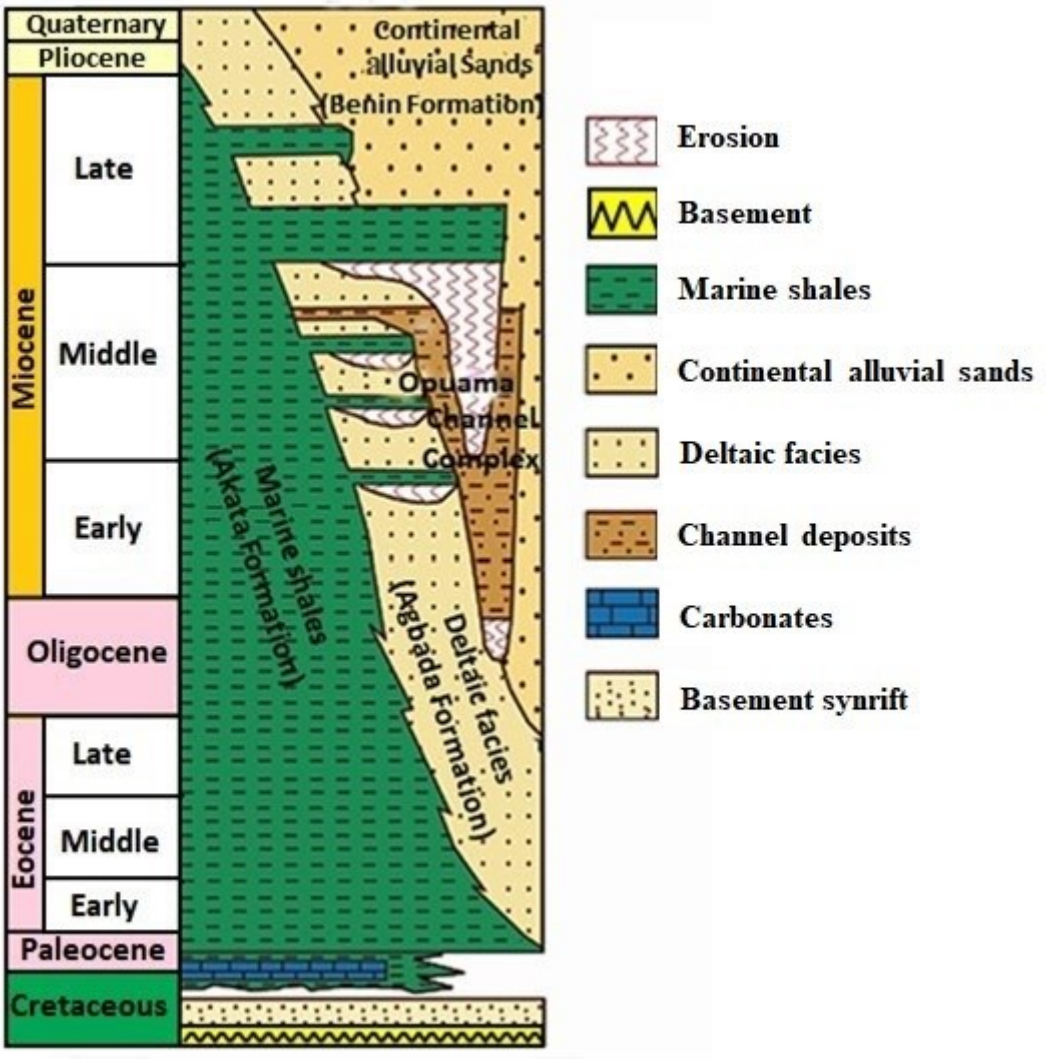

Figure 2.3: Regional stratigraphic scheme of the three diachronous lithologic units (Akata, Agbada, and Benin Formations) in the Niger Delta (modified from Maloney et al. 2010).

Most oil companies arbitrarily define the base of the Benin Formation as the deepest freshwater-bearing sandstone that exhibits high resistivity. Short and Stauble (1967), instead, defined the base of the formation by the first downhole occurrence (last appearance) of marine foraminifera within the underlying shales because the Benin Formation is considered non-

marine. The thickness of the Benin Formation is variable and may reach over 1829 m. In the subsurface, the age of the Benin Formation is Oligocene in the north and progressively becomes younger southwards (Short and Stauble, 1967).

2.2.4. Structural zonation and petroleum system

The Niger Delta Basin was initially divided into three main structural zones (Damuth, 1994): i) an extensional zone of listric growth faults beneath the outer continental shelf; ii) an intermediate translational zone of diapirs and shale ridges beneath the continental slope; and, iii) a compressional zone of imbricated thrusts beneath the lower continental slope and uppermost continental rise. The structural framework was further refined by Corredor et al. (2005) to include five zones/provinces: i) extensional; ii) mud diapirs; iii) inner fold and thrust belt, iv) transitional detachment, and v) outer fold and thrust belt. The structural complexity generally increases from the onshore area in the north to deeper water in the south (Doust and Omatsola, 1990; Tuttle et al., 1999). The fault system consists mostly of normal faults generated by movements of ductile, overpressured, deep-seated marine shale (Ebong et al., 2019). At depth, the faults flatten onto a master detachment plane near the summit of the overpressured marine shales around the base of the sedimentary succession. Most of the hydrocarbon traps in the Niger Delta Basin are structural (e.g., Merki, 1972; Evamy et al., 1978; Doust and Omatsola, 1990; Stacher, 1995; Tuttle et al., 1999), although stratigraphic traps such as clay-filled channels and pinch-outs may also exist and are prospectively as important as the structural traps on the flanks of the delta (Beka and Oti, 1995).

Speculations and debates about the source of the Niger Delta petroleum system continued through many years (e.g., Frankl and Cordry, 1967; Short and Stuable, 1967; Evamy et al., 1978; Ekweozor et al., 1979; Ekweozor and Okoye, 1980; Lambert-Aikhionbare and Ibe, 1984; Nwachukwu and Chukwura, 1986; Bustin, 1988; Doust and Omatsola, 1990). Although Haack et al. (2000) suggested three distinct petroleum systems reflecting different source-rock

organic-matter types – Lower Cretaceous (lacustrine), Upper Cretaceous–Paleocene (marine), and Cenozoic (deltaic) – it is now widely accepted that the Niger Delta has only one identified petroleum system, the Cenozoic Niger Delta (Akata-Agbada) petroleum system (Ekweozor and Daukoru, 1994; Kulke, 1995; Tuttle et al., 1999). The principal source rock is the marine-shale facies of the upper Akata Formation, with possible contributions from the interbedded shale of the lowermost Agbada Formation. Hydrocarbons are mainly produced from the sandstone facies within the paralic Agbada Formation. The upper Akata Formation turbidite sand is another prospective target occurring in deep-water environments and possibly beneath currently-producing intervals onshore (Tuttle et al., 1999).

2.3. Methodology

Thirty-six ditch cuttings (19 shale and 17 sandstone specimens) from hydrocarbon-producing zones of the Agbada Formation (Fig. 2.4, Appendix 2.1) were selected for inorganic geochemical analyses. The sandstone samples are mainly representative of two reservoirs (Fig 2.4), whereas the shale samples belong to units that sealed both the top and bottom of reservoirs. The cuttings were analyzed at Acme Laboratories, Vancouver, Canada, using X-ray Fluorescence (XRF) for major elements and inductive-coupled-plasma mass-spectrometry (ICP-MS) for trace elements, including rare earth elements (REE). The samples were dried at 60°C and pulverized to 85% passing 200 mesh (75 microns) using a mild-steel pulverizer. Powder samples (10 g each) were digested to complete dryness with an acid solution of (2:2:1:1) H_2O-HF-$HClO_4$-HNO_3. The residue was then heated using a mixing hot block after HCl (50% v/v) was added. The solutions were transferred to test-tubes after cooling and brought to volume using dilute HCl. Sample splits of 0.25 g were analyzed for the concentration of trace elements, including rare earth elements (REE), using ICP-MS. Prior to XRF analysis, a predetermined amount for each sample was roasted to measure the loss of ignition (LOI). The roasted sample was fused in a platinum-gold crucible with a commercial lithium tetraborate

flux, and the resulting molten material was cast in a platinum mould. The fused discs were analyzed for major elements using XRF. To ensure accuracy and precision, several standard reference materials, transitional (saprolite-limonite) ore (OREAS 184), and Diorite Gneiss (SY-4), were used for quality assurance (QA) and quality control (QC). The REE data were normalized relative to the chondrite values of Boynton (1984). Eu/Eu* is calculated by the formula, $Eu/Eu^* = Eu_N/(Sm_N \times Gd_N)^{1/2}$, where *N* represents normalization.

2.4. Results

The geochemical results are tabulated in Appendix 2.1, and the summary of their statistics is presented in Table 2.1. The average data for Post-Archean Australian average Shale (PAAS, Taylor and McLennan, 1985), and Upper Continental Crust (UCC, Rudnick and Gao, 2003) are included as references.

2.4.1 Major Elements

The investigated sandstones (Sst) are richer (Table 2.1) in SiO_2 than the shales (Sh), whereas shales have higher concentrations of Al_2O_3, K_2O, Fe_2O_3, and TiO_2. Relative to the PAAS and UCC, sandstones and shales are respectively depleted in Al_2O_3 and SiO_2. Otherwise, they have similar MnO and P_2O_5 and are both enriched in Fe_2O_3 and depleted in CaO, MgO, K_2O, and Na_2O. The TiO_2 content of sandstone and shale samples is higher than the UCC but lower than the PAAS.

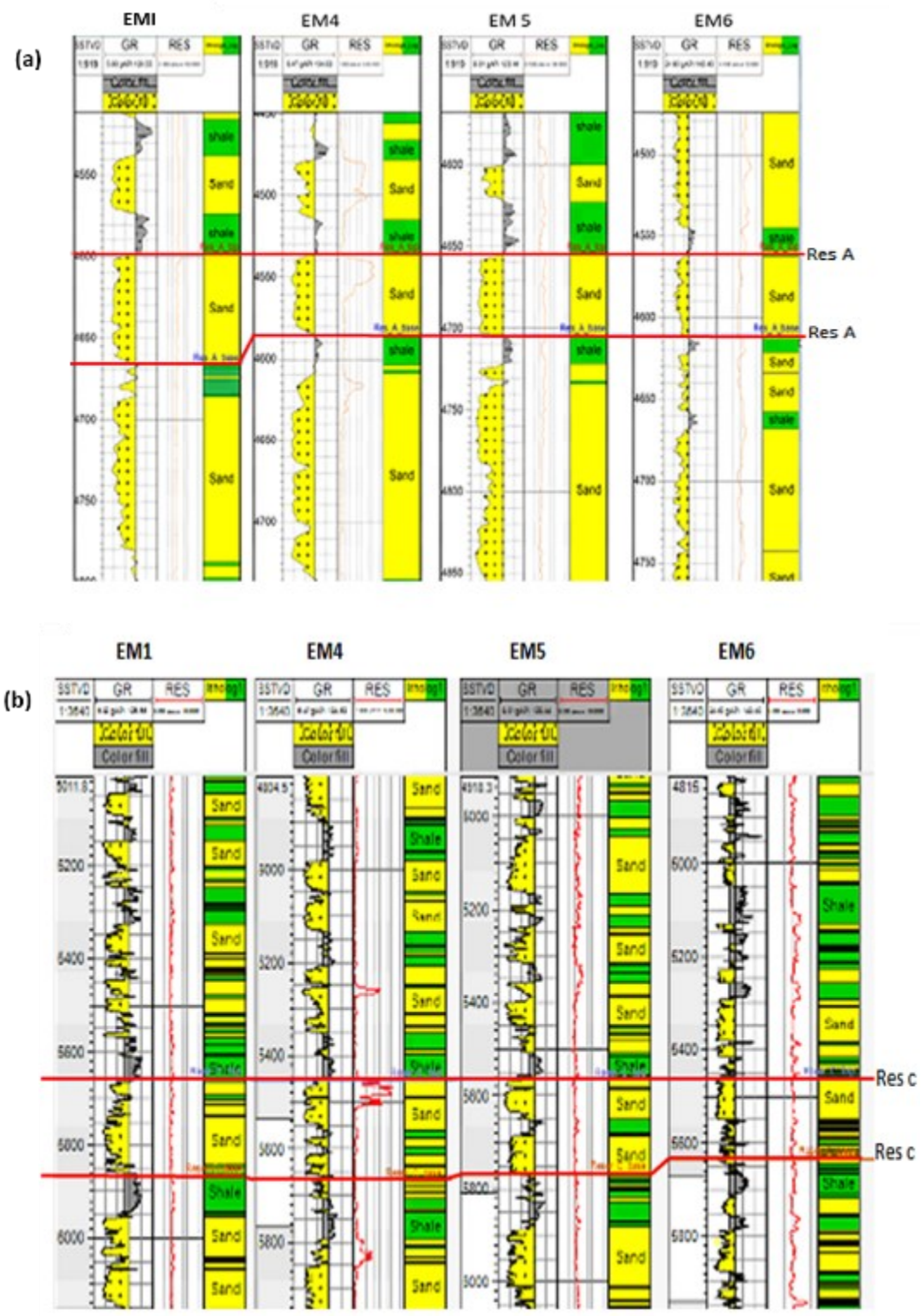

Figure 2.4: Well correlation for (a) Reservoir A (b) Reservoir C

Table 2.1: Concentrations of major oxides and trace elements, including REE, in the investigated sandstone and shale samples.

MAJOR ELEMENTS	SANDSTONES		SHALES		UCC	PAAS
	Range	Mean	Range	Mean		
SiO_2 %	59.80 - 79.10	66.23 ± 5.08	50.23 - 59.10	54.55 ± 2.74	66.00	62.80
Al_2O_3	7.68 - 15.07	11.68 ± 2.37	14.15 - 18.50	16.18 ± 1.43	15.40	18.90
Fe_2O_3	4.47 - 14.40	8.23 ± 2.15	7.41 - 18.10	9.20 ± 2.33	5.04	7.22
CaO	0.34 -1.56	0.96 ± 0.42	0.41 -2.32	1.20 ± 0.57	3.59	1.30
MgO	0.67 - 1.61	1.17 ± 0.25	1.18 - 2.34	1.72 ± 0.32	2.48	2.20
Na_2O	0.37-0.85	0.56 ± 0.13	0.61-0.98	0.72 ± 0.08	3.27	1.20
K_2O	0.96 - 1.78	1.20 ± 0.19	1.24 - 1.92	1.59 ± 0.15	2.80	3.70
MnO	0.05-0.16	0.11 ± 0.03	0.08-0.24	0.12 ± 0.04	0.10	0.11
TiO_2	0.43 - 1.08	0.68 ± 0.16	0.83 - 1.16	0.98 ± 0.08	0.64	1.00
P_2O_5	0.06 - 0.30	0.13 ± 0.06	0.11 - 0.25	0.16 ± 0.04	0.15	0.16
LOI	5.89 - 10.55	8.59 ± 1.28	10.10 - 15.28	12.81 ± 1.79	-	-
Fe_2O_3/K_2O	4.28 - 13.46	7.01 ± 2.28	4.18 - 14.60	5.92 ± 2.20	1.80	1.95
SIO_2/Al_2O_3	4.01 - 10.30	5.98± 1.69	2.92 - 3.85	3.39 ± 0.32	4.29	3.32
K_2O/Na_2O	1.55 - 3.22	2.23 ± 0.47	1.44 - 2.53	2.22 ± 0.30	0.86	3.08
Al_2O_3/TiO_2	13.53 - 19.59	17.34 ± 1.80	14.61 - 19.68	16.61 ± 1.19	24.06	18.90
K_2O/Al_2O_3	0.08 - 0.13	0.10 ± 0.02	0.08 - 0.11	0.10 ± 0.01	0.18	0.20
CIA	73.84 - 83.33	77.96 ± 2.71	77.74 - 82.70	80.24 ± 1.20	52.76	70.39
CIX	84.76 - 90.29	86.75 ± 1.71	86.28 - 89.03	87.46 ± 0.74	-	-
$\alpha^{Al}Na$	3.70 -8.32	4.64 ± 1.41	4.01-5.46	4.77 ± 0.44	-	-
$\alpha^{Al}Ca$	4.06 -9.14	5.47 ± 1.59	4.21 - 10.40	5.80 ± 1.43	-	-
$\alpha^{Al}Mg$	1.02 - 2.34	1.66 ± 0.36	1.05 - 2.08	1.58 ± 0.36	-	-
$\alpha^{Al}K$	1.40 -2.22	1.78 ± 0.27	1.62 -2.39	1.86 ± 0.20	-	-
TRACE ELEMENTS						
Ba (ppm)	293.00 - 3906.00	1705 ± 1153.74	496.00 - 2559.00	1453.95 ± 644.54	628.00	650.00
Co	7.30 - 15.50	12.42 ± 2.13	12.00 - 17.70	14.28 ± 1.34	17.30	23.00
Cs	1.40 - 3.30	2.51 ± 0.53	3.10 - 4.00	3.60 ± 0.25	4.90	4.60
Ga	7.80-19.30	13.94 ± 2.98	17.70 -21.90	19.52 ± 1.37	17.00	20.00

Hf	4.20 - 11.50	6.43 ± 1.85	6.00 - 11.50	9.15 ± 1.45	5.30	5.00
Nb	10.90 - 27.90	17.96 ± 4.25	21.80 - 27.50	25.12 ± 1.52	12.00	19.00
Rb	35.20 - 71.20	49.92 ± 8.61	58.10 - 77.20	68.03 ± 4.35	82.00	160.00
Sr	67.50 - 185.50	123.25 ± 29.91	109.50 - 184.10	157.39 ± 20.00	320.00	200.00
Th	7.40 - 15.10	11.08 ± 2.16	13.70 - 17.50	15.25 ± 0.95	10.50	14.60
U	1.80 - 4.00	2.62 ± 0.58	2.70 - 4.60	3.79 ± 0.49	2.70	3.10
V	40.00 - 92.00	69.18 ± 12.81	83.00 - 107.00	95.05 ± 6.85	97.00	150.00
Zr	158.10- 428.00	239.82 ± 69.94	215.80 - 422.30	341.04 ± 56.30	193.00	210.00
Mo	1.00 - 72.20	19.42 ± 21.49	1.60 – 13.77	5.68 ± 3.85	1.10	1.50
Cu	12.70 - 73.70	29.29 ± 17.00	16.60 - 64.60	23.79 ± 11.67	28.00	50.00
Pb	9.70 - 130.10	49.19 ± 30.02	16.70 - 81.40	31.51 ± 18.88	0.00	0.00
Zn	47.00 - 103.00	66.65 ± 16.16	60.00 - 155.00	75.21 ± 20.48	67.00	85.00
Ni	12.60 - 37.20	20.42 ± 6.09	16.60 - 45.50	20.95 ± 6.45	47.00	55.00
Cr	65.05 - 68.44	66.94 ± 1.10	65.22 - 136.90	81.80 ± 28.73	92.00	110.00
Y	14.90 - 34.30	22.61 ± 5.10	24.70 - 35.50	31.21 ± 2.45	21.00	27.00
$\alpha^{Al}Rb$	1.03 -1.46	1.24 ± 0.13	1.13 - 1.52	1.27 ± 0.09	-	-
$\alpha^{Al}Sr$	1.57-3.06	2.03 ± 0.41	1.60 - 3.51	2.19 ± 0.48	-	-
$\alpha^{Al}Ba$	0.00 -0.04	0.01 ± 0.01	0.25 - 1.52	0.56 ± 0.31	-	-
Cr/V	0.72 - 1.67	1.01 ± 0.22	0.63 - 1.61	0.86 ± 0.31	0.95	0.73
Y/Ni	0.53 - 1.83	1.18 ± 0.38	0.54 - 2.14	1.58 ± 0.34	0.45	0.49
La/Th	3.20 -3.56	3.37 ± 0.11	3.10 -3.61	3.42 ± 0.13	2.95	2.62
Th/Co	0.61 - 1.04	0.90 ± 0.14	0.77 - 1.22	1.08 ± 0.10	0.61	0.63
La/Co	2.14 - 3.51	3.03± 0.44	2.59 - 4.23	3.68 ± 0.35	1.79	1.66
V/Cr	0.60 - 1.40	1.03 ± 0.20	0.62 - 1.59	1.26 ± 0.31	1.05	1.36
Ni/Co	1.25 - 2.40	1.63 ± 0.28	1.17 - 2.57	1.45 ± 0.31	2.72	2.39
Cu/Zn	0.23 - 1.02	0.44 ± 0.22	0.23 - 0.50	0.31 ± 0.07	0.42	0.59
Cr/Th	4.36 - 9.02	6.28 ± 1.31	4.13 - 9.85	5.35 ± 1.81	8.76	7.53
Th/U	3.45 - 5.19	4.28 ± 0.53	3.41 - 5.20	4.09 ± 0.62	3.89	4.71
RARE EARTH ELEMENTS						
La (ppm)	23.70 - 51.60	37.28 ± 7.29	45.80 - 57.70	52.16 ± 2.64	31.00	38.20
Ce	48.20 - 103.30	76.84 ± 14.60	93.40 - 114.20	105.32 ± 5.30	63.00	79.60

Pr	5.56 -12.15	8.79 ± 1.69	10.71 -13.05	12.18 ± 0.62	7.10	8.83
Nd	20.90 - 43.90	32.54 ± 6.43	40.20 - 48.40	44.96 ± 2.40	27.00	33.90
Sm	3.94 - 8.14	5.87 ± 1.13	7.45 - 8.99	8.19 ± 0.42	4.70	5.55
Eu	0.77 - 1.66	1.20 ± 0.23	1.51 - 1.83	1.67 ± 0.09	1.00	1.08
Gd	3.33 - 7.25	5.20 ± 1.04	6.29 - 7.72	7.22 ± 0.35	4.00	4.66
Tb	0.46 - 1.06	0.72 ± 0.15	0.83 - 1.10	1.00 ± 0.06	0.70	0.77
Dy	2.79 - 6.16	4.41 ± 0.89	5.06 - 6.70	6.03 ± 0.37	3.90	4.68
Ho	0.53 - 1.27	0.81 ± 0.19	0.89 - 1.26	1.12 ± 0.08	0.83	0.99
Er	1.41 - 3.63	2.34 ± 0.54	2.48 - 3.66	3.21 ± 0.26	2.30	2.85
Tm	0.22 - 0.56	0.34 ± 0.09	0.34 - 0.55	0.48 ± 0.05	0.30	0.41
Yb	1.42 - 3.60	2.20 ± 0.54	2.32 - 3.46	3.08 ± 0.27	2.00	2.82
Lu	0.22 - 0.56	0.34 ± 0.08	0.36 - 0.54	0.46 ± 0.04	0.31	0.43
∑LREE	117.97 - 255.05	185.12 ± 35.95	223.77 - 277.08	255.70 ± 12.38	133.80	167.16
∑HREE	10.38 - 24.09	16.36 ± 3.45	18.57 - 24.82	22.61 ± 1.35	14.34	17.61
∑LREE/∑HREE	10.51 - 12.29	11.36 ± 0.57	10.68 - 12.12	11.32 ± 0.40	9.33	9.49
∑REE	128.35 - 279.14	201.48 ± 39.30	242.34 - 301.90	278.31 ± 13.51	148.14	184.77
Eu/Eu*	0.61 - 0.70	0.66 ± 0.02	0.62 - 0.69	0.66 ± 0.02	0.66	0.71
Ce/Ce*	0.97 - 1.03	1.00 ± 0.02	0.96 - 1.01	0.98 ± 0.01	1.02	1.03
(La/Lu)N	9.57 - 14.00	11.71 ± 1.33	10.13 - 13.90	11.76 ± 0.97	10.39	9.86
(Gd/Yb)N	1.41 - 1.80	1.59 ± 0.12	1.43 - 1.75	1.59 ± 0.10	1.35	1.61
(La/Sm)N	3.79 - 4.30	4.00 ± 0.14	3.69 - 4.16	4.01 ± 0.12	4.27	4.15
(La/Yb)N	8.51 - 10.92	9.52 ± 0.86	8.41 - 10.61	9.60 ± 0.61	9.15	10.45

LREE/HREE: Light to heavy rare earth element ratio

PAAS: Post-Archean Australian Shales (Taylor and McLennan, 1985)

UCC: Upper Continental Crust (Rudnick and Gao, 2003).

2.4.2 Trace Elements

The shales are richer than sandstones in high field-strength elements (HFSE; Nb, Th, U, Zr, Hf, and Y), transition trace elements (TTE; V, Cr Co, Ni, and Zn), and large ion lithophile elements (LILE; Rb, Cs, and Sr) (Table 2.1). The sandstones, instead, have a higher concentration of Ba and Cu. Relative to the PAAS and the UCC, sandstones are enriched in HFSE elements (e.g., Zr, Hf) but depleted in U, Y, Nb, and Th. Excepting Ba, which is higher than PAAS and UCC compositions, the other LILE (Rb, Sr, and Cs) are depleted. The concentration of most TTE is lower than the PAAS and the UCC, whereas Cu is higher than the UCC.

2.4.3 Rare-Earth Elements (REE)

The chondrite-normalized REE patterns are presented in Figure 2.5. The sandstones and shales of the Agbada Formation have steep LREE and relatively flat HREE patterns. The sediments exhibit distinct negative Eu anomaly (Eu/Eu* = Sst: 0.66 ± 0.02; Sh: 0.66 ± 0.71) similar to UCC.

2.5. Discussion

2.5.1 Geochemical classification and provenance

Previous studies (e.g., Blatt et al., 1972; Pettijohn et al., 1972; Crook, 1974; Herron, 1988; López de Luchi, 2003; Armstrong-Altrin et al., 2004; Do Campo and Guevara 2005; Mikes et al., 2006; Osae et al., 2006; Meinhold et al., 2007; Ramachandran et al., 2016; Akkoca et al., 2019; Overare et al., 2020) have utilized geochemical classification diagrams for terrigenous sedimentary rocks using inorganic geochemical proxies. However, existing geochemical and petrographic classification schemes have come under intense criticism in recent years (e.g., Lindsey, 1999; Basu et al., 2016; Garzanti, 2016). Therefore, caution should be taken when using geochemical data for classification without mineralogical and petrographic information. In the absence of mineralogical data, the classical bivariate plots of Crook (1974) and Herron

(1988) were adopted here by replacing vaguely defined obsolete names such as “greywacke” or “arkose” (Garzanti, 2019) with less ambiguous descriptive terms such as quartz-poor and feldspar-rich sand/sandstone. The studied sandstones are classified essentially as quartz-rich (Fig. 2.6a), although they are lower in SiO_2 (66.2 ± 5.1, Table 2.1) than quartz-rich sandstones (89 wt.%) as defined by Crook (1974). Herron (1988) suggested a bivariate relationship of log(Fe_2O_3/K_2O) vs. log (SiO_2/Al_2O_3) to distinguish different sandstone classes, shales, and other iron-rich siliciclastic sediments. The plot (Fig. 2.6b) of Herron (1988) classifies the studied sandstones and shales as Fe-rich, although it is noteworthy that, because of their high Fe_2O_3, the (Fe_2O_3+MgO)/(K_2O+Na_2O) ratio is so high that samples plot outside the established compositional fields.

Several authors have emphasized the use of geochemical signatures as an additional tool for inferring provenance (e.g., Barbera et al., 2006, Armstrong-Altrin et al., 2004; Meinhold et al., 2007; Amorosi, 2012; Hofers et al., 2013; Baiyegunhi et al., 2017; Xie et al., 2017; Asiedu et al., 2019; Edegbai et al., 2019; Overare et al., 2020). In provenance studies, it is imperative to rely on elements with very low mobility during the processes of weathering, transport, diagenesis, and metamorphism (Wronkiewicz and Condie, 1987). Besides, hydraulic sorting effects must be taken into full account (Garzanti et al., 2010, 2011). The REE, Th, Sc, and the high field strength elements (e.g., Zr, Nb, Hf, Y) are considered to be non-mobile and were thus commonly used to investigate source-rock composition (e.g., Taylor and McLennan, 1985; Floyd et al., 1989; McLennan and Taylor, 1991; McLennan et al., 1993; Bauluz et al., 2000; Armstrong-Altrin et al., 2014; Do Campo and Guevara, 2005).

The pioneering provenance discrimination diagram of Roser and Korsch (1988) differentiates four fields of sedimentary provenance (mafic igneous, intermediate igneous, felsic igneous, and quartzose sedimentary or recycled). The Agbada samples plot mainly in the field of quartzose sedimentary provenance (Fig. 2.7a). Source terrains largely consisting of

quartzose siliciclastic sediments are common in the catchment of the modern Niger River, which today flows for a large tract across the southern edge of the Sahara Desert.

The Hf–La/Th correlation, widely used in provenance studies (e.g., Floyd and Leveridge, 1987; Spalletti et al., 2012; Tao et al., 2014; Xie et al., 2017), also suggests that most of the investigated sandstones fall within the felsic region (Fig. 2.7b). Shale samples display high Hf concentration, which suggests a significant amount of zircon because Hf is preferentially hosted in the zircon lattice. Zircon is a durable ultradense mineral, which is therefore concentrated either in heavy-mineral lags formed by selective hydrodynamic entrainment of less dense minerals in the sedimentary environment or by the selective mechanical and chemical breakdown of less durable minerals during multiple sedimentary cycles (Garzanti, 2017). Other discrimination diagrams concur to a dominantly felsic provenance for the studied sediments (Fig. 2.8a–d: Floyd et al., 1989; Hayashi et al., 1997; Cullers and Berendsen, 1998; Bracciali et al., 2007). The Al_2O_3/TiO_2 vs. SiO_2 plot (Fig. 2.9a; Le Bas, 1986) also confirms a felsic provenance for the sand/sandstones, although it suggests a mixed felsic-intermediate source for the shales. Both Y/Ni vs. Cr/V (Fig. 2.9b; Mongelli et al., 2006) and K(wt.%)-Rb (ppm) plots (Fig. 2.9c; Floyd and Leveridge, 1987) rule out any significant input from mafic-ultramafic sources.

Elemental ratios such as $(La/Lu)_N$, Eu/Eu*, Cr/Th, Th/Co, and La/Co may also help to discriminate provenance from felsic and mafic rocks (e.g., Cullers et al., 1988; Wronkiewicz and Condie, 1989; Cullers, 1994; Cullers and Podkovyrov, 2002; Armstrong-Altrin et al., 2004; Akarish and El-Gohary, 2011; Ramachandran et al., 2016). The Th/Co, La/Co, Cr/Th, $(La/Lu)_N$, and Eu/Eu* ratios of the Agbada sediments (Table 2.2) further support a felsic provenance for the studied sediments.

The REE patterns and the Eu anomaly provide further clues to decrypt source-rock characteristics (e.g., Alkarish and El-Gohary, 2011; Armstrong-Altrin et al., 2014; Tao et al., 2014; Ramachandran et al., 2016). More negative Eu anomaly and higher LREE/HREE ratio point to felsic source rocks, whereas lower LREE/HREE ratio and small Eu anomaly are suggestive of mafic source rocks (Cullers and Graf, 1984; Cullers et al., 1987; Cullers, 1995). The Agbada sandstones and shales show a high LREE/HREE ratio with negative Eu anomaly (Table 2.1), pointing again to provenance from felsic sources. Consistent indications come from the Ni-Cr (Fig. 2.10a; McLennan et al., 1993) and Eu/Eu* vs. $(Gd/Yb)_N$ diagrams (Fig. 2.10b; McLennan and Taylor, 1991). Minor contributions from Archean sources are suggested by $(Gd/Yb)_N$ signatures.

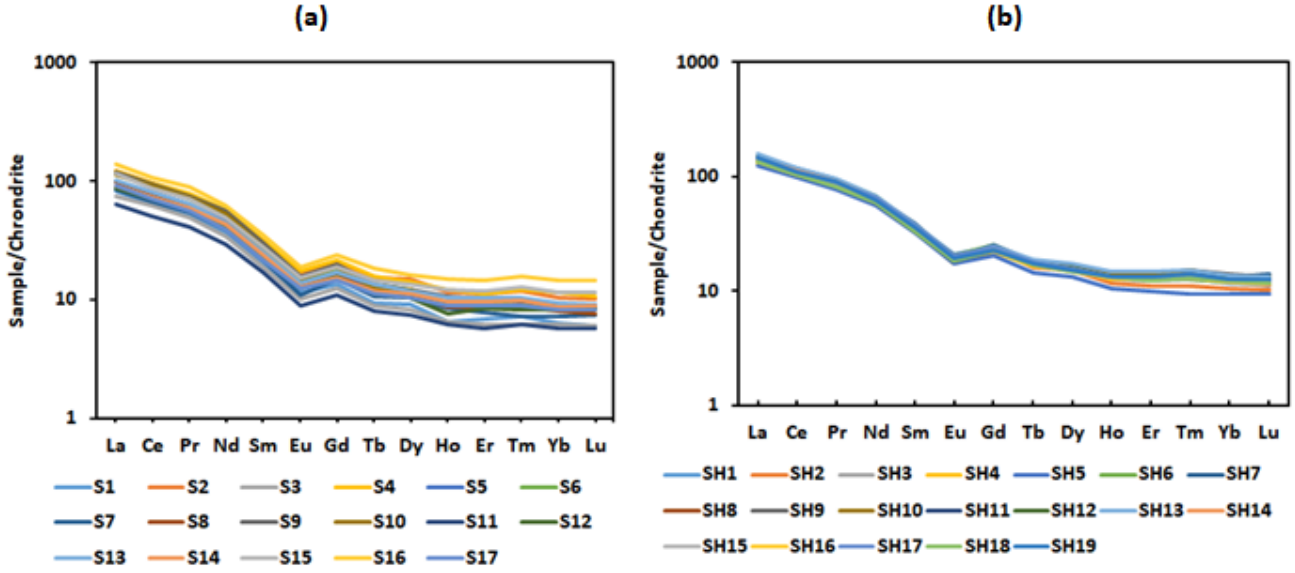

Figure 2.5: Chondrite-normalized REE patterns of the investigated: (a) sandstones; (b) shales.

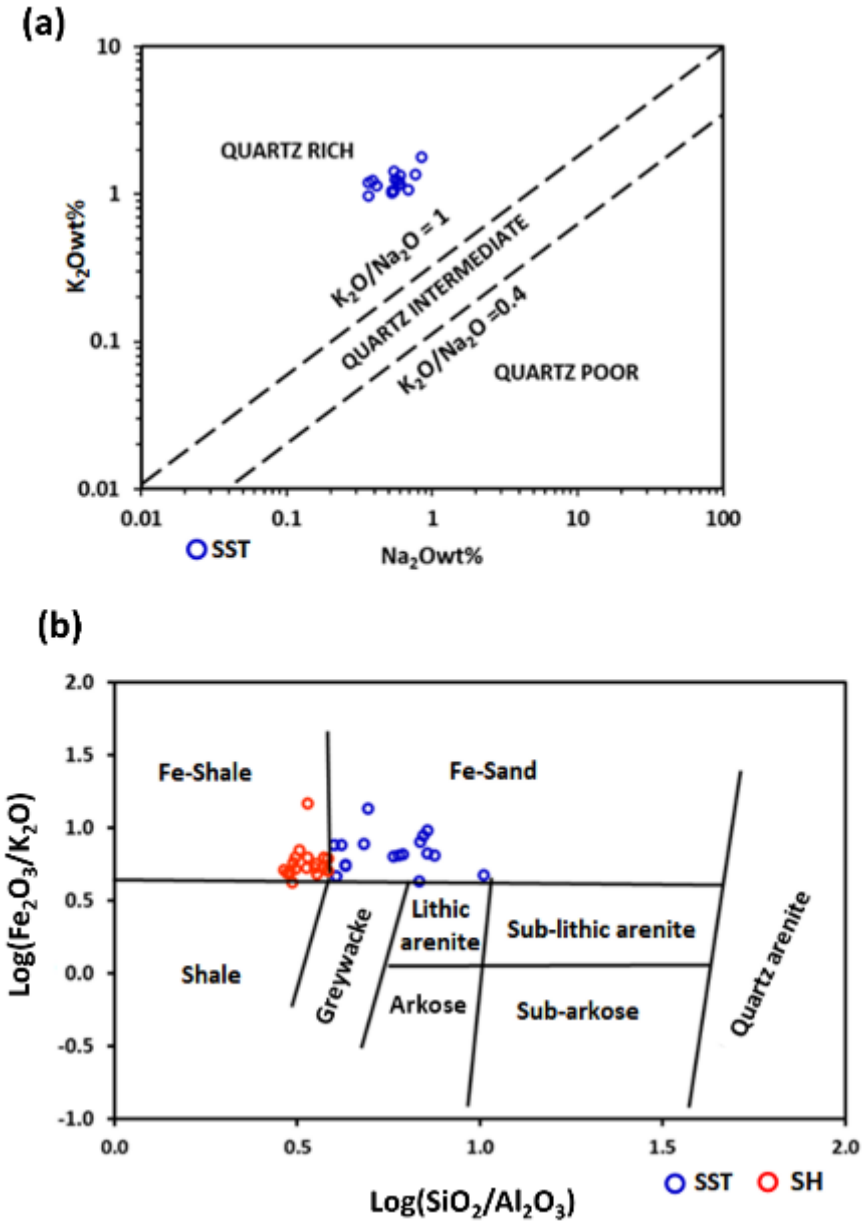

Figure 2.6: Geochemical classification of the sandstones and shales (a) K_2O wt.% versus Na_2O wt.% diagram (Crook,1974), (b) log (SiO_2/Al_2O_3) vs. log (Fe_2O_3/K_2O) diagram (modified from Herron, 1988). Because terms for sandstone classification used in the original diagram are obsolete (Garzanti, 2019), the original terms are modified to indicate: "greywacke" -> quartz-poor sand; "lithic arenite" -> lithic-rich sand; "arkose" -> feldspar-rich sand, "subarkose" -> feldspar-bearing sand; "sub-lithic arenite" -> lithic-bearing sand; "quartz arenite" -> quartzose sand.

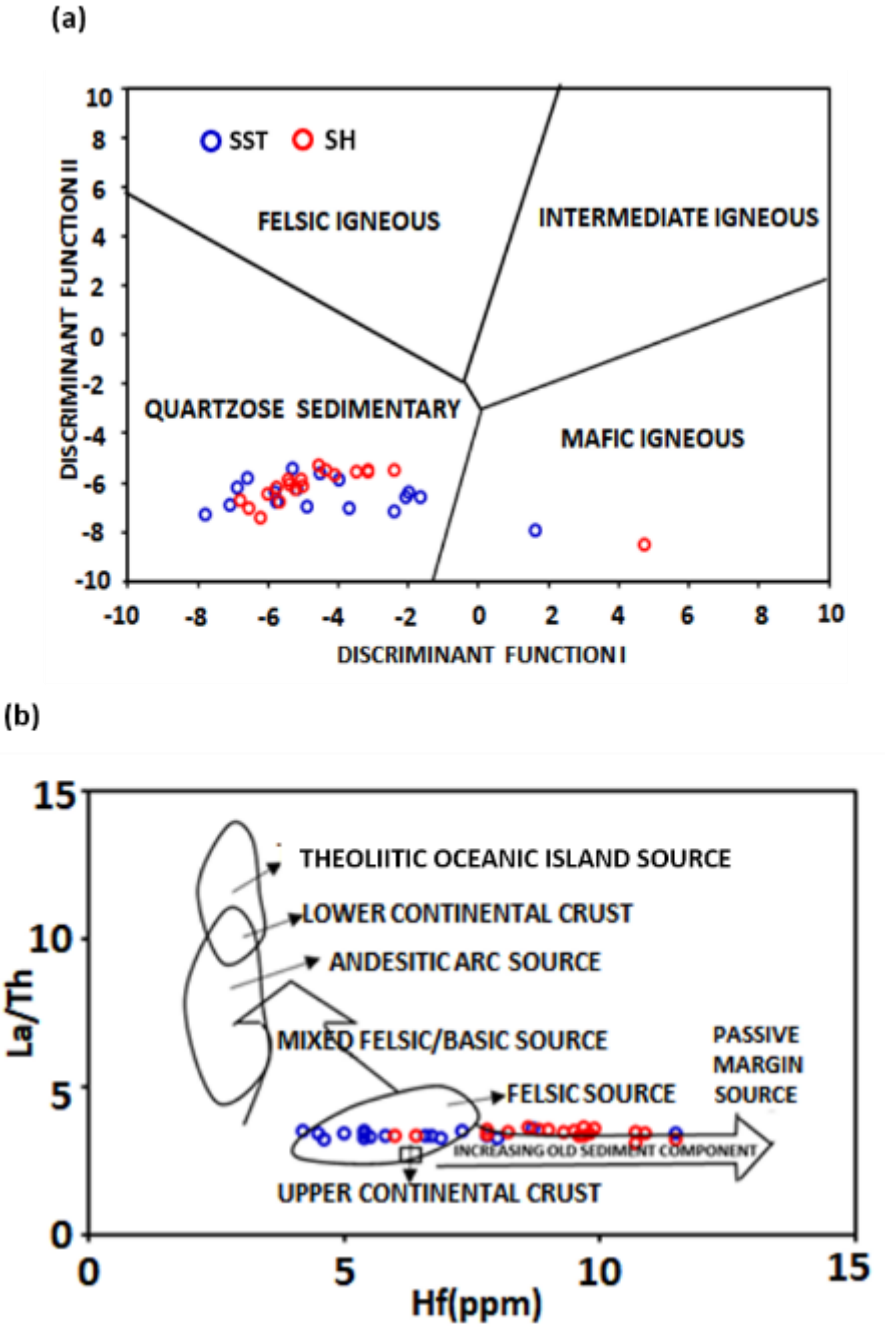

Figure 2.7: (a) Discriminant function diagram for provenance signatures (Roser and Korsch, 1988); and (b) La/Th vs. Hf (ppm) diagram (fields after Floyd and Leveridge, 1987)

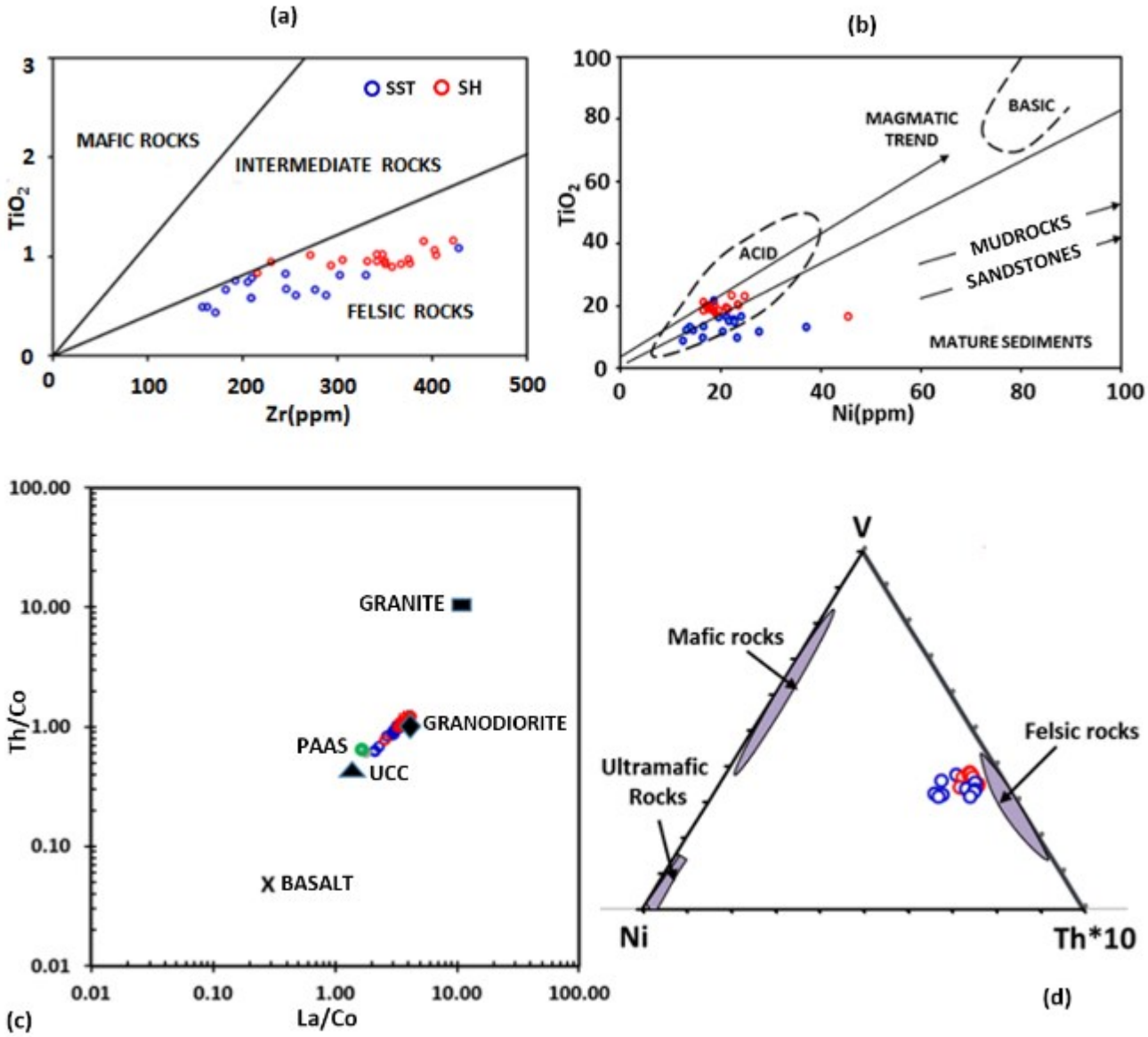

Figure 2.8: (a) TiO_2-Zr correlation for the investigated sediments (Hayashi et al., 1997); (b)TiO_2 vs. Ni plot (fields and trends after Floyd et al., 1989); (c) Th/Co vs. La/Co plot (after Cullers and Berendsen 1998). Average values of granite, basalt, granodiorite (Taylor, 2015), and upper continental crust (Taylor and McLennan, 1985; 1995) are given for comparison; and (d) V-Ni-

Th*10 ternary relationship for Agbada sediments (Bracciali et al., 2007). Shaded areas represent the composition of felsic, mafic, and ultramafic source rocks.

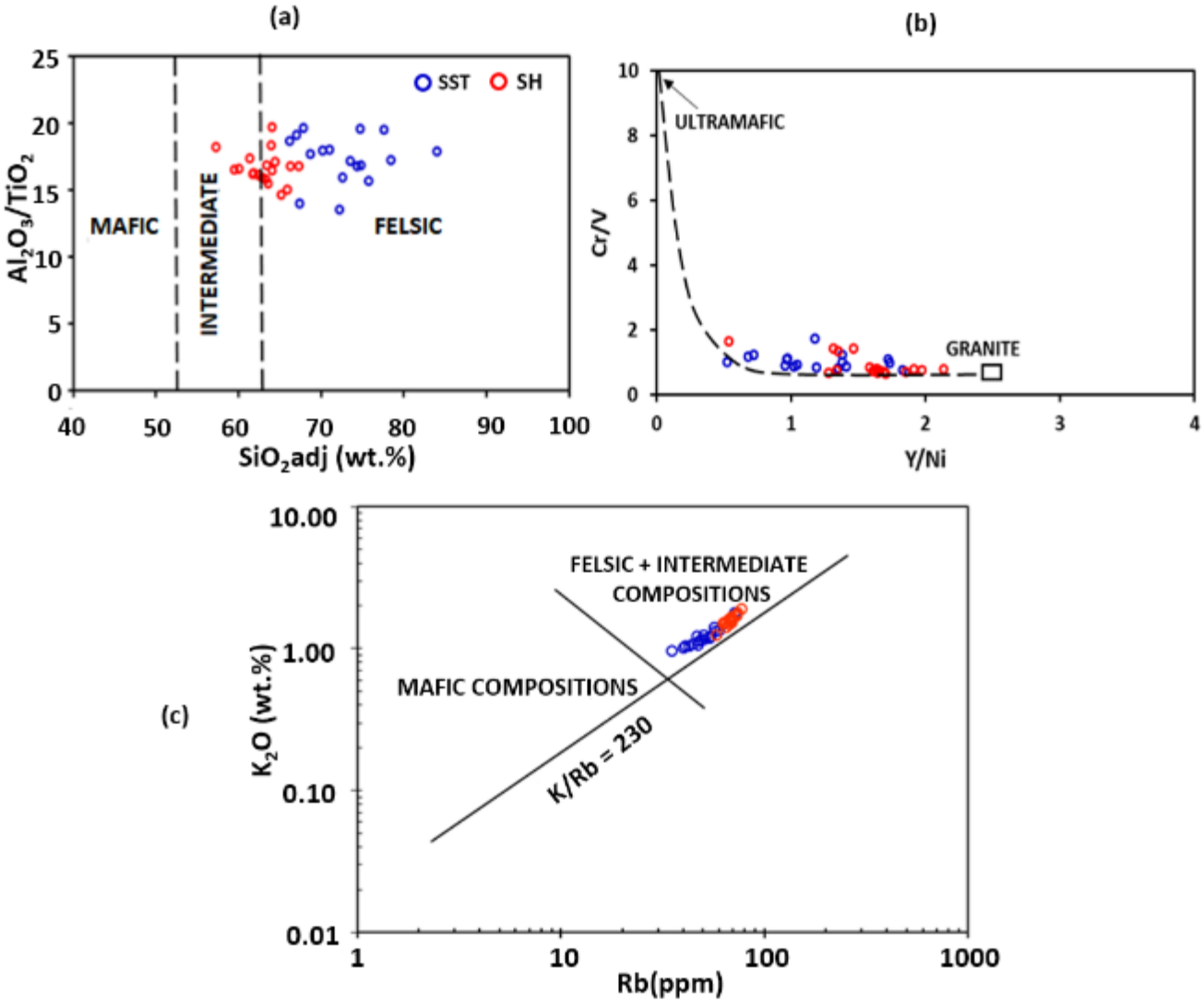

Figure 2.9: (a) Al_2O_3/TiO_2 vs. (SiO_2)adj. (Le Bas et al., 1986) relationship for the studied sediments; (SiO_2)adj = major-element data recalculated to anhydrous (LOI-free) basis and adjusted to 100% ; (b) Cr/V vs. Y/Ni diagram showing modeled mixing between granite and ultramafic end-members (McLennan et al., 1993; Mongelli et al., 2006); c) K_2O vs. Rb plot (Floyd and Leveridge, 1987).

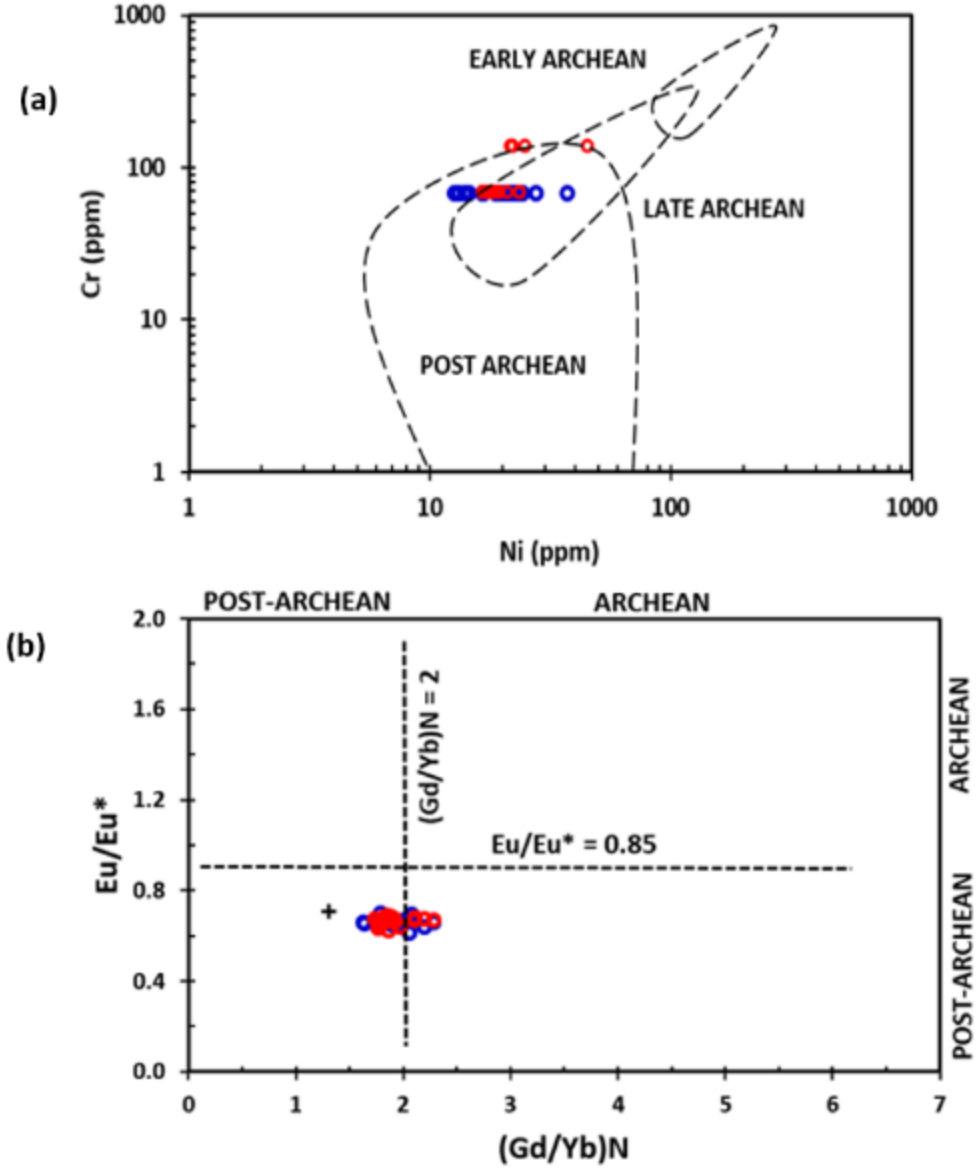

Figure 2.10: (a) Ni-Cr (McLennan et al., 1993); and (b) Eu/Eu* vs. $(Gd/Yb)_N$ (fields after McLennan and Taylor, 1991) diagrams for the Agbada sediments

Table 2.2: Elemental ratios for the studied sandstones and shales compared to ratios in felsic and mafic rocks

Ratios	Sandstones [1]	Shales [1]	Felsic Sources [2]	Mafic Sources [2]	UCC [3]	PAAS [4]
(La/Lu)n	9.57-14.00	10.13-13.90	3.00 – 27.00	1.10 – 7.00	10.39	9.86
Eu/Eu*	0.61- 0.70	0.62-0.69	0.40 – 0.94	0.71 – 0.95	0.66	0.71
Th/Co	0.61-1.04	0.77-1.22	0.67 – 19.40	0.04 – 1.40	0.61	0.63
Cr/Th	4.36 - 9.02	4.13 - 9.85	4.00 – 15.00	25.00 – 500.00	8.76	7.53
La/Co	2.14-3.51	2.59-4.23	1.80 – 13.80	0.14 – 0.38	1.79	1.66

[1]This study.

[2]Cullers et al. (1988), Cullers (1994, 2000), Cullers and Podkovyrov (2000)

[3] Rudnick and Gao (2003).

[4] Taylor and McLennan (1985)

2.5.2 Paleo-weathering and paleoclimate

Although there are several challenges in the use of weathering indices and geochemical parameters as weathering and climatic proxies (Borges et al., 2008; von Eynatten et al., 2012; Garzanti et al., 2010; Garzanti and Resentini, 2016; Dinis et al., 2020), siliciclastic sediments are still considered valuable for the study of past environmental conditions and paleoclimate (e.g., Dinis et al., 2017; Guo et al., 2018). Weak weathering intensity is usually associated with arid and cool conditions, whereas warm temperatures and high precipitation lead to intense silicate weathering (Nesbitt and Young, 1982).

2.5.2.1. Chemical indices

The alteration of rocks during weathering leads to the leaching of mobile alkali and alkaline earth elements with consequent enrichment of non-mobile elements such as aluminium. Several chemical indices have been utilised to quantify the degree of weathering, including the

Chemical Index of Alteration (CIA; Nesbitt and Young, 1982), the Chemical Index of Weathering (CIW; Harnois, 1988), and the Plagioclase Index of Alteration (PIA; Fedo et al., 1995). In this study, weathering indices were considered together with trace-element signatures. Moreover, we evaluated weathering intensity for each mobile element *E* separately by comparing its concentration to non-mobile aluminium in the investigated samples and the Upper Continental Crust standard (UCC; Rudnick and Gao, 2003). These alpha indices, defined as $\alpha^{Al}E=(Al/E)_{sample}/(Al/E)_{UCC}$ by Garzanti et al. (2013a), differ from the alpha values originally defined by Gaillardet et al. (1999) because Al, instead of Ti, Sm, Nd, and Th, is used as a reference for all elements. This is required to minimize hydraulic-sorting bias because Ti, Sm, Nd, and Th are preferentially hosted in the densest minerals (e.g., ilmenite, monazite), the concentration of which may vary by a few orders of magnitude owing to selective-entrainment effects. The value $\alpha^{Al}E = 1$ indicates no net depletion of the considered element *E* relative to the UCC standard, whereas values > 1 and < 1 suggest depletion and enrichment, respectively. The CIA values were calculated using the molecular proportions: $CIA = [Al_2O_3 / (Al_2O_3 + CaO^* + Na_2O + K_2O)] \times 100$, where CaO* is the amount of CaO hosted in the silicate fraction of the rock. Correction for CaO was carried out using the method of McLennan et al. (1993), whereby CaO values are accepted only if $CaO < Na_2O$; wherever $CaO > Na_2O$, then $CaO = Na_2O$ is assumed. In addition, the CIX index of Garzanti et al. (2014b), a modification of the CIA that does not include Ca ($CIX = [Al_2O_3 / (Al_2O_3 + Na_2O + K_2O)] \times 100$), was considered to check for anomalies associated with carbonate content. Phanerozoic shales with CIA values from 70 to 75 suggest moderate weathering, whereas CIA values close to 100 would testify to extreme weathering conditions, resulting in residual minerals such as kaolinite and gibbsite (Bauluz et al., 2000).

The CIA and CIX for the studied sandstone (CIA = 81- 88; 83 ± 2; CIX = 85 – 90; 87 ± 2, Table 2.1) and shale samples (CIA = 83 - 87; 84 ± 1; CIX= 87-90; 87 ± 1, Table 2.1)

suggest moderate to intense weathering. Shales would be expected to display evidence of notably more intense weathering than associated sandstones (McLennan et al., 1990), which, however, is not observed in the Niger Delta. Chondrite-normalized REE plots (Fig. 2.5) for the sandstone and shale samples are also similar, possibly reflecting source-rock inheritance.

The Al_2O_3-(CaO*+ Na_2O)-K_2O (A–CN–K) diagram and the CIA/SiO_2 relationship of Nesbitt and Young (1982) were also applied to appraise the mobility of elements during the progress of chemical weathering. The investigated sandstones and shales (Fig. 2.11a) plot fairly close to the Al_2O_3 pole, suggesting moderate to intense weathering, as confirmed by samples plotting between illite and kaolinite in the CIA-SiO_2 diagram (Fig. 2.11b).

The $\alpha^{Al}E$ values are expected to increase with increasing intensity of weathering in a proportion related to the different mobility of diverse alkali and alkaline-earth metals. The $\alpha^{Al}E$ values are typically found to be higher for Na and Ca, intermediate for Sr and Mg, and lower for K, Rb, and Ba, corresponding to the degree to which these elements are partitioned in unstable plagioclase and heavy minerals versus more stable phyllosilicates and K-feldspar (Garzanti et al., 2013b). Apart from $\alpha^{Al}Ba$, which is enriched, all mobile elements are depleted relative to the UCC in the investigated Agbada sands and shales. The observed order of bulk-sediment mobility is Ca > Na > Sr > K > Mg > Rb. The values obtained for highly mobile Ca and Na are consistent with moderate to intense weathering for the Agbada sediments as suggested by other weathering indices. Sandstones and shales display the same order of bulk-sediment mobility inferred from their $\alpha^{Al}E$ indices, which may reflect source rock inheritance.

The $\alpha^{Al}E$ values observed in this investigation are notably lower than those reported for regions affected by intense weathering, such as subequatorial southern Africa (Garzanti et al., 2014a; Dinis et al., 2017). Also, the order of element mobility is slightly different from those observed in river sediments of central and southern Africa (Garzanti et al., 2013b, 2014b), where Na resulted to be the most mobile element. Moreover, in Agbada sediments, K was more depleted

than Mg (Table 2.1, Appendix 2.1). These differences may be accounted for by diverse factors, including different parent rocks, winnowing of mica in shallow-marine environments, degree of recycling, or inheritance. For instance, in the dry Kalahari Desert, notably high weathering indices and kaolinite content are chiefly inherited from previous sedimentary cycles.

2.5.2.2. Element ratios

Weathering and recycling processes may result in the loss of U, leading to an increase in the Th/U ratio. Thorium and uranium in sedimentary rocks are linked to diverse phases (e.g., clay minerals, feldspars, organic matter, phosphates and heavy minerals; Rufell and Worden, 2000). Weak acids (e.g., humic acid) may dissolve thorium, but uranium is much more soluble because it dissolves even in a neutral aqueous solution (Ullah et al., 2015). Therefore, sediment recycling in an oxidizing environment may lead to the fractionation of U and Th through successive stages of chemical leaching during weathering and/or diagenesis. This fractionation depends on the fact that U^{4+} is easily oxidized to U^{6+}, forming the uranyl ion, which is highly soluble and can be removed from the system, whereas thorium remains relatively insoluble and retains its oxidation state (McLennan and Taylor, 1980). Thus, the Th/U ratio can be used to investigate weathering and/or recycling processes. The Th/U ratio in most upper crustal rocks is between 3.5 and 4.0 (McLennan et al., 1993). Th/U values higher than 4.0 in siliciclastic rocks may indicate intense weathering either in source areas or inheritance from previous cycles through recycling. The Th/U ratio (Fig. 2.11c) in the Agbada sediments is consistent with moderate to intense weathering conditions in source areas and/or considerable recycling.

The relationship between Ga/Rb and K_2O/Al_2O_3 has also been used in paleoclimatic studies (e.g., Roy and Roser, 2013; He et al., 2017). Ga and Al are linked to fine-grained phyllosilicates and enriched in kaolinite, the clay mineral formed by extreme leaching in warm and humid equatorial climates (Beckmann et al., 2005). In contrast, Rb and K are preferentially hosted in illite, a detrital mineral typically produced by physical erosion in dry and cold climates

(Ratcliffe et al., 2010). Low Ga/Rb and high K_2O/Al_2O_3 ratios are thus expected for illite-rich sediments, and high Ga/Rb and low K_2O/Al_2O_3 ratios for kaolinite-rich sediments. Based on this reasoning, the Ga/Rb-K_2O/Al_2O_3 relationship observed in the studied samples from the Agbada Formation (Fig. 2.11d) suggests a warm/humid paleoclimate, consistently with the semiquantitative insight provided by CIA and CIX values (Table 2.1). Humid tropical paleoclimate prevailing during the deposition of the Agbada Formation has been recognized by earlier stratigraphic studies, which used a palynostratigraphic approach to characterize alternating dryer and wetter phases at that time (Bankole et al., 2014).

2.5.3 Depositional Signatures

Some trace elements have contrasting geochemical behaviour in oxic and anoxic environments because of a prominent change in the solubility of their oxyanions (Morford et al., 2005). These trace elements tend to be more soluble in oxidizing conditions, whereas, in reducing conditions, they are less soluble, leading to authigenic enrichment in oxygen-depleted sedimentary facies. Therefore, they may be used to reconstruct paleo-redox conditions and infer the degree of water oxygenation in the depositional environment (e.g., Algeo and Maynard, 2004, 2009; Rimmer, 2004; Rimmer et al., 2004; Gallego-Torres et al., 2007; Tribovillard et al., 2006; 2012; Madhavaraju et al., 2016; Bennett et al., 2020).

It is usually imperative to assess whether trace elements are relatively depleted or enriched when using them to reconstruct paleoenvironmental conditions. The amount of depletion or enrichment is relatively evaluated using a reference such as average crustal rocks or average shale (e.g., Wedepohl, 1971; McLennan, 2001). Sediments can contain variable proportions of diluents such as carbonate or biogenic silica that may influence trace-element abundance in a sample. To minimize these effects, trace element concentrations are commonly normalized to Al content, although certain caveats exist (van der Weijden et al., 2002; Tribovillard et al., 2006). In this study, using average shale as a reference (Wedepohl, 1971),

trace element concentrations were normalized to Al content and enrichment factors calculated for Mo, U, V, Cr, Co, Ni, Cu, and Zn using the relationship; $EF_{element\ X} = (X/Al)_{sample} / (X/Al)_{average\ shale}$, where Al and X are the weight concentrations of Al and the element *X* respectively. Element X is enriched if $EF_X > 1$ and relatively depleted if $EF_X < 1$. EF_X values >10 indicate significant enrichment, whereas those between 1-10 suggest slight enrichment. Several authors have used this approach to evaluate trace-element enrichment in modern and ancient sediments (e.g., Algeo and Tribovillard, 2009; Tribovillard et al., 2012; Bennett et al., 2020; Steinmann et al., 2020). The Enrichment factors (EF) (Appendices 2.1, 2.3) calculated for selected trace elements reveal minor enrichment for U and Mo. However, other trace elements are depleted relative to average shale, suggesting that the environment may not have been oxygen-depleted. Moreso, the EFs for the enriched elements are generally lower than those reported for sediments deposited in reducing environments (e.g., Algeo and Maynard, 2004; Rimmer, 2004).

2.5.3.1 Mo-EF/U-EF covariation

Although there are similarities between U and Mo, including their low contents in the upper continental crust, conservative behaviour in oxic conditions, long residence times in seawater, and nearly uniform contents in global seawater, the enrichment of U commences under suboxic conditions (Fe^{3+} is transforming to Fe^{2+}), but the enrichment of Mo needs euxinic conditions (the presence of H_2S) and the redox cycle of Mo can be influenced by the particulate shuttle process (Algeo and Tribovillard, 2009). This difference in their behaviour makes trends in Mo-U covariation useful for constraining redox conditions during sediment deposition (e.g., Tribovillard et al., 2012; Wang et al., 2017; Ferreira et al., 2020; Wu et al., 2021). The Mo-EF for the Agbada shales (Appendix 2.1, 2.3) under investigation are lower than U-EF, suggesting deposition in water with scarce H_2S. Moreso, the observed Mo-EF/U-EF ratios are less than seawater values (Fig. 2.12), indicating deposition in an oxic-suboxic environment. It is

noteworthy that the Mo–EF vs. U–EF plot does not require information about organic matter and uses only concentrations in Al, U, and Mo to achieve the same interpretations consistent with a multi-parameter dataset (Tribovillard et al., 2012).

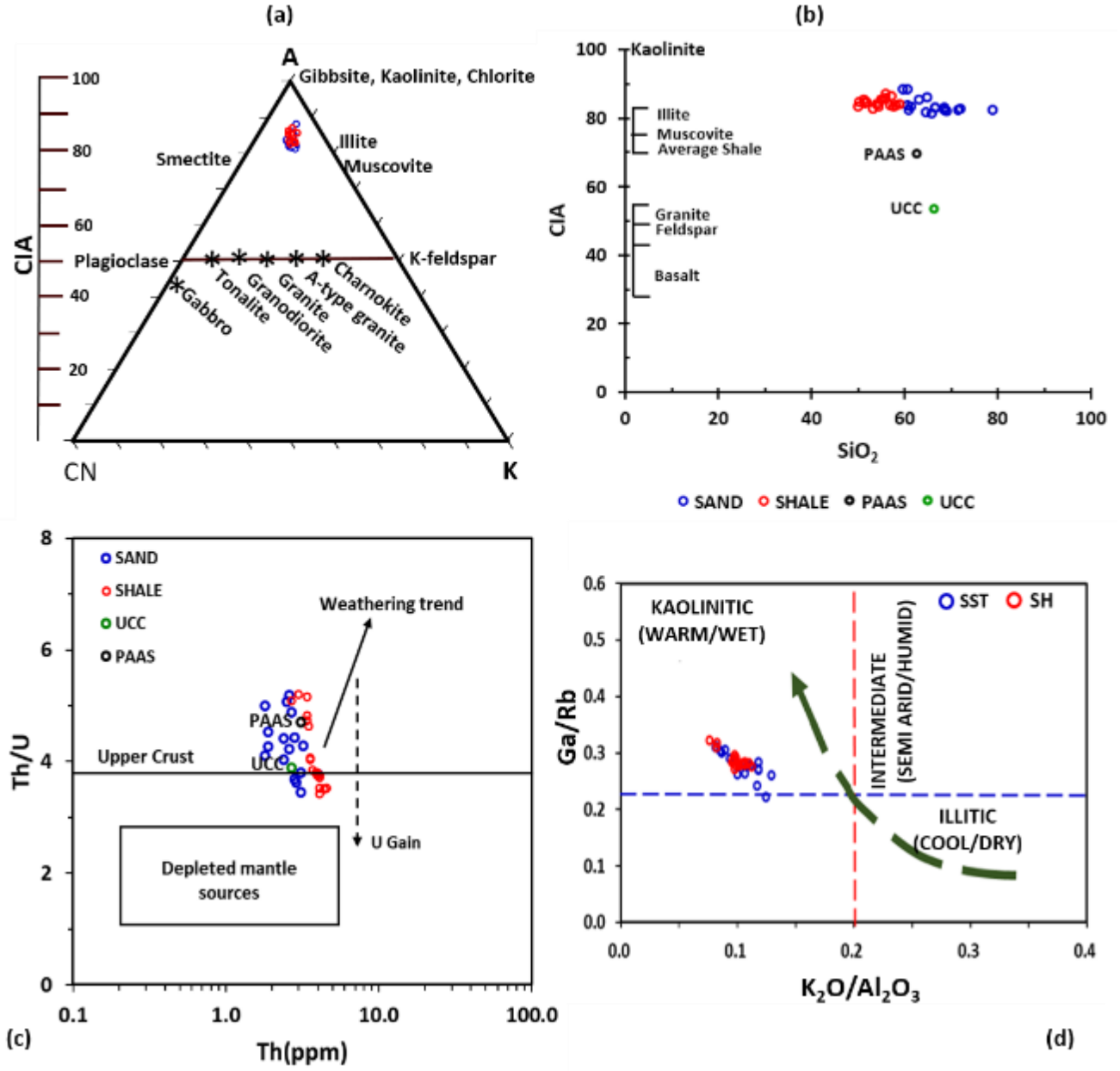

Figure 2.11: (a) Al_2O_3-(CaO*+ Na_2O)-K_2O plot for the studied sediments (Nesbitt and Young, 1982; Fedo et al., 1995), (b) CIA vs. SiO_2 diagram (Nesbitt and Young 1982), (c) Th/U–Th diagram (McLennan et al., 1993), and (d) Ga/Rb vs. (K_2O/Al_2O_3) relationship (Roy and Roser, 2013).

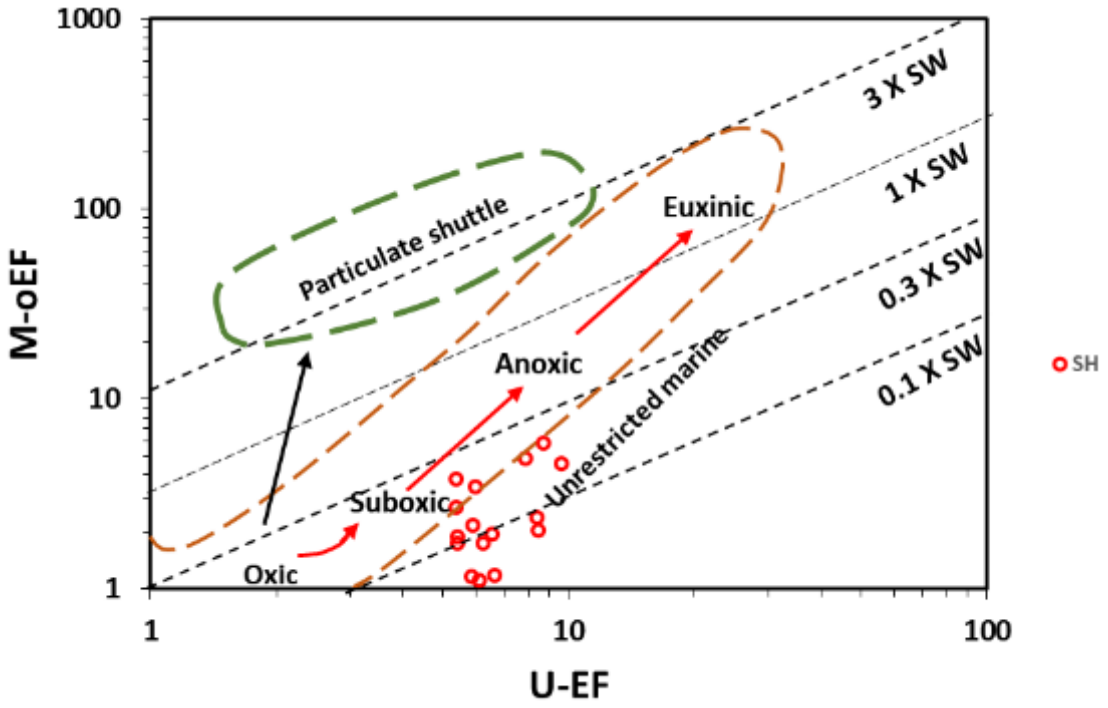

Figure 2.12: Cross plot of Mo-EF vs. U-Ef for the Agbada shales. The diagonal lines depict the Mo/U ratio compared to seawater (SW) and fractions thereof (after Algeo and Tribovillard, 2009)

2.5.3.2 Mo Abundance

Scott and Lyons (2012) suggested that the bulk Mo contents in sediments can be explored to constrain euxinic and non-euxinic depositional conditions after considering the distinct bimodal distribution of Mo enrichment in well-characterized modern sediments. The Mo concentrations in euxinic sediments are usually > 60 ppm, reaching hundreds of ppm in sediments deposited in permanently euxinic environments (e.g., Framvaren Fjord, Cariaco Basin; Algeo and Lyons, 2006). In contrast, sediments deposited in an oxic-suboxic environment, where dissolved sulphide was present but confined to pore-waters (non-euxinic sediments), exhibit Mo values <25 ppm (e.g., Gulf of California, Santa Barbara Basin) but above the range (1–2 ppm) for average crustal abundance (Scott and Lyons, 2012). The difference in Mo contents between

these two settings is usually more complicated and may suggest (i) an unstable or intermittent bottom-water euxinia (e.g., Saanich Inlet, Namibian Shelf) or (ii) a stable euxinic but Mo-depleted bottom-waters (owing to the "basin reservoir effect," as in the Black Sea; Algeo and Lyons, 2006). The low concentration of Mo (Table 2.1, Appendix 2.1) in the investigated shales suggests that hydrogen sulphide was scarcely present in the depositional environment but restricted to sediment pore-waters, overlain by oxic to suboxic bottom-waters.

2.5.3.3 Trace element ratios

Trace element ratios have been widely applied to complement other paleo-redox approaches. The Cu/Zn ratio in sediments may reflect paleo-redox environments, being typically high in reducing conditions and low in oxidizing conditions (Hallberg, 1976). Hatch and Leventhal (1992) used the V/(V+Ni) ratio to constrain paleo-redox conditions and established partly overlapping threshold values of >0.84, 0.54–0.82, and 0.46–0.60 for euxinic, anoxic, and dysoxic depositional conditions, respectively. Jones and Manning (1994) suggested V/Cr ratios of > 4.25, 2-4.25, and < 2, indicative of suboxic to anoxic, dysoxic, and oxic conditions, respectively. Moreover, they suggested Ni/Co ratios of < 5, 5-7, and > 7 indicative of oxic, dysoxic, and anoxic conditions, respectively. Rimmer (2004) suggested that the threshold values for the trace element ratios should be applied with caution, although their relative differences can collectively be applied to evaluate redox conditions. In the investigated Agbada Shales, apart from the V/(V+Ni) ratio that would point to lower paleo-oxygenation, other trace element ratios (e.g., Ni/Co, V/Cr, Cu/Zn, Appendix 2.1) suggest an oxic paleo-depositional environment.

In summary, the geochemical proxies suggest that the studied sediments were mainly deposited in an environment that was not oxygen-depleted (oxic-suboxic), but with possibly localized and short-term anoxia leading to the formation of sulphides and resulting in slightly enriched values for U and Mo. Previous organic geochemical studies (e.g., Akinlua and. Ajayi,

2009; Ekpo et al., 2018) have reported oxic zones in parts of the Agbada Formation, a result confirmed by our inorganic geochemical approach.

2.6 Conclusions

The geochemical signatures of sand/sandstone and interbedded shale in the Agbada Formation (Niger Delta Basin) were used to evaluate their provenance, paleo-weathering, and paleo-depositional conditions. The main conclusions are:

(1) the studied sediments are classified as Fe-rich sand/sandstones and Fe-rich shales based on their geochemical composition;

(2) elemental ratios, LREE-enrichment, flat HREE pattern, and negative Eu anomaly suggest that sources of detritus consisted predominantly of felsic rocks with considerable recycling of post-Archean siliciclastic rocks derived mainly in turn from granitoid basement rocks, older sedimentary basins, and quartzose siliciclastic sediments in the Niger River catchment;

(3) moderate to intense paleo-weathering in a warm/humid climate is inferred from chemical indices and elemental ratios, with element mobility order, Ca > Na > Sr > K > Mg > Rb observed for both sandstone and shale;

(4) geochemical redox proxies suggest deposition in a predominantly oxic-suboxic environment.

This study contributes from an inorganic geochemical perspective to the extensive research previously carried out on the Niger Delta Basin, which has been the object of thorough geological investigation for hydrocarbon exploration in the last half-century. Our results do not and cannot pretend to revolutionize previous views concerning the Niger Delta Basin but do fill a gap as far as geochemical information is concerned and are intended to represent an honest, valuable contribution to the knowledge of this geologically and economically important sedimentary system.

References

Abd El-Rahman, Y., Polat, Y.A., Fryer, B.J., Dilek, Y., El-Sharkawy, M and Sakran, S., 2010. The provenance and tectonic setting of the Neoproterozoic Um Hassa Greywacke Member, Wadi Hammamat area, Egypt: Evidence from Petrography and Geochemistry. Journal of African Earth Science, 58, 185-196.

Ahmad A. H. M., Noufal K. N., Masroor A. M., Tavheed, K., 2014. Petrography and geochemistry of Jumara Dome sediments, Kachchh Basin: Implications for provenance, tectonic setting, and weathering intensity. Chinese Journal of Geochemistry, 33, 9 – 23.

Akarish A.I.M., El-Gohary A.M., 2011. Petrography and geochemistry of lower Paleozoic sandstones, east Sinai, Egypt: Implications for provenance and tectonic setting, Journal of Applied Earth Science, 11(7): 3070-3088.

Akinlua, A., Ajayi, T.R., 2009. Geochemical characterization of central Niger Delta oils. Journal of petroleum geology, 32(4), 373-382.

Akkoca, D.B, Eriş, K.K., Çağatay, M.N., Biltekin, D., 2019. The mineralogical and geochemical composition of Holocene sediments from Lake Hazar, Elazığ, Eastern Turkey: implications for weathering, paleoclimate, redox conditions, provenance, and tectonic setting. Turkish Journal of Earth Sciences, 28, 760-785.

Algeo, T.J., and Maynard, J.B., 2004. Trace-element behaviour and redox facies in core shales of Upper Pennsylvanian Kansas-type cyclothems. Chemical Geology, 206, 289-318.

Algeo, T.J., Lyons, T.W., 2006. Mo-total organic carbon covariation in modern anoxic marine environments: implications for analysis of paleoredox and paleohydrographic conditions. Paleoceanography 21, 1–23. https://doi.org/10.1029/2004PA001112.

Algeo, T.J., Tribovillard, N., 2009. Environmental analysis of paleoceanographic systems based on molybdenum–uranium covariation. Chemical Geology 268, 211–225.

Allen, J.R.L., 1965. Late Quaternary Niger Delta, and adjacent areas-sedimentary environments and lithofacies: AAPG Bulletin, 49, 547-600.

Amorosi, A., 2012. Chromium and nickel as indicators of source-to-sink sediment transfer in a Holocene alluvial and coastal system (Po Plain, Italy). Sedimentary Geology, 280, 260–269.

Armstrong-Altrin, J.S., Lee, Y.I., Verma, S.P., Ramasamy, S., 2004. Geochemistry of Sandstones from the Upper Miocene Kudankulam Formation, Southern India: Implications for Provenance, Weathering, and Tectonic Setting. Journal of Sedimentary Research, 74, 285-297.

Armstrong-Altrin, J.S., Nagarajan, R., LEE, Y.I., Kasper-Zubillaga, J.J., Córdoba-Saldaña, L.P., 2014. Geochemistry of sands along the San Nicolás and San Carlos beaches, Gulf of California, Mexico: implications for provenance and tectonic setting. Turkish Journal of Earth Sciences, 23, 533-558.

Asiedu, D.K., Agoe, M., Amponsah, P.O., Nude, P.M., Anani. C.Y., 2019. Geochemical constraints on provenance and source area weathering of metasedimentary rocks from the Paleoproterozoic (~2.1 Ga) Wa-Lawra Belt, southeastern margin of the West African Craton. Geodinamica Acta, 31(1), 27-39.

Avbovbo, A. A., 1978, Tertiary lithostratigraphy of Niger Delta. American Association of Petroleum Geologists Bulletin, 62(2) 295–300.

Bahlburg, H., 1998. The geochemistry and provenance of Ordovician turbidites in the Argentine Puna. In: Pankhurst, R. J., Rapela, C. W. (eds), The Proto-Andean Margin of Gondwana. Geological Society, London, Special Publications, 142, 127-142.

Baiyegunhi, C., Liu, k., Gwavava, O., 2017. Geochemistry of sandstones and shales from the Ecca Group, Karoo Supergroup, in the Eastern Cape Province of South Africa:

Implications for provenance, weathering and tectonic setting. Open Geosciences, 9, 340–360.

Bankole, S.I., Schrank, E., Osterloff, P.L., 2014. Palynostratigraphy, palaeoclimates and palaeodepositional environments of the Miocene aged Agbada Formation in the Niger Delta, Nigeria. Journal of African Earth Sciences, 95, 41–62.

Barbera, G., Mazzoleni, P., Critelli, S., Pappalardo, A., Lo Giudice, A., Cirrincione, R., 2006. Provenance of shales and sedimentary history of the Monte Soro Unit, Sicily. Periodico di Mineralogia, 75(2-3), 313-330.

Basu, A., Bickford, M.E., Deasy, R., 2016. Inferring tectonic provenance of siliciclastic rocks from their chemical compositions: a dissent. Sedimentary Geology 336, 26-35.

Bauluz, B., Mayayo, M.J., Fernandez-Nieto, C., Lopez J.M.G., 2000. Geochemistry of Precambrian and Paleozoic siliciclastic rocks from the Iberian Range (NE Spain): implications for source-area weathering, sorting, provenance, and tectonic setting. Chemical Geology, 168, 135–150.

Beckmann, B., Flögel, S., Hofmann, P., Schulz M, Wagner. T., 2005. Orbital forcing of Cretaceous river discharge in tropical Africa and ocean response. Nature 437(7056):241–244. https://doi.org/10.1038/nature03976.

Beka, F. T., Oti, M. N., 1995. The distal offshore Niger Delta: frontier prospects of a mature petroleum province, in, Oti, M.N., and Postma, G., (Eds.), Geology of Deltas: Rotterdam, A.A. Balkema, 237-241

Bennett, W.W., Canfield, D.E., 2020. Redox-sensitive trace metals as paleoredox proxies: A review and analysis of data from modern sediments. Earth-Science Reviews, 204, 103175.

Bilotti, F. D., and J. H. Shaw., 2001, Modeling the compressive toe of the Niger delta as a critical taper wedge (abs.): AAPG Annual Meeting Program,10, A18–A19.

Bilotti, F., Shaw, J.H., 2005. Deep-water Niger Delta fold and thrust belt modelled as a critical-taper wedge. The influence of elevated basal fluid pressure on structural styles. American Association of Petroleum Geologists Bulletin 89, 1475–1491.

Blatt, H., Middleton, G., and Murray, R., 1972. Origin of sedimentary rocks: Englewood Cliffs, New Jersey, Prentice-Hall, 634 p.

Borges, J.B., Huh, Y., Moon, S., Noh, H., 2008. Provenance and weathering control on river bed sediments of the eastern Tibetan Plateau and the Russian Far East. Chemical Geology, 254, 52–72.

Boynton, W.V., 1984. Geochemistry of the rare earth elements: meteorite studies. In: Henderson, P. (Ed.), Rare Earth Element Geochemistry. Elsevier, pp. 63–114.

Bracciali, L., Marroni, M., Pandolfi, L., Rocchi, S., 2007. Geochemistry and petrography of Western Tethys Cretaceous sedimentary covers (Corsica and Northern Apennines): From source areas to configuration of margins. Geological Society of America Special Paper, 420, 73-93.

Burke, K., 1972, Longshore drift, submarine canyons and submarine fans in development of Niger delta, AAPG Bulletin, 56, 1975-1983.

Bustin, R. M., 1988. Sedimentology and characteristics of dispersed organic matter in Tertiary Niger delta: Origin of source rocks in a deltaic environment. AAPG Bulletin,72, 277-298.

Chen, B., Liu, G., Wu, D., and Sun, R., 2016. Comparative study on geochemical characterization of the Carboniferous aluminous argillites from the Huainan Coal Basin, China. Turkish Journal of Earth Sciences, 25, 274-287.

Corredor, F., Shaw, J.H., Bilotti, F., 2005. Structural styles in the deep-water fold and thrust belts of the Niger Delta. American Association of Petroleum Geologists Bulletin, 89 (6), 753–780.

Cox, R., Lowe, D.R., Cullers, R.L., 1995. The influence of sediment recycling and basement composition on evolution of mudrock chemistry in the south-western United States. Geochimica et Cosmochimica Acta, 59, 2919-2940.

Crook K.A.W., 1974. Lithogenesis and geotectonics: The significance of compositional variation in flysch arenites (greywackes). Journal of Society of Economic Paleontology and Mineralogist, 19, 304–310.

Cullers, R. L., 1994b. The controls on the major and trace-element variation of shales, siltstones, and sandstones of Pennsylvanian-Permian age from uplifted continental blocks in Colorado to platform sediments in Kansas, USA. Geochimica et Cosmochimica Acta, 58, 4955–4972.

Cullers, R.L., 1995. The controls on the major and trace element evolution of shales, siltstones and sandstones of Ordovician to Tertiary age in the Wet Mountain region, Colorado, USA, Chemical Geology, 123, 107-131.

Cullers, R.L., 2000. The geochemistry of shales, siltstones and sandstones of Pennsylvanian-Permian age, Colorado, USA: Implications for provenance and metamorphic studies. Lithos, 51, 181–203.

Cullers, R.L., Barret, T., Carlson, R., Robinson, B., 1987. Rare earth element and mineralogical changes in Holocene soil and stream sediment: a case study in the Wet Mountains, Colorado, USA. Chemical Geology, 63, 275–295.

Cullers, R.L., Basu, A., Suttner, L., 1988. Geochemical signature of provenance in sand-size material in soils and stream sediments near the Tobacco Root batholith, Montana, USA. Chemical Geology, 70(4), 335- 348.

Cullers, R.L., Berendsen, P., 1998. The provenance and chemical variation of sandstones associated with the Midcontinent Rift System, U.S.A. European journal of mineralogy, 10(5), 987-1002.

Cullers, R.L., Graf, J., 1984. Rare earth element in igneous rocks of the continental crust: intermediate and silicic rocks, ore petrogenesis, in Henderson, P. (Eds.), Rare earth geochemistry, Elsevier, 275-316.

Cullers, R.L., Podkovyrov, V.N., 2000. Geochemistry of the Mesoproterozoic Lakhanda shales in south-eastern Yakutia, Russia: implications for mineralogical and provenance control, and recycling Precambrian Research, 104, 77–93.

Cullers, R.L., Podkovyrov, V.N., 2002. The source and origin of terrigenous sedimentary rocks in the Mesoproterozoic Ui group, south-eastern Russia. Precambrian Research, 117, 157-183.

Damuth, J. E., 1994. Neogene gravity tectonics and depositional processes on the deep Niger Delta continental margin: Marine and Petroleum Geology, 11(3), 320– 346.

Dickinson W.R, Suczek C., 1979. Plate tectonics and sandstone composition. American Association of Petroleum Geologists Bulletin, 63, 2164–2182.

Dickinson, W. R., 1985. Interpreting provenance relations from detrital modes of sandstones. In: Provenance of Arenites, Zuffa GG (ed.). Reide, Dordrecht, Boston, USA: 333–336.

Dickinson, W.R., Beard, L.S., Brakenridge. G.R., Erjavec, J.L., Ferguson, R.C., Inman, K.F., Knepp, R.A., Lindberg, F.A., Ryberg, P.T., 1983. Provenance of North American Phanerozoic sandstones in relation to tectonic setting. Geological Society of America Bulletin, 94, 222–235.

Dim, C.I.P., Onuoha, K.M., Ozumba, B.M., 2020. Hydrocarbon leads and prospects opportunities across a cluster of fields in parts of Onshore Niger Delta Basin. Journal of African Earth Sciences, 164, 103804.

Dinis, P., Garzanti, E., Vermeesch, P., Huvi, J., 2017. Climatic zonation and weathering control on sediment composition (Angola). Chemical Geology, 467, 110–121.

Dinis, P.A., , Garzanti, E., Hahn, A., Vermeesch, P., Cabral-Pinto, M., 2020. Weathering indices as climate proxies. A step forward based on Congo and SW African river muds. Earth-Science Reviews, 201, 103039.

Dinis, P.A., Dinis, J.L., Mendes, M.M., Rey. J., Pais. J., 2016. Geochemistry and mineralogy of the Lower Cretaceous of the Lusitanian Basin (western Portugal): Deciphering paleoclimates from weathering indices and integrated vegetational data. Comptes Rendus Geoscience, 348, 139–149.

Do Campo, D., Guevara, S.R., 2005. Provenance analysis and tectonic setting of late Neoproterozoic metasedimentary successions in NW Argentina. Journal of South American Earth Sciences, 19, 143–153.

Doust, H., and Omatsola, E., 1990. Niger Delta, in J. D. Edwards and P. A. Santogrossi, eds., Divergent/passive margin basins: AAPG Memoir 48, 201–238.

Ebong, E.D., Akpan, A.E., Urang, J.G., 2019. 3D structural modelling and fluid identification in parts of Niger Delta Basin, southern Nigeria. Journal of African Earth Sciences, 158, 103565.

Edegbai, A.J., Schwark, L., Oboh-Ikuenobe, F.E., 2019. Campano-Maastrichtian paleoenvironment, paleotectonics and sediment provenance of western Anambra Basin, Nigeria: Multi-proxy evidences from the Mamu Formation. Journal of African Earth Sciences, 156, 203-239.

Ekpo B.O., Essien, N., Neji, P.A., Etsenake., R.O., 2018. Geochemical fingerprinting of western offshore Niger Delta oils. Journal of Petroleum Science and Engineering, 160, 452–464.

Ekweozor, C. M., Daukoru, E.M, 1994. Northern delta depobelt portion of the Akata-Agbada(!) petroleum system, Niger Delta, Nigeria, in: Magoon, L.B., and Dow, W.G., eds., The

Petroleum System—From Source to Trap, AAPG Memoir 60: Tulsa, American Association of Petroleum Geologists, 599-614.

Ekweozor, C.M., Daukoru, E.M., 1984. Petroleum source bed evaluation of Tertiary Niger Delta, AAPG Bulletin, 68, 390–394.

Ekweozor, C.M., Okogun, J.I., Ekong, D.E.U., Maxwell, J.R., 1979. Preliminary organic geochemical studies of samples from the Niger Delta, Nigeria: part 1, analysis of crude oils for triterpanes. Chemical Geology, 27, 11-28.

Ekweozor, C.M., Okoye, N.V., 1980. Petroleum source-bed evaluation of Tertiary Niger Delta. AAPG Bulletin, 64, 1251-1259.

Evamy, B.D., Haremboure, J., Kamerling, P., Molloy, F.A., Rowlands, P.H., 1978. Hydrocarbon habitat of Tertiary Niger Delta: American AAPG Bulletin, 62,1-39.

Fedo, C.M., Nesbitt, H.W., Young, G.M., 1995. Unravelling the effects of potassium metasomatism in sedimentary rocks and paleosols, with implications for paleo-weathering conditions and provenance. Geology, 23, 921–924.

Ferreira, E., Mateus, A., Azerêdo, A.N., Duarte, L.V., Mendonça-Filho, J., Tassinari, C.C.G., 2020. Tracing bottom-water redox conditions during deposition of Lower and Upper Jurassic organic-rich sedimentary rocks in the Lusitanian Basin (Portugal): Insights from inorganic geochemistry, Marine and Petroleum Geology, 117.104343.

Floyd, P.A., Leveridge, B.E. 1987. Tectonic environment of the Devonian Gramscatho basin, south Cornwall: framework mode and geochemical evidence from turbiditic sandstones. Journal of the Geological Society London, 144, 531-542.

Floyd, P.A., Winchester, J.A., Park, R.G., 1989. Geochemistry and tectonic setting of Lewisian clastic metasediments from the early Proterozoic Loch Maree Group of Gairloch, NW Scotland. Precambrian Research, 45, 203–214.

Frankl, E.J., Cordry, E.A., 1967. The Niger Delta oil province – recent developments onshore and offshore. In: Proceeding of the 7th World Petroleum Congress, Mexico City, V. 1b, 195–209.

Gaillardet, J., Dupré, B., Allègre, C.J., 1999. Geochemistry of large river suspended sediments: Silicate weathering or recycling tracer? Geochim. Cosmochim. Acta, 63, 4037–4051.

Gallala, W., Gaied, M.E., Montacer, M., 2009. Detrital mode, mineralogy, and geochemistry of the Sidi Aïch Formation (Early Cretaceous) in central and southwestern Tunisia: Implications for provenance, tectonic setting and paleoenvironment. Journal of African Earth Sciences, 53, 159–170.

Gallego-Torres, D., Martínez-Ruiz, F., Paytan, A., Jiménez-Espejo, F.J., Ortega-Huertas, M., 2007. Pliocene–Holocene evolution of depositional conditions in the eastern Mediterranean: Role of anoxia vs. productivity at time of sapropel deposition. Palaeogeography, Palaeoclimatology, Palaeoecology, 246, 424–439.

Garva, J.I., Royce. P.R., Smick, T.A., 1996. Chromium and Nickel in Shale of the Taconic Foreland: A case study for the provenance of fine-grained sediments with ultramafic source. Journal of Sedimentary Research, 66(1), 100-106.

Garzanti, E., 2016. From static to dynamic provenance analysis—Sedimentary petrology upgraded. Sedimentary Geology, 336, 3-13.

Garzanti, E., 2017. The maturity myth in sedimentology and provenance analysis. Journal of Sedimentary Research, 87, 353-365.

Garzanti, E., 2019. Petrographic classification of sand and sandstone. Earth-Science Reviews, 192, 545-563.

Garzanti, E., Resentini, A., 2016. Provenance control on chemical indices of weathering (Taiwan river sands). Sedimentary Geology, 336, 81-95.

Garzanti, E., Doglioni, C., Vezzoli, G., Andò S., 2007. Orogenic Belts and Orogenic Sediment Provenances. The Journal of Geology, 15, 315-334.

Garzanti, E., Andò, S., France-Lanord, C., Vezzoli, G., Najman, Y., 2010. Mineralogical and chemical variability of fluvial sediments. 1. Bedload sand (Ganga-Brahmaputra, Bangladesh). Earth Planet. Sci. Lett. 299, 368-381

Garzanti, E., Andò, S., France-Lanord, C., Galy, V., Censi, P., Vignola, P., 2011. Mineralogical and chemical variability of fluvial sediments. 2. Suspended-load silt (Ganga-Brahmaputra, Bangladesh). Earth Planet. Sci. Lett., 302, 107–120.

Garzanti, E., Padoan, M., Setti, M., Peruta, L., Najman, Y., Villa, I.M., 2013a. Weathering geochemistry and Sr-Nd fingerprints of equatorial upper Nile and Congo muds. Geochemistry, Geophysics, Geosystems, 14, 292-316.

Garzanti, E., Padoan, M., Andò, S., Resentini, A., Vezzoli, G., Lustrino, M., 2013b. Weathering and relative durability of detrital minerals in equatorial climate: sand petrology and geochemistry in the East African Rift. The Journal of Geology 121, 547–580.

Garzanti, E., Padoan, M., Setti, M., López-Galindo, A., Villa, I.M., 2014a. Provenance versus weathering control on the composition of tropical river mud (southern Africa). Chemical Geology, 366, 61–74.

Garzanti, E., Vermeesch, P., Padoan, M., Resentini, A., Vezzoli, G., Andò, S., 2014b. Provenance of passive-margin sand (Southern Africa). The Journal of Geology, 122, 17–42.

Guo, Y., Yang, S., Su, N., Li, C., Yin, P., Wang, Z., 2018. Revisiting the effects of hydrodynamic sorting and sedimentary recycling on chemical weathering indices. Geochim. Cosmochim. Acta 227, 48-63.

Haack, R.C., Sundararaman, P., Diedjomahor, J.O., Xiao, H., Gant, N.J., May, E.D., Kelsch, K., 2000. Niger Delta petroleum systems, Nigeria. In: Mello, M.R., Katz, B.J. (Eds.),

Petroleum Systems of the South Atlantic Margins. American Association of Petroleum Geologists Memoir 73, 213-231.

Hallberg, R.O., 1976. A geochemical method for investigation of paleo-redox conditions in sediments. Ambio Special Report, 4, 139-147.

Harnois, L. (1988): The C.I.W Index: a new chemical index of weathering. Sedimentary Geology, 55, 319-322.

Hassan S., Ishiga, H., Roser, B.P., Dozen, K., Naka, T., 1999. Geochemistry of Permian-Triassic shales in the Salt Range, Pakistan: implication for provenance and tectonism at the Gondwana margin. Chemical Geology, 158, 293-314.

Hatch, J.R., Leventhal, J.S., 1992. Relationship between inferred redox potential of the depositional environment and geochemistry of the Upper Pennsylvanian (Missourian) stark shale member of the Dennis Limestone, Wabaunsee County, Kansas, USA. Chemical Geology, 99, 65-82.

Hayashi, K.I., Fujisawa, H., Holland, H.D., Ohmoto, H., 1997. Geochemistry of ~1.9 Ga sedimentary rocks from north-eastern Labrador, Canada. Geochimica et Cosmochimica Acta, 16, 4115-4137.

He, J., Ding, W., Jiang, Z., Jiu, K., Li, A., Sun, U., 2017. Mineralogical and chemical distribution of the Es3 L oil shale in the Jiyang Depression, Bohai Bay Basin (E China): Implications for paleoenvironmental reconstruction and organic matter accumulation. Marine and Petroleum Geology, 81, 196-219.

Herron, M.M., 1988. Geochemical Classification of Terrigenous Sands and Shales from Core or Log Data. Journal of Sedimentary Petrology, 58, 820-829.

Hofer, G., Wagreich, M., Neuhuber, S., 2013. Geochemistry of fine-grained sediments of the upper Cretaceous to Paleogene Gosau Group (Austria, Slovakia): Implications for paleo-environmental and provenance studies. Geoscience Frontiers, 4, 449-468.

Hospers, J., 1965. Gravity field and structure of the Niger Delta, Nigeria, West Africa, Geological Society of American Bulletin, 76, 407-422.

Jones, B., Manning, D.A.C., 1994. Comparison of geochemical indices used for the interpretation of paleo-redox conditions in ancient mudstones. Chemical Geology, 111, 111-129.

Krueger. S.W., Grant, N.T., 2011. The growth history of toe thrusts of the Niger Delta and the role of pore pressure, in K. McClay, J. Shaw, and J. Suppe, eds., Thrust fault-related folding: AAPG Memoir 94, 357 – 390.

Kulke, H. (1995): Nigeria. In: Kulke, H. (Eds), Regional Petroleum Geology of the World. Part II: Africa, America, Australia and Antarctica, Gebru Borntraeger, Berlin, 143–172.

Lambert – Aikhionbare, D.O., Ibe, A.C., 1984. Petroleum source bed evaluation of Tertiary Niger Delta: discussion. AAPG Bulletin, 68, 387–389.

Le Bas M.J., Le Maitre R.W., Streckeisen, A., Zanettin, B., 1986. A chemical classification of volcanic rocks based on the total alkali-silica diagram. Journal of Petrology, 27, 745–750.

Lindsey, D.A., 1999. An Evaluation of Alternative Chemical Classifications of Sandstones. United States Geological Survey Open-File Report 99-346, 23p.

Madhavaraju, J., Ramirez-Montoya, E., Monreal, R., Gonzalez–Leon, C.M., Pi-Puig, T., Espinoza-Maldonado, I.G., Grijalva–Noriega, F.J., 2016. Paleoclimate, paleo-weathering and paleo-redox conditions of Lower Cretaceous shales from the Mural Limestone, Tuape section, northern Sonora, Mexico: Constraints from clay mineralogy and geochemistry. Revista Mexicana de Ciencias Geologicas, 33(1), 34-48.

Maharana, C., Srivastava, D., Tripathi, J.K., 2018. Geochemistry of sediments of the Peninsular rivers of the Ganga basin and its implication to weathering, sedimentary processes, and provenance. Chemical Geology, 483, 1–20.

Maloney, M., Davies, R., Imber, J., Higgins, S., and Kings, S., 2010. New insights into deformation mechanisms in the gravitationally driven Niger Delta deep-water fold and thrust belt. American Association of Petroleum Geologists Bulletin, 94(9)-1401-1424.

Maravelis, A., Zelilidis, A., 2009. Petrography and geochemistry of the late Eocene–early Oligocene submarine fans and shelf deposits on Lemnos Island, NE Greece. Implications for provenance and tectonic setting. Geological Journal, DOI: 10.1002/gj.1183.

McLennan, S M., 1989. Rare earth elements in sedimentary rocks: Influence of provenance and sedimentary processes. Review of Mineralogy, 21, 169-200.

McLennan, S.M., 2001. Relationships between the trace element composition of sedimentary rocks and upper continental crust. Geochemistry, Geophysics, Geosystems 2 (2000GC000109).

McLennan, S.M., Hemming, S., McDaniel, D.K., Hanson, G.N., 1993. Geochemical Approaches to Sedimentation, Provenance, and Tectonics. Geological Society of America Special Papers, 284, 21-40.

McLennan, S.M., Taylor, S.R., 1980. Th and U in sedimentary rocks: crustal evolution and sedimentary recycling. Nature 285: 621–624.

McLennan, S.M., Taylor, S.R., 1991. Sedimentary rocks and crustal evolution: Tectonic setting and secular trends. Journal of Geology, 99, 1-21

McLennan, S.M., Taylor, S.R., McCulloch, M.T., Maynard, J.B., 1990. Geochemical and Nd–Sr isotopic composition of deep-sea turbidites: crustal evolution and plate tectonic associations. Geochimica et Cosmochimica Acta, 54, 2015-2050.

Meinhold, G., Kostopoulos, D., Reischmann, T., 2007. Geochemical constraints on the provenance and depositional setting of sedimentary rocks from the islands of Chios,

Inousses and Psara, Aegean Sea, Greece: implications for the evolution of Palaeotethys. Journal of the Geological Society, London, 164, 1145–1163.

Merki, P., 1972. Structural geology of the Cenozoic Niger delta. In: Dessauvagie, T.F.J., Whiteman, A.J. (Eds.), African Geology. University of Ibadan Press, Ibadan, Nigeria, 635–644.

Mikes, T., Dunkl, I., Eynatten, H., Frisch, W., 2006. Geochemistry of Eocene flysch sandstones in the NW External Dinarides. Acta Geologica Hungarica, 49(2), 103–124.

Mongelli, G., Critelli, S., Perri, F., Sonnino, M., Perrone, V., 2006. Sedimentary recycling, provenance and paleo-weathering from chemistry and mineralogy of Mesozoic continental redbed mudrocks, Peloritani mountains, Southern Italy. Geochemical Journal, 40, 197-209.

Morford J.L., Emerson S., Breckel, E.J., Kim, S.H., 2005. Diagenesis of oxyanions (V, U, Re, and Mo) in pore waters and sediments from a continental margin. Geochimica et Cosmochimica Acta, 69(21), 5021-5032.

Nesbitt, H.W., Young, G.M. 1982. Early Proterozoic Climates and Plate Motions Inferred from Major Element Chemistry of Lutites. Nature, 299, 715-717.

Nwachukwu, J.I., Chukwura, P.I., 1986. Organic Matter of Agbada Formation, Niger Delta, Nigeria. American Association of Petroleum Geologists Bulletin, 70, 48-55.

Nwajide, C.S., 2013. Geology of Nigeria's Sedimentary Basins. CSS Bookshops Limited, Lagos, 565 pp.

Obiadi, I.I., Okoye, F.C., Obiadi, C.M., Irumhe, P.E., Omeokachie, A.I., 2019. 3-D structural and seismic attribute analysis for field reservoir development and prospect identification in Fabianski Field, onshore Niger Delta, Nigeria. Journal of African Earth Sciences, 158,103562.

Ogbe, O.B. Sequence stratigraphic controls on reservoir characterization and architectural analysis: A case study of Tovo field, coastal swamp depobelt, Niger Delta Basin, Nigeria. Marine and Petroleum Geology, 121, https://doi.org/10.1016/j.marpetgeo.2020.104579.

Osae, S., Asiedu, D. K., Banoeng-Yakubo, B., Koeberl, C., Dampare, S.B., 2006. Provenance and tectonic setting of Late Proterozoic Buem sandstones of south-eastern Ghana: Evidence from geochemistry and detrital modes. Journal of African Earth Sciences, 44, 85–96.

Osokpor, J., Lucas, F.A., Osokpor, O.J., Overare, B., Alaminiokuma, G.I., Ogbe, O.B., Izeze, O.E and Daniya, T.S., 2016. Petroleum Potential of Paleogene-Neogene Age Sediments in Well TN-1, Western Niger Delta Basin, Pacific Journal of Science and Technology, 17(1), 288-300.

Overare, B., Osokpor, J., Ekeh, P.C., Azmy, K., 2020. Demystifying provenance signatures and paleo-depositional environment of mudrocks in parts of south-eastern Nigeria: Constraints from geochemistry. Journal of African Earth Sciences. https://doi.org/10.1016/j.jafrearsci.2020.103954.

Padoan, M., Garzanti, E., Haravan, Y., Villa, I.M., 2011. Tracing Nile sediment sources by Sr and Nd isotope signatures (Uganda, Ethiopia, Sudan). Geochimica et Cosmochimica Acta 75, 3627–3644.

Pang, H., Pan, B., Garzanti, E., Gao, H., Zhao, X., Chen. D., 2018. Mineralogy and geochemistry of modern Yellow River sediments: Implications for weathering and provenance. Chemical Geology, 488, 76–86.

Pettijohn, F.J., Potter P.E., Siever, R., 1972. Sand and Sandstone. New York, Springer: 618 p.

Potter, P. E., Maynard, J.B., Depetris, P.J., 2005. Mud and Mudstones: Introduction and Overview, Heidelberg, Springer Verlag, 297p.

Ramachandran, A., Madhavaraju, J., Ramasamy, S., Lee, I.Y., Rao, S., Chawngthu, D.L., Velmurugan, K., 2016. Geochemistry of Proterozoic clastic rocks of the Kerur Formation of Kaladgi-Badami Basin, North Karnataka, South India: implications for, and provenance. Turkish Journal of Earth Sciences, 25, 126-144.

Ratcliffe, K.T., Wright, A.M., Montgomery, P., Palfrey, A., Vonk, A., Vermeulen, J., Barrett, M., 2010. Application of chemostratigraphy to the Mungaroo Formation, the Gorgon field, offshore northwest Australia. Journal of the Australian Petroleum Production & Exploration Association., 371-388.

Reijers, T.J.A., 2011: Stratigraphy and Sedimentology of the Niger Delta, Geologos, 17(3), 133-162.

Reijers, T.J.A., Petters, S.W., Nwajide, C.S., 1996. The Niger Delta Basin, In: T.J.A. Reijers (Eds.), Selected Chapters on Geology: SPDC corporate reprographic services, Warri, Nigeria, 103-114.

Rimmer, S.M., 2004. Geochemical paleoredox indicators in Devonian- Mississippian blacks shales, Central Appalachian Basin (U.S.A.). Chemical Geology, 206: 373-391.

Rimmer, S.M., Thompson, J.A., Goodnight, S.A., Robl, T., 2004. Multiple controls on the preservation of organic matter in Devonian-Mississippian marine black shales: Geochemical and petrographic evidence. Paleogeography, Paleoclimatology, Paleoecology, 215-125-154.

Roser, B.P., Korsch, R.J., 1988. Provenance Signature of Sandstone-Mudstone Suites Determined Using Discriminant Function Analysis of Major Element Data, Chemical Geology, 67, 119-139.

Roy, D.K., Roser, B.P., 2013. Climatic control on the composition of Carboniferous–Permian Gondwana sediments, Khalaspir basin, Bangladesh. Gondwana Research, 23, 1163–1171.

Rudnick, R. L., Gao, S., 2003. The Composition of the Continental Crust, In Treatise on Geochemistry, Elsevier – Pergamon, Oxford–London, 3, 1-64.

Ruffell, A., Worden, R., 2000. Palaeoclimate analysis using spectral gamma-ray data from the Aptian (Cretaceous) of southern England and southern France. Palaeogeography, Palaeoclimatology, Palaeoecology, 155(3-4), 265-283.

Scott, C., Lyons, T.W., 2012. Contrasting molybdenum cycling and isotopic properties in euxinic versus non-euxinic sediments and sedimentary rocks: refining the paleoproxies. Chemical Geology, 324–325, 19–27.

Short, K.C., Stauble, A.J., 1967. Outline of geology of Niger Delta, American Association of Petroleum Geologists Bulletin, 51, 761-779.

Spalletti, L.A., Limarino, C.O., Colombo., Pinol, F., 2012. Petrology and geochemistry of Carboniferous siliciclastics from the Argentine Frontal Cordillera: a test of methods for interpreting provenance and tectonic setting. Journal of South American Earth Sciences, 36, 32–54.

Stacher, P.,1995. Present understanding of the Niger delta hydrocarbon habitat, In: Oti, M. N., and Postma, G., eds., Geology of deltas: Rotterdam, A.A. Balkema, 257-267.

Steinmann, J.W., Grammer, G.M., Brunner, B., Jones, C.K ., Riedinger, N., 2020. Assessing the application of trace metals as paleoproxies and a chemostratigraphic tool in carbonate systems: A case study from the "Mississippian Limestone" of the midcontinent, United States, Marine and Petroleum Geology, 112, 104061.

Tang, S.D.N., Atangana, J.N., Onana, V.L., 2020. Mineralogy and geochemistry of alluvial sediments from the Kadey plain, eastern Cameroon: Implications for provenance, weathering, and tectonic setting. Journal of African Earth Sciences, 163, 103763.

Tao, H., Sun, S., Wang, Q., Yang, X., Jiang, L., 2014. Petrography and geochemistry of Lower Carboniferous greywacke and mudstones in Northeast Junggar, China: Implications for

provenance, source weathering, and tectonic setting. Journal of Asian Earth Sciences, 87, 11–25.

Taylor S.R., McLennan, S.M., 1995. The geochemical evolution of the continental crust", Reviews of Geophysics, 33, 241–265.

Taylor, S.R., 2015. Geochemistry of Andesites. In Origin and Distribution of the Elements, (Eds), L. H. Ahrens. International Series of Monographs in Natural Philosophy, 30, 559-582.

Taylor, S.R., McLennan, S.M., 1985. The Continental Crust: Its Composition and Evolution: An Examination of the Geochemical Record Preserved in Sedimentary Rocks. Blackwell Science, Oxford, 312 p.

Tribovillard, N., Algeo, T. J., Baudin, F., Riboulleau, A. (2012). Analysis of marine environmental conditions based on molybdenum- uranium covariation-Applications to Mesozoic paleoceanography. Chemical Geology, 324-325, 46–58.

Tribovillard, N., Algeo, T., Lyons, T.W., Riboulleau, A., 2006. Trace metals as paleoredox and paleoproductivity proxies: an update. Chemical Geology 232, 12–32.

Tuttle, M. L. W., R. R., Charpentier., M. E. Brownfield, 1999. The Niger delta petroleum system: Niger delta province, Nigeria, Cameroon, and Equatorial Guinea, Africa: USGS Open-file report 99-50-H.

Ullah, F., Arif, M., Shah, M.T., 2015. Petrography and geochemistry of the Kamlial Formation, southwestern Kohat Plateau, Pakistan: implications for paleoclimate of the Western Himalayas. Turkish Journal of Earth Sciences, 24, 276-288.

Van De Kamp, P.C., Leake, B.E., 1985. Petrography and geochemistry of feldspathic and mafic sediments of the north-eastern Pacific margin. Transactions of the Royal Society of Edinburgh, Earth Sciences, 76: 411-449.

van der Weijden, C.H., Reichart, G.J., van Os, B.J.H., 2002. Sedimentary trace element records over the last 200 kyr from within and below the northern Arabian Sea oxygen minimum zone. Marine Geology 231, 69–88.

von Eynatten, H., Barcelò-Vidal, C., Pawlowsky-Glahn, V., 2003. Composition and discrimination of sandstones: a statistical evaluation of different analytical methods. Journal of Sedimentary Research 73, 47–57.

Wang, C., Wang, Q., Chen, G., He, L., Xu, Y., Chen, L., Chen, D., 2017. Petrographic and geochemical characteristics of the lacustrine black shales from the Upper Triassic Yanchang Formation of the Ordos Basin, China: Implications for the organic matter accumulation. Marine and Petroleum Geology, 86, 52-65.

Weber, K.J., Daukoru, E.M., 1975. Petroleum Geology of the Niger Delta: Proceedings of the Ninth World Petroleum Congress, vol. 2. Applied Science Publishers, 210–221.

Wedepohl, K.H., 1971. Environmental influences on the chemical composition of shales and clays. In: Ahrens, L.H., Press, F., Runcorn, S.K., Urey, H.C. (Eds.), Physics and Chemistry of the Earth. Pergamon, Oxford, pp. 305–333.

Wronkiewicz D.J., Condie K.C., 1987. Geochemistry of Archean shales from the Witwatersrand Supergroup, South Africa: Source area weathering and provenance. Geochimica et Cosmochimica Acta, 51, 2401-2416.

Wronkiewicz, D.J., Condie, K.C., 1989. Geochemistry and Provenance of Sediments from the Pongola Supergroup, South Africa: Evidence for 3.0 Ga Old Continental Craton. Geochimica et Cosmochimica Acta, 53, 1537-1549.

Wu, W., Liu, W., Mou, C., Liu, H., Qiao, Y., Pan, J., Ning, S., Zhang, X., Yao, J., Liu, J., 2021. Organic-rich siliceous rocks in the upper Permian Dalong Formation (NW middle Yangtze): Provenance, paleoclimate and paleoenvironment. Marine and Petroleum Geology 123, 104728.

Xie, Y., Yuan, F., Zhan, T., Kang, C., Chi, Y., Ma, Y., 2017. Geochemistry of loess deposits in northeastern China: constraint on provenance and implication for disappearance of the large Songliao palaeolake. Journal of the Geological Society, 175, 146–162.

Zaid, S.M., Al Gahtani, F., 2015. Provenance, diagenesis, tectonic setting, and geochemistry of Hawkesbury Sandstone (Middle Triassic), southern Sydney Basin, Australia. Turkish Journal of Earth Sciences, 24, 72-98.

Zhang, Y., Pe-Piper, G., Piper, D.J.W., 2014. Sediment geochemistry as a provenance indicator: Unravelling the cryptic signatures of polycyclic sources, climate change, tectonism and volcanism. Sedimentology, 61, 383–410.

Zuffa, G.G., 1985. Optical analyses of arenites: influence of methodology on compositional results. In Provenance of Arenites, Zuffa GG (Eds.). NATO ASI Series No 148, D. Reidel Pub. Co, Dordrecht, Boston, USA, 165–189.

Appendix 2.1a: Major oxides, trace, and rare-earth elements composition for the sand/sandstones under investigation

SAMPLE	S1	S2	S3	S4	S5	S6	S7	S8	S9	S10	S11	S12	S13	S14	S15	S16	S17
SiO_2(%)	71.70	63.20	69.10	61.50	66.80	65.10	68.60	60.80	59.80	60.80	79.10	72.10	64.75	68.75	66.05	61.01	66.82
$Al2O_3$	9.53	14.70	9.58	14.30	11.50	13.50	9.74	12.30	14.90	14.50	7.68	10.50	10.49	9.54	10.96	15.07	9.72
Fe_2O_3	6.46	7.17	9.97	7.38	7.25	8.86	9.15	14.40	9.28	9.00	4.47	5.27	8.08	7.46	9.05	8.22	8.52
CaO	1.30	0.75	0.65	1.56	1.33	0.42	0.80	0.63	1.38	1.51	0.34	0.40	1.50	1.01	0.87	0.64	1.17
MgO	1.08	1.20	0.85	1.40	1.23	0.93	0.99	1.00	1.17	1.20	0.67	0.97	1.61	1.51	1.37	1.47	1.16
Na_2O	0.53	0.61	0.55	0.77	0.60	0.61	0.53	0.69	0.39	0.37	0.37	0.59	0.56	0.42	0.55	0.85	0.47
K_2O	1.01	1.32	1.04	1.34	1.15	1.16	1.04	1.07	1.22	1.19	0.96	1.23	1.24	1.13	1.42	1.78	1.08
MnO	0.09	0.08	0.12	0.09	0.10	0.13	0.11	0.16	0.11	0.10	0.05	0.07	0.12	0.10	0.15	0.14	0.10
TiO_2	0.49	0.82	0.49	0.81	0.67	0.75	0.58	0.66	0.78	0.74	0.43	0.61	0.66	0.61	0.81	1.08	0.58
P_2O_5	0.10	0.13	0.11	0.30	0.19	0.10	0.09	0.10	0.10	0.10	0.06	0.09	0.19	0.15	0.14	0.16	0.16
LOI	7.11	9.74	6.65	9.84	8.72	8.34	8.16	7.95	10.55	10.41	5.89	8.05	9.59	8.60	8.13	8.93	9.42
Fe_2O_3/K_2O	6.40	5.43	9.59	5.51	6.30	7.64	8.80	13.46	7.61	7.56	4.66	4.28	6.52	6.60	6.37	4.62	7.89
SIO_2/Al_2O_3	7.52	4.30	7.21	4.30	5.81	4.82	7.04	4.94	4.01	4.19	10.30	6.87	6.17	7.21	6.03	4.05	6.87
K_2O/Na_2O	1.91	2.16	1.89	1.74	1.92	1.90	1.96	1.55	3.13	3.22	2.59	2.08	2.21	2.69	2.58	2.09	2.30
Al_2O_3/TiO_2	19.45	17.93	19.55	17.65	17.16	18.00	16.79	18.64	19.10	19.59	17.86	17.21	15.89	15.64	13.53	13.95	16.76
K_2O/Al_2O_3	0.11	0.09	0.11	0.09	0.10	0.09	0.11	0.09	0.08	0.08	0.13	0.12	0.12	0.12	0.13	0.12	0.11
CIA	82.16	85.27	81.74	83.24	83.03	86.04	82.26	83.73	88.17	88.25	82.14	82.55	81.63	82.88	81.31	82.17	82.79
CIX	86.09	88.39	85.77	87.14	86.79	88.41	86.12	87.48	90.25	90.29	85.24	85.23	85.35	86.02	84.76	85.14	86.25
$\alpha^{Al}Mg$	1.42	1.97	1.82	1.64	1.51	2.34	1.58	1.98	2.05	1.95	1.85	1.74	1.05	1.02	1.29	1.65	1.35
$\alpha^{Al}Ca$	4.19	5.62	4.06	4.33	4.47	7.49	4.28	4.55	8.91	9.14	5.27	6.12	4.37	5.30	4.65	5.49	4.82
$\alpha^{Al}Na$	3.82	5.12	3.70	3.94	4.07	4.70	3.90	3.79	8.11	8.32	4.41	3.78	3.98	4.82	4.23	3.76	4.39
$\alpha^{Al}K$	1.72	2.02	1.67	1.94	1.82	2.12	1.70	2.09	2.22	2.22	1.45	1.55	1.54	1.53	1.40	1.54	1.64
TRACE ELEMENTS (ppm)																	
Ba	507.00	2631.00	605.00	3906.00	2838.00	441.00	3052.00	1969.00	2999.00	2940.00	293.00	313.00	1002.00	1087.00	1521.00	1391.00	1491.00
Co	10.10	14.00	12.80	13.20	11.00	12.60	14.70	15.50	13.70	13.80	7.30	10.50	11.10	10.10	13.70	14.70	12.40
Cs	1.90	3.10	1.90	3.20	2.60	2.60	2.20	2.70	2.90	3.10	1.40	2.10	2.70	2.30	2.60	3.30	2.10
Ga	11.20	17.50	11.30	17.30	12.90	15.40	11.20	14.20	16.80	16.60	7.80	11.30	14.20	12.90	14.70	19.30	12.30
Hf	4.20	6.60	4.50	8.00	6.70	5.40	5.40	5.00	5.80	5.50	4.60	7.80	7.30	6.90	8.70	11.50	5.40
Nb	13.20	21.80	12.30	21.00	17.50	19.90	15.90	16.40	20.40	19.30	10.90	15.00	18.60	17.70	22.80	27.90	14.80
Rb	39.90	57.50	41.00	59.90	49.30	50.80	42.70	47.40	54.20	53.50	35.20	46.90	50.20	47.80	56.70	71.20	44.50

Sr	102.30	132.20	87.60	185.50	142.10	91.60	129.10	111.90	149.30	154.40	67.50	85.20	129.10	117.00	138.20	148.20	124.10
Th	8.60	13.50	8.10	13.70	11.00	12.40	9.00	10.60	13.20	12.70	7.40	9.70	10.70	10.50	11.80	15.10	10.30
U	1.90	2.60	1.90	3.20	2.60	2.80	1.80	2.40	2.70	2.50	1.80	2.40	3.10	2.90	3.10	4.00	2.80
V	62.00	82.00	59.00	84.00	68.00	74.00	56.00	69.00	79.00	77.00	40.00	56.00	71.00	63.00	80.00	92.00	64.00
Zr	158.10	245.40	163.20	302.90	246.60	192.40	209.50	182.60	210.00	205.70	171.40	288.20	276.90	256.40	330.20	428.00	209.50
Mo	19.30	2.80	57.00	1.80	4.40	42.80	39.60	72.20	19.20	18.80	2.00	1.00	5.90	5.70	9.60	2.70	25.30
Cu	21.10	28.70	73.70	29.60	25.30	35.20	38.00	67.90	25.90	25.00	21.60	16.50	12.70	15.80	19.40	18.10	23.50
Pb	33.00	69.00	28.80	27.00	36.10	33.30	64.90	72.40	76.40	130.10	51.50	9.70	26.40	27.60	48.20	20.90	81.00
Zn	56.00	66.00	72.00	64.00	57.00	53.00	81.00	81.00	100.00	103.00	63.00	47.00	56.00	49.00	62.00	60.00	63.00
Ni	16.50	24.20	23.40	21.30	16.70	21.70	27.70	37.20	22.60	22.80	12.60	14.60	13.90	13.20	19.60	18.70	20.50
Cr	67.41	66.66	67.09	65.43	66.15	68.21	68.44	68.16	65.32	67.61	66.73	65.05	67.09	68.32	66.57	65.88	67.92
Y	16.10	28.80	16.00	28.80	23.10	22.80	20.10	19.70	23.10	21.90	14.90	20.20	24.10	22.80	27.70	34.30	19.90
α^{Al}Rb	1.27	1.36	1.24	1.27	1.24	1.42	1.21	1.38	1.46	1.44	1.16	1.19	1.11	1.06	1.03	1.13	1.16
α^{Al}Sr	1.94	2.31	2.27	1.60	1.68	3.06	1.57	2.28	2.07	1.95	2.36	2.56	1.69	1.69	1.65	2.11	1.63
α^{Al}Ba	0.02	0.00	0.01	0.00	0.00	0.02	0.00	0.00	0.00	0.00	0.03	0.04	0.01	0.00	0.00	0.00	0.00
Cr/V	1.09	0.81	1.14	0.78	0.97	0.92	1.22	0.99	0.83	0.88	1.67	1.16	0.94	1.08	0.83	0.72	1.06
Y/Ni	0.98	1.19	0.68	1.35	1.38	1.05	0.73	0.53	1.02	0.96	1.18	1.38	1.73	1.73	1.41	1.83	0.97
La/Th	3.50	3.33	3.40	3.26	3.34	3.42	3.50	3.40	3.33	3.29	3.20	3.33	3.50	3.23	3.56	3.42	3.23
Th/Co	0.85	0.96	0.63	1.04	1.00	0.98	0.61	0.68	0.96	0.92	1.01	0.92	0.96	1.04	0.86	1.03	0.83
La/Co	2.98	3.21	2.15	3.39	3.34	3.37	2.14	2.32	3.20	3.03	3.25	3.08	3.38	3.36	3.07	3.51	2.69
V/Cr	0.92	1.23	0.88	1.28	1.03	1.08	0.82	1.01	1.21	1.14	0.60	0.86	1.06	0.92	1.20	1.40	0.94
Ni/Co	1.63	1.73	1.83	1.61	1.52	1.72	1.88	2.40	1.65	1.65	1.73	1.39	1.25	1.31	1.43	1.27	1.65
Cu/Zn	0.38	0.43	1.02	0.46	0.44	0.66	0.47	0.84	0.26	0.24	0.34	0.35	0.23	0.32	0.31	0.30	0.37
Cr/Th	7.84	4.94	8.28	4.78	6.01	5.50	7.60	6.43	4.95	5.32	9.02	6.71	6.27	6.51	5.64	4.36	6.59
Th/U	4.53	5.19	4.26	4.28	4.23	4.43	5.00	4.42	4.89	5.08	4.11	4.04	3.45	3.62	3.81	3.78	3.68
RARE EARTH ELEMENTS (ppm)																	
La	30.10	44.90	27.50	44.70	36.70	42.40	31.50	36.00	43.90	41.80	23.70	32.30	37.50	33.90	42.00	51.60	33.30
Ce	61.10	92.70	59.90	93.60	76.20	87.80	64.70	74.60	91.20	87.00	48.20	68.30	76.60	69.80	83.30	103.30	68.00
Pr	6.92	10.51	6.72	10.82	8.69	9.73	7.47	8.59	10.25	9.92	5.56	7.93	8.83	8.11	9.60	12.15	7.63
Nd	26.10	40.10	24.20	40.40	32.20	36.00	27.40	31.60	39.50	37.90	20.90	28.40	31.90	30.40	34.60	43.90	27.60
Sm	4.65	7.22	4.39	7.25	6.01	6.21	4.90	5.81	6.88	6.37	3.94	5.23	5.86	5.52	6.50	8.14	4.90
Eu	0.99	1.45	0.88	1.50	1.24	1.29	0.95	1.17	1.35	1.31	0.77	1.08	1.20	1.10	1.32	1.66	1.07
Gd	4.07	6.32	3.77	6.61	5.25	5.56	4.55	4.91	6.02	5.76	3.33	4.81	5.15	4.69	5.80	7.25	4.47
Tb	0.54	0.89	0.51	0.91	0.71	0.77	0.61	0.67	0.78	0.73	0.46	0.65	0.77	0.69	0.84	1.06	0.65

Dy	3.46	5.72	3.09	5.46	4.64	4.59	3.95	4.22	4.66	4.57	2.79	3.94	4.52	4.26	5.12	6.16	3.90
Ho	0.56	0.97	0.56	1.04	0.78	0.79	0.72	0.73	0.90	0.78	0.53	0.65	0.88	0.81	1.04	1.27	0.76
Er	1.72	2.79	1.55	2.77	2.43	2.37	1.96	2.16	2.50	2.27	1.41	2.10	2.56	2.38	2.95	3.63	2.20
Tm	0.26	0.42	0.22	0.43	0.35	0.32	0.26	0.31	0.34	0.31	0.22	0.29	0.37	0.35	0.45	0.56	0.32
Yb	1.59	2.56	1.52	2.83	2.25	2.18	1.79	1.99	2.22	2.05	1.42	2.06	2.31	2.17	2.87	3.60	2.03
Lu	0.23	0.38	0.23	0.41	0.35	0.34	0.28	0.29	0.34	0.31	0.22	0.32	0.35	0.34	0.44	0.56	0.31
∑LREE	145.96	225.68	139.59	227.07	184.14	206.23	157.02	177.47	216.18	206.20	117.97	163.44	185.99	171.63	205.02	255.05	162.40
∑HREE	12.43	20.05	11.45	20.46	16.76	16.92	14.12	15.28	17.76	16.78	10.38	14.82	16.91	15.69	19.51	24.09	14.64
∑LREE/∑HREE	11.74	11.26	12.19	11.10	10.99	12.19	11.12	11.61	12.17	12.29	11.37	11.03	11.00	10.94	10.51	10.59	11.09
∑REE	142.29	216.93	135.04	218.73	177.80	200.35	151.04	173.05	210.84	201.08	113.45	158.06	178.80	164.52	196.83	244.84	157.14
Eu/Eu*	0.70	0.66	0.66	0.66	0.67	0.67	0.61	0.67	0.64	0.66	0.65	0.66	0.67	0.66	0.66	0.66	0.70
Ce/Ce*	0.99	1.00	1.03	1.00	1.00	1.01	0.99	0.99	1.01	1.00	0.98	1.00	0.99	0.99	0.97	0.97	1.00
(La/Lu)N	13.59	12.27	12.41	11.32	10.89	12.95	11.68	12.89	13.40	14.00	11.18	10.48	11.12	10.35	9.91	9.57	11.15
(Gd/Yb)N	1.73	1.51	1.62	1.58	1.56	1.67	1.55	1.71	1.79	1.80	1.53	1.63	1.47	1.41	1.44	1.45	1.54
(La/Sm)N	4.07	3.91	3.94	3.88	3.84	4.30	4.05	3.90	4.02	4.13	3.79	3.89	4.03	3.87	4.07	3.99	4.28
(La/Yb)N	10.70	8.92	9.83	8.88	9.09	10.64	8.97	10.46	10.87	10.92	9.10	9.15	8.90	8.51	8.68	8.61	9.58

Appendix 2.1b: Major oxides, trace, and rare-earth elements composition for the shales under investigation

SAMPLE	SH1	SH2	SH3	SH4	SH5	SH6	SH7	SH8	SH9	SH10	SH11	SH12	SH13	SH14	SH15	SH16	SH17	SH18	SH19
SiO_2(%)	56.1	57.3	57.1	59.1	51.3	51.7	56.1	55.2	57.8	58.2	54.7	51.9	50.4	54.2	54.5	55.3	50.2	53.3	52.0
Al_2O_3	18.5	18.5	15.9	15.4	15.1	17.7	18.3	18.5	15.5	15.1	14.2	16.6	16.1	15.3	16.2	15.6	15.7	14.2	15.3
Fe_2O_3	7.6	8.0	7.4	7.8	18.1	8.7	8.0	8.6	9.2	8.3	9.3	8.4	9.9	8.4	8.5	8.3	11.1	9.4	9.7
CaO	0.5	0.6	0.9	0.7	0.6	0.9	0.4	0.7	0.8	1.3	2.3	1.6	1.8	1.4	1.4	1.6	1.4	2.3	1.6
MgO	1.4	1.4	1.4	1.3	1.2	1.5	1.6	1.6	1.6	1.6	2.0	1.8	2.1	1.8	1.8	1.8	2.3	2.2	2.2
Na_2O	0.8	1.0	0.7	0.7	0.8	0.8	0.8	0.7	0.7	0.7	0.7	0.7	0.7	0.7	0.7	0.6	0.8	0.7	0.6
K_2O	1.5	1.4	1.6	1.5	1.2	1.7	1.9	1.8	1.7	1.7	1.5	1.6	1.6	1.6	1.6	1.5	1.6	1.5	1.6
MnO	0.1	0.1	0.1	0.1	0.2	0.1	0.1	0.1	0.2	0.1	0.1	0.1	0.1	0.1	0.1	0.1	0.2	0.1	0.1
TiO_2	1.0	0.9	1.0	0.9	0.8	1.0	1.2	1.2	1.1	1.0	0.9	1.0	1.0	0.9	1.0	0.9	1.0	0.9	1.0
P_2O_5	0.1	0.1	0.1	0.1	0.1	0.1	0.1	0.1	0.2	0.2	0.2	0.2	0.3	0.2	0.1	0.2	0.2	0.2	0.2
LOI	11.8	10.1	13.6	12.0	10.2	15.0	11.5	11.5	10.4	11.0	12.3	15.3	15.2	14.5	13.3	12.9	14.9	13.5	14.8
Al	9.8	9.8	8.4	8.2	8.0	9.4	9.7	9.8	8.2	8.0	7.5	8.8	8.5	8.1	8.6	8.2	8.3	7.5	8.1
Fe_2O_3/K_2O	5.0	5.7	4.8	5.1	14.6	5.1	4.2	4.8	5.3	5.0	6.1	5.2	6.2	5.3	5.3	5.6	7.0	6.3	6.2
SIO_2/Al_2O_3	3.0	3.1	3.6	3.8	3.4	2.9	3.1	3.0	3.7	3.9	3.9	3.1	3.1	3.5	3.4	3.6	3.2	3.8	3.4
K_2O/Na_2O	2.0	1.4	2.2	2.1	1.6	2.2	2.5	2.5	2.5	2.5	2.2	2.3	2.4	2.4	2.3	2.4	2.0	2.0	2.5
Al_2O_3/TiO_2	18.3	19.7	16.7	16.7	18.2	17.4	15.8	16.1	14.6	15.0	15.5	16.3	16.6	16.5	16.8	17.1	16.5	15.9	16.1
K_2O/Al_2O_3	0.1	0.1	0.1	0.1	0.1	0.1	0.1	0.1	0.1	0.1	0.1	0.1	0.1	0.1	0.1	0.1	0.1	0.1	0.1
CIA	86.8	86.1	83.4	83.9	85.3	84.3	85.5	85.2	83.2	83.5	83.2	84.6	84.6	84.0	84.2	85.2	83.2	82.6	84.5
CIX	89.0	88.6	87.5	87.2	88.3	87.6	87.1	88.1	86.4	86.7	86.6	87.7	87.7	87.1	87.5	88.1	86.8	86.3	87.5
αAlMg	2.1	2.1	1.9	1.9	2.1	1.9	1.9	1.9	1.5	1.5	1.2	1.5	1.2	1.4	1.4	1.4	1.1	1.1	1.1
αAlCa	8.0	7.3	4.2	5.1	5.8	5.2	10.4	6.2	5.2	5.3	4.9	5.5	5.6	5.4	5.3	5.9	4.6	4.5	5.7
αAlNa	5.2	4.0	4.7	4.5	4.2	4.8	5.0	5.5	4.8	4.9	4.4	5.0	5.1	4.9	4.8	5.4	4.2	4.1	5.2
αAlK	2.2	2.4	1.9	1.8	2.2	1.9	1.7	1.9	1.6	1.7	1.7	1.9	1.8	1.7	1.8	1.9	1.8	1.7	1.8
TRACE ELEMENTS																			

Ba(ppm)	2508	496	2502	2559	1302	824	1461	2225	1435	1055	1014	734	818	1391	1962	1784	776	1378	1401
Co	16.3	14.7	12.0	12.0	17.7	14.1	15.3	14.6	14.2	13.7	13.1	14.9	14.8	14.2	14.7	13.9	13.0	14.3	13.8
Cs	3.9	3.8	3.8	3.5	3.1	4.0	3.9	3.7	3.4	3.2	3.4	3.7	3.5	3.4	3.6	3.5	3.9	3.5	3.6
Ga	21.9	20.9	18.3	17.9	18.0	21.0	21.7	21.0	20.1	19.5	17.7	20.7	19.9	18.7	19.4	18.9	18.6	17.8	18.8
Hf	7.8	6.4	9.5	9.7	6.0	9.6	11.5	10.7	10.7	10.9	9.7	9.0	9.9	9.8	8.2	7.8	8.6	9.3	8.8
Nb	26.0	24.5	24.9	24.7	21.8	27.5	26.2	26.7	27.3	25.3	24.7	26.8	26.2	24.3	24.6	23.3	23.7	23.1	25.7
Rb	69.0	64.9	67.6	64.8	58.1	72.7	77.2	73.7	73.1	69.2	63.6	70.2	68.5	66.8	68.7	66.7	67.0	62.9	67.8
Sr	141.4	109.5	162.8	153.5	117.2	145.5	135.8	155.6	158.2	164.8	184.1	172.5	172.9	169.6	170.7	172.2	157.4	180.0	166.8
Th	16.1	15.6	14.6	14.5	13.7	16.2	16.4	17.5	15.2	15.2	14.0	15.4	16.2	15.4	15.4	14.2	14.8	14.4	15.0
U	3.4	3.0	3.6	3.6	2.7	3.5	3.4	3.4	4.1	4.0	4.1	4.4	4.6	4.4	4.1	3.7	3.9	4.1	4.0
V	105.0	97.0	90.0	83.0	84.0	91.0	97.0	102.0	90.0	89.0	92.0	107.0	104.0	94.0	96.0	97.0	101.0	89.0	98.0
Zr	271.7	230.0	350.8	350.8	215.8	342.0	422.3	391.3	402.6	404.7	367.3	347.6	375.1	376.8	305.7	293.3	332.0	358.2	341.7
Mo	1.6	13.2	1.6	2.8	13.8	13.3	6.7	5.8	2.2	5.1	5.9	3.0	4.7	4.1	2.8	4.7	4.2	8.3	4.1
Cu	28.7	28.4	21.3	22.0	64.6	43.0	21.0	22.3	17.5	19.0	17.6	19.9	19.0	19.6	18.7	18.5	17.2	16.6	17.1
Pb	80.8	47.1	20.5	23.2	81.4	37.8	20.1	23.4	20.3	22.9	30.1	21.0	26.5	21.6	24.6	26.7	16.7	32.6	21.3
Zn	79.0	68.0	75.0	73.0	155.0	86.0	68.0	71.0	62.0	60.0	62.0	73.0	76.0	72.0	71.0	81.0	65.0	68.0	64.0
Ni	23.6	21.6	17.7	19.6	45.5	23.5	22.2	24.8	16.6	17.2	16.6	18.8	21.1	18.4	18.1	18.8	17.5	18.9	17.6
Cr	68.3	136.9	67.1	68.4	134.9	66.9	135.5	136.4	67.6	68.2	65.4	67.4	68.5	65.2	66.5	66.8	68.4	67.9	68.1
Y	30.3	28.5	29.2	31.1	24.7	31.5	32.6	33.6	35.5	33.0	32.8	32.1	34.8	29.6	30.1	30.4	32.5	30.9	29.8
αAlRb	1.4	1.5	1.3	1.3	1.4	1.3	1.3	1.3	1.1	1.2	1.2	1.3	1.3	1.2	1.3	1.2	1.2	1.2	1.2
αAlSr	2.7	3.5	2.0	2.1	2.7	2.5	2.8	2.5	2.0	1.9	1.6	2.0	1.9	1.9	2.0	1.9	2.1	1.6	1.9
αAlBa	0.3	1.5	0.3	0.3	0.5	0.9	0.5	0.3	0.4	0.6	0.6	0.9	0.8	0.5	0.3	0.4	0.8	0.4	0.5
Cr/V	0.7	1.4	0.8	0.8	1.6	0.7	1.4	1.3	0.8	0.8	0.7	0.6	0.7	0.7	0.7	0.7	0.7	0.8	0.7
Y/Ni	1.3	1.3	1.7	1.6	0.5	1.3	1.5	1.4	2.1	1.9	2.0	1.7	1.7	1.6	1.7	1.6	1.9	1.6	1.7
La/Th	3.4	3.4	3.5	3.3	3.3	3.4	3.2	3.1	3.4	3.4	3.6	3.6	3.6	3.4	3.4	3.5	3.6	3.4	3.5
Th/Co	1.0	1.1	1.2	1.2	0.8	1.2	1.1	1.2	1.1	1.1	1.1	1.0	1.1	1.1	1.1	1.0	1.1	1.0	1.1
La/Co	3.3	3.6	4.2	4.0	2.6	3.8	3.4	3.7	3.7	3.8	3.9	3.7	3.9	3.7	3.6	3.6	4.1	3.5	3.9
V/Cr	1.5	0.7	1.3	1.2	0.6	1.4	0.7	0.8	1.3	1.3	1.4	1.6	1.5	1.4	1.4	1.5	1.5	1.3	1.4
Ni/Co	1.5	1.5	1.5	1.6	2.6	1.7	1.5	1.7	1.2	1.3	1.3	1.3	1.4	1.3	1.2	1.4	1.4	1.3	1.3

Cu/Zn	0.4	0.4	0.3	0.3	0.4	0.5	0.3	0.3	0.3	0.3	0.3	0.3	0.3	0.3	0.3	0.2	0.3	0.2	0.3
V/(V+Ni)	0.8	0.8	0.8	0.8	0.7	0.8	0.8	0.8	0.8	0.8	0.9	0.9	0.8	0.8	0.8	0.8	0.9	0.8	0.9
Cr/Th	4.2	8.8	4.6	4.7	9.9	4.1	8.3	7.8	4.4	4.5	4.7	4.4	4.2	4.2	4.3	4.7	4.6	4.7	4.5
Th/U	4.7	5.2	4.1	4.0	5.1	4.6	4.8	5.2	3.7	3.8	3.4	3.5	3.5	3.5	3.8	3.8	3.8	3.5	3.8
Co-EF	0.8	0.7	0.8	0.8	0.8	0.8	0.8	0.8	0.9	0.9	0.9	0.8	0.9	0.9	0.8	0.8	0.8	0.9	0.9
U-EF	8.5	9.6	6.9	6.7	8.7	7.9	8.4	8.5	5.9	5.9	5.4	5.9	5.5	5.4	6.2	6.6	6.3	5.4	6.0
V-EF	0.7	0.7	0.7	0.7	0.7	0.7	0.7	0.7	0.8	0.8	0.8	0.8	0.8	0.8	0.8	0.8	0.8	0.8	0.8
Mo-EF	0.6	4.6	0.7	1.2	5.9	4.8	2.4	2.0	0.9	2.2	2.7	1.2	1.9	1.7	1.1	1.9	1.7	3.8	3.4
Cu-EF	0.6	0.6	0.5	0.5	1.6	0.9	0.4	0.5	0.4	0.5	0.5	0.5	0.4	0.5	0.4	0.4	0.4	0.4	0.4
Zn-EF	0.8	0.7	0.8	0.8	1.8	0.9	0.7	0.7	0.7	0.7	0.8	0.8	0.8	0.8	0.8	0.9	0.7	0.8	0.7
Ni-EF	0.3	0.3	0.3	0.3	0.7	0.3	0.3	0.3	0.3	0.3	0.3	0.3	0.3	0.3	0.3	0.3	0.3	0.3	0.3
Cr-EF	0.7	1.4	0.8	0.8	1.7	0.7	1.4	1.4	0.8	0.8	0.9	0.8	0.8	0.8	0.8	0.8	0.8	0.9	0.8
RARE-EARTH ELEMENTS																			
La(ppm)	54.1	52.2	50.8	48.4	45.8	54.2	52.7	54.3	52.2	51.9	50.5	54.7	57.7	52.8	53.0	49.9	53.4	49.4	53.1
Ce	114.2	106.9	104.3	100.1	93.4	109.3	110.4	110.7	104.6	103.2	99.8	108.9	113.0	107.7	106.0	99.9	104.1	99.1	105.5
Pr	13.1	12.4	12.1	11.6	10.7	12.6	12.5	12.6	12.1	12.0	11.4	12.9	13.0	12.5	12.3	11.8	12.1	11.2	12.4
Nd	48.3	46.4	44.1	42.8	40.2	48.4	47.2	46.3	42.9	42.8	41.7	46.7	48.1	45.6	45.2	44.4	46.5	42.2	44.5
Sm	8.8	8.1	8.1	7.9	7.5	8.5	9.0	8.4	8.2	8.0	7.7	8.4	8.7	8.0	8.3	7.8	8.4	7.5	8.2
Eu	1.8	1.7	1.6	1.5	1.5	1.8	1.7	1.7	1.7	1.6	1.6	1.8	1.7	1.7	1.7	1.6	1.8	1.6	1.7
Gd	7.6	7.3	7.2	6.9	6.3	7.7	7.7	7.4	7.4	7.2	7.1	7.3	7.6	7.0	7.2	7.0	7.4	6.9	7.1
Tb	1.0	0.9	1.0	1.0	0.8	1.0	1.1	1.1	1.0	1.0	1.0	1.0	1.1	1.0	1.0	1.0	1.1	1.0	1.0
Dy	6.2	5.8	5.9	6.1	5.1	6.3	6.4	6.5	6.5	6.1	6.1	6.2	6.7	5.8	6.0	5.7	5.9	5.7	5.8
Ho	1.1	1.0	1.1	1.1	0.9	1.1	1.2	1.2	1.2	1.2	1.2	1.2	1.3	1.1	1.1	1.1	1.1	1.1	1.1
Er	3.1	2.8	3.0	3.2	2.5	3.3	3.4	3.4	3.4	3.5	3.3	3.3	3.7	3.2	3.2	3.2	3.2	3.1	3.3
Tm	0.5	0.4	0.5	0.5	0.3	0.5	0.5	0.5	0.5	0.5	0.5	0.5	0.6	0.5	0.5	0.5	0.5	0.5	0.5
Yb	2.9	2.6	3.0	3.2	2.3	3.0	3.3	3.2	3.5	3.3	3.2	3.2	3.4	3.1	3.1	3.0	3.2	3.0	3.2
Lu	0.4	0.4	0.4	0.4	0.4	0.5	0.5	0.5	0.5	0.5	0.5	0.5	0.5	0.4	0.5	0.5	0.5	0.5	0.5
∑LREE	270.6	256.2	250.2	243.4	223.8	266.3	266.1	267.7	257.3	252.5	245.6	265.5	277.1	257.9	256.6	245.8	258.8	241.9	255.2
∑HREE	22.8	21.1	22.1	22.2	18.6	23.3	24.1	23.7	24.1	23.3	22.8	23.2	24.8	22.1	22.6	21.8	22.7	21.7	22.4

∑LREE/∑HREE	11.9	12.1	11.3	11.0	12.1	11.4	11.1	11.3	10.7	10.8	10.8	11.5	11.2	11.7	11.4	11.3	11.4	11.1	11.4
∑REE	263.1	248.8	243.1	234.5	217.6	258.1	257.6	257.8	245.9	242.8	235.5	256.6	267.1	250.4	249.1	237.2	249.1	232.7	247.9
Eu/Eu*	0.7	0.7	0.6	0.6	0.7	0.7	0.6	0.7	0.7	0.7	0.7	0.7	0.7	0.7	0.7	0.7	0.7	0.7	0.7
Ce/Ce*	1.0	1.0	1.0	1.0	1.0	1.0	1.0	1.0	1.0	1.0	1.0	1.0	1.0	1.0	1.0	1.0	1.0	1.0	1.0
(La/Lu)N	13.1	13.9	12.6	11.4	13.2	12.0	10.1	11.1	10.6	10.6	10.7	11.8	11.8	12.5	12.0	11.5	11.8	11.4	11.5
(Gd/Yb)N	1.7	1.8	1.7	1.5	1.8	1.7	1.6	1.5	1.4	1.5	1.5	1.6	1.5	1.6	1.7	1.6	1.6	1.5	1.6
(La/Sm)N	3.9	4.1	4.0	3.9	3.9	4.0	3.7	4.1	4.0	4.1	4.1	4.1	4.2	4.1	4.0	4.0	4.0	4.1	4.1
(La/Yb)N	10.2	10.5	10.0	8.9	10.6	9.9	9.3	9.3	8.4	9.0	8.8	9.8	9.5	10.2	10.1	9.4	9.4	9.2	10.2

Appendix 2.2: Depths of the analyzed samples.

Well	Sample	Depth (ft)	Lithology
EM 1	S1	4540-5460	Sandstone
	SH1	4580-4600	Shale
	S2	4600-4620	Sandstone
	SH2	4680-4700	Shale
	SH3	5600-5620	Shale
	S3	5780-5800	Sandstone
	SH4	5900-5920	Shale
	S4	5960-5980	Sandstone
	SH5	6660-6680	Shale
EM 4	S5	4480-4500	Sandstone
	SH6	4520-4540	Shale
	S6	4540-4560	Sandstone
	SH7	4580-4600	Shale
	S7	4620-4640	Sandstone
	SH8	5380-5400	Shale
	S8	5460-5480	Sandstone
	SH9	5740-5760	Shale
	S9	5860-5880	Sandstone
	SH10	6000-6020	Shale
EM 5	S10	4600-4620	Sandstone
	SH11	4620-4640	Shale
	S11	4680-4700	Sandstone
	SH12	4700-4720	Shale
	SH13	5520-5540	Shale
	S12	5700-5720	Sandstone
	SH14	5860-5880	Shale
	S13	5920-5940	Sandstone
	SH15	6040-6060	Shale
EM 6	S14	4500-4520	Sandstone
	SH16	4540-4560	Shale
	S15	4580-4600	Sandstone
	SH17	4620-4640	Shale
	SH18	5400-5420	Shale
	S16	5500-5520	Sandstone
	SH19	5660-5680	Shale
	S17	5820-5840	Sandstone

Appendix 2.3: Enrichment factors (EF) for selected trace elements in Agbada shales

Element	Min	Max	Range	Mean
Co	0.74	0.89	0.74 - 0.89	0.83 ± 0.04
U	5.38	9.62	5.38 - 9.62	6.81 ± 1.35
V	0.66	0.83	0.66 - 0.83	0.76 ± 0.06
Mo	0.56	5.86	0.56 - 5.86	2.34 ± 1.50
Cu	0.41	1.59	0.41 - 1.59	0.83 ± 0.04
Zn	0.65	1.80	0.65 - 1.80	0.82 ± 0.25
Ni	0.26	0.74	0.26 - 0.74	0.32 ± 0.10
Cr	0.68	1.66	0.68 - 1.66	0.93 ± 0.28

Chapter III

Diagenetic imprints in the reservoirs of Agbada Formation, Niger Delta Basin: Implication for reservoir quality and appraisal of calcite cement

Brume Overare [a, b*], Karem Azmy[a], Eduardo Garzanti[c], Enivwenaye Oghenero Avwenagha[d], Juliet Edafiwogho Emudianughe[b]

[a]Department of Earth Sciences, Memorial University of Newfoundland, St. John's, NL, A1B 3X5, Canada.

[b]Department of Earth Sciences, Federal University of Petroleum Resources, P.M.B 1221, Effurun, Delta State, Nigeria

[C]Laboratory for Provenance Studies, Department of Earth and Environmental Sciences, University of Milano-Bicocca, Piazza Della Scienza 4, 20126 Milano, Italy.

[d]Department of Earth Sciences, Arthur Jarvis University, Akpabuyo, P.M.B 1404, Calabar, Cross River State, Nigeria

[e]Department of Geology, Faculty of Sciences, Federal University Lokoja, Lokoja, Nigeria

*Corresponding author's e-mail address: boverare@mun.ca.

Marine and Petroleum Geology 163 (2024) 106746

https://doi.org/10.1016/j.marpetgeo.2024.106746

Abstract

The main exploration targets for hydrocarbons in the Niger Delta Basin are within the Agbada sandstone reservoirs. The current study utilizes a multitechnical approach (SEM-MLA, SEM-EDS, XRD and LA-ICP-MS) to evaluate the roles of framework composition and diagenetic processes, particularly calcite cementation on reservoir quality in Miocene intervals of the Agbada Formation sandstone, Niger Delta Basin. Petrographic analysis reveals that the sandstones are feldspatho-quartzose to quartzose sandstones, with a preponderance of quartzose sandstones. The overall diagenetic imprints suggest minimal compaction and lack of pervasive cement, which have contributed significantly to the high porosity. Although the degree of mechanical compaction is generally low, it has comparatively exercised a better control on porosity than the growth of cements, excluding some intervals with considerable cementation (siderite and ferroan calcite) where compactional porosity-loss was minimal. The occurrence of ferroan calcite cement ($CaCO_3$ = 95.9 ± 0.4, $MgCO_3$ = 0.8 ± 0.1, $FeCO_3$ = 2.9 ± 0.2 mol%) is generally small, probably discontinuous and unlikely to represent significant barriers to fluid flow with their localized influence, but understanding their locally significant influence may still contribute to building good reservoir models. Petrographic observations suggest that the precipitation of "poikilitic" calcite was early, but the shale normalized REY patterns do not mimic seawater patterns (Y/Ho ratios; 36.3 ± 1.6) due to possible contributions from clastic or detrital grains and/or incorporation of particulate matter that can preferentially scavenge LREEs from the overlying water column. A possible concern during reservoir production is the occurrence of clay mineral matrix (mostly kaolinitic) anticipated to cause the production of fines and formation damage, but this can be mitigated with proper reservoir management.

3.1. Introduction

A crucial part of hydrocarbon exploration and production in sedimentary basins involves understanding and predicting the temporal and spatial variations of reservoir quality within a diagenetic framework since it can significantly modify reservoir quality by reducing porosity through compaction and cementation or enhance it through dissolution. For instance, calcite cementation in sandstone reservoirs may dramatically reduce the reservoir quality because the cemented intervals may act as barriers to fluid flow, although early calcite cements can provide a framework that has the potential to resist burial compaction and therefore retain porosity until decarbonatization at greater depth (e.g., Hesse and Abid, 1998; Blamey et al., 2014; Liu et al., 2014; Caracciolo et al., 2014; Xiong et al., 2016; Civitelli et al., 2023).

The siliciclastic Niger Delta province, located on the continental margin of West Africa, has been a hub for hydrocarbon exploration and production for over six decades. It hosts several great discoveries in both onshore and offshore parts of the deltaic system and has been extensively studied by many authors (e.g., Allen, 1965; Short and Stauble, 1967; Evamy et al., 1978; Ekweozor and Okoye, 1980; Ejedawe and Coker, 1984; Stacher, 1995; Eneogwe, 2004; Owoyemi and Willis, 2006; Akinlua and Ajayi, 2008; Reijers 2011; Anomneze et al., 2015; Osokpor et al., 2016; Chudi et al., 2018; Akinlua et al., 2020; Ogbe et al., 2021). These studies, which are mostly skewed toward understanding the petroleum system of the basin, make up a rich platform for discussing and projecting various aspects of the basin's geology. However, little has been done to determine the origin of diagenetic cements and their impact on reservoir quality. Considering the geologic settings of the area and the large siliciclastic influx, calcite cemented intervals are rare but do locally occur. Given that calcite cementation influences the porosity and permeability of reservoirs, thereby affecting fluid flow during production, understanding the controls on calcite cement distribution has important economic implications (Dutton 2008). Even though the calcite cement in the sandstones of the Agbada Formation is

scarce and requires a rigorous examination to identify, its influence may still be locally considerable. Therefore, this study attempts to examine the diagenetic imprints of the sediments and the influence of rare calcite cemented intervals. The purpose is to support reservoir quality prediction in the subsurface by ascertaining whether there is a relationship or connection between diagenetic minerals and porosity distribution. The main objectives are to (i) investigate the petrographic characteristics of the Agbada sandstones and the diagenetic evolution of their cements, (ii) shed light on the paragenetic sequence of the cementation events and highlight their influence on porosity distribution, (iii) determine the diagenetic processes that have been more influential in shaping the reservoir quality, and (iv) elucidate the origin of calcite cements and their influence on porosity development.

3.2. Geologic Setting

The study area is located in the Niger Delta Basin (Fig. 3.1). The Cenozoic Niger Delta Basin is situated in the southern part of Nigeria, bordering the Atlantic Ocean and the Gulf of Guinea, and it represents a classic example of a modern regressive delta (Doust and Omatsola, 1990). The basin evolution, sediment provenance, stratigraphy, and petroleum system have been extensively discussed by earlier studies (e.g., Allen, 1965; Short and Stauble, 1967; Burke, 1972; Weber and Daukoru, 1975; Evamy et al., 1978; Avbovbo, 1978; Whiteman, 1982; Doust and Omatsola, 1990; Kulke, 1995; Stacher, 1995; Tuttle et al., 1999; Osokpor et al., 2015; Overare et al., 2021; Nwajide, 2022; Pastore et al., 2023); therefore only a summary is presented in the current study.

The impact of basement tectonics as a structural control on the evolution of the Niger Delta was notably restricted to movements along the fracture zones of the Equatorial Atlantic Oceanic, which extended beneath the delta and shaped the initial locus into which the proto-Niger River has built its delta (Reijers et al., 1997). The delta's growth during the Cenozoic was initially promoted by pulses of sedimentation and deposition on a continental basement

dipping ocean-ward into the Gulf of Guinea, followed by progradation over a landward-dipping oceanic basement. As the delta advanced onto the oceanic crust, repeated subsidence of the oceanic basement produced the accommodation required to accumulate the thick prograding sedimentary sequence (Evamy et al., 1978; Hospers, 1971). The Niger Delta flexes in a seaward direction due to increased sediment loading, subsiding gradually in response to the slow thermal cooling of the underlying lithosphere (Reijers, 2011).

It is widely accepted that a distinctive combination of syn-sedimentary growth faults divides the basin into various depositional belts (Doust and Omatsola, 1990). The depobelts are thought of as transient basinal areas that succeed one another in space and time as the delta progrades southward, with each depobelt constituting an independent unit delimited by major bounding faults (Doust and Omatsola, 1990). Sedimentation within the depobelts depended on the depositional and subsidence rate, with syn-sedimentary growth faults largely upsetting the delicate balance (Evamy et al., 1978), a mechanism described as an "escalator regression" model (Knox and Omatsola,1989).

Boreholes penetrating the subsurface sequence usually encounter three siliciclastic units (Fig. 3.2) reflecting a proximal to basinward transition from continental to paralic facies and to distal pro-delta marine shales. These lithostratigraphic units are strongly diachronous and have been identified as Benin (Oligocene-Recent), Agbada (Eocene-Recent) and Akata (Paleocene-Recent) formations. In addition, the siliciclastic sequence consists of intraformational shale members (e.g., the Opuama and Afam Members) believed to reflect submarine paleochannels (Knox and Omatsola, 1989; Jubril and Amajor, 1991). Considering their characteristics, distribution and role in the formation of stratigraphic traps, they are of considerable interest to petroleum explorationists.

The Akata Formation (Fig. 3.2) consists of thick marine shale units, with sandy and silty beds representing turbidites and continental-slope channel fills (Tuttle et al., 1999). The

shales, widely regarded as the major hydrocarbon source rock in the basin, are typically overpressured, providing a mobile base for synsedimentary growth faults linked to the deposition of the overlying paralic units. The formation may reach 7000 m in thickness (Doust and Omatsola, 1990) in areas around the central part of the basin; however, in deep-water environments, it is ~5000m (Bilotti et al., 2005; Corredor et al., 2005).

The Agbada Formation (Fig. 3.2) represents the paralic sequence that overlies the Akata Formation, comprising channel sands and shoreface facies with minor shale in the upper parts and predominantly interbeds of shale and sands of roughly equal proportion in the lower section. It represents a transitional environment between the underlying Akata Formation and the freshwater-bearing sandstones of the Benin Formation evidenced in various recognised subenvironments; fluviatile, backswamp and lagoonal sediments, barrier bar sand, barrier foot comprising interbedded sand, silt, and clays, marine clay, and transgressive deposits (Weber and Daukoru, 1975). Although the Agbada Formation thins northward and towards the northwestern and eastern flanks of the delta, it attains a maximum thickness of 3940m in the central part of the delta (Avbovbo, 1978).

The Benin Formation (Fig. 3.2) represents an upper delta-top lithofacies of white, fine to coarse and pebbly, poorly sorted continental sands, with thin local interbeds of greyish brown shale containing plant fragments. Lignite occurs as thin streaks or finely dispersed fragments. The shales were deposited in back-swamps and oxbow lakes, whereas sandstones document point-bar deposits, channel fills, or natural levees (Reijers, 2011). The base of the Benin Formation is identified in boreholes as the first downhole occurrence of marine shale that contains distinctive marine microfauna (Short and Stauble, 1967). The thickness of the formation is variable, reaching a thickness of ~1970 m around the Warri-Degema area, which is considered the depocenter (Avbovbo, 1978), although Whiteman (1982) suggests it may exceed 2100 m.

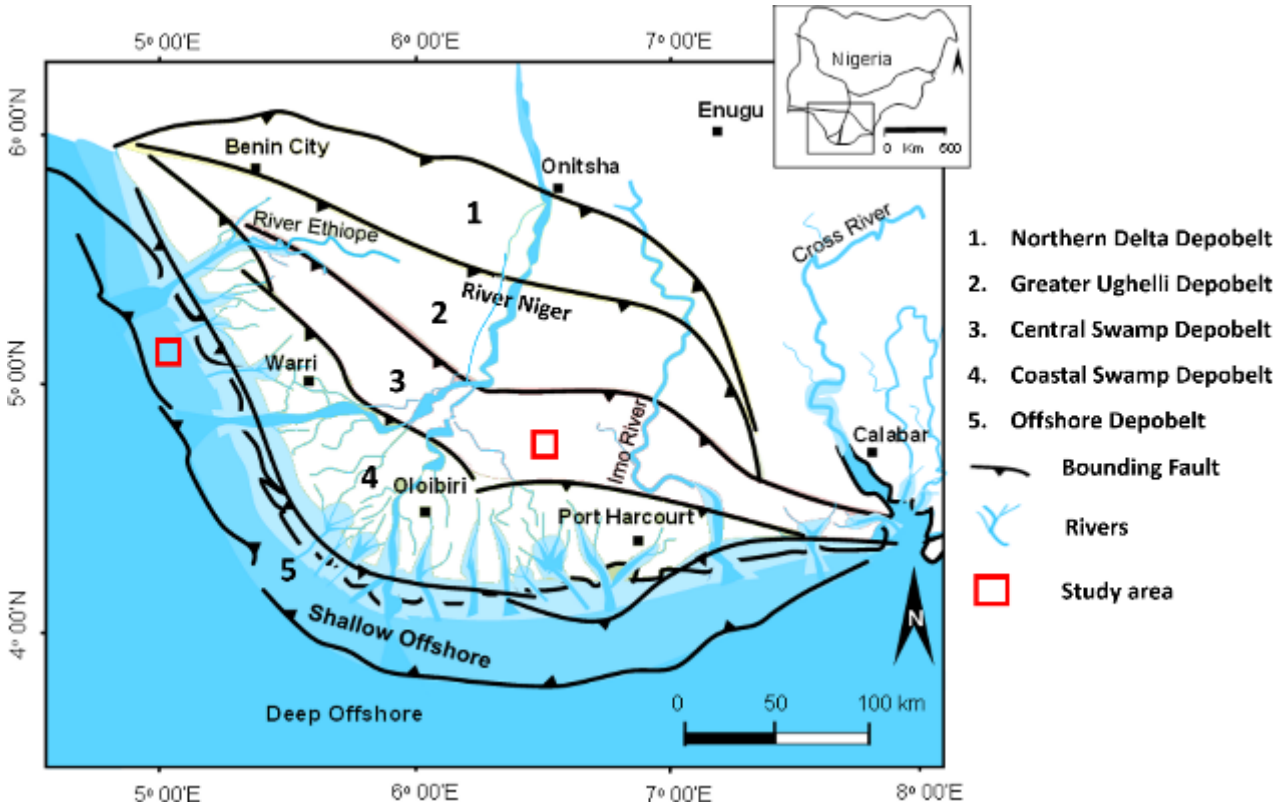

Figure 3.1: Simplified map of the Niger Delta indicating the study area. Structural limits and depobelts. Inset: Nigeria and Niger Delta region (modified from Overare et al., 2021).

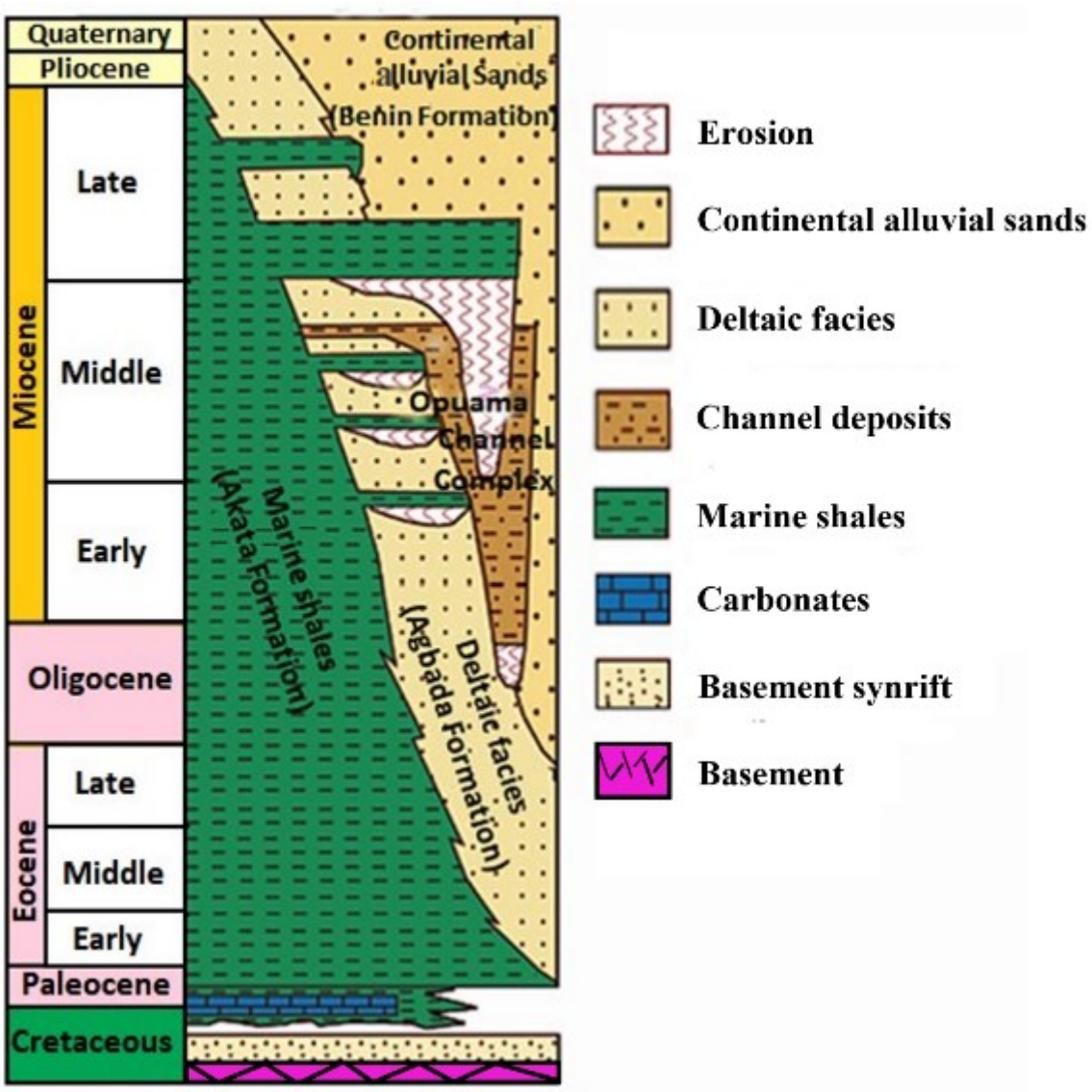

Figure 3.2: Regional stratigraphic framework of the Niger Delta (Maloney et al., 2010; Overare et al., 2021). Lithologic units in the subsurface are defined as Akata (Paleocene-Recent), Agbada (Eocene-recent) and Benin (Oligocene-Recent) formations.

One of the most noteworthy features in the Niger Delta Basin is the penecontemporaneous deformation of deltaic sediments, resulting in the formation of growth faults (Fig. 3.3) in response to the swift sedimentation and gravitational instability during the

deposition of the Agbada Formation over the under-compacted, highly pressured, and mobile shales of the Akata Formation (Merki, 1972; Hospers, 1971; Evamy et al., 1978). Associated with the growth faults are rollover anticlinal structures. Moreso, the lateral flow and extrusion of the Akata Shales and related extensional processes account for diapiric structures on the Niger Delta continental slope (Reijers et al., 1997). Details about these structures have been discussed by several authors (e.g., Merki, 1972; Weber and Daukoru, 1975; Evamy et al., 1978; Weber, 1987; Doust and Omatsola, 1990; Damuth, 1994; Stacher, 1995; Tuttle et al., 1999; Corredor et al., 2005; Krueger and Grant, 2011; Benesh et al., 2014). The growth faults and rollover structures comprise some of the most prominent hydrocarbon trapping systems in the Niger Delta Basin, but stratigraphic traps are not uncommon (Beka and Oti, 1995; Tuttle et al., 1999). The trapping system is connected to regional top seals formed from the transgressive marine shales, with faults often providing the framework for lateral seals. The integrity and properties of the reservoirs are generally influenced by the ratios of sandstone/shale and the sealing potential of the faults. The stratigraphic traps are mainly paleochannel fills, regional sand pinch-outs, and truncations (e.g., Orife and Avbovbo, 1982; Stacher, 1995). Although the upper Akata Formation turbidite sand facies are considered prospective targets for exploration, hydrocarbons in the basin are mainly produced from the Agbada Formation sandstone reservoirs (Tuttle et al., 1999).

There have been several views about the source rocks of the Niger Delta petroleum system (including deep-marine Akata Shales, interbedded marine shale intervals in the Agbada Formation, and Cretaceous shale at lower stratigraphic levels, e.g., Frankl and Cordry, 1967; Short and Stauble, 1967; Reed, 1969; Weber and Daukoru, 1975**;** Evamy et al., 1978; Ekweozor et al. 1979**;** Ekweozor and Okoye, 1980; Ejedawe et al., 1984; Ekweozor and Daukoru, 1984; Lambert-Aikhionbare and Ibe, 1984; Nwachukwu and Chukwura, 1986; Doust and Omatsola, 1990; Kulke 1995; Stacher, 1995; Tuttle et al., 1999; Haack et al. 1997; 2000;

Osokpor and Overare, 2019). However, it is widely accepted that the hydrocarbon in the Cenozoic Niger Delta Basin is sourced mainly from the marine-shale facies of the upper Akata Formation, with possible contributions from the lowermost shale facies of the Agbada Formation.

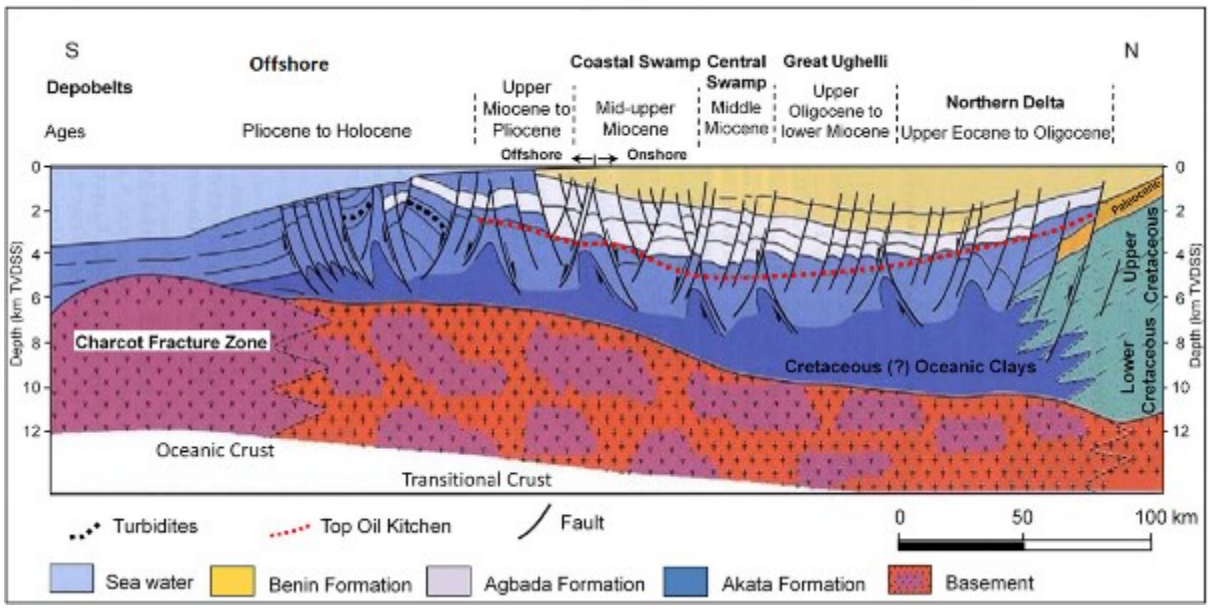

Figure 3.3: Section across the Cenozoic Niger Delta Basin illustrating depositional belts, diachronous lithostratigraphic units, and associated depositional structures (after Ogbe et al., 2020).

3.3 Methodology

Core samples acquired from oil companies operating in the Niger Delta Basin were thoroughly examined using various analytical techniques, including petrography, Scanning Electron Microscopy (SEM), Mineral Liberation Analysis (MLA), X-ray diffraction (XRD), and Laser ablation – inductively coupled plasma –mass spectrometry (LA-ICP-MS). Several challenges were encountered in this research, including the small size of many samples and the inability to invariably obtain fully adequate core samples and data due to constraints and limitations on their release and use. Moreover, many samples are poorly consolidated and thus difficult to prepare in the laboratory for an investigation focused on diagenetically precipitated minerals.

3.3.1. Petrography

Thirty-six (36) samples were thin-sectioned for petrographic examination, taking care to preserve the texture and fabric of interstitial cements. Most thin sections were impregnated with blue epoxy to highlight the pore spaces. The modal composition was obtained by counting 300 points for each thin section. Sandstones were classified according to the relative abundance of the three main groups of framework components (Q, quartz; F, feldspar; L, lithic fragments) considered if exceeding 10%QFL (classification scheme after Garzanti, 2016; 2019). Feldspatho-quartzose sand is thus defined as Q > F > 10%QFL > L, formally distinguishing between feldspar-rich (Q/F < 2) and quartz-rich (Q/F > 4) compositions (Garzanti et al. 2018a; Critelli et al., 2023).

A Nikon Eclipse E600POL microscope equipped with 4 x, 10 x, 20 x and 40 x lenses was used for routine petrographic examinations. Photomicrographs were taken with a Nikon DXM 1200F digital camera attached to the petrographic microscope and were used to estimate porosity by extracting colours on scanned thin sections using threshold methods. Image analysis was conducted with *JMicroVision* software.

3.3.2. Mineral Liberation Analyses (MLA)

A FEI MLA 650F scanning electron microscope (SEM; FEI, Hillsboro, OR USA) was used to carefully identify and quantify textures, cements, secondary alteration/phases, and pore space. The method uses backscattered-electron imaging of polished sections to delineate grain boundaries and uses different X-ray emissions with an energy-dispersive detector to assign mineral compositions based on elemental chemistry. MLA maps were made at 25kV, using the MLA GXMAP method, frame size 1.5mm x 1.5 mm, Fran resolution 500 x 500 pixels, and X-ray collection time 18 ms. Analysis was conducted in the Core Research Equipment and Instrument Training (CREAIT) facility at the Memorial University of Newfoundland (St. John's, Canada). Additional samples were analyzed at Brandon University Micro-analytical facility (Manitoba, Canada) with a JEOL JSM-6390 LV analytical scanning electron microscope (SEM) equipped with an Oxford instrument ULTIM MAX 100 Energy Dispersive Spectrometer (EDS), characteristic X-ray detector, and Aztec 4.1 analytical software. A 6.1 μm carbon coat was applied to the thin sections using a Leica EM ACE600 to make the samples conductive and eliminate surface charging. The samples were run at an acceleration voltage of 20 kV, working distance of 11 mm, and process time of 3 sec, with a minimum of 300,000 counts collected per analyzed spot/area. During analyses, copper tape was used for optimization and as an external standard before and every 2 hours. Because samples were coated with carbon, carbon was not included in the composition and results were normalized to 100%. Caution was taken in identifying and labeling minerals because surrounding minerals can influence analyses of tiny, micron-sized grains. Representative areas were processed using *ImageJ* software to estimate pore space.

3.3.3 X-ray diffraction (XRD)

Clay mineralogy in representative samples was determined by quantitative X-ray diffraction analysis and clay speciation at Activation Laboratories Limited (Ancaster, Ontario, Canada). A split of pulverized sample was mixed with corundum (also used as an internal standard) and packed into a standard holder. For clay speciation, another split of the sample was dispersed in distilled water, and clay minerals (< 2 μm fraction) were separated by settling of suspended particles. Oriented slides of the < 2 μm fraction were prepared by placing a portion of the suspension onto a glass slide. The oriented slides were analyzed dried after treatment with ethylene glycol and heating at 375°C. XRD analysis was performed using a Bruker D8 Endeavour diffractometer equipped with Cu X-ray source. Operational conditions were 40 kV and 40 mA, range 4-70 deg 2θ for random specimens and 3–30 deg 2θ for oriented specimens, step size 0 0.02 deg 2θ, time per step 0.5 sec, fixed divergence slit, angle 0.3°, and sample rotation 1 rev/sec. The PDF4/Minerals ICDD database was used for mineral identification. Quantities of mineral phases were determined using the Rietveld method based on the calculation of the full diffraction pattern from crystal-structure data. Semi-quantitative amounts of clay minerals in the < 2 μm fraction were calculated using the relative ratios of basal-peak areas.

3.3.4. Elemental Geochemistry

Representative samples of carbonate cement were ablated and analysed with a GeoLas 193nm ArF excimer laser (Coherent, Göttingen, Germany) coupled to an Element XR (Thermo Fisher Scientific, Bremen, Germany) for major, trace and rare-earth elements + Yttrium (REY) at the CREAIT Network (MUN, Memorial University of Newfoundland, Canada). The ICP-MS was tuned daily for high sensitivity and low oxide formation rate (ThO^+ / Th^+ < 0.3%). The laser was operated with a repetition rate of 5 Hz, an energy density of 4 J/cm^2, and a crater size of 40 μm. The background was recorded for 30 s at the beginning of each measurement, and

ablation was performed for 50 s. A carrier gas flow of lL/min of Helium was applied. NIST SRM 610 was used for standardization and MACS-1 as a quality control standard. Data evaluation was done with SILLS (Guillong et al. 2008). To verify that ablated pits were located within the spots of interest, samples were confirmed by careful petrographic examination under the FEI SEM-EDS system (MUN) after the analyses. The concentration of Ca was predetermined with an electron probe micro-analyzer (EPMA) at CREAIT Network (MUN). The technique is explained in detail by Olanipekun and Azmy (2022). The REY concentrations were normalized using Post Archaean Australian Shales (PAAS; McLennan, 1989) and anomalies were defined using established conventions (e.g., Bau and Dulski, 1996; Webb and Kamber, 2000). Y has been included in this investigation, considering its identical charge and similarity in atomic radii to its neighbours (Bau and Dulski, 1999; Jiang et al., 2015). For convenience, REY is used to denote rare earth elements and Yttrium throughout this study.

3.4. Results

3.4.1 Sandstone petrography

The studied sandstones are mostly fine to medium-grained (but vary from very fine to coarse grains) and well to moderately sorted, but some intervals are laminated and poorly sorted. Grains are mainly subangular to rounded, with mostly tangential contacts within a loosely packed framework; long contacts are rare. Composition is fairly homogeneously quartzose to quartz-rich feldspatho-quartzose (Appendices 3.1-3.2, Fig. 3.4, Fig. 3.5a-d, 3.6a-f), with no obvious variations in the wells (Fig. 3.4, Appendix 3.1). Accounting for 78–95 % of the sandstone framework, quartz consists of monocrystalline quartz locally, showing slightly undulose extinction and subordinate polycrystalline quartz with crenulated crystal boundaries (Fig. 3.6a-c). Feldspars, which comprise 3–18% of the sandstone framework, are mostly microcline (Fig. 3.6a-b), orthoclase with subordinate plagioclase (Fig. 3.6e-f), and rare occurrence of perthite. K-feldspar and plagioclase may be moderately altered (Fig. 3.6d-f), but

plagioclase sometimes appears slightly more altered. Metamorphic, plutonic, and sedimentary rock fragments represent ≤ 6% of framework grains.

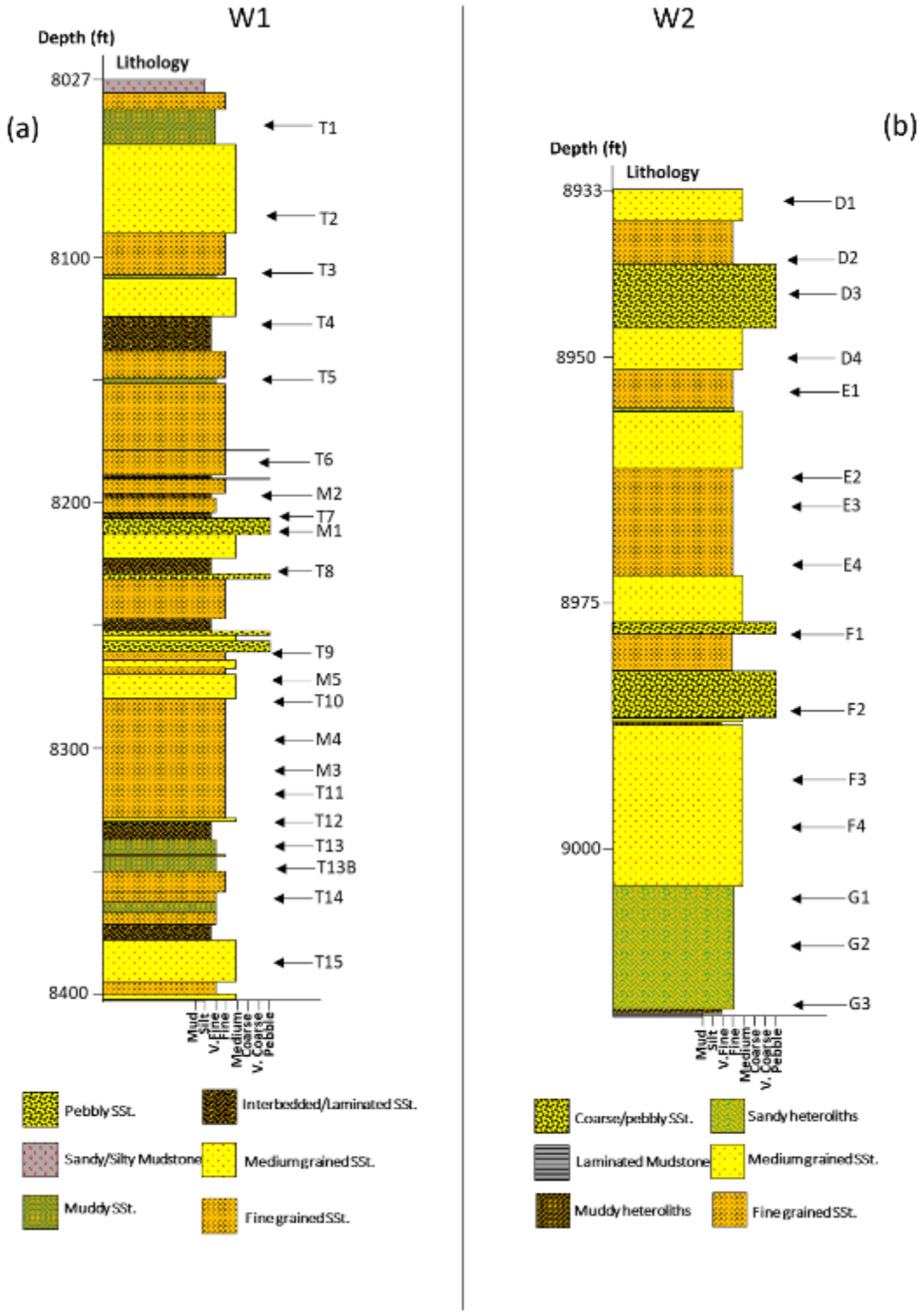

Figure 3.4: Simplified lithologic framework of the investigated wells.

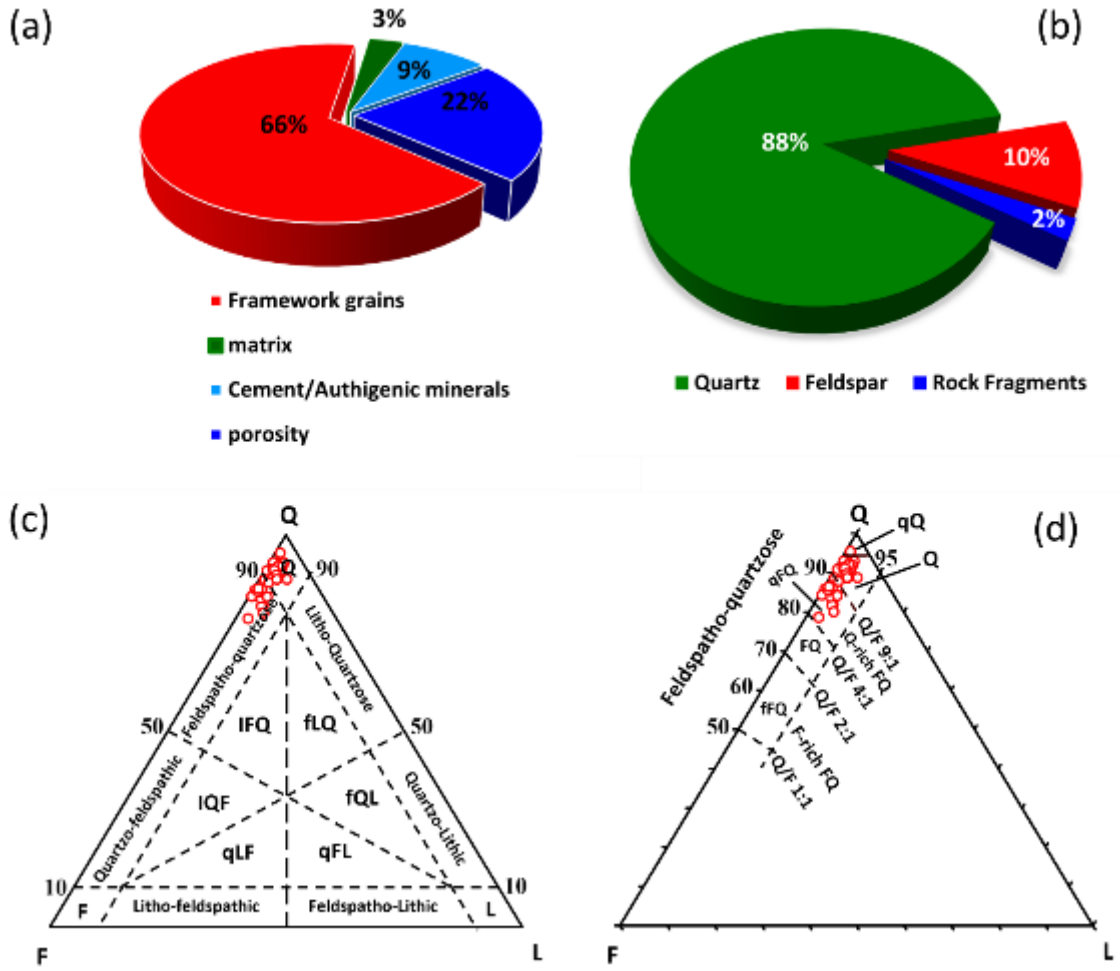

Figure 3.5: Petrography of the Agbada sandstones: (a) average rock composition; (b) average QFL modes; (c,d) classification as quartz-rich feldspatho-quartzose to quartzose sandstones (compositional field in the QFL diagram after Garzanti, 2019: Q, quartzose; pQ, pure quartzose; F, feldspathic; L, lithic; FQ, feldspatho-quartzose; fFQ, feldspar-rich feldspatho-qurtzose; qFQ, quartz-rich feldspatho-quartzose; lFQ, Litho-feldspatho-quartzose; lQF, litho-quartzo-feldspathic; qLF, quartzo-litho-feldspathic; qFL, quartzo-feldspatho-lithic; fQL, feldspatho-quartzo-lithic; fLQ, feldspatho-litho-quartzose).

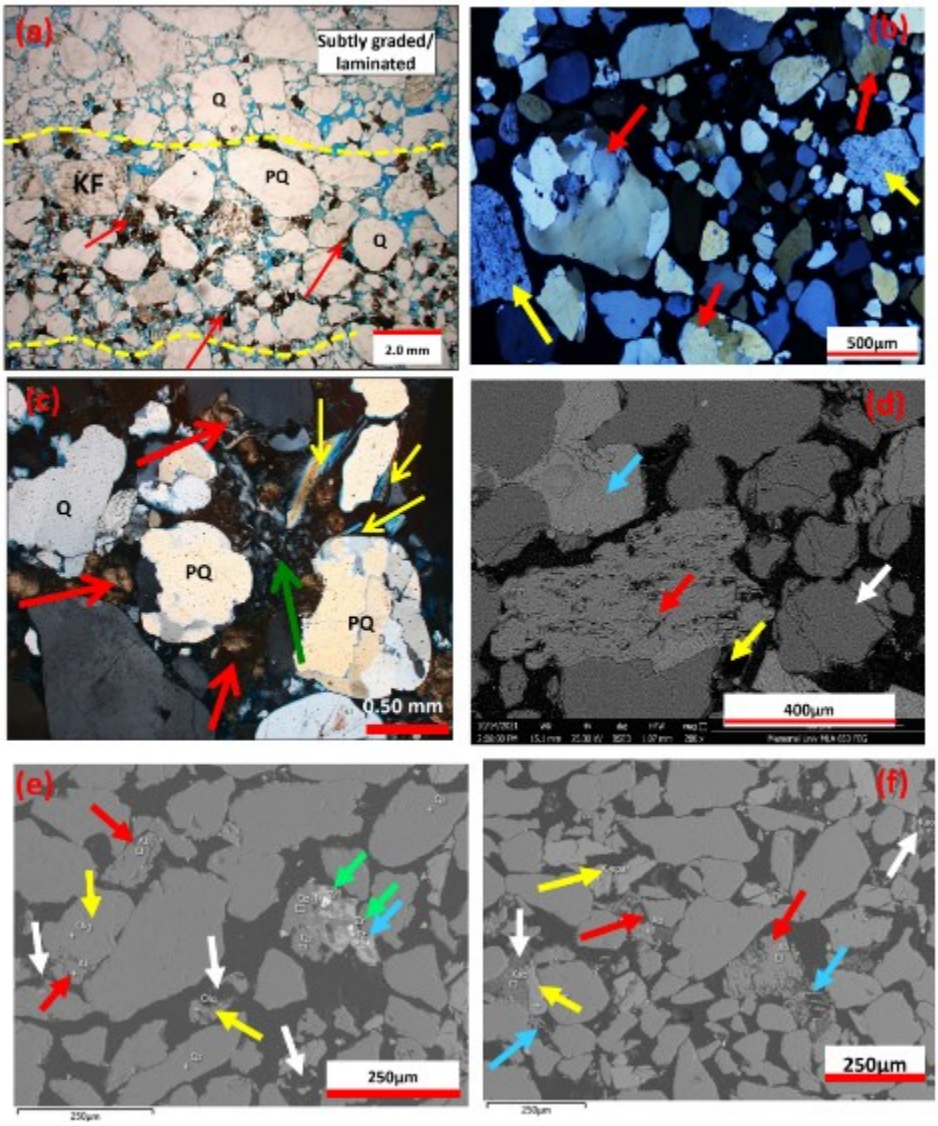

Figure 3.6: Photomicrographs and SEM images of the Agbada sandstone : (a) laminated quartz-rich feldspatho-quartzose sand. Interparticle porosity (IP) is high but locally occluded by siderite (red arrow). Minor secondary porosity is associated with partial dissolution of feldspars and rock fragments, PL; (b) Monocrystalline quartz associated with polycrystalline quartz (red arrow) and K-feldspar (yellow arrow). Note poor compaction and high interparticle porosity; XP, (c) Siderite (red arrows) and kaolinite (green arrows) occluding pores. Note the presence of slightly deformed muscovite (yellow arrows) and polycrystalline quartz grains, PX; (d) K-feldspar alteration to kaolinite (red arrow). The white arrow points at fractured quartz grain, the blue arrow at calcite cement, and the yellow arrow at dissolution pores, SEM; (e) quartz

grain with authigenic overgrowth, and inclusions of euhedral zircon (green arrows) and rutile intergrowths (blue arrow). White arrows point at dissolution pores, red and yellow arrows point at altered albite and oligoclase, respectively; SEM (f) backscattered-electron image of interlocking quartz, K-feldspar (yellow arrows), and albite (red arrows) with minor interstitial clay derived from the alteration of feldspar (kaolinite; white arrow). Blue arrows point at secondary porosity originating from the dissolution of feldspars or other unstable grains, SEM.

Elongated or tiny mica flakes (Fig. 3.6c) are common and frequently gently bent by compaction or slightly altered. Heavy minerals (Fig. 3.6e, Appendix 3.2) include zircon, rutile, and subordinately garnet, tourmaline, apatite, and iron oxide (hematite). Bioclasts are sporadically observed as well as phosphatic pellets (Fig. 3.7a-b) or green to greenish brown, slightly deformed to undeformed glauconite grains (Fig. 3.7a, 3.7c). Rare cryptocrystalline and euhedral rhombic carbonate grains (up to 50 μm in diameter; Fig. 3.7b) are also observed. Finer-grained samples may contain significant constituents of silt and clay. Clay minerals and organic matter occur in laminae as fine fragments associated with pyrite (Fig 3.7d-f).

3.4.2 Diagenetic minerals

Cementation in the Agbada sandstone is generally minimal, with replacement minerals/other authigenic phases also constituting a small portion. However, petrographic, SEM, BSEM, SEM-EDS, and SEM-MLA analyses revealed a variety of diagenetic minerals.

Siderite is the most common authigenic phase in the sandstones (Fig. 3.6a, 3.6c, 3.7e-f, 8a-c), although its proportion is variable. It is more abundant than calcite and appears light to very dark brown in thin sections, being the dominant carbonate cement in the Agbada sandstones. It occurs with no preferred orientation, with some zones reflecting substantial cementation by siderite. The interstitial siderite is microcrystalline and commonly replaces clay matrix (Fig. 3.7f, 3.8a), but occurs more commonly as a larger granular/spherulitic/rhombic

crystalline intergranular cement (Fig. 3.6a, 3.6c, 3.7e, 3.8b-c), that significantly fills pores and scarcely as rare thin rim (coatings) on grains.

Calcite (mainly ferroan) cement is subordinate to siderite in occurrence. Although SEM images provided a clearer picture of its occurrence, it occurs sporadically in relatively loose and undercompacted zones as pore-filling cement and occasionally as grain replacements. The calcite cement is mostly poikilitic, being the dominant pore-occluding cement in the zones of its occurrence as it causes a network of floating grains, leaving very little pore space visible in thin sections (Fig. 3.8d-f).

Appearing as alteration products, pore filling, detrital grains replacement types, and rims around detrital grains, clay minerals are mainly kaolinite which accounts for 81–98 % of the < 2 μm clay fractions that also contains illite (8–15 %) (Table 3.1-3.2, Fig. 3.9). Their concentration, textures and/or morphologies have been captured (Fig. 3.6c, 3.6f, 3.7f, 3.10a-d).

Authigenic pyrite is commonly disseminated as micron-sized framboids associated with clay and organic matter in finer-grained samples or found in blocky habits in open pore space, within patches of organic matter, between sheets of mica grains, or as replacement of grains or cement (Fig. 3.7d, 3.10e-f)

Quartz cementation is rare, but a few overgrowths (Fig. 3.6e, 3.8f, 3.10a, 3.11a) seem to occur on some detrital quartz grains with faint or no demarcation lines between the primary grain and secondary quartz overgrowth, but their mostly irregular surfaces oppose to whether they are diagenetic, suggesting possible inherited from the recycling of older sandstones (e.g., Barbera et al., 2011; Xiong et al., 2016; Critelli et al., 2018; Olanipekun and Azmy, 2022).

Diagenetic albitization of detrital feldspars also occurs locally, but it is hard to quantify; albite may also fill secondary pores generated by feldspar dissolution (Fig. 3.6e-f). Hematite

plausibly originated from the dissolution of unstable ferromagnesian heavy minerals as interstitial pore filling or as rare coatings on quartz grains (Fig. 3.8d, 3.10e, 3.11b-f).

3.4.3 Elemental and REE geochemistry of carbonate cement

The summary of the trace element concentrations of the investigated cements is presented in Table 3.3. The calcite cements (in mol %) consist of $CaCO_3$: 94.9–96.4 (95.9 ± 0.4), $MgCO_3$: 0.6–0.8 (0.7± 0.1), and $FeCO_3$: 2.9–3.7 (3.3 ± 0.2). Trace element composition of the calcite (in ppm) comprises Sr: 320–631 (459 ± 113), Mn: 2190 – 4428 (3582 ± 760), and U: 0.1–0.2 (0.1 ± 0.04).

The siderite cements (in mol %) contain $CaCO_3$: 6.5–10.9 (8.4 ± 1.4), $MgCO_3$: 25.5–28.1 (21.5 ± 2.1), and $FeCO_3$: 54.6–62.4 (56.8 ± 2.6). Trace element composition (in ppm) consists of Sr: 222 – 353 (290 ± 44), Mn: 1690–2892 (2509 ± 361), and U: 0.9–3.3 (1.5 ± 0.8).

The summary of the rare earth elements (REY) analyses of the Agbada sandstone calcite cements is presented in Table 3.4. The PAAS-normalized REY patterns of the calcite cements are illustrated in Figure 3.12. The calcite cements are similar in composition, exhibiting features that indicate: (1) slight LREE enrichment (Nd_{SN}/Yb_{SN} = 0.96-2.42; 1.42 ± 0.34), (2) Y/Ho ratios of 34.31 – 38.87; 36.30 ± 1.35, (3) no significant Ce and La anomaly, (4) a positive Gd anomaly with Gd_{SN}/Gd^*= 1.18–1.33; 1.25 ± 0.05 (5) a positive Eu anomaly defined by Eu_{SN}/Eu^* of 1.41-1.70; 1.59 ± 0.08.

3.5. Discussion

3.5.1 Paragenetic sequence

The reconstruction of paragenetic sequence encompasses the various stages of fluid flow that promoted the precipitation of authigenic minerals/cements and the dissolution of detrital framework grains. The Agbada sandstones generally reflect minimal diagenetic imprints and diagenetic minerals do not seem to be closely associated. Moreover, due to the constraints from a lack of geothermometric data, possible overlap in the growth sequence of

the cements, spatial characteristics and distribution of the growth sites, the timing of cementation can only be approximated. The general diagenetic sequence for the investigated Miocene Agbada sandstones was deciphered from textural relationships observed in thin-section slides and SEM images. The paragenetic sequence is presented in Figure 3.13.

The earliest diagenetic events are possibly the growth of glauconite and pyrite framboids and the formation of clays and/or iron oxides coating, followed by siderite and calcite cementations. Siderite cement and locally abundant ferroan calcite cements fill intergranular volume, thus occluding porosity, whereas other minerals are volumetrically insignificant to dramatically influence the reservoir's quality.

Minor grain coating clays (Fig. 3.7e) developed shortly after deposition through bioturbation activity or mechanical infiltration while sediments were exposed at the sea floor (Matlack et al., 1989; Moraes and De Ros, 1990, 1992; McIlroy et al., 2003; Needham et al., 2005; Worden et al., 2006; Rahman et al., 2016). Connected to bioturbation activities, the admixing and infiltration of detrital clays into newly deposited sediments opened a window for the distribution of clays as dispersed matrix and locally in laminae (Fig. 3.7d-f). Associated with detrital clay are pyrite framboids (3.7d, 3.10e-f, 3.14a), which also grew near the sediment-water interface, although framboidal pyrite occurs in dissolution pores (Fig. 3.10e), suggesting possible formation at later diagenetic stages.

Siderite precipitation (Fig. 3.6a, 3.6c, 3.7e-f, 3.8a-c, 3.11d-e) seems to have occurred early and continued for a while with the understanding that Fe was enriched in the depositional system, which is evident from the prevalence of siderite cement, especially with the absence of quartz overgrowths and the loose grain framework. Though locally abundant in the sandstones, some samples are cemented with calcite (ferroan) cement (Fig. 3.8d-f, 3.11c-d), which occurs as poikilitic crystals intergranular pores, engulfing framework grains (floating texture), thus suggesting precipitation before significant compactional porosity loss.

A relative sea-level fall almost certainly causes an influx of meteoric water during which the sandstones are flushed with low-saline marine pore waters (Morad et al., 2010; Bukar et al., 2021). When sandstones are subjected to conditions of acidic fluids such as meteoric water and/or organic acids, the dissolution of chemically unstable grains and feldspars becomes apparent (e.g., Critelli and Nilsen, 1996; Caracciolo et al., 2014; Lai et al., 2018c; Morad et al., 2010; Bjørlykke, 1998; Lei et al., 2019; Civitelli et al., 2023; Critelli et al., 2023). This event led to the dissolution of grains and the development of secondary intragranular pores (Fig. 3.8b), with feldspars and rock fragments being the most chemically labile. However, the dissolution might also have started earlier, presumably during weathering and sediment transport, but continued after the deposition (e.g., Le Pera et al., 2001; Scarciglia et al., 2005). The dissolution offers a condition of low pH that is suitable for the precipitation of kaolinite. The dissolved/partly decomposed feldspar grains (Fig. 3.6d-f, 3.8a, 3.14b-c) could easily have sourced the kaolinite, and this suggests that the feldspar grains were more abundant before their partial or complete dissolution. The low pH conditions connected to the influence of meteoric waters also led to the partial/complete dissolution of calcite cement (Fig. 3.14d). The dissolution process in the sandstone is believed to have continued through and after the onset of initial mechanical compactional processes and grain restructuring. Nevertheless, despite some evidence of compaction (Fig. 3.14b-c, 3.14e), it is generally considered low, as indicated by the dominant point contacts between grains explaining the lack of pressure dissolution and the minimal amount of quartz cement (Fig. 3.6e, 3.8f, 3.10a, 3.11a).

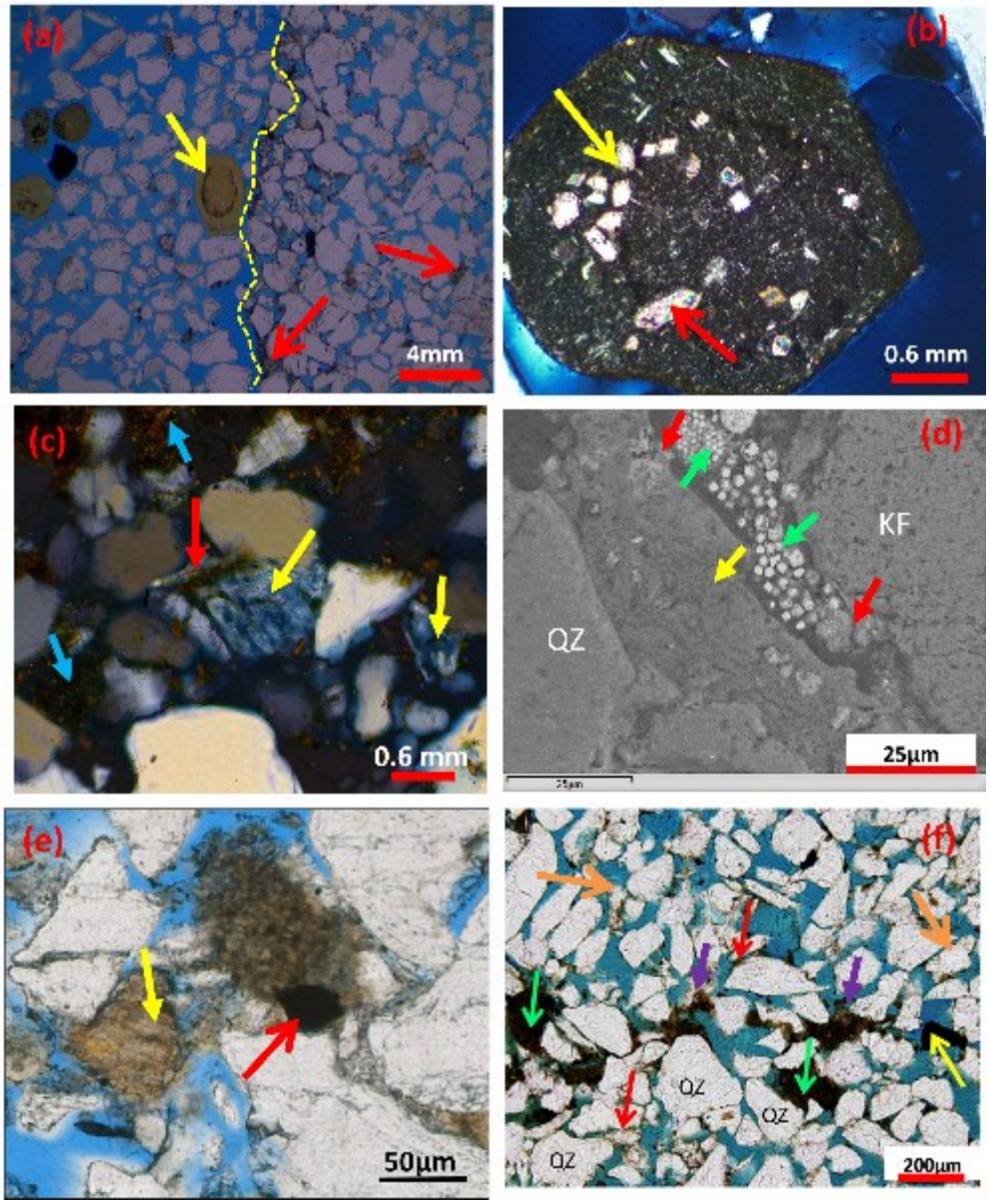

Figure 3.7: Photomicrographs and SEM features of the Agbada sandstone: (a) contact (dashed yellow line) between medium-coarse sand (left) and oversized intraformational pebble (right). Yellow arrow points at large phosphatic pellet with sub-circular concentration of opaques. Red arrows point at glaucony grains, PL; (b) enlarged view of the pellet in (a), depicting a 100-µm-long euhedral tourmaline crystal (red arrow) and dolomite rhombs at centre left (yellow arrow), PX; (c) glaucony grains (yellow arrows), broken into smaller fragments and altered around edges to darker material rich in iron and organic matter (blue arrows). Red arrow points at

deformed muscovite, PX; (d) backscattered electron image of pyrite framboids (green arrows) with hematite (red arrows) reaction rims, along with iron and chlorite-rich clay (yellow arrow) infilling void between quartz (Qz) and K-felspar (KF) clast, SEM; (e) replacement pyrite (red arrow) in a chlorite rich clay-matrix and patchy (yellow arrow) siderite cement, PL; (f) Altered potassium feldspars (orange arrows), minor clay coats (red arrows), blocky pyrite (yellow arrow) and siderite cement (green arrows) replacing clay matrix (purple arrows) in a porous network of grains, PL.

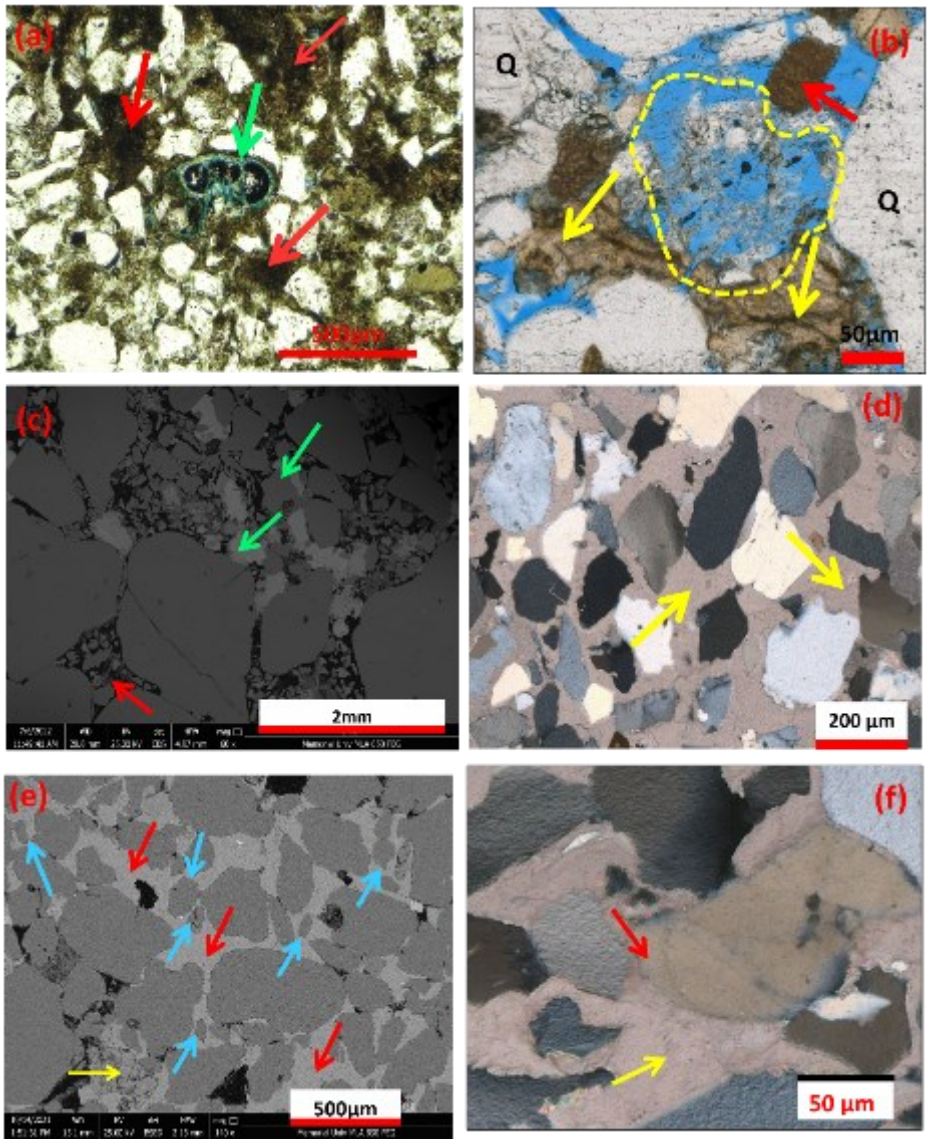

Figure 3.8: Photomicrographs and SEM features of the Agbada sandstone: (a) fine quartz-rich sandstone with abundant brown siderite cement (red arrows) associated with organic matter and opaque iron-oxides. Green arrow points at benthic foraminifera, PL; (b) pore-filling siderite cement (yellow arrows). Dashed yellow contour outlines porosity that originated from feldspar dissolution. Red arrow points at argillaceous rock fragments, PL; (c) illitic clay intergrown with muscovite (red arrow) and pore-filling siderite locally replacing matrix (green arrow), SEM; (d) poikilitic calcite cement occluding pores in a network of grains that appear to float, PX; (e) Floating grains (blue arrows) in a framework of calcite cement (red arrow)

with local replacement of feldspar (yellow arrows), SEM; (f) rare quartz overgrowths (red arrow) enclosed by poikilitic calcite cements (yellow arrow), PX.

Progressive burial and the associated higher temperature favoured the precipitation of illite (Fig. 3.8c, 3.11e) and conversion of some kaolinite to illite by reaction with K^+ supplied from the dissolution of K-feldspar (Bjørlykke, 2014). Minor authigenic chloritic Fe-clays (Fig. 3.7d, 3.11e) might have also occurred in this stage, occluding some porosity outside the calcite cemented areas. Blocky pyrite cements seem (Fig. 3.7f) to have been deposited at the latest diagenetic stages since they replaced chlorite.

3.5.2 Cement Sources

3.5.2.1 Pyrite Framboids

Pyrite precipitated by bacterial sulphate reduction phase during early diagenesis in a deoxygenated environment at a relatively shallow burial, confirming the influence of marine sedimentary environment. Framboidal pyrite (3.7d, 3.10e-f, 3.14a) formed by bacterial sulphate reduction in the interstitial waters (Berner, 1981). Sulphate-reducing bacteria utilise sulphate from seawater to consume organic fragments in sediment, leading to the formation of H_2S and subsequently pyrite formation when H_2S reacts with iron oxides within the oxic-anoxic interface (sediment-water interface; Berner, 1970, 1981; Morad, 1986). The sulphide was probably derived from reduced marine aqueous sulphate and the iron was from Fe-rich clastic sediments in the depositional system.

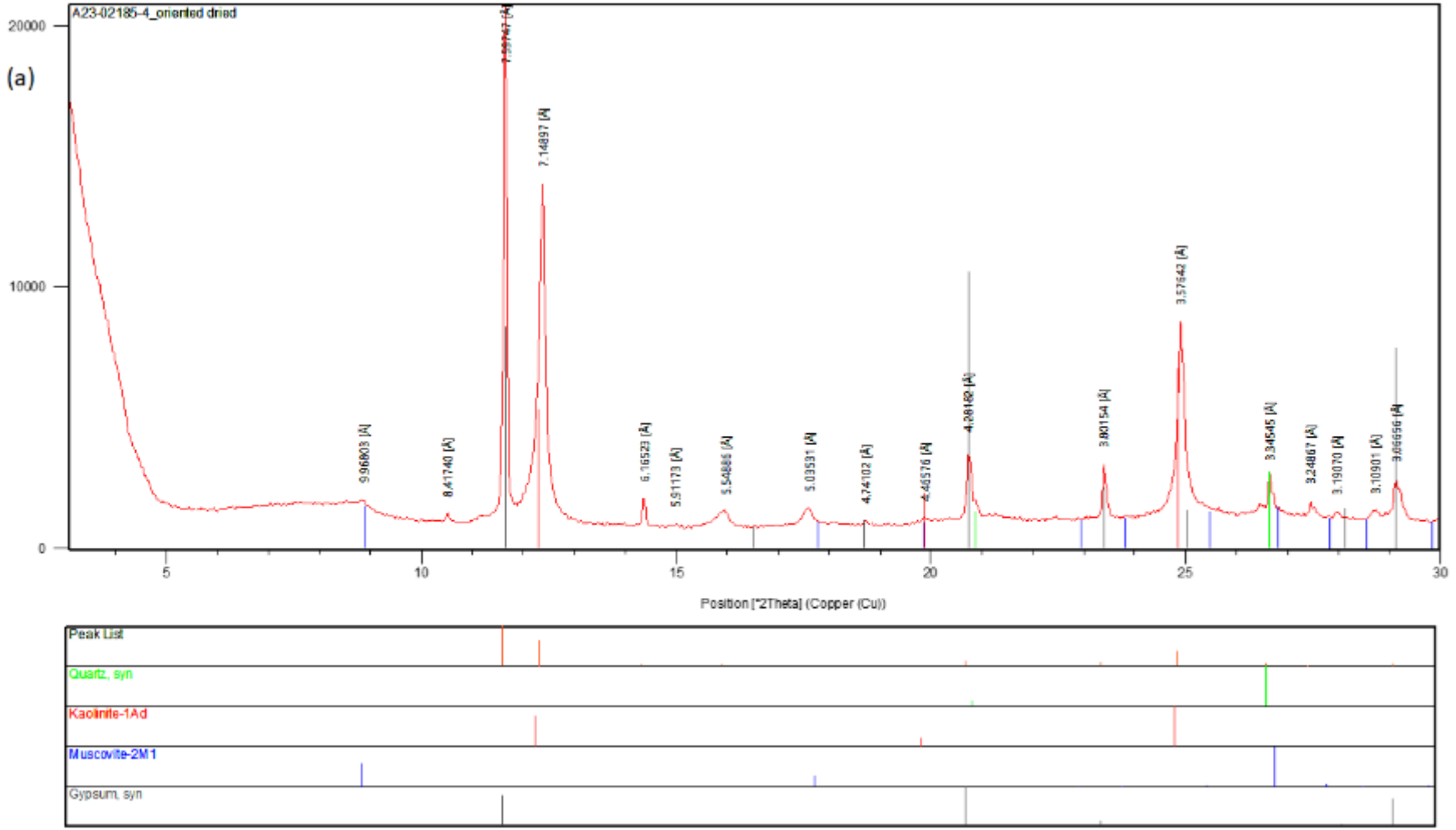
A23-02185-4_oriented dried
(a)
20000
10000
0
7.14897 [Å]
9.96603 [Å]
8.41740 [Å]
6.16523 [Å]
5.91173 [Å]
5.54886 [Å]
5.03591 [Å]
4.74102 [Å]
4.46576 [Å]
4.28182 [Å]
3.80154 [Å]
3.57642 [Å]
3.34545 [Å]
3.24887 [Å]
3.19070 [Å]
3.10901 [Å]
3.06556 [Å]
5
10
15
20
25
30
Position [°2Theta] (Copper (Cu))
Peak List
Quartz, syn
Kaolinite-1Ad
Muscovite-2M1
Gypsum, syn

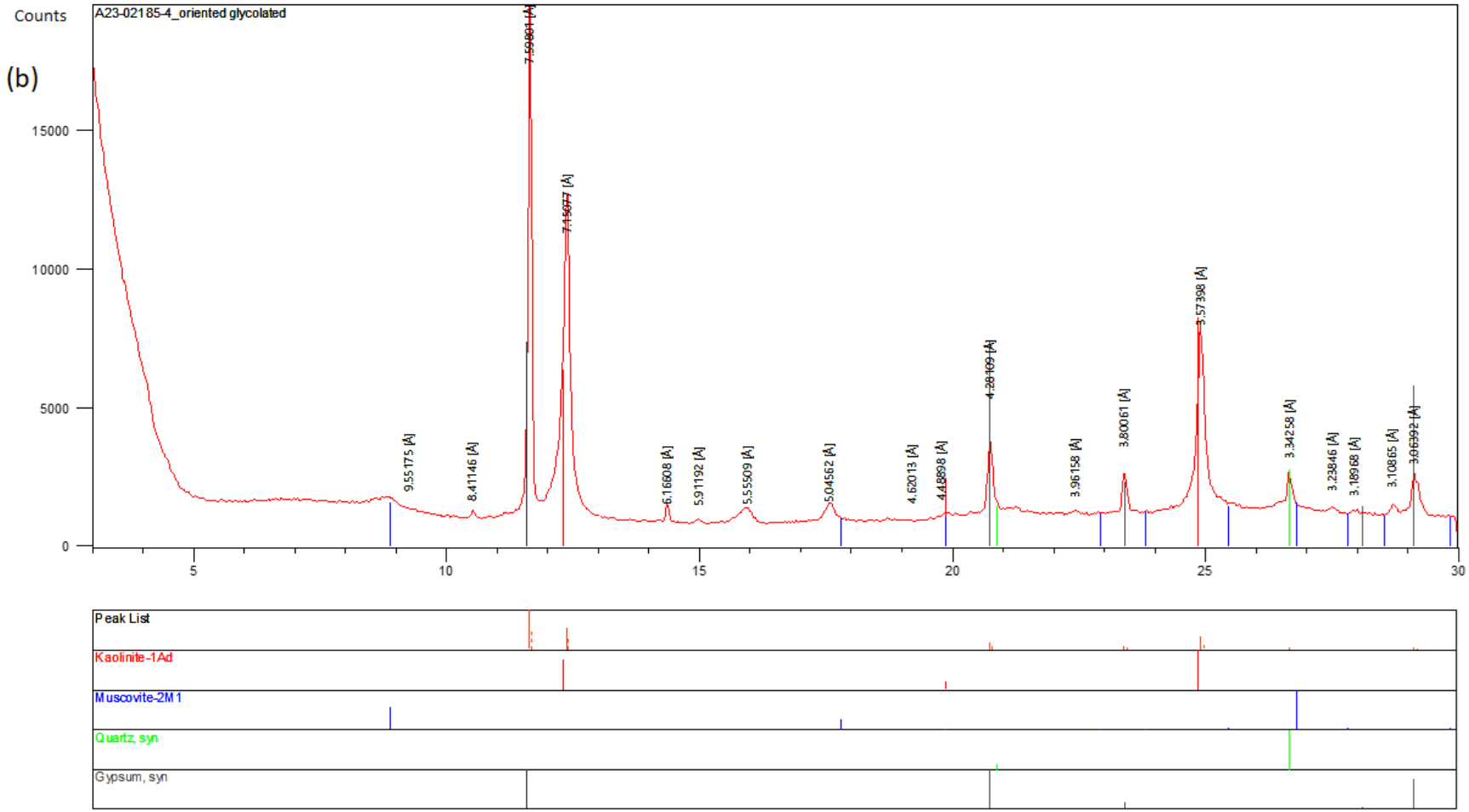
Counts
A23-02185-4_oriented glycolated
(b)
15000
10000
5000
0
5
10
15
20
25
30
9.55175 [Å]
8.41146 [Å]
7.59801 [Å]
7.15077 [Å]
6.16608 [Å]
5.91192 [Å]
5.55509 [Å]
5.04562 [Å]
4.62013 [Å]
4.48898 [Å]
4.28169 [Å]
3.96158 [Å]
3.80061 [Å]
3.57398 [Å]
3.34258 [Å]
3.23846 [Å]
3.18968 [Å]
3.10865 [Å]
3.06392 [Å]
Peak List
Kaolinite-1Ad
Muscovite-2M1
Quartz, syn
Gypsum, syn

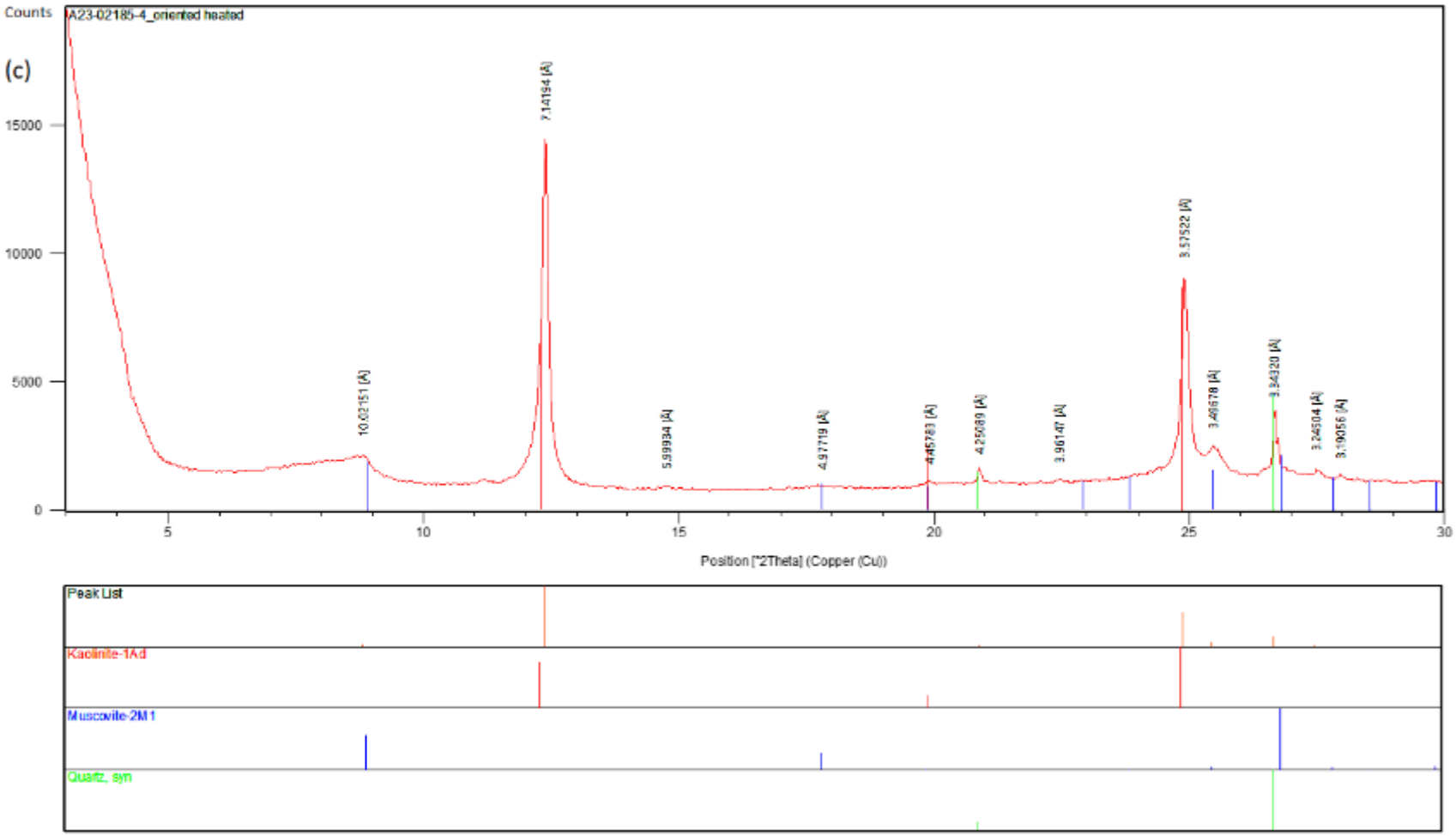
Counts
A23-02185-4_oriented heated
(c)
15000
10000
5000
0
10.02151 [Å]
7.14194 [Å]
5.99934 [Å]
4.97719 [Å]
4.45783 [Å]
4.25589 [Å]
3.96147 [Å]
3.57522 [Å]
3.49678 [Å]
3.34320 [Å]
3.24504 [Å]
3.19056 [Å]
5
10
15
20
25
30
Position [°2Theta] (Copper (Cu))
Peak List
Kaolinite-1Ad
Muscovite-2M1
Quartz, syn

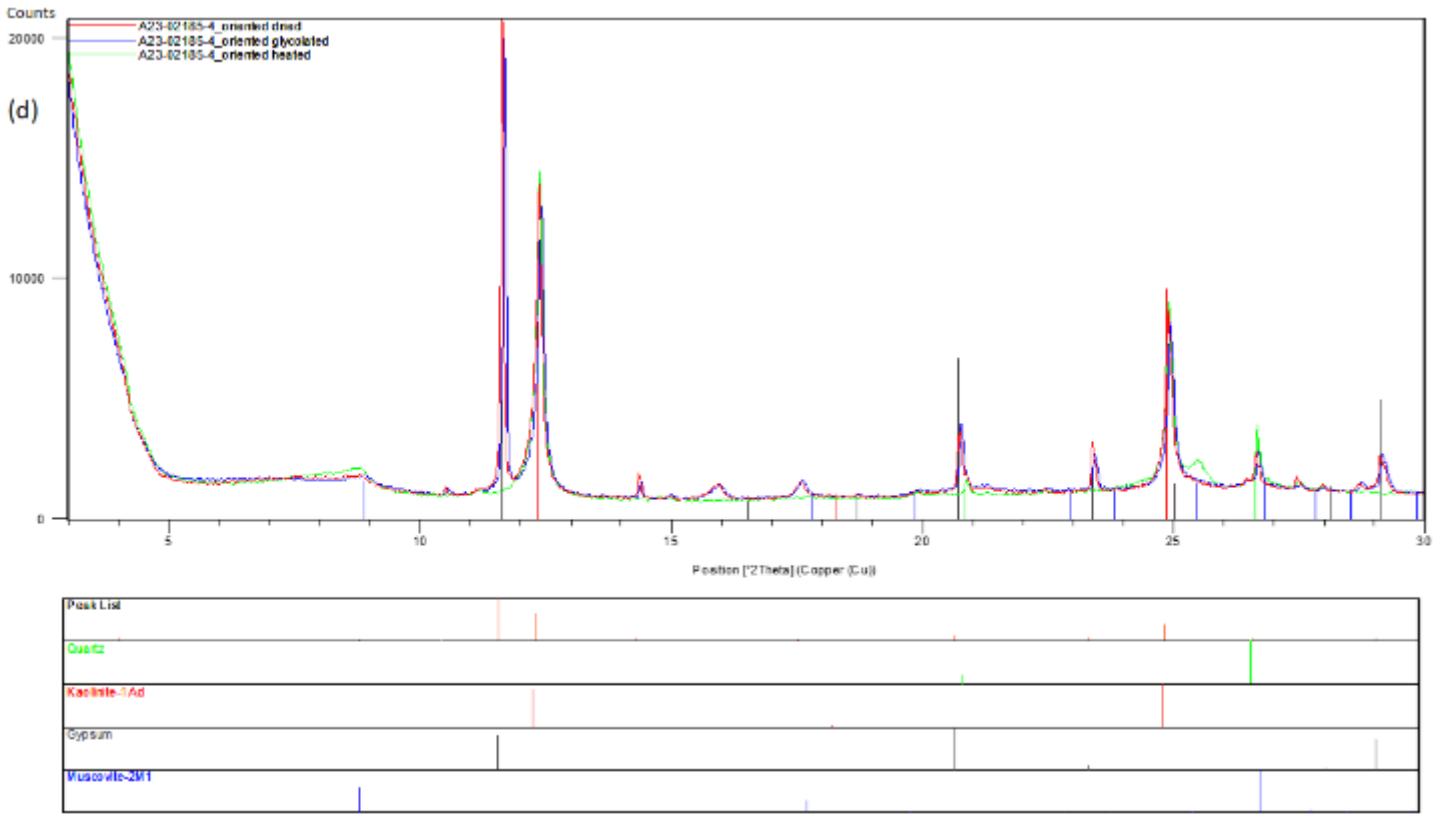

Fig. 3.9. Representative XRD patterns of < 2 µm fraction of the Agbada Sandstones (a) Oriented dried (b) ethylene glycol treated (EG) oriented aggregate (c) oriented heated (d) XRD patterns of (a), (b) and (c)

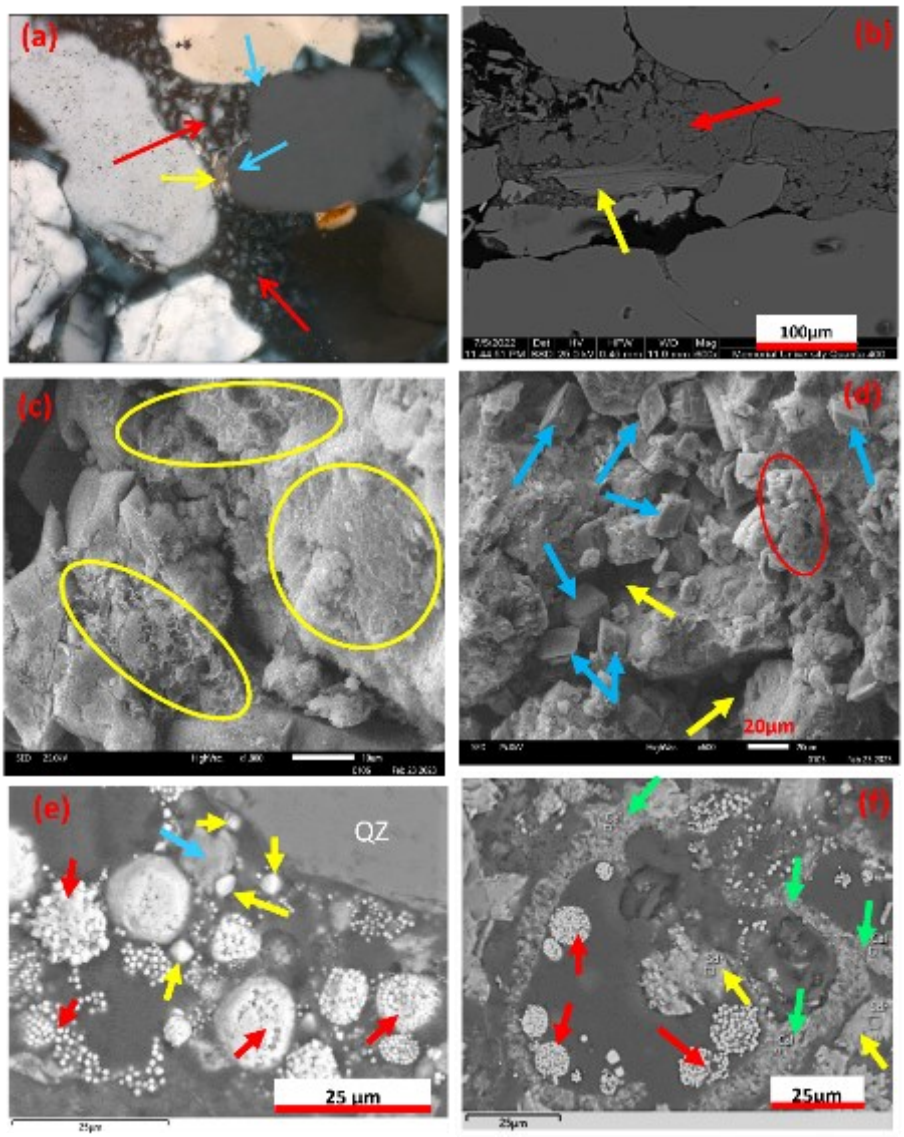

Figure 3.10: Photomicrographs and SEM features of the Agbada sandstone: (a) pore-filling kaolinite (red arrows). Blue and yellow arrows point at rare quartz overgrowths and bent muscovite, respectively, PX; (b) kaolinite (red arrow) occluding pore spaces. Note the transformation of biotite (yellow) to kaolinite (yellow arrow), SEM; (c) rare thin grain coating illite/smectite mixed layer clay (yellow circles), SEM; (d) minor grain coating kaolinite platelets (red circle), grain coating/pore lining granular/rhombs (blue arrows) of siderite occluding intergranular pore system (yellow arrows), SEM; (e) Framboidal pyrite (red arrows), appears to be an open pore filling, with some hematite alteration (blue arrow). Note the presence of minor euhedral pyrites (yellow arrows), SEM; and (f) backscattered electron image

reflecting pyrite agglomerates (red arrows), which appears to be an open space filling of void along with calcite (green arrow) and siderite (yellow arrow), SEM.

Table 3.1: Whole-sample XRD mineralogical composition (%) of the Agbada sandstones

Sample	M1	M4	M5	T6	T7	T12	T13e	T13
Quartz	94.1	60.7	72.0	77.2	70.8	41.6	88.6	78.0
K. Feldspar	3.6	10.73	11.6	10.5	14.9	14.3	6.1	11.0
Plagioclase	0.8	7.4	14.3	9.8	9.62	6.3	3.7	8.6
Kaolinite	1.0	13.3	2.1	2.4	4.6	11.8	0.8	2.3
Calcite	-	-	-	-	-	1.69	-	-
Ankerite	-	-	-	-	-	3.1	-	-
Siderite	Trace	7.2	Trace	Trace	-	21.2	Trace	Trace
Muscovite/illite	Trace	0.67	trace	-	-	0.10	0.8	-
Halite	0.5	-	-	-	-	-	-	-
Gypsum	-	-	-	-	-	-	Trace	-

Table 3.2: The <2 μm fraction mineralogical composition (%) of the Agbada sandstones

Sample	M1	M5	T7	T13e
Kaolinite	92	81.9	98.4	87
Illite	8	15.9	-	13
Mica-Vermiculite	Trace	-	-	-
Halite	-	-	1.5	-
Quartz	-	2.2	0.1	-
	-	-	-	-

Table 3.3: Statistical summary of minor and trace element contents of calcite and siderite cements in the investigated sandstones

Sample	Cement	Statistics	$CaCO_3$ (mol%)	$FeCO_3$(mol%)	$MgCO_3$(mol%)	Mn(ppm)	Sr(ppm)	U(ppm)
		n	3	3	3	3	3	3
T9	F. Calcite	mean	95.5	3.0	0.9	4131	478	0.1
		S. D	0.4	0.1	0.0	309	125	0.1
		Max	95.9	3.0	0.9	4428	625	0.21
		Min	94.9	2.9	0.8	3704	320	0.07
M5	F. Calcite	n	4	4	4	4	4	4
		mean	96.2	2.7	0.8	3447	382	0.1
		S. D	0.2	0.1	0.1	726	37	0.0
		Max	96.4	2.9	0.9	3900	414	0.1
		Min	95.8	2.6	0.7	2190	320	0.1
T10	F. Calcite	n	3	3	3	3	3	3
		mean	95.7	3.0	0.9	3639	436	0.1
		S. D	0.2	0.2	0.1	828	123	0.0
		Max	96.0	2.8	1.0	4403	608	0.2
		Min	95.4	3.3	0.8	2488	336	0.1
T13	F. Calcite	n	4	4	4	4	4	4
		mean	96.2	2.8	0.8	3262	539	0.10
		S. D	0.2	0.2	0.1	746	81	0.04
		Max	96.4	2.9	0.8	4359	631	0.17
		Min	95.9	2.5	0.7	2258	410	0.08
T5	Siderite	n	2	2	2	2	2	2
		mean	6.8	57.7	24.9	1784	244	3.2
		S. D	0.4	3.0	1.3	94	13	0.2
		Max	7.2	60.7	26.2	1877	257	3.3
		Min	6.5	54.6	23.6	1690	231	3.0
T7	Siderite	n	2	2	2	2	2	2
		mean	8.4	56.3	27.2	2649	286	0.9
		S. D	0.2	1.6	0.8	77	8	0.0
		Max	8.7	57.9	28.0	2726	294	1.0
		Min	8.2	54.6	26.4	2572	277	0.9
M1	Siderite	n	2	2	2	2	2	2
		mean	9.8	56.3	25.6	2660	341	1.1
		S. D	0.3	1.6	0.7	78	10	0.0
		Max	10.1	57.9	26.3	2738	351	1.1
		Min	9.5	54.6	24.8	2583	331	1.1
T13B	Siderite	n	2	2	2	2	2	2
		mean	8.0	56.4	27.3	2804	284	1.0
		S. D	0.3	1.8	0.9	88	9	0.0
		Max	8.2	58.2	28.1	2892	293	1.0
		Min	7.7	54.6	26.4	2716	275	0.9
E4	Siderite	n	4	4	4	4	4	4
		mean	8.8	57.2	24.0	2579	291	1.3
		S. D	1.9	3.2	2.3	209	56	0.1
		Max	10.9	62.4	26.6	2809	353	1.5
		Min	6.50	54.6	20.5	2249	222	1.3

Table 3.4: Summary of REY concentrations in the calcite cement of the Agbada Formation sandstone reservoirs

Sample	Cement	Statistics	La	Ce	Pr	Nd	Sm	Eu	Gd	Tb	Dy	Y	Ho	Er	Tm	Yb	Lu
T9	Calcite	n	4	4	4	4	4	4	4	4	4	4	4	4	4	4	4
		mean	9.72	49.16	7.79	40.01	12.39	3.44	11.17	1.36	6.89	39.26	1.08	2.73	0.31	2.02	0.26
		S. D	4.76	19.69	2.80	13.22	3.57	0.78	2.55	0.33	1.71	10.55	0.26	0.72	0.08	0.53	0.05
		Max	16.18	74.15	11.23	55.84	16.18	4.26	14.03	1.75	8.97	52.37	1.39	3.45	0.42	2.77	0.32
		Min	5.70	30.78	5.01	26.92	8.55	2.58	8.36	0.97	5.03	27.43	0.80	1.92	0.24	1.49	0.21
M5	Calcite	n	3	3	3	3	3	3	3	3	3	3	3	3	3	3	3
		mean	5.87	29.69	4.70	24.46	7.92	2.31	7.23	0.93	4.73	27.79	0.77	1.97	0.23	1.51	0.21
		S. D	1.86	10.41	1.46	8.37	2.35	0.64	2.01	0.26	1.13	5.22	0.14	0.38	0.03	0.18	0.03
		Max	7.37	38.62	5.72	31.02	9.87	2.76	8.76	1.16	5.54	31.22	0.89	2.28	0.26	1.63	0.23
		Min	3.78	18.25	3.03	15.02	5.30	1.57	4.95	0.65	3.44	21.78	0.61	1.54	0.20	1.30	0.17
T10	Calcite	n	4	4	4	4	4	4	4	4	4	4	4	4	4	4	4
		mean	5.99	30.86	5.10	26.60	8.76	2.65	8.66	1.08	5.42	33.15	0.90	2.26	0.29	1.72	0.24
		S. D	1.57	6.57	0.78	3.64	1.16	0.31	1.43	0.17	0.97	6.69	0.16	0.42	0.06	0.41	0.05
		Max	8.22	40.26	6.25	31.96	10.32	2.96	10.04	1.25	6.64	39.96	1.10	2.80	0.36	2.29	0.30
		Min	4.69	25.32	4.63	24.05	7.64	2.29	7.43	0.92	4.58	27.31	0.76	1.90	0.24	1.35	0.20
T13	Calcite	n	3	3	3	3	3	3	3	3	3	3	3	3	3	3	3
		mean	7.65	39.95	6.41	33.75	10.86	3.27	10.51	1.33	6.69	38.88	1.07	2.67	0.32	2.19	0.28
		S. D	0.36	0.60	0.20	1.81	0.45	0.17	0.74	0.18	0.90	6.70	0.13	0.36	0.04	0.48	0.05
		Max	8.05	40.61	6.63	35.78	11.35	3.39	11.35	1.54	7.68	46.53	1.21	3.08	0.36	2.71	0.34
		Min	7.38	39.43	6.24	32.30	10.46	3.08	9.93	1.23	5.94	34.03	0.97	2.45	0.30	1.77	0.25

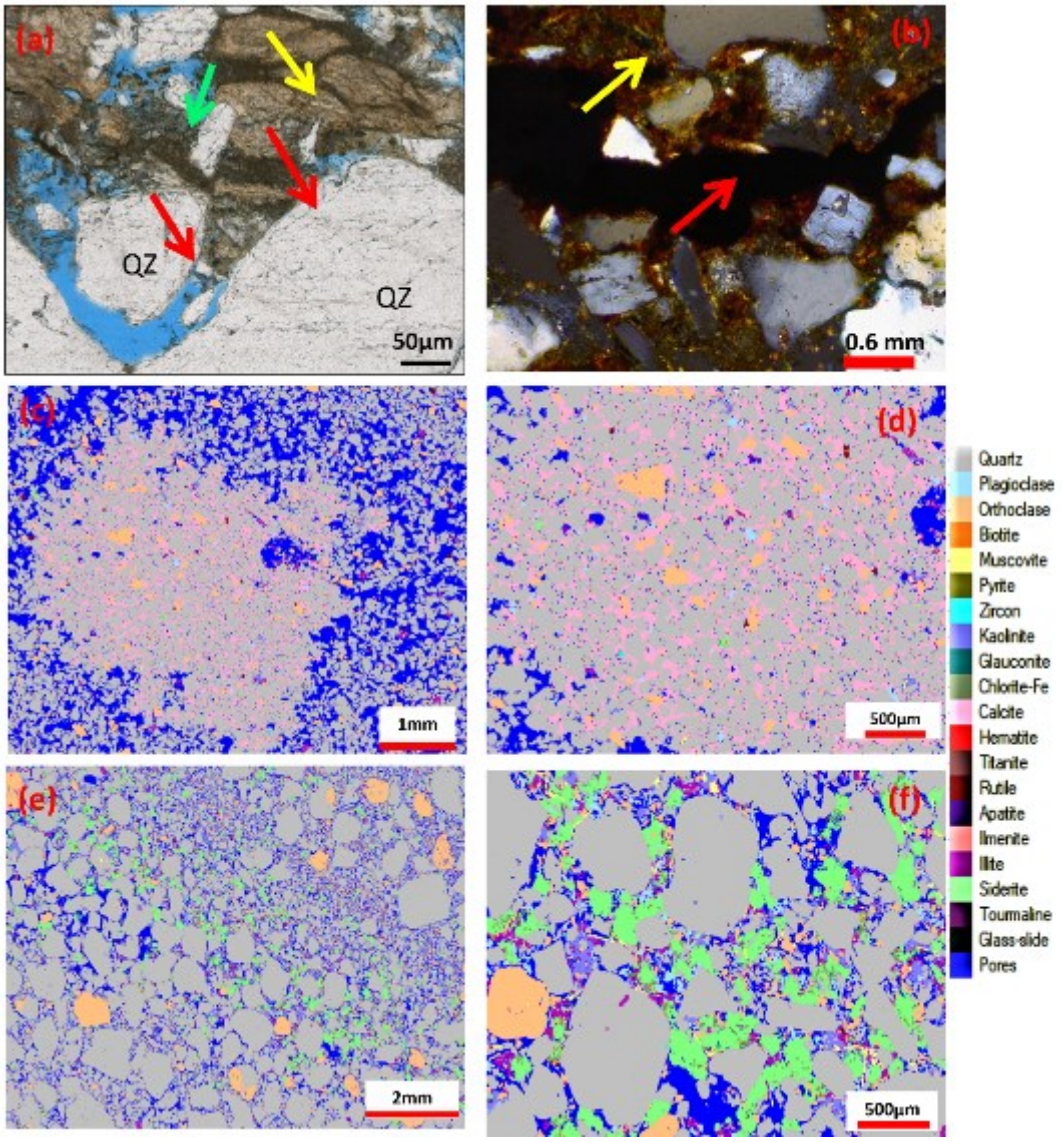

Figure 3.11: Photomicrographs, SEM image and MLA maps of the Agbada sandstone (a) rare quartz overgrowths (red arrows) within a siderite (yellow arrow) cemented horizon, with organic matter and clay matrix (green arrow), PX; (b) a horizon with significant organic matter (red arrow) and iron oxide (red arrow) cement, PX; (c) MLA map of a zone reflecting significant calcite cementation (d) magnified view of (*c)*; (e) MLA map of a zone with significant siderite cementation; (f) magnified view of siderite cementation in (*e)*, MLA map.

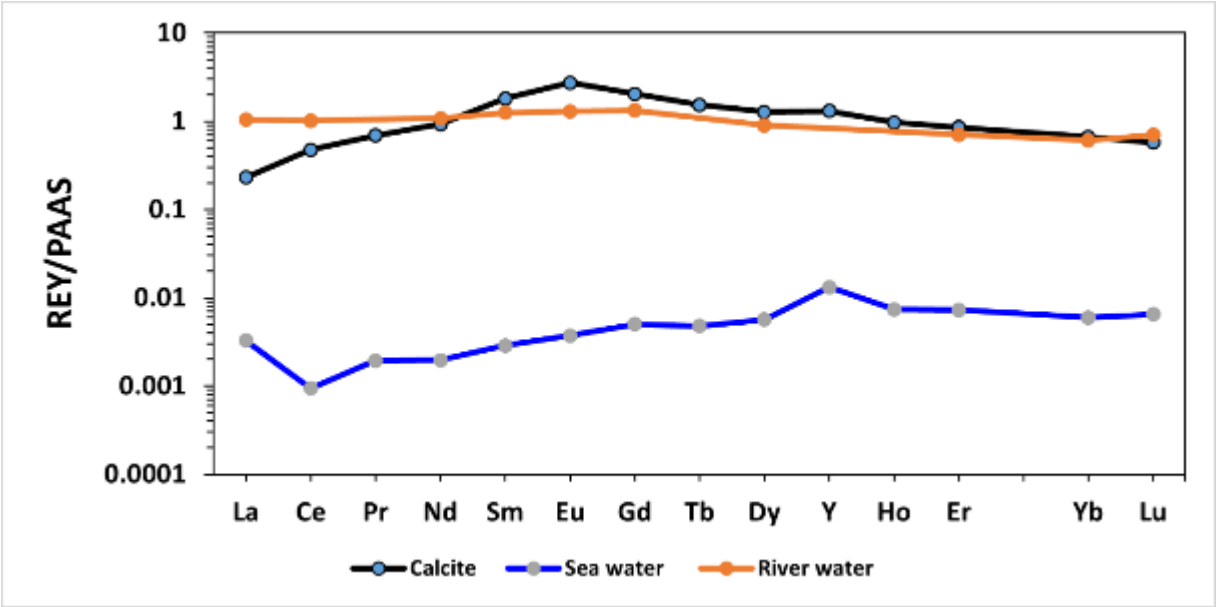

Figure 3.12: Mean PAAS-normalized REY patterns of calcite cement in Agbada sandstones. REY patterns of seawater (Lennard Shelf cements; Nothdurft et al., 2004) and suspended load from modern river water reflecting fluvial input (Goldstein and Jacobsen, 1988)

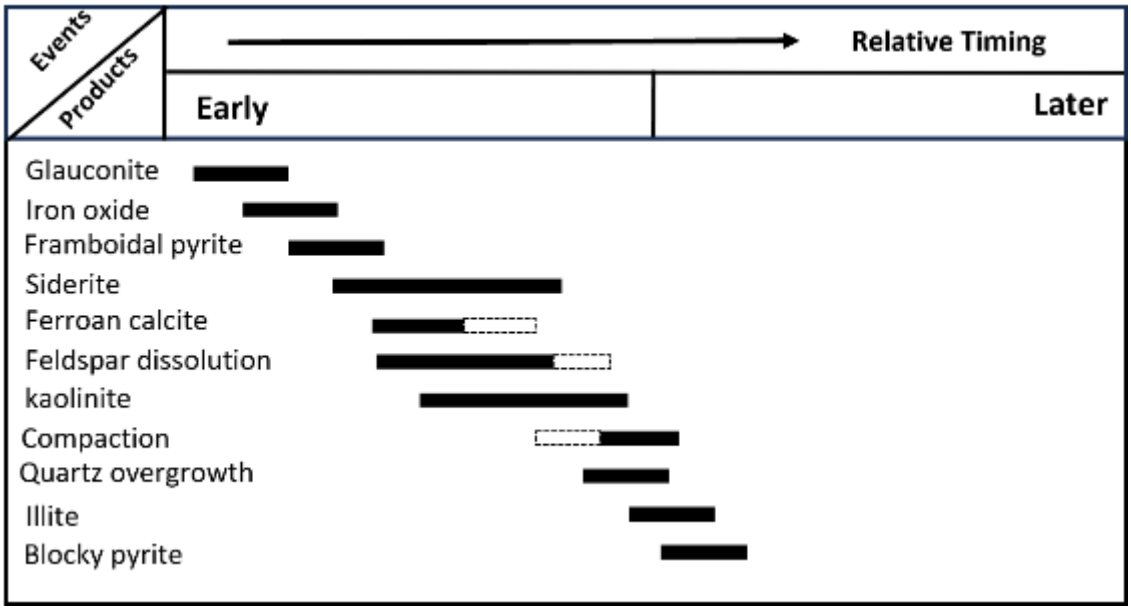

Figure 3.13: Paragenetic sequence of the diagenetic events in the Agbada sandstones reconstructed based on petrographic relationships.

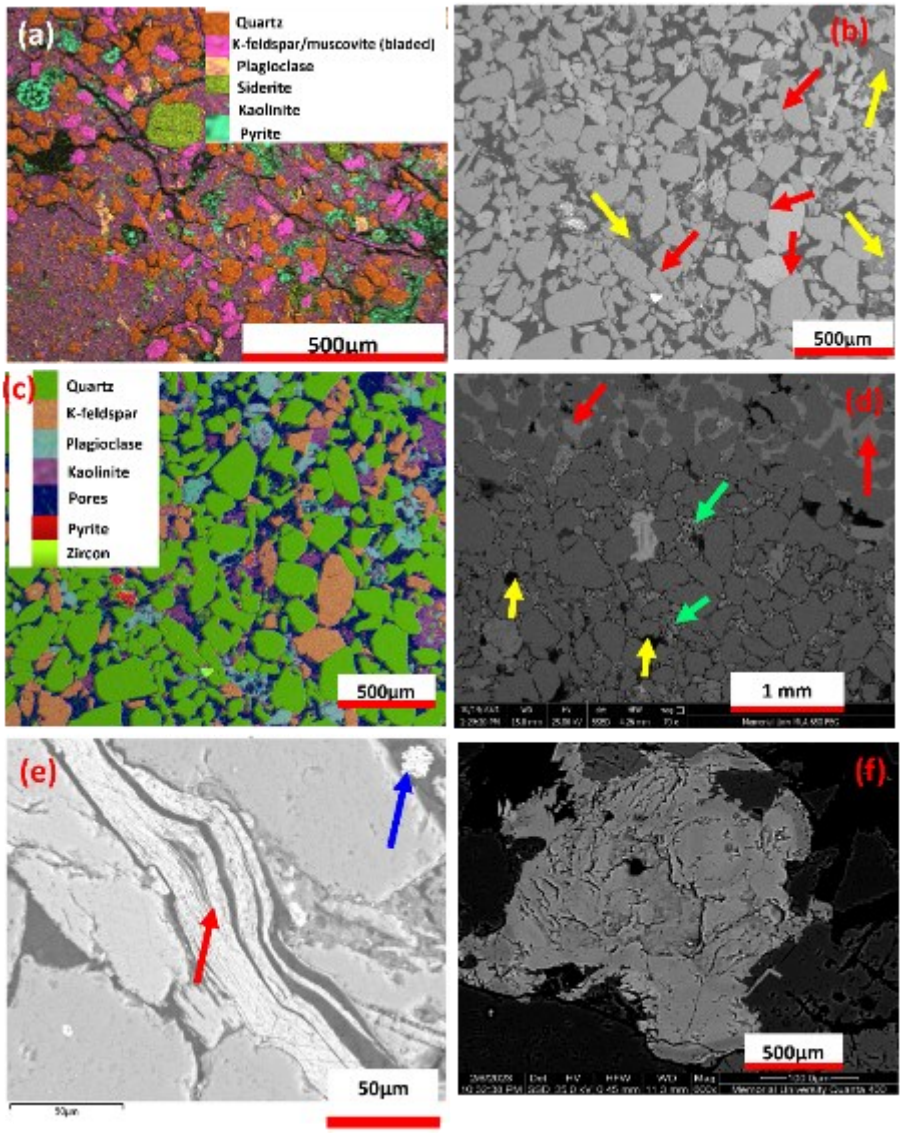

Figure 3.14: Photomicrographs and SEM features of the Agbada sandstone (a) SEM-EDS mineralogy of a very fine-grained sandstone (b) BSE image showing long grain contacts (red arrows) and kaolinite locally occluding pore spaces (yellow arrows); (c) SEM-EDS mineralogy of *b.* Note that the plagioclase is significantly altered; (d) calcite cement (yellow arrow) showing partial (green arrows) to complete dissolution (yellow arrows); SEM (e) squeezed/deformed biotite grain and framboidal pyrite (blue arrow), BSE (f) SEM image of siderite exhibiting zonation. The darker portions are richer in Mg content.

3.5.2.2 Quartz cement

Sandstones are commonly subjected to various conditions during diagenesis, initiating sources of silica for quartz cementation. Sandstones usually show significant overgrowths if compaction and diagenesis progress normally. Quartz overgrowths are generally most important at depths >2 km (e.g., Wilson and Stanton, 1994; Barbera et al., 2011; Bjørlykke, 2015; Olanipekun and Azmy, 2022; Civitelli et al., 2023), and some parts of the Agbada Formation sandstones are within or have possibly transcended the overburden threshold for initiating such processes (broadly around 3000m: Worden and Burley, 2003). However, its formation in the Agbada sandstones is limited, as low concentration of silica in formation water and restriction of overgrowth development by other diagenetic events have been advanced as reasons for poor silica cementation (Lambert-Aikhionbare, 1982). This is not unconnected to under-compaction, the presence of clay coatings on some quartz grains and possibly the influence of early calcite cementation.

Petrographic evidence in this study suggests that syntaxial quartz overgrowths (Fig. 3.6e, 3.8f, 3.10a, 3.11a) are not common and possibly present before deposition as abraded overgrowths of quartz grains (Fig. 3.8f), recycled from quartzose parent sandstones (Xiong et al., 2016; Olanipekun and Azmy, 2022). Considering the loose grain packing defined by common point contacts and the near absence of pressure dissolution, there is unequivocal evidence to support that pressure dissolution and stylolites did not contribute significantly to the silica available for quartz cementation. Without a considerable amount of pressure solution, it is unlikely that a sufficient amount of silica will be present in the solution to support the development of large overgrowths. Moreover, evidence from photomicrographs and SEM images reflects few or no biogenic grains; hence, a significant contribution from the dissolution of biogenic amorphous silica is unlikely. Although the illitization of smectite may release silica, the absence or minimal occurrence of mixed-layer I/S clays (Fig. 3.10c) and volcanic detritus

in the investigated sandstones, argue against it (Lambert-Aikhionbare, 1982). Moreover, even if the interbedded shales in the Agbada reservoirs have suffered some degree of illitization of their detrital clays, the paucity of overgrowths reflects that their silica contribution is not apparent in the diagenetic transformations of the associated sandstones. Thus, the evident dissolution of feldspar and/or alteration of feldspars and micas into clay minerals in the Agbada sandstones seems likely to have contributed to the silica for the limited quartz overgrowths (e.g., McKinley et al., 2003; Worden and Morad 2003; Lawan et al., 2021).

3.5.2.3 Clay minerals

Petrographic, SEM, and XRD analyses reveal several clay minerals (Tables 3.1-3.2, Fig. 3.6c, 3.6f, 3.7f, 9,10a-d), but kaolinite is the most dominant. Kaolinite formation requires feldspar dissolution in low salinity and/or low pH (acidic) formation water (Bauluz et al., 2008; Harris, 1992; Marfil et al., 2003; Amendola et al., 2016). Kaolinite appeared to be closely associated with partly decomposed feldspar grains and was thus likely sourced from the alteration of detrital feldspars (Fig. 3.6d-f, 3.8a, 3.14b-c). The rare pore-filling chlorite might have originated from the transformation of detrital or eogenetic clay minerals, whereas illite was possibly sourced from the conversion of kaolinite to illite by incorporating the K^+ released from the dissolution of K-feldspar at greater depths and higher temperatures.

3.5.2.4 Siderite

Earlier studies have documented the origin of siderite in various depositional systems and diagenetic settings utilizing their distribution patterns and composition (Matsumoto and Iijima, 1981; Curtis et al., 1986; Mozley, 1989; Pye et al., 1990; Mozley and Carothers, 1992; Morad et al., 1994; Baker et al., 1996; Huggett et al., 2000; Rossi et al., 2001; El-ghali et al., 2006; Pe-piper and Piper 2019; Lawan et al., 2021). There is a disparity in the chemistry of early marine and freshwater siderite because the purity of siderite is dependent on the extent to which Mg and Ca substitute for Fe in the crystal structure, which is influenced by the

composition of pore water at the time of precipitation (Mozley, 1989). Siderite precipitated in freshwater is commonly purer with > 90 mol% $FeCO_3$, significant Mn (> 2 mol% $MnCO_3$) and Ca/Mg ratios, whereas marine siderite may contain up to 41 mol% $MgCO_3$ and 15 mol% $CaCO_3$, with lower Ca/Mg ratio and much lower Fe and Mn (<1 mol% $MnCO_3$).

Siderite in the Agbada sandstone (Fig. 3.6a, 3.6c, 7e-f, 3.8a-c, 3.11d-e, Table 3.3) shows minimal variations in Fe^{2+}, Mg^{2+}, Mn^{2+}, and Ca^{2+}, with high Mg and to a lesser extent Ca suggesting precipitation from either marine pore water (Mozley, 1989) or evolved formation water (Curtis and Coleman, 1986; Morad et al., 1994; Rezaee and Schulz-Rojah, 1998; Rossi et al., 2001). The composition ($CaCO_3$ = 8.4 ± 1.4, $MgCO_3$ = 25.5 ± 2.1, $FeCO_3$ = 56.8 ± 2.6 mol%, Table 3.3) of the investigated siderite favours precipitation from marine pore water, consistent with shallow burial, although the compositional zonation (Fig. 3.14f) shown by some siderite crystals, indicates variations in pore-water chemistry, possibly associated with an influx of meteoric waters. The Fe^{2+} and CO_3^{2-} needed for siderite cementation were likely provided by the dissolution of Fe-rich detrital components (e.g., Oluwadebi et al., 2018; Luo et al., 2019; Yang et al., 2021). Also, siderite precipitation might have been fostered by the alteration of micas and clay-bearing intraclasts rich in organic matter (Boles and Johnson, 1984).

3.5.2.5 Calcite cement

Calcite cements in sandstones have been linked to several potential sources spanning internal, external, and mixed sources relative to the sandstone (Walderhaug, 1998; Dutton et al., 2002). Internal sources are related to the dissolution of detrital carbonate rock fragments, skeletal debris, and Ca-bearing feldspars (Morad et al., 1990), whereas external sources are linked to pore fluids reflecting Ca^{2+}, Mg^{2+} and Fe^{2+} that are possibly sourced from interbedded mudstones or adjacent source rocks during their evolution (Sun et al., 2020). The decarboxylation of organic matter that may interact with clay-bearing lithologies is also another possible source (e.g., Irwin et al., 1977; Thyne, 2001; Liu et al., 2012). These assertions are

well documented in the literature, with many previous investigations highlighting that calcite cements reflect the initial distribution of skeletal debris, carbonate rock fragments, ooids, dissolving and reprecipitating within the sandstones and therefore ascribing the origin of the calcium carbonate to internal sources (e.g., Bjørkum and Walderhaug, 1990; Morad et al., 1990; Hendry et al., 1996; Morad, 1998; Walderhaug and Bjørkum, 1998; Dutton, 2008; Gier et al., 2008; Zhixue et al. 2010; Worden et al., 2019, Barshep and Worden, 2021). Other reports have suggested that the source could be either external (especially when there is a paucity of evidence linking the calcite to internal sources) or mixed (e.g., Sullivan and McBride, 1991; Moraes and Surdam, 1993; McBride et al., 1995; Anjos et al., 2000; Dutton et al., 2000; Thyne, 2001; McBride and Milliken, 2006; Zhang et al., 2009; Xiong et al., 2016; Dutton and Loucks, 2010). To suggest a possible origin for the calcite cement (Fig. 3.8d-f, 3.11c-d) in the Agbada sandstones, we shall consider three notions: (1) the detrital carbonates and skeletal material within the sandstone acted as the source of calcium carbonate, (2) calcium carbonate was sourced externally and (3) the source is linked to both external and internal sources.

Considering the geologic setting and the large siliciclastic influx, the provenance and composition of the sandstones in the Niger Delta reflect minimal amounts of detrital carbonate grains/bioclasts. This does not suggest that much $CaCO_3$ was initially present during the deposition, with the understanding that some carbonates were probably subsequently dissolved. Deemed as a subordinate source, calcite can be sourced from feldspar dissolution (mainly plagioclase) and/or alteration. However, given that Ca-bearing feldspars are relatively small in the sandstone, it is doubtful that the feldspar alterations supplied enough prerequisites to form significant calcite cement. Bearing in mind that the distribution and average volume of authigenic calcite are generally minimal in the sandstone reservoirs, it seems reasonable to link the source and distribution of the calcite cement solely to the initial scanty detrital carbonate materials or skeletal debris, which can be easily redistributed as cement locally or by diffusion

over a short distance within the sandstone. However, the possible internal source (dissolution and reprecipitation of shelly material deposited with the sediment) for the calcite cement may not be sufficient alone to account for the volume of authigenic calcite in some intervals and perhaps some parts of the basin where its occurrence exhibits better local abundance in contrast to its general diminutive nature (Lambert-Aikhionbare, 1981; Nwajide, 2013). Hence, the source is connected to internal (the original scanty detrital grains and bioclasts) and/or external sources (calcareous shells in coeval interbedded shales and possibly shells washed into the marine from the onshore environment). Some bioclastic materials must have been present in shoreface environments and possibly represent a plausible source of irregularly distributed calcite cement. Moreover, during their diagenetic transformation, the interbedded shales may have released ions required for calcite precipitation to pore waters that migrated into the adjacent sandstones during mechanical compaction. Contributions from external sources seem plausible because of the scarcity of detrital carbonate grains and bioclasts in the sandstones. Moreover, since calcite is an early diagenetic phase, fluids might have exchanged freely and locally with bottom waters captured in the syndepositional stage owing to the shallow depth of burial of the reservoir sediments and the better connectivity that reflects the initial high porosity and permeability at the time of deposition.

3.5.3 Timing of calcite cementation

To establish the timing of calcite cement in the sandstones, it is important to consider some clues that are useful for its reconstruction. These include, but are not limited to, the intergranular volume of the calcite-cemented zones, the habitat of the calcite cement, the contacts and the structure of the grain framework, the abundance or absence of deformed ductile grains, fluid-inclusion homogenization data and the growth relationships between calcite cement and other diagenetic minerals. In addition, rare earth element geochemistry and stable isotopes are particularly useful for this reconstruction. However, the calcite cement generally

occurs in insufficient quantities to be separated for isotopic analyses. Moreover, the calcite cements do not contain measurable fluid inclusions suitable for microthermometry, so it was impossible to estimate the precise temperature at which calcite cement formed.

Evidence from petrographic observation (Fig. 3.8d-f, 3.11c-d) supports that calcite precipitation is an early diagenetic event. The poikilitic calcite and the fact that it is primarily distributed in intergranular pores that connect framework grains that are relatively loose and sometimes appear to float suggest that it was deposited before significant compaction. Besides, quartz overgrowth is scarce or possibly underdeveloped and deformed ductile grains are generally absent in the calcite-cemented zones. In addition, the evidence of calcite cement engulfing quartz overgrowths is also scarce, as the cements have mostly direct contact with detrital framework grains. This observation suggests that their temperature of formation is likely lower than typical temperatures (~75^0C) required for quartz cement precipitation (Walderhaug, 1994), although their precipitation seems to have continued to the early stage of progressive burial to locally replace framework grains (Fig. 3.8e) and engulf rare quartz grains with overgrowths (Fig. 3.8f).

Moreso, the intergranular volume has been explored to provide clues on the timing of cement growth relative to compaction and therefore can be used to interpret the relative timing of cement growth (Stephenson et al., 1992; Ehrenberg, 1995; Dutton, 1997; Worden et al., 2019). Since most sandstones have an initial porosity of up to 40–45% at the time of deposition (Beard and Weyl 1973), the intergranular volume (Fig. 3.16) for the calcite cemented samples suggests that growth probably happened immediately after deposition before any significant burial-induced compaction occurred. The calcite cements enhance the capability of the sandstone to resist compaction and preserve the original intergranular pores.

3.5.4 Geochemical signatures of the calcite cements

The elemental concentrations of diagenetic carbonates depend largely on the precursor carbonates, the bulk constituents of the diagenetic fluid, and the distribution coefficient values of the respective elements (e.g., Brand and Veizer, 1980; Veizer, 1983). The elevated content of Fe in the calcite cement ($CaCO_3$ = 95.9 ± 0.4, $MgCO_3$ = 0.8 ± 0.1, $FeCO_3$ = 2.9 ± 0.2 mol%, Table 3.3) suggests they are mainly ferroan, as the syn-depositional pore water was enriched in Fe and underwent variable marine influence that promoted the early formation of pyrite under reducing conditions. The Sr concentration of the Agbada calcite cements (320–631 ppm, Table 3.3) does not seem to suggest pristine marine (Sr ≥1000ppm) conditions (Banner, 1995; Taylor et al., 2000). It is inconsistent with those that have either experienced significant diagenetic transformation (Sr <100 ppm) or initially contain low magnesium calcite (LMC) mineralogy (Tucker and Wright 1990), suggesting possible fluviomarine influence. However, the high-end member Sr values (e.g., 631 ppm; Table 3.3) might reflect an aragonitic precursor and possible dissolution of aragonitic shells (Thomas et al., 2004; Xiong et al., 2016).

The proportion of rare earth elements (REE) incorporated by marine carbonates reflects the chemistry of seawater from which they precipitated (e.g., Webb and Kamber, 2000; Nothdurft et al., 2004). REE are sensitive diagenetic proxies because diagenetic alteration causes significant enrichment in their total concentration (∑REE), although their precursor shale normalized patterns are commonly retained at low water/rock interaction ratios (Webb et al., 2009; Azmy et al., 2011). In marine geochemical studies, yttrium (Y), which exhibits identical charge and similar atomic radii to its neighbours, is particularly of interest (Bau and Dulski, 1999; Jiang et al., 2015). Holmium (Ho) is scavenged at a rate considered two times faster than Y (Nozaki et al., 1997), Y/Ho ratio is thus much higher in seawater (Y/Ho = 44–74; Bau, 1996) than in the upper crust (Y/Ho ~28; Kamber et al., 2005). Marine carbonates exhibit shale-normalized REY patterns consistent with modern seawater, characterized by LREE

depletion, negative Ce anomaly, positive La anomaly, small positive Gd anomaly, and super chondritic Y/Ho ratio (e.g., Elderfield and Greaves, 1982; De Baar et al., 1985; Zhang and Nozaki, 1996; Webb and Kamber, 2000; Nothdurft et al., 2004; Frimmel, 2009; Allwood et al., 2010; Zhou et al., 2023).

Apart from the slightly positive Gd anomalies (Gd_{SN}/Gd^*= 1.18-1.33; 1.25 ± 0.05) of the Agbada calcite cements, which are consistent with those of modern seawaters (e.g., de Baar et al., 1985; Alibo and Nozaki, 1999; Li and Jones; 2014) and ancient sediments (Bau and Dulski, 1996), their shale-normalized REY patterns (Fig. 3.12) do not seem to mimic that of seawater due to weak LREE depletion relative to HREE, enriched MREE phases, and lack of distinctive negative Ce. The overall signature suggests precipitation from a parent fluid that could be modified seawater (mixed with meteoric water), meteoric water, or a fluid circulated in sediments enriched in LREE (Nothdurft et al., 2004). The Y/Ho ratios (34.3–38.9, 36.3 ± 1.36) are also inconsistent with that of seawater (Y/Ho = 44–74; Bau, 1996) as they are slightly higher than those of the average upper continental crust (Y/Ho=28, Kamber et al., 2005) and continental carbonates (Bolhar and Van Kranendonk, 2007; Lawrence et al., 2006), suggesting possible contamination from detrital grains and/or contributions from other sources (e.g., Nothdurft et al., 2004; Frimmel, 2009; Webb et al., 2009; Allwood et al., 2010; Liang and Jones; 2021).

River waters tend to be enriched in MREE relative to HREE (e.g., Elderfield et al., 1990; Andersson et al., 2006; Liang and Jones, 2021). In addition, pore fluids below the sediment-water interface in marine settings may contain MREE-enriched phases formed by the release of MREE from Fe-oxides as terrigenous sediments are reduced in early anoxic diagenesis (Haley et al., 2004). Thus, a reasonable explanation for the Agbada calcite cements REY trend may be ascribed to river influx and the associated particulate matter that preferentially scavenged LREEs from the overlying water column, leading to an increased (∑REE), decreased

LREE depletion, La anomaly and Y/Ho, as particles scavenge less La relative to neighbouring REEs and little Y relative to Ho (Della Porta et al., 2015).

Previous studies have utilized Cerium anomaly (Ce/Ce*) as a proxy for redox conditions (e.g., Elderfield and Greaves, 1982; De Baar et al., 1988; German and Elderfield, 1990; Wilde et al., 1996**;** Madhavaraju and González-León, 2012**;** Piper and Bau, 2013; Bellefroid et al., 2018; Overare et al., 2020; Lanz et al., 2021; Shembilu et al., 2021; Luan et al., 2023; Zhou et al., 2023). Unlike seawater, the investigated Agbada calcite cement exhibits no Ce anomaly (Fig. 3.15), suggesting possible dysoxic/anoxic conditions within an early diagenetic environment as Ce is quickly released into early marine burial suboxic pore fluids from oxide crusts on water column particles, reducing the negative Ce anomaly to unity (Haley et al. (2004). The investigated Agbada calcite cements reflect shallow marine settings and should contain some input from seawater (fluviomarine environment). The lack of a negative Ce anomaly may have resulted from siliciclastic contamination and REE-scavenging marine particles in the water column, representing an additional source of Ce without the need to invoke a shallow oxygen minimum zone (Della Porta et al., 2015). Nevertheless, a shallow oxygen minimum zone could also have been locally developed, considering the abundance of framboidal pyrites and the virtually inexistent Ce-anomaly. This local impingement of the oxygen minimum zone favours the reduction of Fe^{3+} and the release of Fe^{2+} into pore water, leading to the growth of ferroan calcite cement (Zhang and Li, 2020). Therefore, we suggest that the slight Ce enrichment is possibly attributed to changes in the geochemistry of the parent fluids due to contributions from riverine waters and mixing with fluids that were progressively circulated in REE-rich, particularly Ce, siliciclastic rocks in the basin (Shields and Stille, 2001; Abanda and Hannigan, 2006; Xiong et al., 2016; Shembilu et al., 2021).

Europium, which is present as Eu^{3+} in seawater, is not substantially fractionated during the precipitation–dissolution processes, as is the case for Ce (Shields and Stille, 2001). Under

reducing conditions, Eu^{3+} in seawater is reduced to Eu^{2+} within interstitial fluids (MacRae et al., 1992; Shields and Stille, 2001), giving rise to a strongly positive Eu anomaly. Europium is commonly enriched in highly reducing hydrothermal fluids and in Ca-rich early magmatic minerals, such as plagioclase feldspar, where Eu^{2+} may replace Sr^{2+} due to their similar ionic radii (Michard and Albarede, 1986; Olivarez and Owen, 1991; Shields and Stille, 2001). Considering the geologic settings of the Niger Delta Basin on a passive continental margin and the rarity of basalts within the siliciclastics system, a widespread hydrothermal activity is improbable, but basinal deposits are known to commonly contain detritus derived from igneous/metamorphic basement and recycled from siliciclastic deposits, which contain Eu-rich feldspars (e.g., Sverjensky, 1984; Lee et al., 2003; Bau et al., 2010; Luan et al., 2023). Circulation of diagenetic fluids may lead to the dissolution of feldspars and release of Eu that may cause positive Eu anomalies in the PAAS-normalized REY patterns of the calcite cements precipitated from those fluids (e.g., Xiong et al., 2016). Therefore, we suggest that the Eu/Eu* shown by the Agbada calcite cements may be attributed mainly to the dissolution of plagioclase feldspars during the circulation of the parent diagenetic fluids through the sandstones (e.g., Xiong et al., 2016; Lanz et al., 2021; Luan et al., 2022a, b).

3.5.5 Diagenetic control on reservoir quality

Depending on the intensity of diagenetic influence on sandstone reservoirs during burial, diagenetic signatures can irreversibly obliterate reservoir intergranular porosity, although some porosity destruction attributed to cementation is temporal, dissolving during later diagenetic episodes**.** The relative importance of compaction and cementation as porosity controls in the Agbada sandstone was evaluated within considerations deemed acceptable using established conventions (Equations 1–3, Fig. 3.16, Ehrenberg, 1989; Paxton et al., 2002).

$$COPL = [100 (P_o - 1GV) - 2 (P_o . IGV)]/ (100 - IGV) \quad (1)$$

$$CEPL = (P_o - COPL). (CEM /1GV) \quad (2)$$

IGV = IGP + IGCm + Ma…… (3)

Where COPL = compactional porosity loss, CEPL = cementational porosity loss, CEM = total cement, P_o = original porosity, IGV= intergranular volume, IGP= Intergranular porosity, IGCm = Intergranular cement, and Ma = depositional matrix.

All values in equations (1) and (2) are expressed as a percentage of the rock volume.

COPL and CEPL were computed using (i) an assumed P_o of 40% (Houseknecht, 1987; Wilson and McBride, 1988) and (ii) thin section to estimate the values of the Trask sorting coefficient (So) with the help of the reference images of Beard and Weyl (1973) and eventually using the relationship of Scherer (1987):

Po = 20.91 + (22.9/So) ……. (4)

However, there was no significant disparity in the interpretation trends of COPL and CEPL when both methods were applied in the current investigation; therefore, the first method was utilized for the compactional porosity loss in sandstone.

The proximity of framework grains has been utilized to shed light on compactional features in sandstones. IGV is ~ 26% for quartz-rich, well-sorted sandstones that have experienced mechanical compactional processes, with the consideration that a further decline (<26%) in intergranular volume would require obvious intergranular pressure solution (Paxton et al., 2002). Although some bending/squeezing of mica flakes (Fig. 3.6c) and the rearrangement of detrital grains in the rock texture defined by a few long contacts (Fig.3.14b-c) are observed in the Agbada sandstones, most samples (~69%) reflect IGV > 26% (Fig. 3.16), indicating mechanical compaction and chemical compaction (pressure solution) is low, which is consistent with petrographic observations (dominance of point-to-null- contacts between grains). The sandstones also reflect minimal content of cements, replacements, and other authigenic phases. Since the sandstones generally lack evenly distributed and sufficient early diagenetic rigid cement to resist mechanical compaction, cementation appears to have been less influential in

shaping the porosity of the sandstones. Thus, apart from 18% of the samples (dashed purple circle, Fig. 3.16) that contain considerable carbonate cementation (mainly ferroan calcite and siderite cement) that stabilized the rock texture and therefore less compactional control, mechanical compaction seems to be the dominant control on porosity loss for 77% of the samples. No significant difference in compaction effects among wells was detected, which was expected given the similar facies association and restricted range of sand-body geometries in Niger Delta reservoirs (Weber, 1971; Nwajide, 2013).

3.5.6. Influence of calcite cement

The timing, influence, and extent of calcite cementation are important considerations in sandstone reservoirs. Moreover, developing reservoir characterization models and identifying controls on carbonate cementation in reservoirs are essential for understanding resource placement and reservoir potential in fields where carbonate cementation occurs. Early diagenetic cementation by calcite can preserve a good portion of reservoir porosity during burial compaction until it is recovered by carbonate dissolution at greater depths. As already established, calcite-cemented zones are not abundant in the Agbada sandstones and the presence of “poikilitic” calcite cement in a network of grains that appear to float coupled with the prevalence of tangential contacts implies that it is an early diagenetic event and filled pores prior to significant mechanical compaction. This prevented grain reorganization and crushing by strengthening the grain-framework and effectively counteracting vertical stress. Although this event may generally offer cohesion and rigidity to the rock, it diminishes the effect of further mechanical compaction and porosity loss by causing low grain contact and consequently little pressure-solution unlikely for considerable silica to be present for overgrowths to occlude porosity. Samples above and below the calcite cemented zones have little or no calcite cements, suggesting that the pore-filling calcite is probably vertically discontinuous. This observation is possibly attributed to the unfavourable conditions in the depositional system for dwelling

organisms with carbonate shells, leading to the scarcity of significant sources of carbonate in the sediments with the understanding that some of the early cement formed was subsequently dissolved when pore fluids became undersaturated with respect to carbonates.

Whether replacing or pore-filling, when carbonate cements in sandstones experience significant dissolution, it is of great importance in reservoir characterization (Taylor, 1990; Taylor et al., 2010; Hesse and Abid, 1998). Relics of partly/completely dissolved calcite cements (Fig. 3.14d) are found in the Agbada sandstones and their optical signatures imply that they are part of the same network of poikilitic calcite cement being isolated due to partial dissolution. Even though the sandstones might have been influenced by meteoric waters that contributed to calcite dissolution, it is not entirely excluded that the cement dissolution produced only small amounts of secondary porosity, particularly with insignificant sources of carbonates (e.g., carbonate rock fragments, marine shells,) and minimum calcite cementation. However, due to data constraints and the rare occurrence of the calcite cement in the investigated succession, it is impossible to determine the lateral extent of the cemented intervals or effectively correlate any of the cemented zones. Moreover, the lateral extent of those intervals cannot be pinpointed with certainty using a few subsurface well datasets that are widely spaced since cemented layers may not be laterally continuous but discontinuous stratabound concretions (Dutton, 2008). Although the Agbada sandstone calcite-cemented zones might not form impermeable barriers that may significantly impact reservoir quality, it can cause a local reduction in the average permeability of the reservoir, increase the tortuosity of flow paths, and modify sweep efficiency in a reservoir (Dutton et al., 2002). Therefore, a clear understanding of their origin and distribution may still contribute to the development of realistic reservoir models. Developing reservoir characterization models and identifying controls on carbonate cementation in reservoirs are essential for understanding resource placement and reservoir potential in fields where carbonate cementation occurs.

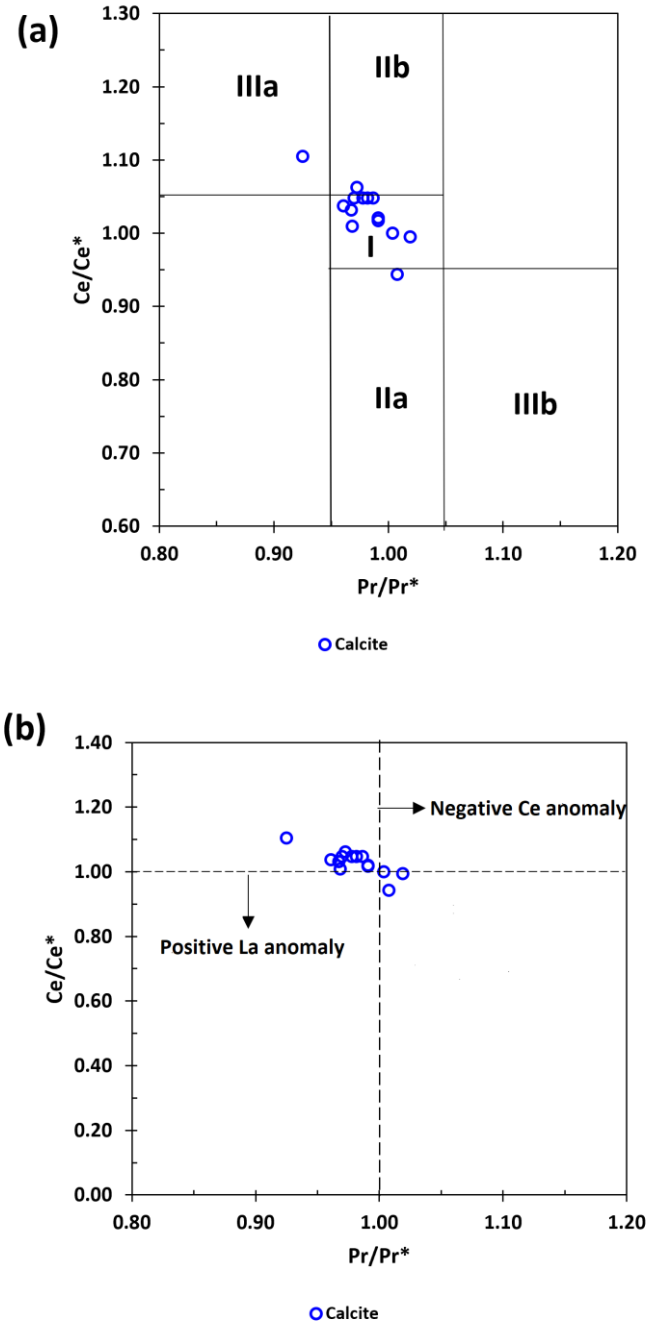

Figure 3.15: Cross plot highlighting the relationship between Ce/Ce* and Pr/Pr* for the investigated sediments using the method of Bau and Dulski (1996) (a) Field I: neither Ce nor La-anomaly, field IIa: positive La-anomaly, no Ce-anomaly, field IIb: negative La anomaly, no Ce-anomaly, field IIIa: positive Ce-anomaly, field IIIb: negative Ce-anomaly. Note that most data points clustered in field I, indicating no anomaly. (b) Ce/Ce* and Pr/Pr* plots depicting samples clustering away from the classical region of modern seawater.

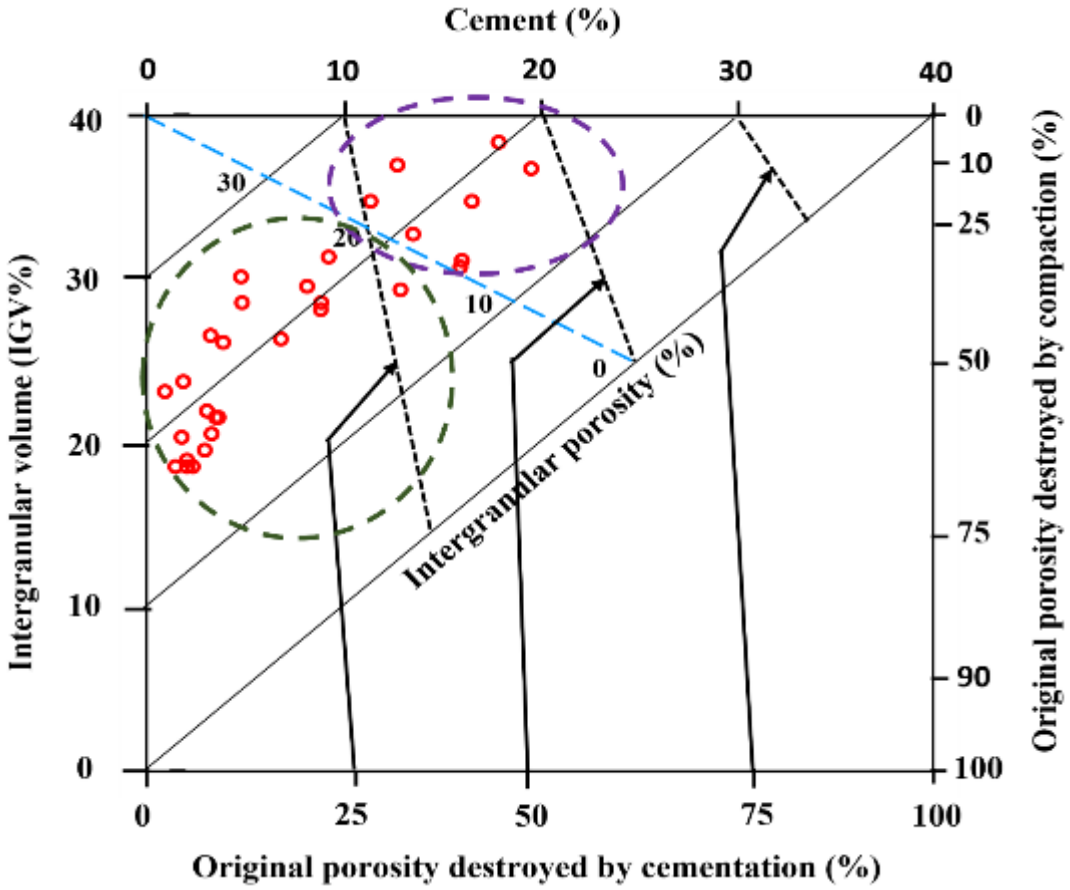

Figure 3.16: Illustrative diagram highlighting the relative importance of compaction and cementation to porosity development in sandstone (Houseknecht, 1987; modified by Ehrenberg, 1989). Purple dashed lines are samples with considerable carbonate cement (siderite and calcite) reflecting porosity attributed to cementation, whereas the green dashed lines are samples with little or no cement where compactional porosity loss has been more dominant.

3.5.7 Implication for porosity development and exploration

The main processes that significantly affect and modify porosity in the different diagenetic environments are the dissolution of existing phases and/or the precipitation of new phases. The general lack of pervasive cements and minimal compaction are significant features of the Agbada sandstones that contributed to the high porosity and excellent reservoir quality despite the depth of burial of the sandstones. The early calcite cementation, where abundant and almost completely occluding primary porosity, was sufficient to strengthen the framework against compaction as its role for porosity preservation is optimized. However, new porosity is generated where the dissolution of the early calcite cement was not compensated by new cement formation. In addition, the partial and complete dissolution of unstable detrital grains (e.g., feldspars, micas) added to the effect and enhanced the secondary porosity in the reservoir.

The minimal compaction and the presence of a clay-rich matrix in the sandstones may lead to the production of fines and formation damage during reservoir production. However, the prevalence of kaolinite in the matrix and quartz in the grain framework implies smaller compactional intensity from the overburden pressure than for quartz-poor sandstone with smectite-rich matrix (Lambert-Aikhionbare, 1982; Corrado et al., 2019; Adamolekun et al., 2022). Although significant smectite has been reported in parts of the Niger Delta Basin (Lambert-Aikhionbare, 1981; Lambert-Aikhionbare and Shaw, 1982), requiring a cautious approach in the selection of drilling fluid when penetrating the smectite-bearing horizons, the investigated samples do not contain significant smectite and should not pose an issue during production. In addition, even if the significant presence of kaolinite in the sandstones could be of concern, it is not likely to cause much damage to permeability compared to other authigenic clays that are far more destructive (Selley, 2000). Moreover, permeability loss can be minimized when a suitable reservoir management and development plan is applied (Akinmosin et al., 2018; Adamolekun et al., 2022).

3.5.8 Comparison of the Agbada Sandstone reservoirs to some Miocene reservoirs

In comparison to other Miocene sandstones (buried to depths > 2000 m) in several sedimentary basins worldwide (e.g. the Gulf of Mexico, Asia, Central Europe and California) that have been evaluated and assessed for reservoir quality, the Agbada sandstone reservoirs share similar features common to them as a result of the rapid accumulation of sediments. The Agbada sandstones exhibit significant alteration of feldspar grains, particularly plagioclase, which is prevalent in most Miocene sandstones (e.g., Boles and Ramseyer, 1987; Dutton et al., 2012; Gier et al., 2008; Hirt et al., 1993; Rahman et al., 2016). Moreover, clay minerals in most Miocene sandstones are yet to achieve the illite-dominated characteristics distinctive of older sandstone buried to depths of over 3,000 m (>100^{o}C), and this is particularly true for the investigated Miocene Agbada sandstone reservoirs. The Agbada sandstones are quartz-rich and therefore, exhibit reasonably comparable detrital modal composition to those of Lower Miocene sandstones from offshore Louisiana and Miocene sandstones (Surma Group) of the Bengal Basin, Bangladesh but differ from some other Miocene sandstones that are poorer in quartz, including those of offshore Texas, Burgos Basin, northern Mexico, Veracruz Basin, southern Mexico, and Vienna Basin, Austria (Dutton et al., 2012; Gier et al., 2008; Rahman et al., 2016). Diverse factors, including different parent rocks and degree of recycling, may account for the variations in mineralogical composition. Considering the loose grain packing defined by common point contacts and the near absence of pressure dissolution, quartz cementation is scarce in the Agbada sandstone, and just like Miocene sandstones in the Vienna Basin, Austria, it is of minimal significance in the reservoir quality control of the sandstones.

3.6 Conclusions

This research examined the diagenetic imprints and the influence of rare calcite cemented intervals on the reservoir quality of Agbada sandstone, highlighting the petrographic characteristics, the diagenetic evolution of the cements and the relationship or connection between diagenetic processes and porosity distribution, and therefore determining the processes that have been more influential in shaping the reservoir quality.

The Agbada Formation sandstones consist of quartzose and subordinately quartz-rich feldspatho-quartzose sandstones with relatively high porosity and excellent reservoir quality owing to the lack of pervasive diagenetic cements and minimal compaction. Although the degree of mechanical compaction in the sandstone is generally low, it might have generally exerted more control on porosity than cementation, with exceptions to horizons that contain comparatively more amounts of early cements (particularly siderite and ferroan calcite) in which compactional porosity-loss was minimal.

The deltaic depositional setting and syn-depositional pore waters underwent variable marine influence that promoted the early formation of pyrite. The influence of meteoric waters and their modification contributed to the dissolution of framework grains (mainly unstable feldspars) and the formation of authigenic kaolinite. Ferroan calcite cements also dissolved, representing only a small percentage of the investigated sandstones, being locally present in a few intervals. Siderite, subordinate ferroan calcite, and pyrite growth suggest iron enrichment in pore waters during early diagenesis.

The shale normalized REY pattern of the calcite cement does not match that of seawater and suggests a parent fluid that could be modified seawater (mixed with meteoric water, meteoric water, or a fluid circulated in sediments enriched in LREE). Although calcite cements are minor, probably discontinuous and unlikely to represent significant barriers to fluid flow with their localized influence, a clear understanding of their origin and distribution may still

contribute to the development of realistic reservoir characterization models because identifying the controls on carbonate cementation in reservoirs are essential for resource placement and evaluating the reservoir potential in fields where carbonate cementation occurs.

Besides carbonate cements, detrital and authigenic clay (mostly kaolinite), pyrite, and rare Fe oxides and perhaps quartz overgrowths contributed to a slight additional loss of reservoir porosity, compensated by the partial dissolution of unstable detrital grains and calcite cements. Although the occurrence of clay-rich matrix in the sandstones could be of concern due to the possible production of fines and formation damage during reservoir production, this can be mitigated with proper reservoir management, considering the clays are dominated by kaolinite rather than other clay minerals that are far more prone to cause significant damage to permeability.

References

Abanda, P.A., Hannigan, R.E., 2006. Effect of diagenesis on trace element partitioning in shales. Chemical Geology, 230, 42–59.

Adamolekun, O.J., Busch, B., Suess, M.P., Molenaar, N., Hilgers, C., 2022. Petrography and reservoir quality controls in shallow transitional marine Cretaceous-Paleogene deposits in the Dahomey Basin, Nigeria. Journal of African Earth Sciences, 186, 104437.

Akinlua, A., Ibeachusim, B.I., Adekola, S.A, Adedosu, T.A., Li, Y., Xiong, Y.Q., 2020. Diamondoid geochemistry of Niger Delta source rocks: implication for petroleum exploration. Energy Sources, Part A: Recovery, Utilization, and Environmental Effects, DOI: 10.1080/15567036.2020.1840672.

Akinlua, A., Torto, N., Ajayi, T.R., 2008. Determination of rare earth elements in Niger Delta crude oils by inductively coupled plasma-mass spectrometry. Fuel, 87, 1469-1477.

Akinmosin, A., Bankole, S.I., Eyogwe, S.O., 2018. Reservoir geology and effects on exploitation of natural bitumen deposits (Nigerian deposits as a case study). J. Petroleum Exploration Prod. Technol. 9, 191–205.

Alibo, D.S., Nozaki, Y., 1999. Rare earth elements in seawater: particle association, shale-normalization, and Ce oxidation. Geochem. Cosmochim. Acta 63 (3–4), 363–372.

Allen, J.R.L., 1965. Late Quaternary Niger Delta, and adjacent areas-sedimentary environments and lithofacies: AAPG Bulletin, 49, 547-600.

Allwood, A.C., Kamber, B.S., Walter, M.R., Burch, I.W., Kanik, I., 2010. Trace elements record depositional history of an Early Archean stromatolitic carbonate platform. Chem. Geol. 270, 148–163.

Amendola U., Perri F., Critelli S., Monaco P., Cirilli S., Trecci T., and Rettori R., 2016. Composition and provenance of the Macigno Formation (Late Oligocene-Early Miocene) in the Trasimeno Lake area (Northern Apennines): Marine and Petroleum Geology 69, 146-167, doi: 10.1016/j.marpetgeo.2015.10.019.

Andersson, K., Dahlqvist, R., Turner, D., Stolpe, B., Larsson, T., Ingri, J., Andersson, P., 2006. Colloidal rare earth elements in a boreal river: changing sources and distributions during the spring flood. Geochimica et Cosmochimica Acta 70, 3261–3274.

Anjos, S. M. C., De Ros, L. F., Souza, R. S., Silva, C. M. A., Sombra, C. L., 2000. Depositional and diagenetic controls on the reservoir quality of Lower Cretaceous Pendeˆncia sandstones, Potiguar rift basin, Brazil: AAPG Bulletin, 84, 1719–1742.

Anomneze, D.O., Okoro A.U., Ajaegwu, N.E., Akpunonu, E.O., Ahaneku, C.V., Ede, T.A.D, Okeugo, G.C., Ejeke, C.F., 2015. Application of seismic stratigraphy and structural analysis in the determination of petroleum plays within the eastern Niger Delta Basin, Nigeria. J Petrol Explor Prod Technol, 5(2),113–122.

Avbovbo, A.A., 1978. Tertiary lithostratigraphy of Niger delta. AAPG (Am. Assoc. Pet. Geol.) Bull. 62 (2), 295–300.

Azmy, K., Brand, U., Sylvester, P., Gleeson, S.A., Logan, A., Bitner, M.A., 2011. Biogenic and abiogenic low-Mg calcite (bLMC and aLMC): evaluation of seawater-REE composition, water masses and carbonate diagenesis. Chem. Geol. 280, 180-190.

Baker, J.C., Kassan, J., Hamilton, P.J., 1996. Early diagenetic Siderite as indicator of depositional environment in the Triassic Rewan Group, southern Bowen Basin, eastern Australia. Sedimentology 43, 77–88.

Banner, J.L., 1995. Application of the trace element and isotope geochemistry of strontium to studies of carbonate diagenesis. Sedimentology 42, 805–824.

Barbera G., Critelli S., Mazzoleni P., 2011, Petrology and geochemistry of Cretaceous sedimentary rocks of the Monte Soro Unit (Sicily, Italy): constraints on weathering, diagenesis and provenance. Journal of Geology, v. 119, p. 51-68, doi: 10.1086/657340.

Barshep, D.V., Worden, R.H., 2021. Reservoir quality of upper Jurassic Corallian Sandstones, weald basin. Geosciences, 11, 446. https://doi.org/10.3390/geosciences11110446

Bau M., 1996. Controls on fractionation of isovalent trace elements in magmatic and aqueous systems: Evidence from Y/Ho, Zr/Hf, and lanthanide tetrad effect. *Contrib. Mineral.* Petrol. 123**,** 323–333.

Bau, M., Balan, S., Schmidt, K., Koschinsky, A., 2010. Rare earth elements in mussel shells of the Mytilidae family as tracers for hidden and fossil high-temperature hydrothermal systems. Earth Planet Sci. Lett. 299, 310–316.

Bau, M., Dulski, P., 1996. Distribution of Yttrium and rare-earth elements in the Penge and Kuruman iron-formations, Transvaal Supergroup, South Africa. Precambrian Res. 79, 37–55.

Bau, M., Dulski, P., 1999. Comparing Yttrium and rare earths in hydrothermal fluids from the Mid-Atlantic Ridge: Implications for Y and REE behaviour during near-vent mixing and for the Y/Ho ratio of Proterozoic seawater. Chem. Geol. 155 (1), 77–90.

Bauluz, B., Mayayo, M.J., Yuste, A., Gonzalez Lopez, J.M., 2008. Genesis of kaolinite from Albian sedimentary deposits of the Iberian Range (NE Spain): analysis by XRD, SEM and TEM. Clay Miner. 43, 459–475.

Beard, D.C., Weyl, P.K., 1973. Influence of texture on porosity and permeability of unconsolidated sand. AAPG (Am. Assoc. Pet. Geol.) Bull. 57, 349–369.

Beka, F.T., Oti, M.N., 1995. The distal offshore Niger Delta: frontier prospects of a mature petroleum province. In: Oti, M.N., Postma, G. (Eds.), Geology of Deltas. A.A. Balkema, Rotterdam, 237–241.

Bellefroid, E.J., Hood, A.V.S., Hoffman, P.F., Thomas, M.D., Reinhard, C.T., Planavsky, N.J., 2018. Constraints on Paleoproterozoic atmospheric oxygen levels. Proc. Natl. Acad. Sci. 115, 8104–8109.

Benesh, N P., Plesch, A., Shaw, J. H.., 2014. Geometry, kinematics, and displacement characteristics of tear-fault systems: an example from the deep-water Niger Delta. AAPG Bull. 98, 465–482.

Berner, R. A., 1970. Sedimentary pyrite formation. American Journal of Science, 268, 1-23.

Berner, R. A., 1981. A new geochemical classification of sedimentary environments. Journal of Sedimentary Petrology, 51(2), 359-365.

Bilotti, F. D., Shaw, J. H., Cupich, R. M., Lakings, R. M., 2005. Detachment fold, Niger Delta, in J. H. Shaw, C. Connors, and J. Suppe, eds., Seismic interpretation of contractional fault related folds: AAPG Studies in Geology 53, 103– 104.

Bjørkum, P. A., Walderhaug, O., 1990. Geometrical arrangement of calcite cementation within shallow marine sandstones, Earth-Science Reviews, 29, 145–161.

Bjorlykke, K., 2015. Petroleum Geoscience: From Sedimentary Environments to Rock Physics. Springer Berlin Heidelberg: Berlin, Heidelberg, 1, IX, p. 508.

Bjørlykke, K., 1998. Clay mineral diagenesis in sedimentary basins-a key to the prediction of rock properties. Examples from the North Sea Basin. Clay Miner. 33 (1), 15–34.

Bjørlykke, K., 2014. Relationships between depositional environments, burial history and rock properties. Some principal aspects of diagenetic process in sedimentary basins. Sediment. Geol. 301, 1–14.

Blamey, N.J.F., Azmy, K., Brand, U., 2014. Provenance and burial history of cement in sandstones of the Northbrook Formation (Carboniferous), western Newfoundland, Canada: a geochemical investigation. Sediment. Geol. 299, 30-41.

Boles, J.R., Johnson, K.S. 1984. Influence of mica surfaces on pore-water pH. Chemical Geology 43, 303-317.

Boles, J.R., Ramseyer, K., 1987. Diagenetic carbonate in Miocene sandstone reservoir, San Joaquin basin, California. Am. Assoc. Pet. Geol. Bull. 71, 1475–1487.

Bolhar, R., Van Kranendonk, M.J., 2007. A non-marine depositional setting for the northern Fortescue Group, Pilbara Craton, inferred from trace element geochemistry of stromatolitic carbonates. Precambrian Res.155, 229–250

Brand, U., Veizer, J., 1980. Chemical diagenesis of a multicomponent carbonate system: 1. Trace elements. J. Sediment. Petrol. 50, 1219–1236.

Bukar, M., Worden, R.H., Bukar, S., Shell., 2021. Diagenesis and its controls on reservoir quality of the Tambar oil field, Norwegian North Sea. Energy Geoscience, 2, 10-31.

Burke, K., 1972, Longshore drift, submarine canyons and submarine fans in development of Niger delta, AAPG Bulletin, 56, 1975-1983.

Caracciolo L., Arribas J., Ingersoll R.V., Critelli S., 2014., The diagenetic destruction of porosity in plutoniclastic petrofacies: The Miocene Diligencia and Eocene Maniobra

formations, Orocopia Mountains, southern California, USA, in R.A. Scott, H.R. Smyth, A.C. Morton & N. Richardson (eds.), Sediment Provenance Studies in Hydrocarbon Exploration and Production. Geological Society, London, Special Publication, 386, 49-62, doi: 10.1144/SP386.9.

Civitelli, M., Ravidà, D.C.G., Borrelli, M., Criniti, S., Falsetta, E., 2023. Diagenesis and petrophysics of Miocene sandstones within southern Apennines foreland, Italy. Marine and Petroleum Geology, 155, 106411, 1-16, doi: 10.1016/j.marpetgeo.2023.106411.

Corrado, S., Aldega, L., Perri, F., Critelli, S., Muto, F., Schito, A., Tripodi, V., 2019. Detecting syn-orogenic and sediment provenance of the Cilento wedge top basin (southern Apennines, Italy) by mineralogy and geochemistry of fine grained sediments and petrography of dispersed organic matter. Tectonophysics 750, 404-418, doi 10.1016/j.tecto.2018.10.027.

Chudi, OK., Lewis, H., Stow, D.A.V., Buckman, J.O., 2018. Reservoir quality prediction of deep-water Oligocene sandstones from the west Niger Delta by integrated petrological, petrophysical and basin modelling. In PJ Armitage, AR Butcher, JM Churchill, AE Csoma, C Hollis, RH Lander, JE Omma & RH Worden (eds), Reservoir Quality of Clastic and Carbonate Rocks: Analysis, Modelling and Prediction. Geological Society Special Publication, vol. 435, Geological Society of London, pp. 245-264. https://doi.org/10.1144/SP435.8

Corredor, F., Shaw, J.H., Bilotti, F., 2005. Structural styles in the deep-water fold and thrust belts of the Niger Delta. AAPG (Am. Assoc. Pet. Geol.) Bull. 89 (6), 753–780.

Critelli, S., Nilsen, T.H., 1996, Petrology and diagenesis of the Eocene Butano Sandstone, LaHonda Basin, California. The Journal of Geology, 104, 295-315, doi: 10.1086/629826.

Curtis, C.D., Coleman, M.L., 1986. Controls on the precipitation of early diagenetic calcite, dolomite, and siderite concretions in complex depositional sequence. In: Gautier, D.L. (Ed.), Roles of Organic Matter in Sediment Diagenesis, Society of Economic Palaeontologists and Mineralogists, Special Publication, 38, 23–33.

Critelli, S., Perri, F., Arribas, J., Herrero, M.J., 2018. Sandstone detrital modes and diagenetic evolution of Mesozoic continental redbeds from western-central circum-Mediterranean orogenic belts, in Ingersoll, R.V., Lawton, T.F., Graham, S., eds., Tectonics, Sedimentary Basins and Provenance: A Celebration of William R. Dickinson's Career: Geological Society of America Special Paper 540, 119-132.

Critelli, S., Criniti, S., Ingersoll, R.V., and Cavazza, W., 2023. Temporal and Spatial significance of volcanic particles in sand (stone): implications for provenance and paleotectonics, in Di Capua, A., De Rosa, R., Kereszturi, G., Le Pera, E., Rosi, M. and Watt, S. F.L., eds., Volcanic Processes in the Sedimentary Record: When Volcanoes Meet the Environment: Geological Society of London Special Publication 520, 311-325, doi: 10.1144/SP520-2022-99.

Damuth, J. E., 1994. Neogene gravity tectonics and depositional processes on the deep Niger Delta continental margin: Marine and Petroleum Geology, 11(3), 320– 346.

De Baar, H.J., German, C.R., Elderfield, H., van Gaans, P., 1988. Rare earth element distributions in anoxic waters of the Cariaco Trench. Geochim. Cosmochim. Acta 52, 1203–1219. http://dx.doi.org/10.1016/0016-7037(88)90275-X.

De Baar, H.J.W., Bacon, M.P., Brewer, P.G., Bruland, K.W., 1985. Rare earth elements in the Pacific and Atlantic oceans. Geochimica et Cosmochimica Acta 49, 1943–1959.

Della Porta, G., Webb, G.E., McDonald, I., 2015. REE patterns of microbial carbonate and cements from Sinemurian (Lower Jurassic) siliceous sponge mounds (Djebel Bou Dahar, High Atlas, Morocco). Chem. Geol.400, 65–86.

Doust, H., and Omatsola, E., 1990. Niger Delta, In J. D. Edwards and P. A. Santogrossi, eds., Divergent/passive margin basins: AAPG Memoir 48, 201–238.

Dutton, S. P., 2008. Calcite cement in Permian deep-water sandstones, Delaware Basin, west Texas. Origin, distribution, and effect on reservoir properties. AAPG Bulletin, 92(6): 765–787.

Dutton, S. P., B. J. Willis, C. D. White, and J. P. Bhattacharya, 2000. Outcrop characterization of reservoir quality and interwell-scale cement distribution in a tide influenced delta, Frontier Formation, Wyoming, USA: Clay Minerals, 35, 95–105.

Dutton, S. P., Loucks, R. G., 2010. Reprint of: Diagenetic controls on evolution of porosity and permeability in lower Tertiary Wilcox sandstones from shallow to ultradeep (2000–6700 m) burial, Gulf of Mexico Basin, U.S.A. Marine and Petroleum Geology, 27, 1775–1787.

Dutton, S.P., Loucks, R.G., Day-Stirrat, R.J., 2012. Impact of regional variation in detrital mineral composition on reservoir quality in deep to ultradeep lower Miocene sandstones, western Gulf of Mexico. Mar. Pet. Geol. 35, 139–153.

Dutton, S. P., White, C. D., Willis, B. J., Novakovic, D., 2002. Calcite cement distribution and its effect on fluid flow in a deltaic sandstone, Frontier Formation, Wyoming, USA: AAPG Bulletin, 86, 2007–2021.

Dutton, S.P., 1997. Timing of compaction and quartz cementation from integrated petrographic and burial history analyses, Lower Cretaceous Fall River Formation, Wyoming and South Dakota. Journal of Sedimentary Research, 67, 186–196.

Ehrenberg, S.N. 1995. Measuring sandstone compaction from modal analysis of thin sections – how to do it and what the results mean. Journal of Sedimentary Research Section a – Sedimentary Petrology and Processes, 65, 369–379.

Ehrenberg, S.N., 1989. Assessing the relative importance of compaction processes and cementation to reduction of porosity in sandstones: discussion; compaction and porosity evolution of Pliocene sandstones, Ventura basin, California. Discussion. AAPG Bull. 73, 1274–1276.

Ejedawe, J. E., and S. J. L. Coker, 1984. Dynamic interpretation of organic-matter maturation and evolution of oil-generative window: AAPG Bulletin, 68, 1024-1028.

Ejedawe, J.E., Coker, S.J., Lambert-Aikhionbare, D.O., Alofe, K.O and Adoh, F.O., 1984. Evolution of oil-generative window and oil and gas occurrence in Tertiary Niger Delta Basin. American Association of Petroleum Geologists Bulletin 68, .1744–1751.

Ekweozor, C. M., and Daukoru, E.M, 1984. Petroleum source bed evaluation of Tertiary Niger Delta--reply: American Association of Petroleum Geologists Bulletin, 68, 390-394.

Ekweozor, C.M., Okogun, J.I., Ekong, D.E.U., Maxwell, J.R., 1979. Preliminary organic geochemical studies of samples from the Niger Delta, Nigeria: part 1, analysis of crude oils for triterpanes. Chemical Geology, 27, 11-28.

Ekweozor, C.M., Okoye, N.V., 1980. Petroleum source-bed evaluation of Tertiary Niger Delta. AAPG Bulletin, 64, 1251-1259.

Elderfield, H., Greaves, M.J., 1982. The rare earth elements in seawater. Nature 296, 214–219.

Elderfield, H., Upstill-Goddard, R., Sholkovitz, E.R., 1990. The rare earth elements in rivers, estuaries and coastal sea waters: processes affecting crustal input of elements to the ocean and their significance to the composition of seawater. Geochim. Cosmochim. Acta 54, 971–991.

El-ghali, M.A.K., Tajori, K.G., Mansurbeg, H., Ogle, N., Kalin, R.M., 2006. Origin and timing of siderite cementation in Upper Ordovician glaciogenic sandstones from the Murzuq Basin, SW Libya. Marine and Petroleum Geology, 23, 459–471.

Eneogwe, C.I 2004., The invariance ratio in isoheptanes: a powerful tool for oil-oil correlation in the Tertiary Niger Delta, Nigeria. Organic Geochemistry, 35, 989– 992.

Evamy, B.D., Haremboure, J., Kamerling, P., Molloy, F.A., Rowlands, P.H., 1978. Hydrocarbon habitat of Tertiary Niger Delta: American AAPG Bulletin, 62,1-39.

Frankl, E.J. and Cordry, E.A., 1967. The Niger Delta oil province recent developments onshore and offshore. 7th World Petroleum Congr., Mexico City Proc. IB, p. 195-209.

Frimmel, H.E., 2009. Trace element distribution in Neoproterozoic carbonates as palaeoenvironmental indicator. Chem. Geol. 258, 338–353.

Garzanti, E., 2016. From static to dynamic provenance analysis—sedimentary petrology upgraded. Sediment. Geol. 336, 3–13.

Garzanti, E., 2019. Petrographic classification of sand and sandstone. Earth-Science Reviews, 192, 545-563

Garzanti, E., Dinis, P., Vermeesch, P., Ando, S., Hahn, A., Huvi, J., Limonta, M., Padoan, M., Resentini, A., Rittner, M., Vezzoli, G., 2018a. Dynamic uplift, recycling, and climate

control on the petrology of passive-margin sand (Angola). Sediment. Geol. 375, 86–104.

German, C.R., Elderfield, H., 1990. Application of the Ce anomaly as a paleoredox indicator: the ground rules. Paleoceanography, 5, 823-833

Gier, S., Worden, H. R., Johns, D. W., Kurzweil, H., 2008. Diagenesis and reservoir quality of Miocene sandstones in the Vienna Austria. Marine and Petroleum Geology, 25, 681–695.

Goldstein, S.J., Jacobsen, S.B., 1988. Rare earth elements in river waters. Earth Planet Sci. Lett. 89, 35–47.

Guillong, M., Meier, D.L., Allan, M.M., Heinrich, C.A., Yardley, B.W.D., 2008. Appendix A6; SILLS; a MATLAB-based program for the reduction of laser ablation ICP-MS data of homogeneous materials and inclusions, 40. Short Course Series Mineralogical Association of Canada, pp. 328–333.

Haack, R.C., Sundararaman, P., and Dahl, J., 1997. Niger Delta petroleum System, *in*, Extended Abstracts, AAPG/ABGP Hedberg Research Symposium, Petroleum Systems of the South Atlantic Margin, November 16-19, 1997, Rio de Janeiro, Brazil.

Haack, R.C., Sundararaman, P., Diedjomahor, J.O., Xiao, H., Gant, N.J., May, E.D., Kelsch, K., 2000. Niger Delta petroleum systems, Nigeria. In: Mello, M.R., Katz, B.J. (Eds.), Petroleum Systems of the South Atlantic Margins. American Association of Petroleum Geologists Memoir 73, 213-231.

Haley, B.A., Klinkhammer, G.P., McManus, J., 2004. Rare earth elements in pore waters of marine sediments. Geochimica et Cosmochimica Acta, 68 (6), 1265–1279.

Harris, N.B., 1992. Burial diagenesis of Brent sandstones: A study of Statfjord, Hutton and Lyell fields. Geological Society London Special Publications, 61(1), 351-375

Hendry, J. P., Trewin, N. H., Fallick, A. E., 1996. Low-Mg calcite marine cement in Cretaceous turbidites: Origin, spatial distribution and relationship to seawater chemistry. Sedimentology, 43, 877–900.

Hesse, R., Abid, L.A., 1998. Carbonate cementation-the key to reservoir properties of four sandstone levels (Cretaceous) in the Hibernia Oilfield, Jeanne d'Arc Basin, Newfoundland, Canada. In: Morad, S. (Ed.), Carbonate Cementation in Sandstones: Distribution Patterns and Geochemical Evolution, International Association of Sedimentologists Special Publication 26, pp. 363-393.

Hirt, W.G., Wenk, H.R., Boles, J.R., 1993. Albitization of plagioclase crystals in the Stevens sandstone (Miocene), San Joaquin Basin, California and the Frio Formation (Oligocene), Gulf coast, Texas, a TEM AEM study. Geol. Soc. Am. Bull. 105, 708–714.

Hospers, J., 1971. The geology of the Niger Delta area, in the geology of the East Atlantic continental margin, Great Britain, Institute of Geological Science. Report 70(16), 121–141.

Houseknecht, D. W., 1987. Assessing the relative importance of compaction processes and cementation to reduction of porosity in sandstones. Bulletin American Association Petroleum Geologists 7l, 633-642.

Huggett, J., Dennis, P., Gale, A., 2000. Geochemistry of early siderite cements from the Eocene succession of Whitecliff Bay, Hampshire Basin, UK. Journal of Sedimentary Research 70, 1107–1117.

Irwin, H., Curtis, C., Coleman, M., 1977. Isotopic evidence for source of diagenetic carbonates formed during burial of organic rich sediments. Nature 269, 209–2133.

Jiang, L., Cai. C., Worden, R.H., Li, K., Xiang, L., Chu, X., Shen, A., Li, W., 2015. Rare earth element and yttrium (REY) geochemistry in carbonate reservoirs during deep burial diagenesis: Implications for REY mobility during thermochemical sulfate reduction. Chemical Geology, 415, 87–101.

Jubril, M.A., Amajor, L.C., 1991. The Afam Clay Member: a Lower Miocene incised channel in the southeastern Niger Delta Marine Petroleum Geology, 8, 163-173.

Kamber, B.S., Greig, A., Collerson, K.D., 2005. A new estimate for the composition of weathered young upper continental crust from alluvial sediments, Queensland, Australia. Geochim. Cosmochim. Acta 69, 1041–1058.

Knox, G.J. and Omatsola, M.E., 1989. Development of the Cenozoic Niger Delta in terms of the escalator regression model. In: Coastal Lowlands. Geology and Geotechnology, Proc. K. Ned.. Geol. Mijnbouwk. Genoot., p. 181-202.

Krueger, S.W., Grant, N.T., 2011. The growth history of toe thrusts of the Niger Delta and the role of pore pressure. In: McClay, K., Shaw, J., Suppe, J. (Eds.), Thrust Fault- Related Folding: AAPG Memoir, 94, 357–390.

Kulke, H. (1995): Nigeria. In: Kulke, H. (Eds), Regional Petroleum Geology of the World. Part II: Africa, America, Australia and Antarctica, Gebru Borntraeger, Berlin, 143–172.

Lai, J., Wang, G., Cai, C., Fan, Z., Wang, S., Chen, J., Luo, G., 2018c. Diagenesis and reservoir quality in tight gas sandstones. Geol. J. 53, 629–646. https://doi.org/10.1002/gj.2917.

Lambert – Aikhionbare, D.O., Ibe, A.C., 1984. Petroleum source bed evaluation of Tertiary Niger Delta: discussion. AAPG Bulletin, 68, 387–389.

Lambert-Aikhionbare, D.O., 1981. Sandstone Diagenesis and its Relation to Petroleum Generation and Migration in the Niger Delta. Imperial College of Science and Technology London (Ph.D. thesis), pp. 1–298.

Lambert-Aikhionbare, D.O., 1982. Relationship between diagenesis and pore fluid chemistry in Niger Delta oil-bearing sands. J. Petrol. Geol. 4 (3), 287–298.

Lambert-Aikhionbare, D.O., Shaw, H.F., 1982. Significance of clays in the petroleum geology of the Niger Delta. Clay Miner. 17, 91–103.

Lanz, M. del R., Azmy, K., Cesaretti, N.N., Fortunatti, N.B., 2021. Diagenesis of the Vaca Muerta Formation, Neuqu´en Basin: evidence from petrography, microthermometry and geochemistry. Mar. Petrol. Geol. 124, 104769.

Lawan, A.Y., Worden, R.H., Utley, J.E.P., Crowley, S.F., 2021. Sedimentological and diagenetic controls on the reservoir quality of marginal marine sandstones buried to moderate depths and temperatures: Brent Province, UK North Sea. Marine and Petroleum Geology, 128, 104993.

Lawrence, M.G., Greig, A., Collerson, K.D., Kamber, B.S., 2006. Rare earth element and yttrium variability in Southeast Queensland waterways. Aquat. Geochem.12, 39–72.

Lee, S.G., Lee, D.H., Kim, Y., Chae, B.G., Kim, W.Y., Woo, N.C., 2003. Rare earth elements as indicators of groundwater environment changes in a fractured rock system: evidence from fracture-filling calcite. Appl. Geochem. 18, 135–143.

Lei, Z., Xu, H., Li, Q., Li, W., Yan, D., Li, S., Lei, P., Yan, M., Li, J., 2019. The influence of multiple-stage oil emplacement on deeply buried marine sandstone diagenesis: A case study on the Devonian Donghe sandstones, Tabei Uplift, Tarim Basin, NW China. Marine and Petroleum Geology, 110, 299–316.

Le Pera, E., Arribas, J., Critelli, S., Tortosa, A., 2001, The effects of source rocks and chemical weathering on the petrogenesis of siliciclastic sand from the Neto River (Calabria, Italy): implications for provenance studies. Sedimentology, 48, 357-378, doi 10.1046/j.1365-3091.2001.00368.x.

Li, R., Jones, B., 2014. Evaluation of carbonate diagenesis: a comparative study of minor elements, trace elements, and rare-earth elements (REE+ Y) between Pleistocene corals and matrices from Grand Cayman, British West Indies. Sedimentary Geology, 314, 31–46.

Liang, T., Jones, B., 2021. Characteristics of primary rare earth elements and yttrium in carbonate rocks from the Mesoproterozoic Gaoyuzhuang Formation, North China: Implications for the depositional system. Sedimentary Geology, 415, 105864.

Liu, C., Zheng, H., Hu, Z., Yin, W., Li, S., 2012. Characteristics of carbonate cementation in clastic rocks from the Chang 6 sand body of Yanchang Formation, southern Ordos Basin. Sci. China Earth Sci. 55, 58–66.

Liu, S., Huang, S., Shen, Z., Lü, Z., Song, R., 2014. Diagenetic fluid evolution and water-rock interaction model of carbonate cements in sandstone: an example from the reservoir sandstone of the Fourth Member of the Xujiahe Formation of the Xiaoquan-Fenggu area, Sichuan Province, China. Sci. China Earth Sci. 57, 1077-1092.

Luan, G., Azmy, K., Dong, C. Lin, C., Ren, L., Shi, C., 2022a. Carbonate cements in Eocene turbidite sandstones, Dongying depression, Bohai Bay Basin: Origin, distribution, and effect on reservoir properties. AAPG Bulletin, 106(1), 209–240

Luan, G., Azmy, K., Berra, F., Della Porta, G., Nembrini, M., 2022b. Origin of dolomites in oolitic carbonates of the middle Jurassic Dorgali formation, eastern Sardinia, Italy: petrographic and geochemical constraints. Mar. Petrol. Geol. 135, 105395.

Luan, G., Azmy, K., Meyer, R., Olanipekun, B., Dong, C., 2023. Origin of carbonate cements in Ben Nevis sandstones of Jeanne d'Arc Basin: Insights from geochemistry. Mar. Petrol. 148, 106033.

Lundegard, P.D., 1992. Sandstone porosity loss; a “big picture” view of the importance of compaction. J. Sedimen. Res. 62 (2), 250–260.

Luo, L., Meng, W., Gluyas, J., Tan, X., Gao, X., Feng, M., Kong, X., Shao, H., 2019. Diagenetic characteristics, evolution, controlling factors of diagenetic system and their impacts on reservoir quality in tight deltaic sandstones: typical example from the Xujiahe Formation in Western Sichuan foreland basin, SW China. Mar. Petrol. Geol. 103, 231–254.

MacRae, N.D., Nesbitt, H.W., Kronberg, B.I., 1992. Development of a positive Eu anomaly during diagenesis. Earth Planet. Sci. Lett. 109, 585–591.

Madhavaraju, J., González-León, C.M., 2012. Depositional conditions and source of rare earth elements in carbonate strata of the Aptian-Albian Mural Formation, Pitaycachi section, northeastern Sonora, Mexico. Revista Mexicana de Ciencias Geológicas, 29(2), 478–491.

Maloney, M., Davies, R., Imber, J., Higgins, S., Kings, S., 2010. New insights into deformation mechanisms in the gravitationally driven Niger Delta deep-water fold and thrust belt. AAPG Bull. 94 (9), 1401–1424.

Marfil, R., Delgado, A., Rossi, C., Iglesia, A.L., Ramseyer, K., 2003. Origin and diagenetic evolution of kaolin in reservoir sandstones and associated shales of the Jurassic and Cretaceous, Salam Field, Western Desert (Egypt). Clay Miner. Cement Sandstones 319–342.

Matlack, K.S., Houseknecht, D.W., Applin, K.R., 1989. Emplacement of clay into sand by infiltration. J. Sediment. Petrol. 59, 77-87.

Matsumoto, R., Iijima, A., 1981. Origin and diagenetic evolution of Ca– Mg–Fe carbonates in some coalfields of Japan. Sedimentology, 28, 239–259.

McBride, E. F., and K. L. Milliken, 2006. Giant calcite cemented concretions, Dakota Formation, central Kansas, USA. Sedimentology, 53, 1161–1179.

McBride, E. F., Milliken, K. L., Cavazza, W., Cibin, U., Fontana, D., Picard, M. D., Zuffa, G. G., 1995. Heterogeneous distribution of calcite cement at the outcrop scale in Tertiary sandstones, northern Apennines, Italy: AAPG Bulletin, 79, 1044–1063.

McIlroy, D., Worden, R.H., Needham, S.J., 2003. Faeces, clay minerals and reservoir potential. J. Geol. Soc. 160, 489-493.

McKinley, J.M., Worden, R.H., Ruffell, A.H., 2003. Smectite in sandstones: a review of the controls on occurrence and behaviour during diagenesis. In: Worden, R.H., Morad, S. (Eds.), Clay Mineral Cements in Sandstones, vol. 34. Special Publication of the International Association of Sedimentologists, Oxford, Blackwells, p. 109–128.

McLennan, S.M., 1989. Rare earth elements in sedimentary rocks: influence of provenance and sedimentary processes. Rev. Mineral. 21, 169–200.

Merki, P., 1972. Structural geology of the Cenozoic Niger delta. In: Dessauvagie, T.F.J., Whiteman, A.J. (Eds.), African Geology. University of Ibadan Press, Ibadan, Nigeria, 635–644.

Michard, A., Albare`de, F., 1986. The REE content of some hydrothermal fluids. Chem. Geol. 55, 51–60.

Morad, S., 1986. Pyrite-chlorite and pyrite-biotite relations in sandstones. Sedimentary Geology, 49, 177-192.

Morad, S., 1998. Carbonate cementation in sandstones; distribution patterns and geochemical evolution. In: Morad, S. (Ed.), Carbonate Cementation in Sandstones, 26. International Association of Sedimentologists, (Special Publication),1–26.

Morad, S., Al-Ramadan, K., Ketzer, J.M., De Ros, L.F., 2010. The impact of diagenesis on the heterogeneity of sandstone reservoirs: a review of the role of depositional facies and sequence stratigraphy. AAPG Bull. 94 (8), 1267-1309.

Morad, S., Ben Ismail, H., De Ros, L.F., Al-Aasm, I.S., Serrihin, N.E., 1994. Diagenesis and formation waters chemistry of Triassic reservoir sandstones from southern Tunisia. Sedimentology 41, 1253–1272.

Morad, S., Bergan, M., Knarud, R., Nystuen, J.P., 1990. Albitization of detrital plagioclase in Triassic reservoir sandstones from the Snorre Field, Norwegian North Sea. J. Sediment. Res. 60, 411-425.

Moraes, M.A. S., Surdam, and R.C., 1993. Diagenetic heterogeneity and reservoir quality: fluvial, deltaic, and turbiditic sandstone reservoirs, Potiguar and Reconcavo rift basins, Brazil, AAPG Bulletin, 77, 1142–1158.

Moraes, M.A.S., De Ros, L.F., 1990. Infiltrated clays in fluvial Jurassic sandstones of Reconcavo Basin, northeastern Brazil. J. Sediment. Petrol. 60, 809-819.

Moraes, M.A.S., De Ros, L.F., 1992. Depositional, infiltrated and authigenic clays in fluvial sandstones of the Jurassic Sergie Formation, Reconcavo Basin, northeastern Brazil. In: Houseknecht, D.W., Pittman, E.D. (Eds.), Origin, Diagenesis and Petrophysics of Clay Minerals in Sandstones. SEPM Special Publication, 197-208.

Mozley, P.S. and Carothers, W.W., 1992. Elemental and isotopic composition of siderite in the Kuparuk Formation, Alaska; effect of microbial activity and water sediment interaction on early pore-water chemistry. J. Sed. Res., 624, 681–692.

Mozley, P.S., 1989. Relationship between depositional environment and the elemental composition of early digenetic siderite. Geology 17, 704–706.

Needham, S.J., Worden, R.H., McIlroy, D., 2005. Experimental production of clay rims by macrobiotic sediment ingestion and excretion processes. J. Sediment. Res. 75, 1028-1037.

Nothdurft, L.D., Webb, G.E., Kamber, B.S., 2004. Rare earth element geochemistry of Late Devonian reefal carbonates, Canning Basin, Western Australia: confirmation of a seawater REE proxy in ancient limestones. Geochimica Cosmochimica Acta 68, 263-283.

Nozaki, Y., Zhang, J., Amakawa, H., 1997. The fractionation between Y and Ho in the marine environment. Earth Planet. Sci. Lett. 148, 329–340. http://dx.doi.org/10.1016/S0012-821X(97)00034-4.

Nwachukwu, J.I., Chukwura, P.I., 1986. Organic matter of Agbada Formation, Niger Delta, Nigeria. AAPG (Am. Assoc. Pet. Geol.) Bull. 70, 48–55.

Nwajide, C.S., 2013. Geology of Nigeria's Sedimentary Basins. CSS Bookshops Limited, Lagos, p.565.

Nwajide, C.S., 2022. Geology of Nigeria's Sedimentary Basins, 2nd Edition Albishara Educational Publications, Enugu, p. 693p.

Ogbe, O.B., Okoro, A.U., Ogagarue, D.O., Osokpor, J., Overare, B., Ocheli, A., Opatola, A.O., Oluwajana, O.A., 2021. Reservoir hydrocarbon prospectivity and productivity evaluations of sands S-600 and S-700 of Fega field, onshore Niger Delta Basin, Nigeria. Journal of African Earth Sciences, 184, 104311.

Ogbe, O.B., Orajaka, I.P., Osokpor, J., Omeru, T., Okunuwadje, S.E., 2020. Interaction between sea-level changes and depositional tectonics: implications for hydrocarbon prospectivity in the western coastal swamp depobelt, Niger Delta Basin, Nigeria. AAPG Bull 104, 477–505.

Olanipekun, B., Azmy, K., 2022. Carbonate cementation in the Tithonian Jeanne d'Arc sandstone, terra nova field, Newfoundland: implications for reservoir quality evolution. Sedimentology, 69 (2), 461–500.

Olivarez, A.M., Owen, R.M., 1991. The europium anomaly of seawater: implications for fluvial versus hydrothermal REE inputs to the oceans. Chem. Geol. 92, 317–328.

Oluwadebi, A.G., Taylor, K.G., Dowey, P.J., 2018. Diagenetic controls on the reservoir quality of the tight gas Collyhurst Sandstone Formation, Lower Permian, East Irish Sea Basin, United Kingdom. Sedimentary Geology, 371, 55–74.

Orife, J.M. and Avbovbo, A.A., 1982. Stratigraphic and unconformity traps in the Niger Delta. In: M.T. Halbouty (Editor), The Deliberate Search for the Subtle Trap. AAPG Mem., 32, 251-265.

Osokpor J., Overare, B., 2019. Source Rock Evaluation and Hydrocarbon Potentials in the Northern Depobelt, Niger Delta Basin. Journal of Mining and Geology. 55(1), 17-28.

Osokpor, J, Lucas, F. A., Osokpor, O.J, Overare, B., Izeze., O.E., Avwenagha., E.O., 2015. Palynozonation and lithofacies cycles of Paleogene to Neogene age sediments in PML-1 well, northern Niger Delta Basin. Pacific Journal of Science and Technology, 16, 286 – 297

Osokpor, J., Lucas, F.A., Osokpor, O.J., Overare, B., Alaminiokuma, G.I., Ogbe, O.B., Daniya, T.S., Avwenagha E.O., 2016. Petroleum potential of Paleogene-Neogene age sediments in well TN-1, western Niger Delta basin. Pacific Journal of Science and Technology 17 (1), 288–300.

Overare, B., Osokpor, J., Ekeh, P.C., Azmy, K., 2020. Demystifying provenance signatures and paleo-depositional environment of mudrocks in parts of south-eastern Nigeria: constraints from geochemistry. J. Afr. Earth Sci. 172, 103954.

Overare., B., Azmy, K., Garzanti, E., Osokpor, J., Ogbe, O.B., Avwenagha, E.O., 2021. Decrypting geochemical signatures in subsurface Niger delta sediments: Implication for provenance, weathering, and paleo-environmental conditions. Marine and Petroleum Geology, 126, 104879.

Owoyemi, A.O., Willis, BJ., 2006. Depositional patterns across syndepositional normal faults, Niger delta, Nigeria. Journal of Sedimentary Research, 76, 346–363.

Pastore, G., Garzanti, E., Vermeesch, P., Bayon, G., Resentini, A., Braquet, N., Overare, B., 2023. The zircon story of the Niger River: Time-structure maps of the West African Craton and discontinuous propagation of provenance signals across a disconnected sediment-routing system. J. Geophys. Res.: Earth Surface 128, e2023JF007342. doi:10.1029/2023JF007342.

Paxton, S.T., Szabo, J.O., Ajdukiewicz, J.M., Klimentidis, R.E., 2002. Construction of an intergranular volume compaction curve for evaluating and predicting compaction and porosity loss in rigid-grain sandstone reservoirs. American Association of Petroleum Geologists Bulletin 86, 2047-2067.

Pe-Piper, G., Piper, D.J., 2019. Significance of the chemistry and morphology of diagenetic siderite in clastic rocks of the Mesozoic Scotian Basin. Sedimentology 67 (2), 782–809.

Piper, D.Z., Bau, M., 2013. Normalized rare earth elements in water, sediments, and wine: identifying sources and environmental redox conditions. Am. J. Anal. Chem. 4, 69–83. http://dx.doi.org/10.4236/ajac.2013.410A1009.

Pye, K., Dickson, J.A.D., Schiavon, N., Coleman, M.L., Cox, M., 1990. Formation of siderite-Mg-calcite-iron sulphide concretions in intertidal marsh and sandflat sediments, north Norfolk, England. Sedimentology 37, 325–343.

Rahman, M.J.J., Worden, R.H., 2016. Diagenesis and its impact on the reservoir quality of Miocene sandstones (Surma Group) from the Bengal Basin, Bangladesh. Marine and Petroleum Geology, 77, 898-915.

Reed, K.J., 1969, Environment of deposition of source beds of high-wax oil: American Association of Petroleum Geologists Bulletin, 53, 1502-1506.

Reijers, T.J.A., 2011. Stratigraphy and sedimentology of the Niger Delta. Geologos,17 (3) 133–162.

Reijers, T.J.A., Petters, S.W., and Nwajide, C.S., 1997. The Niger Delta Basin, *in* Selley, R.C., ed., African Basins--Sedimentary Basin of the World 3: Amsterdam, Elsevier Science, 151-172. doi.org/10.1016/S1874-5997(97)80010-X

Rezaee, M.R., Schulz-Rojah, J.P., 1998. Application of quantitative backscattered electron image analysis in isotope interpretation of siderite cement: Tirrawarra Sandstone, Cooper basin, Australia. In: Morad, S. (Ed.), Carbonate Cementation in Sandstones, 26. International Association of Sedimentologists (Special Publication). p. 461–481.

Rossi, C., Rafaela, M., Ramseyer, K., Permanyer, A., 2001. Facies-related diagenesis and multiphase siderite cementation and dissolution in the reservoir sandstones of the Khataba formation, Egypt's western desert. Journal of Sedimentary Research, 71, 459–472.

Scarciglia F., Le Pera E., Critelli S., 2005. The interplay of geomorphic processes and soil development in an upland environment, Calabria, South Italy. Geomorphology 64, 1-23. doi: 10.1016/j.geomorph.2005.01.003.

Scherer, M., 1987. Parameters influencing porosity in sandstones: a model for sandstone porosity prediction. AAPG Bull. 71 (5), 485–491.

Selley, R.E., 2000. Applied Sedimentology. Academic Press, Cambridge, p.523.

Shembilu, N., Azmy, K., Blamey, N., 2021. Origin of Middle-upper Cambrian dolomites in eastern Laurentia: a case study from Belle Isle Strait, western Newfoundland. Mar. Petrol. Geol. 125, 104858

Shields, G., Stille, P., 2001. Diagenetic constraints on the use of cerium anomalies as palaeo-seawater redox proxies: an isotopic and REE study of Cambrian phosphorites. Chem. Geol. 175, 29–48. https://doi.org/10.1016/S0009-2541(00)00362-4.

Short, K.C., Stauble, A.J., 1967. Outline of geology of Niger Delta, American Association of Petroleum Geologists Bulletin, 51, 761-779.

Stacher, P.,1995. Present understanding of the Niger delta hydrocarbon habitat, In: Oti, M. N., and Postma, G., eds., Geology of deltas: Rotterdam, A.A. Balkema, 257-267.

Stephenson, L.P., Plumley, W.J., Palciauskas, V.V. 1992. A model for sandstone compaction by grain interpenetration. Journal of Sedimentary Petrology, 62, 11–22.

Sullivan, K. B., McBride, E. F., 1991. Diagenesis of sandstones at shale contacts and diagenetic heterogeneity, Frio Formation, Texas, AAPG Bulletin, 75, 121–138.

Sun, N., Zhong, J., Hao, B., Ge, Y., Swennen, R., 2020. Sedimentological and diagenetic control on the reservoir quality of deep lacustrine sedimentary gravity flow sand reservoirs of the Upper Triassic Yanchang Formation in Southern Ordos Basin, China. Marine and Petroleum Geology, 112, 104050.

Sverjensky, D.A., 1984. Europium redox equilibria in aqueous solution. Earth Planet. Sci. Lett. 67, 70–78.

Taylor, K.G., Gawthorpe, R.L., Curtis, C.D., Marshall, J.D., Awwiller, D.N., 2000. Carbonate cementation in a sequence-stratigraphic framework: upper Cretaceous sandstones, Book Cliffs, Utah-Colorado. Journal Sedimentary Research, 70, 360-372.

Taylor, T. R., M. R. Giles, L. A. Hathon, T. N. Diggs, N. R. Braunsdorf, G. V. Birbiglia, M. G. Kittridge, C. I. Macaulay, and I. S. Espejo, 2010. Sandstone diagenesis and reservoir quality prediction: Models, myths, and reality: AAPG Bulletin, 94 (8), 1093–1132.

Taylor, T.R., 1990. The influence of calcite dissolution on reservoir porosity in Miocene sandstones, Picaroon field, offshore Texas Gulf Coast. Journal of Sedimentary Petrology, 60 (3), 322-334.

Thomas, C., Graham, C., Ellam, R., Fallick, A., 2004. $^{87}Sr/^{86}Sr$ chemostratigraphy of Neoproterozoic Dalradian limestones of Scotland and Ireland: constraints on depositional ages and time scales. Journal of the Geological Society, 161, 229-242.

Thyne, G., 2001, A model for diagenetic mass transfer between adjacent sandstone and shale: Marine and Petroleum Geology, 18 (6), 743–755.

Tucker, M.E., Wright, V.P., 1990. Carbonate Sedimentology. Blackwell Science Ltd., Oxford, 496. https://doi.org/10.1002/9781444314175.

Tuttle, M.L.W., Charpentier, R.R., Brownfield, M.E., 1999. The Niger Delta Petroleum System: Niger Delta Province, Nigeria, Cameroon, and Equatorial Guinea. USGS Open-file, Africa report 99-50-H.

Veizer, J., 1983. Trace elements and isotopes in sedimentary carbonates. In: Reeder, R. J. (ed.) Carbonates, Mineralogy and Chemistry. Reviews in Mineralogy, 11, 265–299.

Walderhaug, O., 1994. Temperatures of quartz cementation in Jurassic sandstones from the Norwegian continental shelf: evidence from fluid inclusions. Journal of Sedimentary Research 64, 311–323.

Walderhaug, O., and P. A. Bjørkum, 1998. Calcite growth in shallow marine sandstones: Growth mechanisms and geometry, in S. Morad, ed., Carbonate cementation in sandstones. International Association of Sedimentologists, Special Publication 26, 179–192.

Webb, G.E. and Kamber, B.S. 2000. Rare earth elements in Holocene reefal microbialites: a new shallow seawater proxy. Geochim. Cosmochim. Acta, 64, 1557–1565.

Webb, G.E., Nothdurft, L.D., Kamber, B.S., Kloprogge, J.T., Zhao, J.X., 2009. Rare earth element geochemistry of scleractinian coral skeleton during meteoric diagenesis: a sequence through neomorphism of aragonite to calcite. Sedimentology 56, 1433–1463.

Weber, K.J., 1971. Sedimentological aspects of oil fields in the Niger Delta. Geologie en Mijnbouw, 50, 559–576.

Weber, K.J., 1987. Hydrocarbon distribution patterns in Nigerian growth fault structures controlled by structural style and stratigraphy. J. Petrol. Sci. Eng. 1, 91–104.

Weber, K.J., Daukoru, E.M., 1975. Petroleum Geology of the Niger Delta: Proceedings of the Ninth World Petroleum Congress, vol. 2. Applied Science Publishers, 210–221.

Whiteman, A., 1982. Nigeria: Its Petroleum Geology, Resources and Potential: London, Graham and Trotman, 394 pp.

Wilde, P., Quinby, M.S., Erdtmann, B.D., 1996. The whole-rock cerium anomaly: a potential indicator of eustatic sea-level changes in shales of anoxic facies. Sediment. Geol. 101, 43–53.

Wilson, M.D. and Stanton, P.T., 1994. Diagenetic mechanisms of porosity and permeability reduction and enhancement. In: Reservoir Quality Assessment and Prediction in Clastic Rocks (Ed. Wilson, M.D.). SEPM Society for Sedimentary Geology, p. 60.

Worden, R. H., and S. D. Burley, 2003, Sandstone diagenesis: The evolution from sand to stone, in S. D. Burley and Worden, R. H., eds., Sandstone diagenesis: Recent and ancient: Gent, Belgium, International Association of Sedimentologists Reprint Series, v. 4, p. 3–44.

Worden, R.H., Morad, S., 2003. Clay minerals in sandstones: controls on formation, distribution and evolution. In: Worden, R.H., Morad, S. (Eds.), Clay Mineral Cements in Sandstones, vol. 34. Special Publication of the International Association of Sedimentologists, Oxford, Blackwells, p. 3–41.

Worden, R.H., Morrall, G.T., Kelly, S., Mc Ardle, P., Barshep, D.V., 2019. A renewed look at calcite cement in marine-deltaic sandstones: the Brent Reservoir, Heather Field, northern North Sea, UK. Geological Society, London, Special Publications, 484, 305 – 335. https://doi.org/10.1144/SP484-2018-43

Worden, R.H., Needham, S.J., Cuadros, J., 2006. The worm gut; a natural clay mineral factory and a possible cause of diagenetic grain coats in sandstones. J. Geochem. Explor. 89, 428-431.

Xiong, D; Azmy, K., Blamey N.J.F., 2016**.** Diagenesis and origin of calcite cement in the Flemish Pass Basin sandstone reservoir (Upper Jurassic): Implications for porosity development. Marine and Petroleum Geology, 70, 93-118.

Yang, P., Zhang, L., Liu, K., Cao, B., Gao, J., Qiu, Q., 2021. Diagenetic history and reservoir evolution of tight sandstones in the second member of the Upper Triassic Xujiahe

Formation, western Sichuan Basin, China. Journal of Petroleum Science and Engineering 201, 108451. https://doi.org/10.1016/j.petrol.2021.108451

Zhang, J., Nozaki, Y., 1996. Rare earth elements and yttrium in seawater: ICP-MS determinations in the East Caroline, Coral Sea, and South Fiji basins of the western South Pacific Ocean. Geochim. Cosmochim. Acta 60, 4631–4644.

Zhang, L., Bai, G., Luo, X., Ma., X., Chen, M., Wu, M., Yang, W., 2009. Diagenetic history of tight sandstones and gas entrapment in the Yulin Gas Field in the central area of the Ordos Basin, China. Marine and Petroleum Geology, 26, 974–989.

Zhang, Y., Li, F., 2020. Origin of multiple-phase carbonate cements in the sandstones of the third member of the Shahejie Formation in the Niuzhuang Sag, Bohai Bay Basin. Interpretation, 8 (3), SM83-SM101.

Zhixue, S., Zhilei, S., Hongjiang, L., Xijie, Y., 2010. Characteristics of carbonate cements in sandstone reservoirs: A case from Yanchang Formation, middle and southern Ordos Basin, China. Petrol. Explor. Develop., 37(5), 543–551.

Zhou, L., Wang, G., Zhang, Y., Qiao, Y., Hao, F., Xu, R., Quan, L., 2023. Characteristics and origin of Lower Triassic Feixianguan Formation dolostones on the west side of Kaijiang–Liangping Trough, northeastern Sichuan Basin, China. Marine and Petroleum Geology 147, 105956.

Appendix 3.1: Petrographic composition of the Agbada Formation sandstones

Sample number	T1	T2	T3	T4	T5	T6	M2	T7	M1	T8	T9	M5	T10	M4	M3	T11	T12	T13
Monocrystalline quartz (%)	46.0	44.6	56.6	58.0	38.2	57.0	51.6	42.8	39.6	42.2	58.4	61.0	57.8	60.0	51.6	51.4	48.6	58.0
Polycrystalline quartz	1.2	10.4	3.6	1.6	1.8	7.6	5.2	10.2	12.4	12.0	2.4	4.0	2.2	4.0	3.8	3.2	4.4	3.0
K-feldspar	4.0	3.2	3.8	7.4	5.6	1.8	5.6	3.2	3.2	2.8	3.6	2.4	3.2	4.0	4.8	3.6	2.2	3.8
Plagioclase	4.0	2.0	1.0	2.2	1.4	1.0	3.4	0.0	0.0	0.0	0.8	0.0	0.8	1.0	3.2	1.0	1.0	0.8
Chert	0.6	0.0	0.0	0.0	0.0	0.0	0.0	0.0	0.4	0.4	0.0	0.0	0.0	0.0	0.0	0.0	0.0	0.0
Argillaceous rock fragment	1.4	0.0	0.2	0.0	0.4	0.2	0.4	0.4	0.8	0.8	0.8	0.0	0.6	0.0	1.0	0.4	0.0	0.6
Sedimentary rock fragment	0.4	0.4	0.0	0.0	0.0	0.0	0.0	0.0	0.4	0.4	0.0	0.0	0.0	0.4	0.8	0.6	0.0	0.0
Metamorphic rock fragment	0.0	0.0	0.4	0.4	0.8	0.4	0.0	0.4	0.0	0.0	0.0	0.4	0.0	0.4	0.0	0.4	0.8	0.8
Plutonic rock fragment	0.0	0.0	1.8	1.2	0.8	1.6	0.0	0.2	0.4	0.4	0.0	0.4	0.0	0.4	0.0	1.0	1.0	0.0
Glauconite	0.4	0.0	0.0	0.0	0.4	0.0	0.0	0.0	0.0	0.0	0.0	0.0	0.0	0.0	0.0	0.0	0.0	0.0
Carbonate/Shell fragment	0.4	0.0	0.0	0.0	0.8	0.0	0.0	0.0	0.0	0.0	0.0	0.0	0.0	0.0	0.0	0.0	0.0	0.0
Organic matter	1.4	0.4	0.0	0.0	2.6	0.0	0.0	0.0	0.0	0.0	0.0	0.0	0.0	0.0	0.4	0.4	0.4	0.0
Micas	1.0	2.6	0.0	0.0	1.0	0.0	0.8	1.4	1.6	2.8	0.0	0.4	1.2	0.4	0.8	1.2	2.2	0.8
Heavy mineral	1.0	1.4	1.2	2.0	1.6	1.6	0.4	1.0	0.0	0.0	2.4	0.4	1.2	0.4	0.4	1.6	1.4	1.8
Detrital/dispersed Clay	1.4	1.2	2.0	0.4	1.2	2.0	2.0	0.0	0.0	0.0	0.0	0.0	0.0	0.0	2.0	1.8	2.4	0.0
Laminated Clay	3.0	2.8	0.0	0.0	4.6	0.0	0.0	0.0	0.0	0.0	0.0	0.0	0.0	0.0	0.0	0.6	2.4	0.0
Kaolinite	1.8	1.6	0.0	0.0	0.8	0.0	1.8	2.6	1.6	1.2	0.4	1.0	0.6	0.4	1.8	1.6	1.0	0.4
Chlorite	0.0	0.0	0.0	0.0	0.0	0.0	0.0	0.0	0.0	0.0	0.8	0.0	0.4	0.0	0.0	0.0	0.0	0.6
Undifferentiated Clay	0.0	0.0	0.0	0.0	0.6	0.0	1.4	2.2	2.0	1.6	0.4	0.0	0.0	0.0	1.6	1.2	2.0	0.4
Clay coats	2.0	0.0	0.4	0.4	1.2	0.0	0.6	0.4	0.0	0.0	0.0	0.0	0.0	0.2	0.0	0.4	1.4	0.0
Calcite cement	0.0	0.0	0.0	0.0	0.0	0.0	0.0	0.0	0.0	0.0	5.2	2.2	5.6	0.0	0.0	0.0	0.0	3.2

Siderite cement	6.2	3.0	1.8	3.2	12.0	0.4	2.0	10.0	12.0	10.0	0.4	2.0	0.4	3.0	3.0	6.4	4.0	0.4
Quartz overgrowth	0.0	0.0	0.4	0.4	0.0	0.4	0.0	2.4	2.4	2.4	9.2	1.4	8.4	1.2	0.4	0.4	0.0	7.2
Pyrite	2.4	1.2	1.2	0.4	3.8	1.2	2.4	0.2	0.0	0.0	0.0	2.0	1.0	2.0	2.4	2.2	2.2	1.0
Hematite	0.0	0.0	1.0	0.0	0.0	0.0	0.0	0.0	0.0	0.0	2.0	1.0	2.0	1.0	0.0	0.0	0.6	2.0
Intergranular porosity	12.0	18.8	14.8	15.8	14.2	14.6	16.0	16.4	16.8	17.6	12.0	19.0	12.4	18.8	16.0	15.8	15.6	13.8
Secondary porosity	9.4	6.4	9.8	6.6	6.2	10.2	6.4	6.2	6.4	5.4	1.2	2.4	2.2	2.4	6.0	4.8	6.4	1.4

Sample number	T13B	T14	T15	D1	D2	D3	D4	E1	E2	E3	E4	F1	F2	F3	F4	G1	G2	G3
Monocrystalline quartz	50.4	47.6	51.6	54.8	57.6	57.2	48.4	59.6	49.4	57.6	39.2	56.0	57.6	57.2	53.6	50.2	37.8	53.8
Polycrystalline quartz	2.2	4.4	2.8	3.6	1.6	2.0	1.2	1.2	2.2	2.8	3.0	1.2	2.8	1.4	3.2	1.0	1.0	1.4
K-feldspar	4.8	3.2	5.4	7.4	3.2	6.2	6.8	5.0	5.6	8.4	4.6	5.2	8.4	4.8	5.2	6.0	5.2	4.4
Plagioclase	2.0	1.0	2.2	2.0	0.4	2.2	1.2	0.2	2.4	0.4	3.2	1.2	0.8	2.0	2.4	3.2	4.0	2.8
Chert	0.0	0.0	0.0	0.4	0.0	0.0	0.0	0.4	0.0	0.0	0.0	0.0	0.0	0.0	0.0	0.0	0.4	0.0
Argillaceous rock fragment	0.4	0.0	0.6	0.4	0.0	2.4	0.4	0.0	0.4	0.0	0.8	0.4	0.0	0.0	0.0	0.4	0.0	0.0
Sedimentary rock fragment	0.6	0.4	0.0	0.0	0.0	0.0	0.0	0.4	0.0	0.0	0.4	0.0	0.0	0.0	0.0	0.0	0.0	0.0
Metamorphic rock fragment	0.0	0.4	0.2	0.0	2.0	0.0	0.0	0.4	0.0	0.4	0.6	0.0	0.0	0.4	0.0	0.0	1.0	0.0
Plutonic rock fragment	1.0	1.0	0.4	0.6	2.0	0.4	1.2	1.4	0.4	0.4	1.0	1.2	1.2	0.4	0.0	0.0	0.0	0.0
Glauconite	0.0	0.2	0.0	0.4	0.0	0.0	0.4	0.0	0.0	0.0	0.0	0.0	0.0	0.0	0.0	0.8	0.0	0.0
Carbonate/Shell fragment	0.0	0.0	0.0	0.0	0.8	0.0	0.0	0.0	0.0	0.0	0.4	0.0	0.0	0.0	0.0	0.0	0.4	0.0
Organic matter	0.8	0.8	1.0	0.4	0.0	1.4	0.4	0.0	2.0	0.0	0.0	1.0	0.0	0.4	0.4	0.8	2.4	0.4
Micas	1.2	2.2	1.4	0.6	0.6	0.8	0.4	1.0	0.8	0.0	0.4	0.4	0.4	0.4	0.4	1.4	1.0	0.8
Heavy mineral	1.6	1.4	0.4	0.0	1.4	0.4	0.8	1.0	0.4	0.8	1.4	0.0	0.0	0.6	1.6	0.4	0.4	1.2
Detrital/dispersed Clay	1.8	2.4	1.6	3.4	2.0	1.4	11.6	0.0	2.4	1.6	1.2	4.8	0.4	6.0	7.0	8.8	5.6	6.8
Laminated Clay	0.0	2.4	3.4	0.0	0.0	0.0	0.0	0.0	4.6	0.0	0.0	0.0	0.0	0.0	0.0	0.0	5.8	0.0

Kaolinite	1.6	1.0	1.8	0.0	0.0	0.0	0.4	0.0	2.0	0.0	0.0	0.0	0.4	0.0	0.0	0.0	0.8	0.0
Chlorite	0.0	0.0	0.2	0.0	0.0	0.0	0.0	0.0	0.0	0.0	0.0	0.0	0.0	0.0	0.0	0.0	0.0	0.0
Undifferentiated Clay	0.0	2.0	0.2	0.0	0.0	0.0	0.0	0.4	0.0	0.0	0.0	0.0	0.0	0.6	0.0	0.0	0.0	0.0
Clay coats	0.4	1.4	0.6	1.2	0.0	0.4	0.4	1.0	0.4	0.4	0.6	0.4	0.4	0.0	0.8	0.0	1.6	0.0
Calcite cement	0.0	0.0	0.0	0.0	0.0	0.4	0.0	0.0	2.2	0.0	0.0	0.0	0.0	0.0	0.0	0.0	0.0	0.0
Siderite cement	6.4	4.0	3.4	0.4	0.6	2.4	3.6	1.6	3.4	1.6	16.4	0.8	0.4	0.4	0.8	2.8	6.2	2.4
Quartz overgrowth	0.0	0.0	0.0	0.0	0.8	0.0	0.0	0.8	0.0	0.4	0.0	0.4	0.8	0.0	0.0	0.0	0.4	0.0
Pyrite	2.2	2.2	1.4	0.8	1.4	0.8	1.2	0.8	2.6	0.8	3.6	2.4	0.8	0.8	0.8	1.2	4.4	2.4
Hematite	0.0	0.0	0.0	0.0	0.0	0.0	0.0	0.0	0.4	0.0	0.0	0.6	0.0	2.0	0.0	0.0	0.0	0.0
Intergranular porosity	15.8	15.6	15.0	14.6	14.2	14.2	13.0	15.0	13.0	13.8	15.0	13.2	15.4	14.0	14.4	13.8	12.2	14.6
Secondary porosity	6.8	6.4	6.4	9.0	11.4	7.4	8.6	9.8	5.4	10.6	8.2	10.8	10.2	8.6	9.4	9.2	9.4	9.0

Appendix 3.2**:** MLA composition of the Agbada Formation sandstones

Sample	T7	M1	T9	T10	F1	E2
Quartz (%)	68.62	72.63	73.79	61.67	68.32	74.41
Orthoclase	7.97	8.21	5.18	4.44	7.92	5.21
Plagioclase	2.59	2.71	1.18	0.97	2.49	1.24
Siderite	4.04	6.36	0.35	0.20	4.00	0.36
Calcite	0.01	0.01	4.35	3.52	0.01	4.49
Kaolinite	2.26	1.81	0.61	0.51	1.63	1.37
Illite	1.25	1.27	1.25	1.00	1.20	0.62
Muscovite	0.00	0.66	0.09	0.07	0.58	0.00
Chlorite-Fe	0.58	0.63	0.05	0.04	0.51	0.07
Glauconite	0.00	0.12	0.03	0.02	0.10	0.00
Tourmaline	0.10	0.11	0.06	0.04	0.09	0.06
Biotite	0.00	0.07	0.02	0.01	0.06	0.00
Rutile	0.03	0.05	0.25	0.13	0.03	0.25
Titanite	0.02	0.03	0.23	0.14	0.02	0.23
Hematite	0.01	0.03	0.00	0.20	0.01	0.00
Apatite	0.00	0.01	0.10	0.07	0.01	0.00
Pyrite	0.01	0.02	0.02	0.01	0.01	0.02
Ilmenite	0.01	0.01	0.02	0.01	0.01	0.02
Zircon	0.01	0.01	0.05	0.02	0.01	0.05
Pores	12.50	5.26	12.36	26.92	13.00	11.60
Total (%)	100.00	100.00	100.00	100.00	100.01	100.00

Chapter IV

Paleosalinity signals deciphered from parts of the Agbada Formation, Niger Delta Basin: A geochemical approach

Corresponding author's e-mail address: boverare@mun.ca.

Prepared for submission to the Journal of Geosystems and Geoenvironment

Abstract

Trace-element signatures are widely used to reconstruct sedimentary environments, including to articulate insights on paleosalinity, particularly for the qualitative distinction of freshwater, coastal marine/brackish, and full-marine depositional conditions. The Agbada Formation (Niger Delta Basin) is a classic example of paralic facies representing unique spatial and temporal variations in sediment characteristics, water chemistry, and hydrodynamic systems. Elemental ratios (B/Ga, Sr/Ba, and S/TOC) and their general utility for reconstructing paleosalinity have not been demonstrated in the Agbada Formation. Therefore, several trace element proxies (elemental ratios and boron-derived paleosalinity proxies) are integrated in this study to provide a better insight into the paleosalinity conditions that are prevalent in the Agbada Formation. The signals from B/Ga (1.8–5.9, 3.4 ± 1.1), Sr/Ba (0.1–1.6, 0.3 ± 0.4) and S/TOC (0.1–0.9, 0.4 ± 0.3) suggest mainly low saline, brackish conditions with inputs from fresh and marine waters. All the boron-derived paleosalinometric tools: equivalent boron (117–423ppm, 249 ± 75ppm) Adam's (4.4–34.3‰, 17.3‰ ± 7.3), Landergren and Carvajal's (1.6–43.1‰, 15.5‰ ± 10.2) and Couch's (12.8–26.7‰, 19.3‰ ± 4.1) methods are consistent with the insights from the elemental ratios, also pointing to low saline, brackish settings with

considerable inputs from both fresh and marine waters. The perceptions from the various paleosalinity proxies are consistent with paralic facies of the Agbada Formation and represent the interplay between freshwater and seawater that are susceptible to lateral and/or vertical salinity gradients, with zones of lower salinities linked to reduced seawater or increased freshwater inputs and zones of greater seawater inputs reflecting relatively higher salinities. This research contributes to the geology of the Niger Delta, particularly from an inorganic geochemical perspective, and corroborates the faunal evidence in the Agbada Formation, comprising numerously of terrestrially derived pollen and spores with significant marine-derived dinoflagellate cysts and foraminiferal test linings. Integrating the various proxies is essential for refining paleosalinity perceptions and improving confidence in interpretation. Therefore, we suggest a similar approach would be suitable for paleosalinity watermass reconstruction in other ancient siliclastic systems.

4.1. Introduction

Salinity is an important feature of watermasses commonly reported in modern aqueous systems, being a significant factor for the preservation and enrichment of organic matter. It may control the primary productivity, thus providing insight into the paleoecological and paleoenvironmental studies. Paleosalinometric tools have been in the literature for several decades, although caution is recommended for their general applicability due to certain limitations or drawbacks. A common method for evaluating paleosalinity depends on signals from biological evidence (e.g., Bukry, 1974; Van Geel, 2001**;** Buatois et al., 2010; Jaglarz and Ucham, 2010; Bankole et al., 2014). However, they are feasible only when fossils are deposited and preserved; and in some cases, assemblages are only crudely diagnostic of salinity level and it is almost impossible to guarantee that all microfossils are in situ rather than transported from distal regions reflecting different environmental conditions (e.g**.,** Matthiessen, 1995; Wei and Algeo, 2020). Some other techniques, that have been utilized for reconstructing paleosalinity,

include sedimentological studies, biomarkers and organic geochemical data, authigenic iron sulfides, isotope geochemical signatures, sulfur/organic carbon ratio (S/TOC), and bulk sediment geochemical proxies (e.g., Degens et al., 1957; Frederickson and Reynolds, 1960; Adams et al., 1965; Walker and Price, 1963; Nelson, 1967; Couch, 1971; Berner et al.,1979; Berner and Raiswell, 1983, 1984; Pirrus, 1992; Ingram et al., 1996; Holmden et al., 1997; Barakat and Rullkotter, 1997; Reinhardt et al., 1998; Hasegawa et al. 2010; Spear et al., 2014; Zhang et al., 2017; Wei et al., 2018; Retallack et al., 2020; Remírez and Algeo, 2020; Wei and Algeo, 2020; Quan et al., 2020; Song et al., 2021; Wei et al., 2022; Cheng et al., 2023; Zhang et al., 2023). Nevertheless, most of these approaches have limitations and require caution and/or integration with other methods.

The Agbada Formation, Niger Delta Basin, is a classic example of paralic facies that represents the dominant hydrocarbon-bearing reservoir in the basin, attracting numerous publications from academia and stakeholders in the oil and gas industries (Short and Stauble 1967; Ejedawe et al., 1984; Lambert-Aikhionbare and Ibe, 1984; Doust and Omatsola, 1990; Tuttle et al., 1999; Ekpo et al., 2018; Anyiam and Uzuegbu 2020; Osokpor and Overare; 2019; Ogbe et al., 2021). Paralic environments are sometimes complex to understand due to their unique spatial and temporal variations in sediment source and composition, water chemistry, and hydrodynamic systems. Their convolution reduces the ability of geologists to effectively decipher geological histories and reconstruct paleoenvironments from the rock record in such settings. Due to the signature inputs from fresh and marine water, defining transition zones (coastal terrestrial or marginal-marine settings) in sedimentary succession hinges upon perceptions of paleosalinity reconstructions. Hence, the availability of proxies that can reliably decode sensitive changes in water mass salinity in space and time and/or complement other techniques for this type of system is desired. Geochemical evidence for water mass salinity is a tool commonly used as an alternative to complement other techniques or refine intervals,

especially where signals from fossil assemblage and/or other methods are inconclusive. Bulk sediment geochemical proxies (e.g., B/Ga, Sr/Ba, S/TOC) for reconstructing paleosalinity and their general applicability to fine-grained siliciclastic sediments in the Agbada Formation have not been demonstrated. Therefore, this investigation focuses on reconstructing paleosalinity using geochemical signatures encoded in Agbada Formation, Niger Delta Basin. The purpose is to utilize several geochemical proxies (B/Ga, Sr/Ba, S/TOC) to establish the salinity conditions prevalent in the paleodepositional environment. In addition, boron-derived paleosalinity reconstructions are also considered to provide quantitative insight and offer a platform for integrating various proxies and improving confidence in the interpretation.

4.2. Geologic settings

The study areas (Fig. 4.1) are located in the Cenozoic Niger Delta Basin, within the fringe of the Gulf of Guinea, on the Atlantic coast of West Africa and the west coast of Central Africa. The Niger Delta has received a variety of publications that defines its evolution, stratigraphy, and petroleum system and provenance of the sediments (e.g., Short and Stauble, 1967; Avbovbo, 1978; Evamy et al., 1978; Ekweozor and Okoye, 1980; Ejedawe and Coker 1984; Whiteman, 1982; Doust and Omatsola, 1990; Tuttle et al., 1999; Nwajide, 2013; Osokpor et al., 2015; Anomneze et al., 2020; Overare et al., 2021; Osokpor and Ogbe, 2023; Obi et al., 2024). The evolution of the Niger Delta is connected to the failed arm of a triple junction system (aulacogen) along a series of rift zones of different orientations that initially developed in the Mesozoic due to the separation of South American and African land masses (Doust and Omatsola, 1990). The southwestern and southeastern coast of Nigeria and Cameroon, harboring two arms, formed the West African passive continental margin, whereas the Benue Trough developed from the failed third arm (Lehner and De Ruiter, 1977). The formation of the delta commenced when the influx of sediments supplied from the Niger River and adjacent highlands progressively filled up the Benue Trough as the equatorial Atlantic Ocean was

opening. During the late Eocene, the progradation of the siliciclastic wedge in the basin began to accumulate beyond the confines of the continental slope (Burke, 1972). This progradation (active to date) led to the development of depobelts corresponding to discrete periods of the delta's evolutionary history (Doust and Omatsola, 1990; Ekweozor and Daukoru, 1984).

The Cenozoic Niger Delta Basin consists of outcropping (including Imo, Ameki, Ogwashi-Asaba, and Benin Formations, Fig. 4.2) and subsurface units (diachronous prograding lithostratigraphic units; Akata, Agbada, and Benin formations, Fig. 4.3). The Akata Formation is typically overpressured, consisting predominantly of thick marine shale units, with signatures of sandy and silty beds defined as turbidites and continental-slope channel fill (Tuttle et al., 1999). It is ~5 km thick in deep-water settings (Bilotti et al., 2005; Corredor et al., 2005) but attains a thickness of ~7 km in the central part of the delta (Doust and Omatsola, 1990). The paralic facies (Agbada Formation), which represent a transitional environment between those of the Akata and Benin Formations, consist of channel sands and shoreface facies with minor shale in the upper parts and predominantly interbeds of shale and sands of roughly equal proportion in the lower section. The Agbada Formation is the thickest in the coastal and central swamp depobelts (up to 3940m, Avbovbo, 1978) but thinnest on the present-day shelf in response to Akata shale diapirism. Representing an upper delta top lithofacies, the Benin Formation consists mostly of sand/sandstone (70–100%) with only local thin shale interbeds (Avbobvo, 1978) that lack distinctive marine or brackish-water microfauna, suggesting the first downhole occurrence of marine shale that contains a distinctive marine microfauna reflecting the Agbada shales can be roughly regarded as its base (Short and Stauble, 1967). The shales suggest back-swamp deposits and oxbow fills, whereas the sandstones document point-bar deposits, channel fills, or natural levees (Reijers, 2011). The unit attains a maximum thickness of 1970–2100 m in the Warri-Degema area, which is the depocenter (Avbovbo, 1978; Whiteman, 1982).

Penecontemporaneous deformation (Fig. 4.4) of the deltaic sediments resulted in growth faults (mostly trending NE/SW or NW/SE; Hosper, 1971) with associated rollover anticlinal structures and shale diapirs from shale upheaval ridges. The growth and characteristics of these structures have been discussed by many authors (e.g., Hosper, 1971; Merki, 1972; Weber and Daukoru, 1975; Evamy et al., 1978; Weber, 1987; Doust and Omatsola, 1990; Damuth, 1994; Stacher, 1995; Tuttle et al., 1999; Corredor et al., 2005; Maloney et al., 2010; Krueger and Grant, 2011; Benesh et al., 2014; Jolly et al., 2016). Together with stratigraphic traps (e.g., pinch outs, clay-filled channels), which are common along flanks of the delta, the growth fault systems and their associated rollover structures comprise the prominent hydrocarbon trapping mechanisms in the Niger Delta Basin (Beka and Oti, 1995; Tuttle et al., 1999). Turbidite facies in the upper Akata Formation are prospective exploration targets, but hydrocarbons are produced from the sandstone reservoirs within the Agbada Formation (Tuttle et al., 1999), with the remaining hydrocarbon resources reflecting several well-imaged targets from shallow zones or poorly imaged zones from deeper targets (Adereti et al., 2012).

There have been speculations about the source sediments since the early days of petroleum exploration in the Niger Delta Basin (Frankl and Cordry, 1967; Short and Stauble, 1967; Evamy et al., 1978; Ekweozor et al., 1979; Ekweozor and Okoye, 1980; Ejedawe et al., 1984; Ejedawe and Coker 1984; Ekweozor and Daukoru, 1984; Lambert-Aikhionbare and Ibe, 1984; Nwachukwu and Chukwura, 1986; Doust and Omatsola, 1990; Kulke 1995; Stacher, 1995; Tuttle et al., 1999; Haacket al. 1997; 2000; Osokpor et al., 2016; Osokpor and Overare 2019). These postulations were championed by divergent views and a tangling assemblage of datasets with source speculations including the deep marine Akata Shales, the marine interbedded shale intervals of the Agbada Formation, and Cretaceous shale probably occurring at lower stratigraphic levels. Nevertheless, it is widely accepted that the hydrocarbon is sourced

predominantly from the marine shale facies of the upper Akata Formation, with contributions from the lowermost shale facies of the Agbada Formation. The Niger Delta crudes are sourced from mixed organic matter: mainly from land plant materials reflecting high resins and waxes and from structureless organic matter that depicts significant contributions from marine sources (Reijers et al., 1997). The substantial contributions from land-derived plant source material are evident in Nigerian crudes characterized by low sulfur contents (< 0.4%, Reijers et al., 1997).

4.3. Methodology

Representative core samples (shales) acquired from oil companies operating in the Niger Delta Basin were examined with various analytical methods.

4.3.1 Geochemistry

Trace element analyses were conducted with High-Resolution Inductively Coupled Plasma Mass Spectrometry (HR-ICP-MS). Sample powders were weighted to about 80–100 mg in cleaned PFA beakers. The powders were dissolved with a mix of concentrated HF-HNO_3 and put on a hot plate for 24h at 100°C. Samples were evaporated to dryness and complete redissolution was achieved with a mix of concentrated HCl-HNO_3, and were put on a hot plate for 24h at 100°C. The residues were dissolved in 5 ml HCl 6N and centrifuged to remove organic matter, and they were kept as archive solutions. Trace elements were measured on an HR-ICP-MS Thermofisher Scientific Element XR at PSO (Pôle de Spectrométrie Océan, IUEM, Brest, France).

An aliquot of the archive solution was diluted in 2.5% HNO_3 doped with indium as an internal standard to correct the signal drift during measurements. Sample concentrations were calibrated using in-house external calibration standards. The standard BHVO2 and procedural blanks were also prepared and run with the samples. Uncertainty of analyses was better than 5%.

The Elemental Isotope Cube in Ján Veizer Laboratory, University of Ottawa, was used to determine the N%, C%, H%, and S%. Representative samples were acidified using 50% HCI. The carbonate-free residues were then dried overnight in an oven at 25°C. Up to 200mg of the powdered samples were weighed into tin capsules; material with concentrations down to 0.01% can be analyzed on the Elemental Cubes due to their large capacity capabilities. Tungsten oxide (WO_3) acted as a combustion catalyst and a binder and was added to take care of resilient solids, such as salts, (inorganic) sulfur-bearing minerals, iron oxides, or alkalis before being closed. The closed capsules are re-weighed on the microbalance. Calibrated standards were prepared in a range of weights and run with the samples. A "blind" standard was also run as a check for the calibration. The prepared capsules were loaded into the carousel of the autosampler. A sample falls into the top of a column of solid chemicals at 1150°C and is flash-combusted at 1800°C for a few seconds with the addition of oxygen. Ultra-pure helium is used to carry the resulting gases through the column of chemicals to finally obtain N_2, CO_2, H_2O, and SO_2, then through a series of adsorption traps to separate them ("Trap and purge" method). The thermoconductivity detector (TCD) measures the gases as they are released. The Elementar's software that controls the EA in stand-alone mode is used to process the results from the TCD using various calibration curves, usually linear regression. The analytical precision (2 sigma) for the analyses is ± 0.2%.

4.3.2 Clay mineralogy

The <2 μm fractions of representative samples were analyzed for their mineralogical compositions at Activation Laboratories Limited (Ancaster, Ontario, Canada) using X-ray diffraction analysis (XRD). A split of samples was dispersed in distilled water, and clay minerals (< 2 μm fraction) were separated by settling suspended particles. Oriented slides (< 2 μm fraction) were carefully prepared by placing a portion of the suspension onto a glass slide. The oriented dry slides were analyzed after treatment with ethylene glycol and heating at

375°C. A Bruker D8 Endeavour diffractometer equipped with Cu X-ray source was utilized for the XRD analysis, with operational conditions: 40 kV and 40 mA, range 4-70 deg 2θ for random specimens and 3–30 deg 2θ for oriented specimens, step size 0 0.02 deg 2θ, time per step 0.5 sec, fixed divergence slit, angle 0.3°, and sample rotation 1 rev/sec. Mineral identification was performed with the help of the PDF4/Minerals ICDD database. Quantities of mineral phases were determined using the Rietveld method based on the calculation of the full diffraction pattern from crystal-structure data. Semi-quantitative amounts of clay minerals in the < 2 μm fraction were calculated using the relative ratios of basal-peak areas.

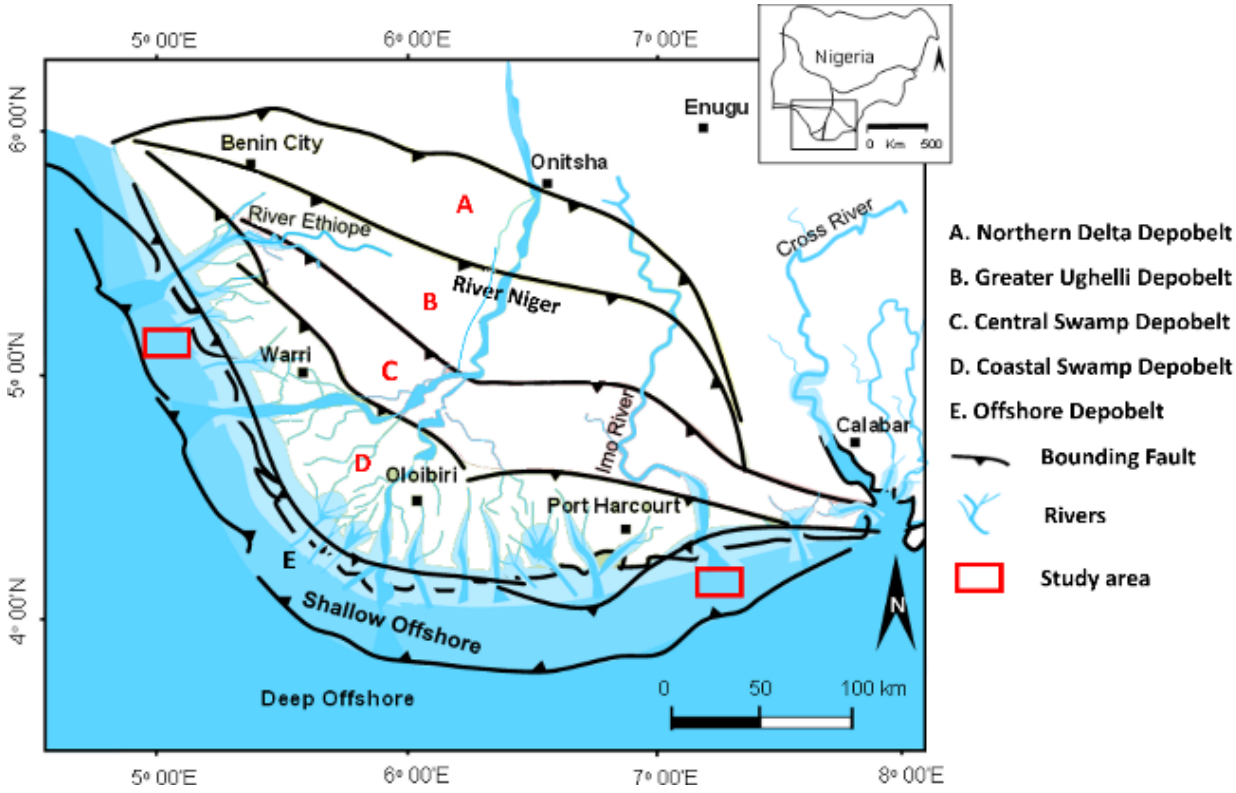

Figure 4.1: Simplified map of the Cenozoic Niger Delta Basin depicting the study area, structural limits, and depobelts. Inset: Nigeria and Niger Delta region (modified from Overare et al., 2021).

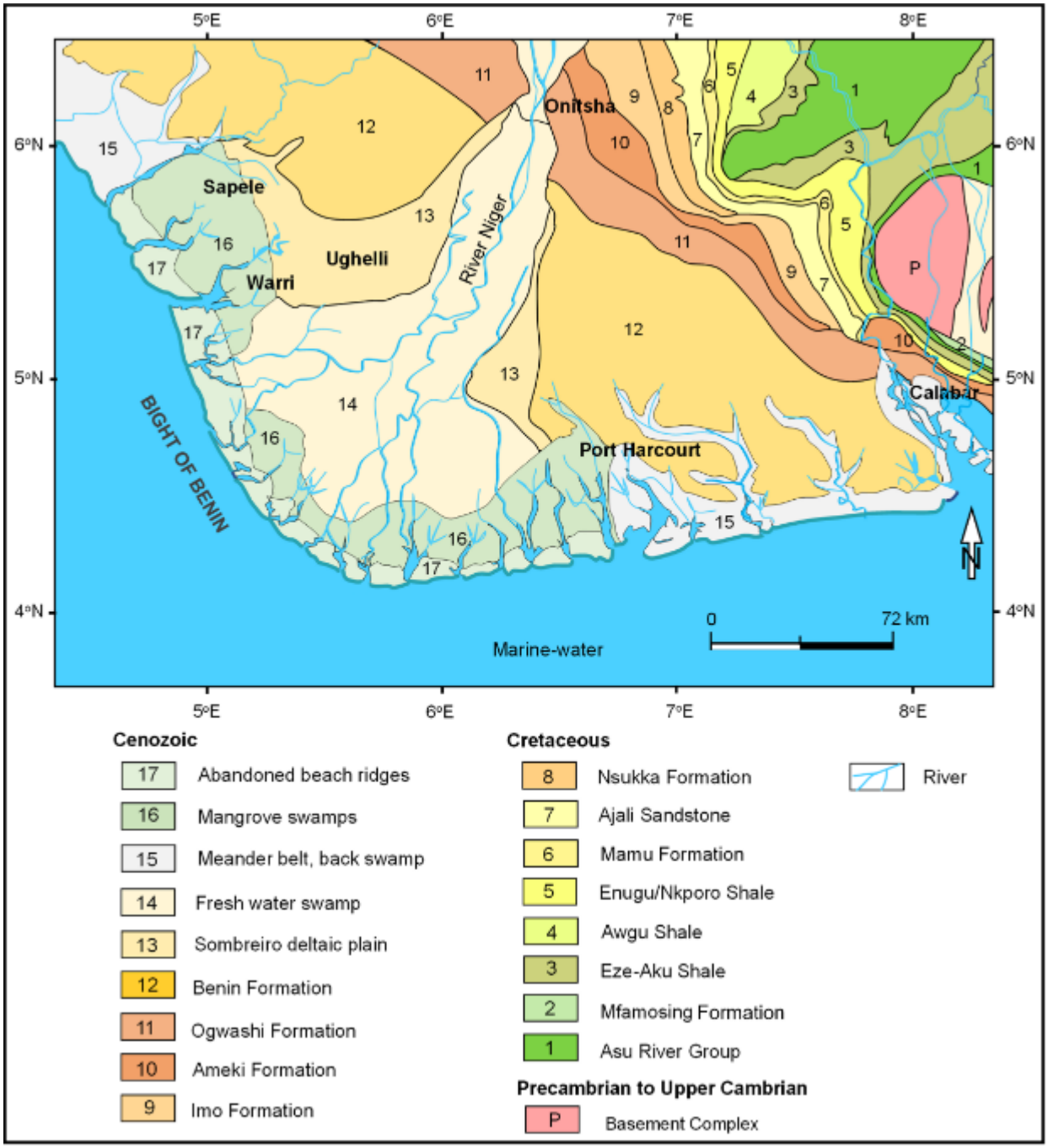

Figure 4.2. Geologic map of onshore Niger Delta and adjacent areas (Redrawn and modified from Reijers et al., 2011). Note the presence of basement rocks and Cretaceous units belonging to older sedimentary basins in the northeastern part of the map.

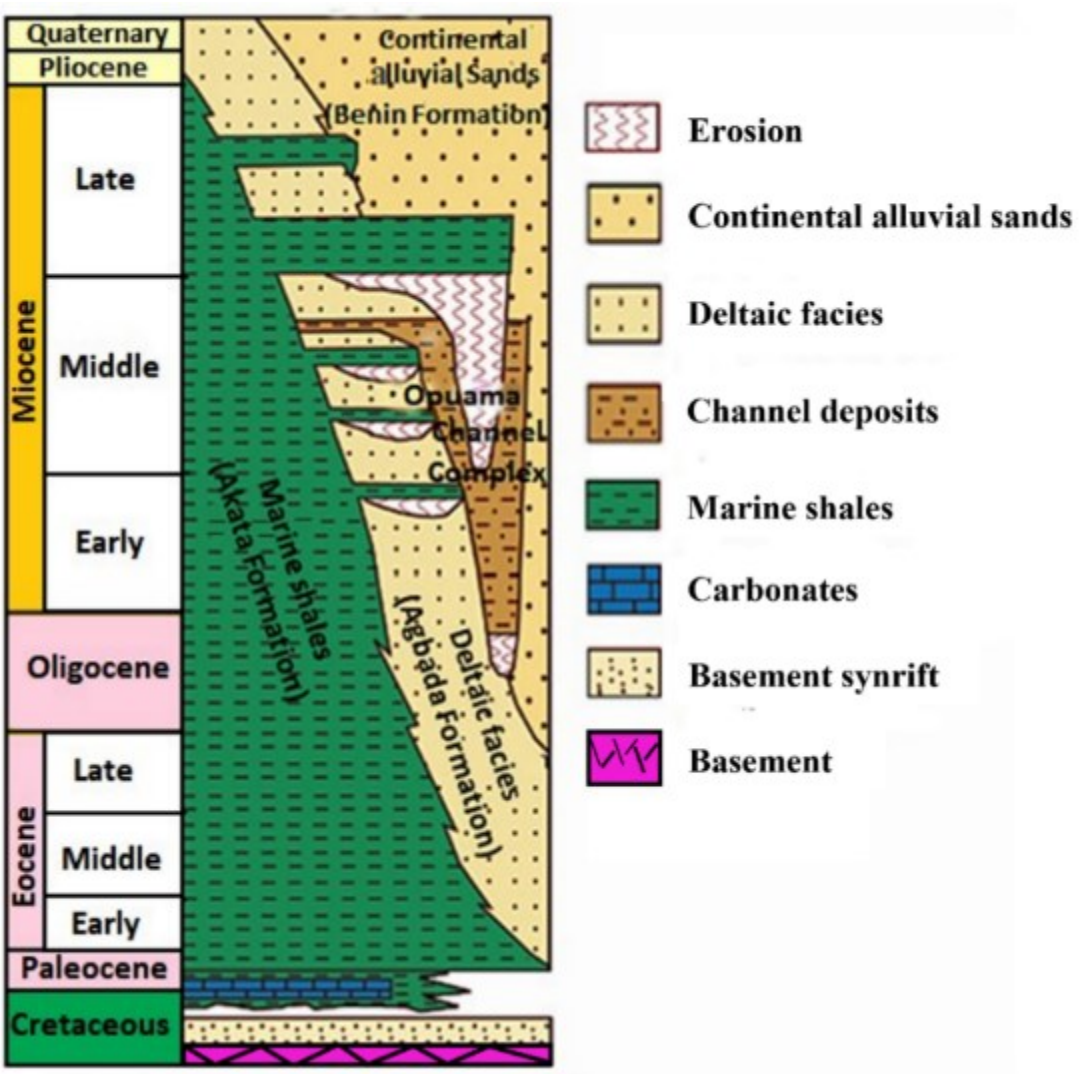

Figure 4.3: Stratigraphy of the Niger Delta indicating the diachronous subsurface lithologic units: Akata, Agbada, and Benin Formations. (Maloney et al., 2010; Overare et al., 2021).

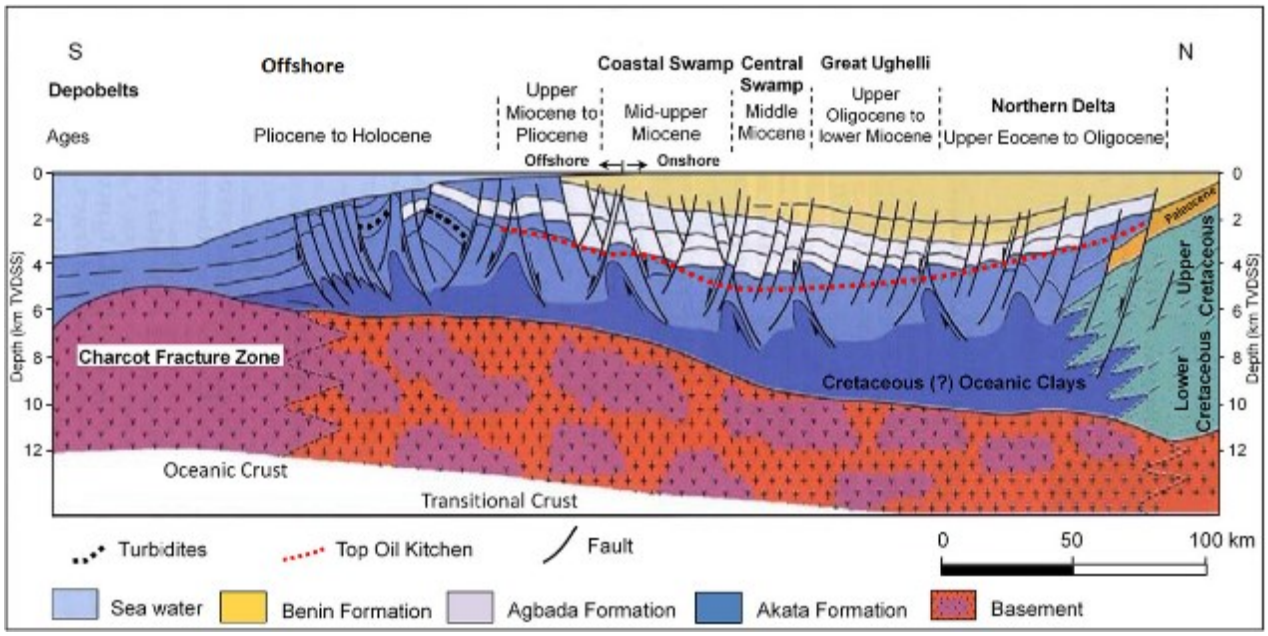

Figure 4.4: Section across the Niger Delta Basin highlighting diachronous lithostratigraphic units, depositional belts, and associated depositional structures (after Ogbe et al., 2020).

4.3.3 Paleosalinity reconstruction methods

Three elemental ratios (S/TOC, B/Ga, and Sr/Ba, Fig. 4.5) and boron in clay paleosalinity proxies are utilized in this investigation for the paleosalinity reconstruction of the Agbada Formation. The background and ideas behind their utility are concisely discussed in the next section.

4.3.3.1 The sulfur/total organic carbon (S/TOC) ratios

The significant disparity in the concentrations of aqueous sulfate between brackish/marine (moderate to high sulphate) and freshwater (low-sulphate) depositional systems in organic-rich sedimentary rocks presents a framework for using the S/TOC ratios for paleosalinity studies (e.g., Goldhaber and Kaplan, 1974, Berner and Raiswell, 1983;1984; Hasegawa et al., 2010; Hofer et al., 2013; Wei et al. 2018; Remírez and Algeo, 2020; Quan et al., 2020; Song et al., 2021; Wu et al., 2021; Bokanda et al., 2022). In contrast to other paleosalinity proxies, such as Sr/Ba or B/Ga linked to the clay fractions, the S/TOC depends on the organic and sulfide fractions of the sediment. Most freshwater settings contain low aqueous sulfate ions and generate only a minimal supply of reduced sulfur-derived materials, but microbial sulfate reduction can dominate the anaerobic oxidation process of organic matter in marine conditions, leading to the formation of reduced sulfur species (e.g., sulfide minerals such as pyrite) that can significantly accumulate in the sediments (Berner, 1980). Consequently, the S/TOC ratios in marine facies are higher than that of freshwater facies, with S/TOC thresholds of <0.1 and >0.1, suggesting freshwater and brackish/marine facies, respectively (Wei and Algeo, 2020). As a precautionary measure, applying the S/TOC paleosalinometric method to rocks with low organic carbon (<1%) is futile; thus, only samples with TOC>1 were utilized for this investigation. Moreover, the sediments do not contain a significant amount of sulfate minerals that will influence the results for the total sulfur (Berner and Raiswell, 1984).

4.3.3.2 Boron/Gallium (B/Ga) ratio

It has been established from previous studies that B/Ga ratios can be utilized for reconstructing paleosalinity (e.g., Chen et al., 1997; He et al., 2017; Zhang et al., 2017; Song et al., 2018; Wei et al., 2018; Wei and Algeo, 2020; Remírez and Algeo, 2020; Song et al., 2021; Wei et al. 2021). Both elements can have long aqueous residence times (Livingstone, 1963; Spivack et al., 1987; Song et al., 2021), and their transmission to sediment is linked to their aqueous concentration and the processes regulating their relative uptake and dynamics, accounting for the disparity in concentration between marine and freshwater sediments (Wei and Algeo, 2020). Boron is one of the trace elements with higher concentrations in seawater facies relative to freshwater facies, reflecting a positive linear relationship with the salinity of sedimentary depositional systems (Reynolds, 1965; Walker, 1968; Potter et al., 1963; Zhang et al., 2017). It is strongly absorbed by clay minerals (may replace Si or Al in the lattice of clay minerals) in coastal to marine environments (Frederickson and Reynolds, 1960; Couch, 1971., Dominik and Stanley, 1993; Zhang et al., 2017), and its uptake by sediments have been described to take place under all salinity conditions, but it is generally enhanced for marine facies possibly due to the increased alkaline water-mass chemistry (Palmer et al., 1987; Spivack et al., 1987; Wei and Algeo, 2020). Moreso, mafic minerals (e.g., olivine, orthopyroxene, and chlorite), which are major constituents of the oceanic crust, contain a significant amount of B, causing its enrichment in seawater via crustal-fluid exchange (Spivack et al., 1987; Tenthorey and Hermann, 2004).

Gallium is commonly depleted in seawater relative to freshwater and is mostly derived from detrital silicate minerals such as the weathering of quartzose and feldspathic silicate rocks (Chen et al., 1997; Wei et al., 2018). Although Ga is relatively less reactive than B, it is capable of adsorbing onto clay minerals in sediments, with the pH conditions (neutral to alkaline pH provides the ideal settings for stronger uptake) of the aqueous sedimentary depositional system

providing a significant control on its uptake by sediments (Wei and Algeo, 2020). Generally speaking, most dissolved Ga tends to precipitate as hydroxides in sediments or soils before their transportation to the ocean (Shiller and Frilot, 1996; De Vos and Tarvainen, 2006) due to the low solubility of $Ga(OH)_3$, its dominant hydroxide. Since the primary source of Ga is linked to terrestrial runoff, the concentrations of Ga in seawater are generally low.

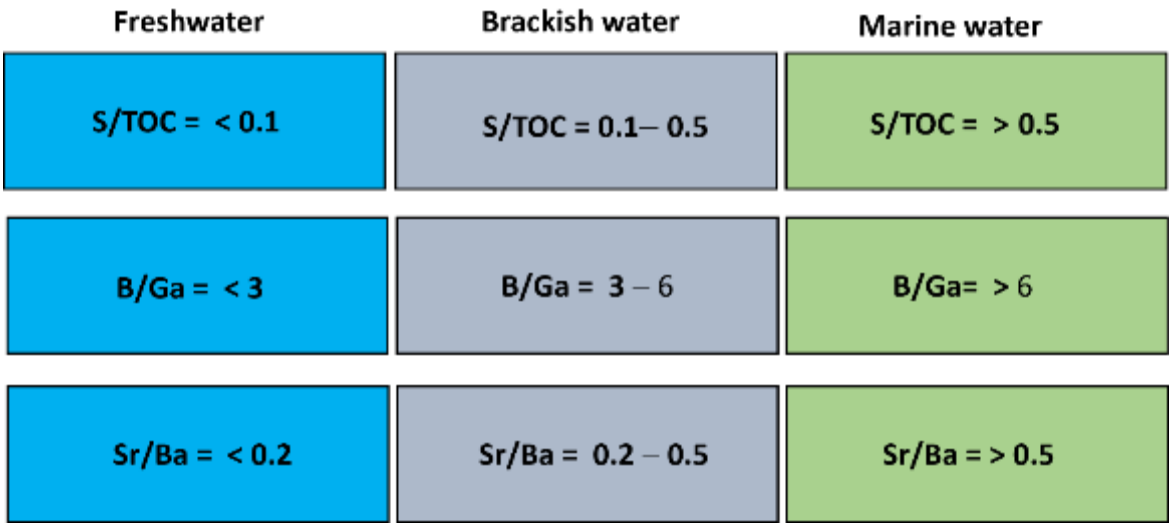

Figure 4.5: Paleosalinity thresholds (Wei and Algeo, 2020).

The different sources and geochemical behaviors of B and Ga provide a framework for using the B/Ga ratio as a paleosalinity tool, with recently established B/Ga thresholds of >6, 3–6, and <3 depicting marine, brackish, and freshwater facies, respectively (Wei and Algeo, 2020), although thresholds of >4.0 (shallow marine lithofacies), 3.0–4.0 (brackish lithofacies) and < 3 (terrigenous lithofacies) were proposed earlier by Chen et al. (1997), values of < 2.5 (Freshwater sediments), 2.5–5.0 (brackish-water sediments) >5.0 (marine sediments) had also been utilized (Wei et al., 2018). Notably, B/Ga thresholds assigned to discriminate various depositional salinity conditions are more effective for sediments with a certain degree of enrichments (B >75 ppm and Ga >25 ppm; Wei et al., 2018).

4.3.3.3 Strontium/barium (Sr/Ba)

The relationship between Sr and Ba in sedimentary records has been utilized to reconstruct the salinity of various sedimentary depositional systems (e.g., Chen et al., 2016; Li et al., 2018; Wei et al., 2018; Zhang et al., 2020; Overare et al. 2020; Wei and Algeo, 2020; Zuo et al., 2020). However, as with other paleosalinity proxies, concerns about its paleosalinometric efficacy have also been raised (e.g., Remírez and Algeo, 2020; Wang et al., 2021; Jewuła et al., 2022). The geochemical behaviors of Sr and Ba are distinctive under different sedimentary environments (variable salinity conditions), with increasing salinity conditions pointing to higher Sr/Ba ratios (Chen et al., 1997; Zeng et al., 2015). For instance, the ratio of Sr/Ba in freshwater water systems is generally low compared to that in seawater due to the faster liberation of Sr relative to Ba in sediments during weathering in terrestrial settings (Yang et al., 2004a, 2006; Wei et al., 2018). In addition, earlier investigations have noted that the concentration of Sr relative to Ba is significantly higher in seawater, with Ba only occurring in very minimal or trace concentrations because barium carbonate, sulfate, and phosphate minerals have low aqueous solubilities (Neff, 2002; Pyle et al., 2017; Wei and Algeo, 2020). As the water salinity increases in a depositional system, Ba is usually the first to precipitate, whereas the significant precipitation of Sr depends mainly on higher salinity conditions (Zhang et al., 2017). Thresholds of >0.5, 0.2–0.5, and <0.2 for Sr/Ba points to marine, brackish, and freshwater depositional salinities, respectively, but a significant overlap may exist for brackish and marine conditions (Wei and Algeo, 2020).

4.3.3.4 Boron-derived paleosalinity proxies

Boron-derived paleosalinity proxies in fine-grained siliciclastics have been utilized for several decades (Goldschmidt and Peters, 1932; Landergren, 1945) but not without controversies, as some researchers either challenged or supported its efficacy (Degens et al., 1957; Frederickson and Reynolds, 1960; Harder, 1961; Tourtelot et al., 1961; Walker and Price, 1963; Walker, 1968; Couch, 1971; Bohor and Gluskoter, 1973; Brockamp, 1973; Ye et al., 2016; Zhang et al., 2017; Zhang et al., 2014; Song et al., 2018; Li et al., 2021; Zuo et al., 2021; Wang et al., 2021; Jewuła et al., 2022). Several methods (e.g. Walker's equivalent boron, Adam's, Landergren and Carvajal's, and Couch's quantitative approach) utilizing boron in clay were used for reconstructing paleosalinity in this investigation. The boron contents of fine-grained siliciclastic sediments have been found to correlate fairly with paleosalinity. For instance, illites are known to contain a small quantity of boron, which may substitute for silicon in the illite lattice, and the amount of boron uptake into the structure is influenced by the grain size of the illite, potassium content, and the salinity conditions at the time of deposition (Walker and Price, 1963). Since there is a relationship between the boron content of illite in clays and the potassium mass fraction, the true boron content of pure illite can be computed (Walker, 1962) using the relationship

$$\text{Adjusted boron } (B_a) = B \times 8.5 / K_2O \quad (1)$$

Where B = observed boron (ppm) and K_2O refers to the K_2O content in percentage (%)

However, converting B_a to equivalent boron (B_e) concentrations is usually imperative for comparative analysis reflecting the same conditions, and departure curves can be utilized to convert "B_a" to B_e (the B_a that would exist at equilibrium in illite containing 5% K_2O from the same salinity medium; Walker and Price, 1963; Walker 1968). The B_e values < 200pm, 200–300 ppm, and 300–400 ppm suggest low-salinity water and brackish and normal marine

environments, respectively. Although this approach cannot quantitatively estimate paleosalinity, it may provide qualitative insights.

Adams et al. (1965) provided a quantitative approach for estimating salinity, which is utilized in the current investigation. The authors conducted their investigation using Recent sediments of the Dovey Estuary over a mean salinity range of 16-33‰, establishing a direct relationship between depositional salinity and B_e using the equation:

$$S_p = 0.0977\ B_e - 7.043 \quad (2)$$

where S_p = salinity of the water (‰) and B_e = Walker's equivalent boron (ppm).

Also adopted in this investigation is the method Landergren and Carvajal (1969). The mass fraction of boron (B) measured in clay minerals can be linked to the salinity (S_p) of seawater using a relationship known as the Freundlich isotherm adsorption equation.

$$\log B = C_1 \log S_p + C_2 \quad (3)$$

where B = boron uptake (ppm), S_p = salinity of the water (‰); C_1 and C_2 are constants dependent on the type of clay mineral.

Landergren and Carvajal (1969) evaluated the concentration of boron in certain modern clays and were able to relate boron content in the clays to water salinity through a Freundlich adsorption isotherm;

$$\text{Log } B = 0.43 \log S_p + \log 27.9 \quad (4)$$

where B = observed boron content (ppm), and S_p = salinity of the water (‰).

In addition, Couch's boron-derived paleosalinometer was also utilized. It is a quantitative approach that utilizes the adsorption capacities of various clay minerals instead of only the illite fraction. Most clay minerals are capable of adsorbing boron from natural waters, although illite is the main host, extracting approximately four times as much as kaolinite and about twice as much as montmorillonite (Couch 1971), which is expressed by the equation:

$B_C = B/(Xk + 2Xm + 4Xi)$ (5)

Where B_C = Couch adjusted B content (ppm), B = measured boron concentration (ppm), and Xk, Xm, and Xi represent the weight fractions of kaolinite, montmorillonite, and illite, respectively

Utilizing data from the Niger Delta clays, Couch was able to resolve the coefficients (C_1 and C_2) in equation (1) so that; $\log B_C = 1.28\log S_p + 0.11$ (6)

where B_C = adjusted boron (ppm) and Sp = paleosalinity (‰).

4.4. Results

The elemental geochemistry of the investigated samples is listed in Appendix 1, and their statistics are summarized in Table 4.1 and the box plots (Fig. 4.6a–d). The results of the boron-derived paleosalinometric tools (Adams: 4.4–34.3‰, 17.3 ± 7.3‰; Landergren and Carvajal: 1.6–43.1‰, 15.5 ± 10.2‰ and Couch: 12.8–26.7‰, 19.3 ± 4.1‰) are presented in Appendix 1 and summarized in Table 1 and Figure 4.6d. All the boron-derived paleosalinometric tools show good correlations with each other and correlate well with B and fairly with B/Ga (r = 0.57–0.95; Figs. 4.7 and 4.8). However, B/Ga is negatively correlated with Sr/Ba (r = –0.34) and S/TOC (r = –0.72).

Representative XRD patterns of the <2 μm clay mineral fractions and their quantitative composition are presented in Appendix 1 and Figures 4.9 and 4.10. The clays are mostly kaolinite (65–94%, 82.4% ± 9.3), although illite (6–25%, 12.3% ± 5) and montmorillonite (0–25%, 5.3% ± 6.4) may occur. The <2 μm fractions were selectively utilized to minimize error since different size fractions of clay generally contain different concentrations of boron (Landergren, 1958; Walker, 1963; Couch and Grim, 1968; Couch, 1971).

4.5. Discussion

Although dissolved elements are comparatively lesser in fresh/brackish waters than in seawater, the elemental concentration of some elements generally reflects more abundance in seawater (e.g., B and Sr) or freshwater (e.g., Ga and Ba) on a salinity-normalized basis, thus providing a signature platform (B/Ga, Sr/Ba) that can be used to delineate the depositional conditions of sediments. In addition, sulfate concentration is commonly more abundant in brackish/seawater than in freshwater, making S/TOC a useful paleosalinometric proxy.

The Agbada shales Sr/Ba, B/Ga, and S/TOC values (Figs. 4.11, 4.12, 4.13, and 4.14) suggest freshwater/brackish depositional conditions with variable marine influence, brackish/freshwater conditions and brackish/marine depositional conditions with freshwater input, respectively. The insights from these proxies collectively indicate low saline (brackish settings) conditions that contain inputs from freshwater with little marine influence. This trend is generally observed in both wells, with depths ~5600ft and 5825ft, reflecting increasing salinity conditions for W1 and mostly fluctuating salinity conditions for W2 (Fig. 4.14). The overall trend from the various proxies is consistent with the transitional settings of the Agbada Formation, which represents an interplay between fresh and seawaters that are prone to lateral and/or vertical salinity gradients, with zones of lower salinities linked to reduced seawater or increased freshwater inputs and zones of greater seawater inputs reflecting relatively higher salinities.

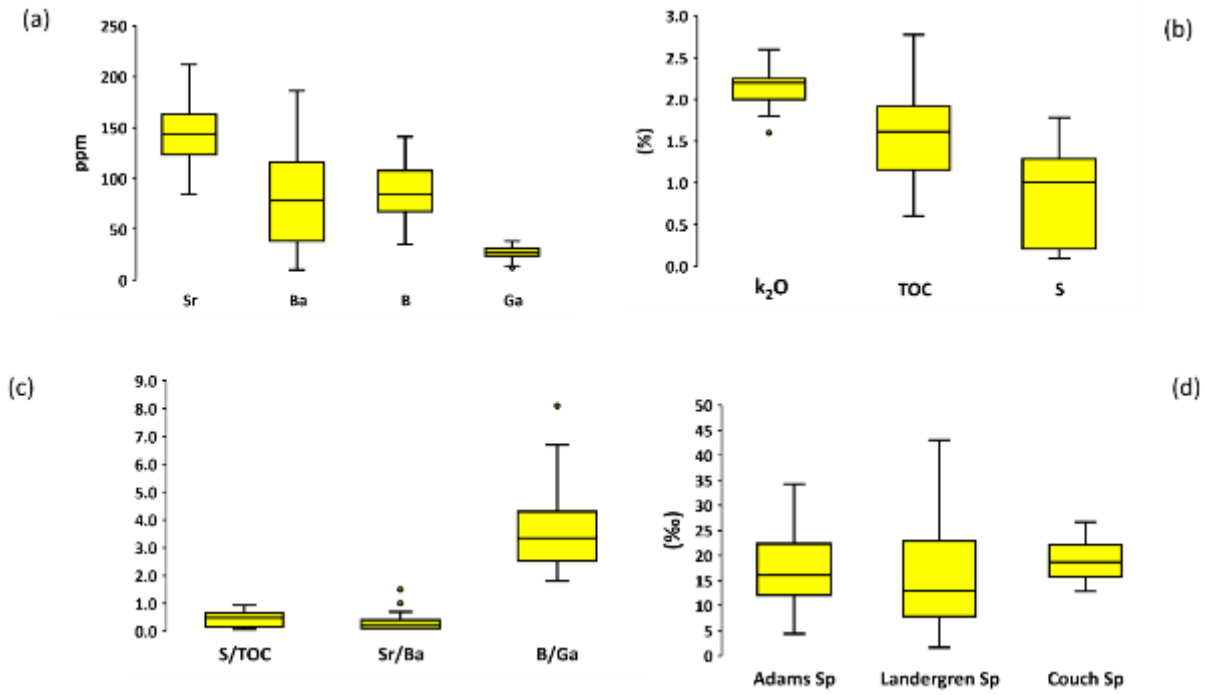

Figure 4.6: Elemental composition and paleosalinity values: (a) and (b), selected elemental compositions, (c) elemental ratios, and (d) calculated paleosalinity values. Note that the Ba concentration is in $x10^{-1}$ppm

Table 4.1: Statistical summary of elemental compositions and ratios, clay mineral contents (< 2 µm fraction), Total organic carbon (TOC) values, and paleosalinity analysis of the Agbada shales. K-Kaolinite, I-illite, M-Montmorillonite, Csp- Couch's paleosalinity (Couch, 1971), Eb-Equivalent boron (Walker and Price, 1963), Adam's paleosalinity (Adams et al., 1965), L-Paleosalinity of Landergren and Carvajal (Landergren and Carvajal, 1969).

	Sr (ppm)	**Ba (ppm)**	**B (ppm)**	**Ga (ppm)**	**K_2O (%)**	**S (%)**	**K (%)**	**I (%)**	**M (%)**	**TOC (%)**	**Sr/Ba**	**B/Ga**	**S/TOC**	**CSp (‰)**	**Eb (ppm)**	**A (‰)**	**L (‰)**
n	45	45	45	45	45	23	23	23	23	34	45	45	23	23	45	45	45
Max	212	1862	140.7	38.1	2.6	1.8	94	25	20	2.8	1.6	5.9	0.9	26.7	423	34.3	43.1
Min	84.4	99.9	34.6	5.2	1.6	0.1	65	6.0	0.0	0.6	0.1	1.8	0.1	12.8	117	4.4	1.6
Mean	146.5	809.8	85.8	26.2	2.1	0.9	82.4	12.3	5.3	1.6	0.3	3.4	0.4	19.3	249	17.3	15.5
Stdev	31.0	512.5	25.5	7.6	0.3	0.6	9.3	5.0	6.4	5.5	0.4	1.1	0.3	4.1	75	7.3	10.2

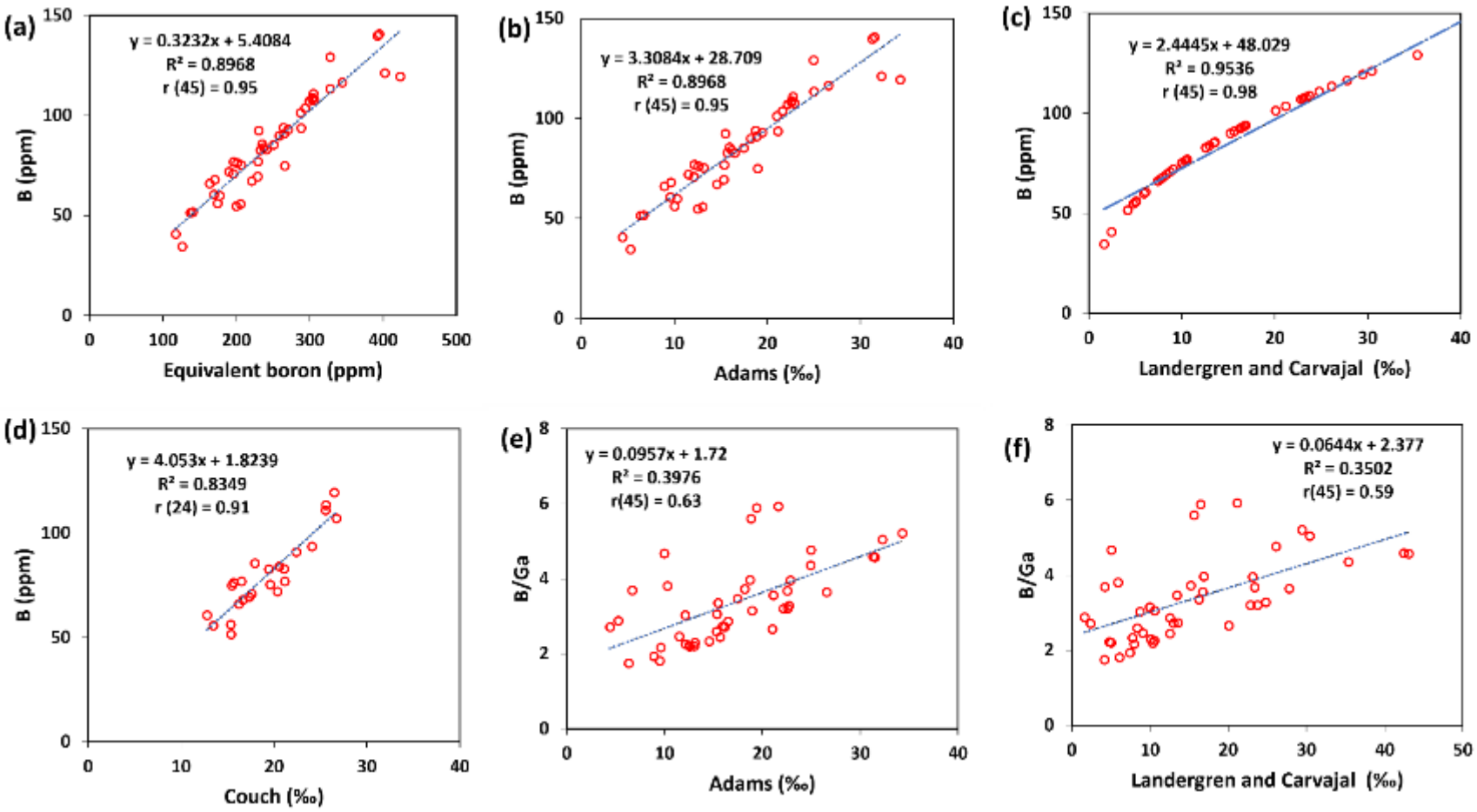

Figure 4.7: Cross plots of paleosalinity proxies for the Agbada shales (a) B vs Equivalent boron, (b) B vs Adams Sp, (c) B vs. Landergren and Carvajal Sp, (d) B vs Couch Sp, (e) B/Ga vs. Adams Sp, and (f) B/Ga vs. Landergren and Carvajal Sp

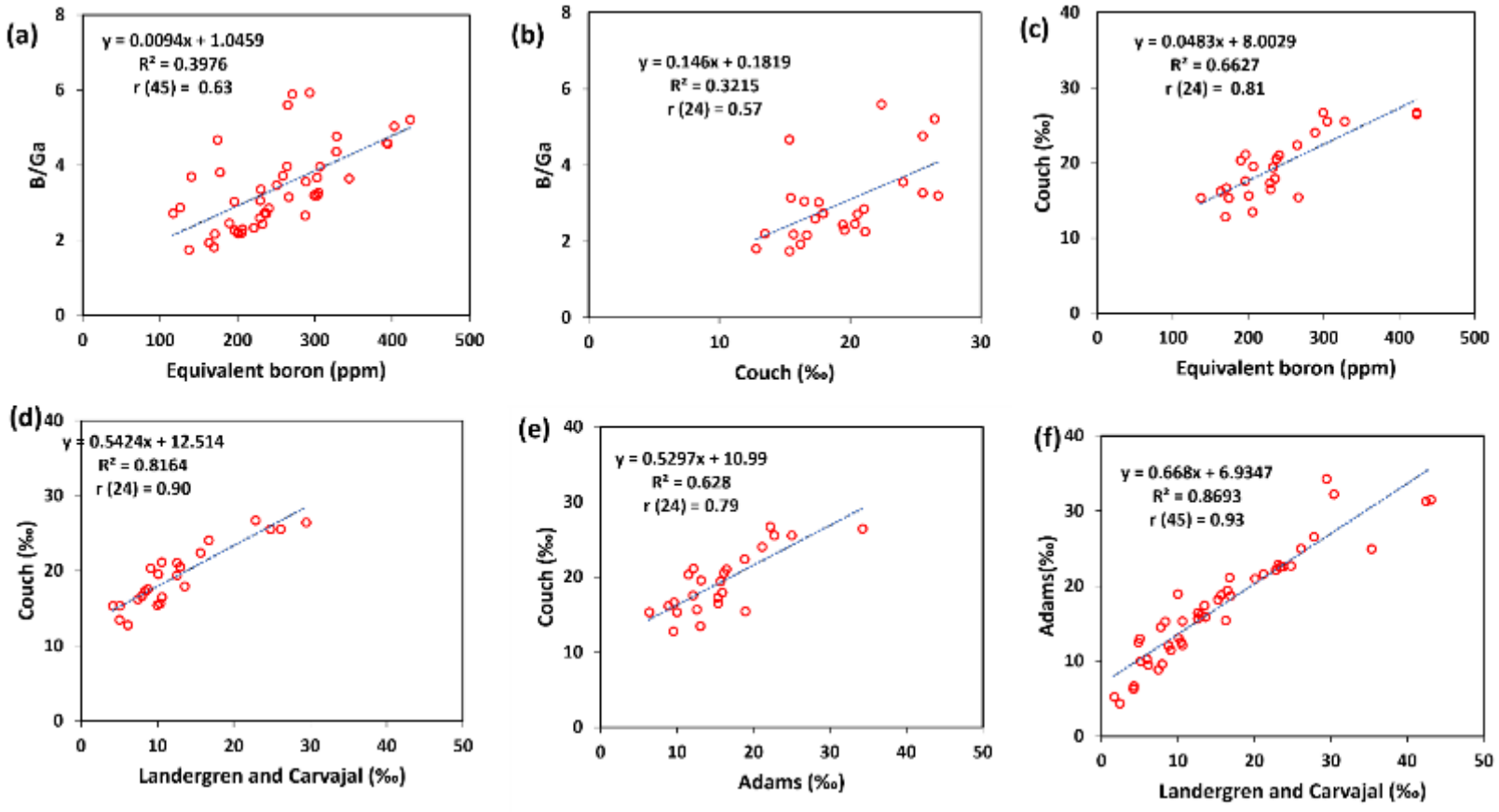

Figure 4.8: Crossplots of paleosalinity proxies for the Agbada shales (a) B/Ga vs Equivalent boron, (b) B/Ga vs Couch Sp, (c) Couch Sp vs. Equivalent boron, (d) Couch Sp vs. Landergren and Carvajal Sp, (e) Couch Sp vs. Adams Sp, and (f) Adams Sp vs. Landergren and Carvajal Sp

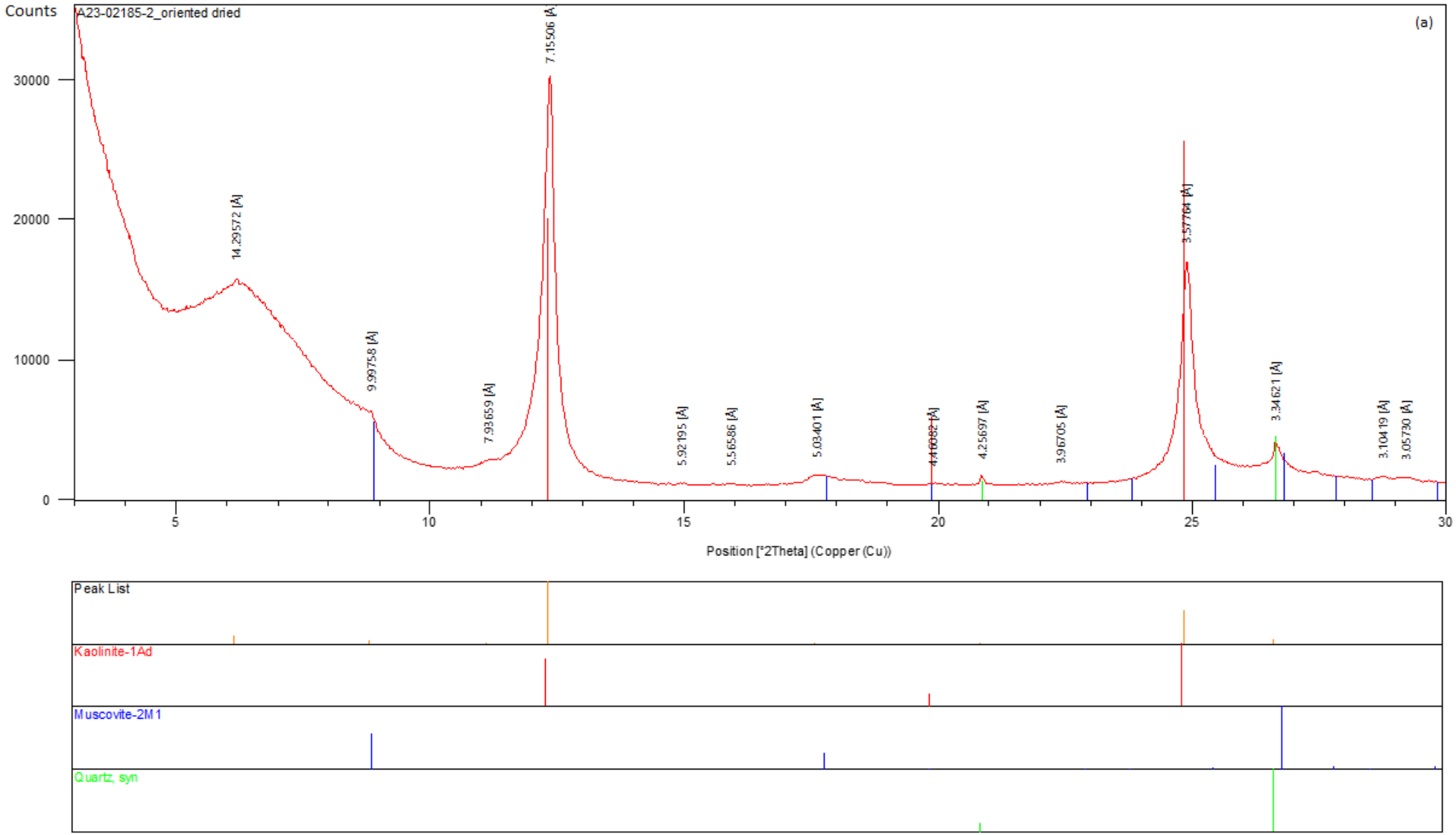
Counts
A23-02185-2_oriented dried
(a)
30000
20000
10000
0
14.29572 [Å]
9.99758 [Å]
7.93659 [Å]
7.15506 [Å]
5.92195 [Å]
5.56586 [Å]
5.03401 [Å]
4.46082 [Å]
4.25697 [Å]
3.96705 [Å]
3.57764 [Å]
3.34621 [Å]
3.10419 [Å]
3.05730 [Å]
5
10
15
20
25
30
Position [°2Theta] (Copper (Cu))
Peak List
Kaolinite-1Ad
Muscovite-2M1
Quartz, syn

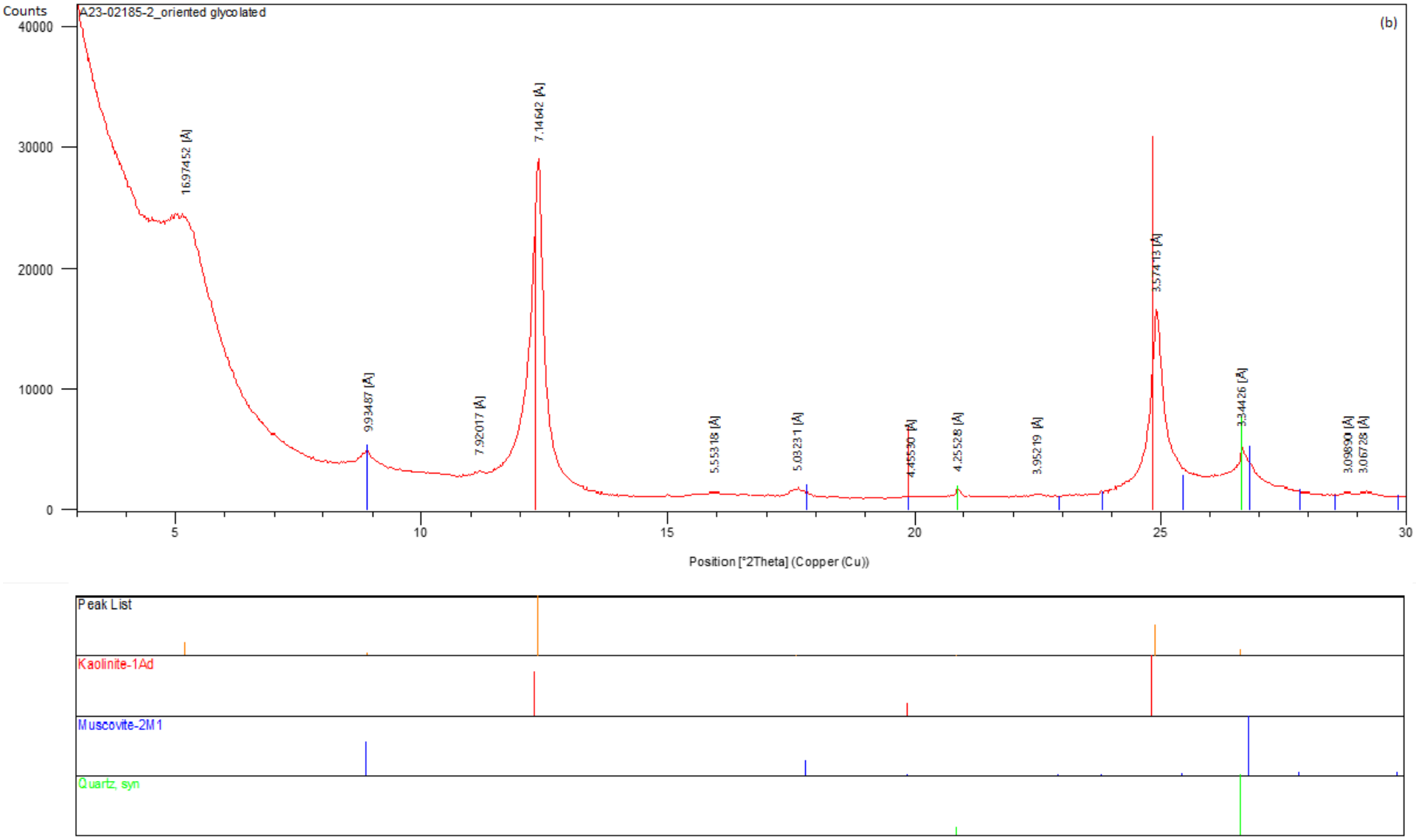
Counts
A23-02185-2_oriented glycolated
(b)
40000
30000
20000
10000
0
16.97452 [Å]
9.93487 [Å]
7.92017 [Å]
7.14642 [Å]
5.55318 [Å]
5.03231 [Å]
4.45530 [Å]
4.25528 [Å]
3.95219 [Å]
3.57413 [Å]
3.34426 [Å]
3.09690 [Å]
3.06728 [Å]
5
10
15
20
25
30
Position [°2Theta] (Copper (Cu))
Peak List
Kaolinite-1Ad
Muscovite-2M1
Quartz, syn

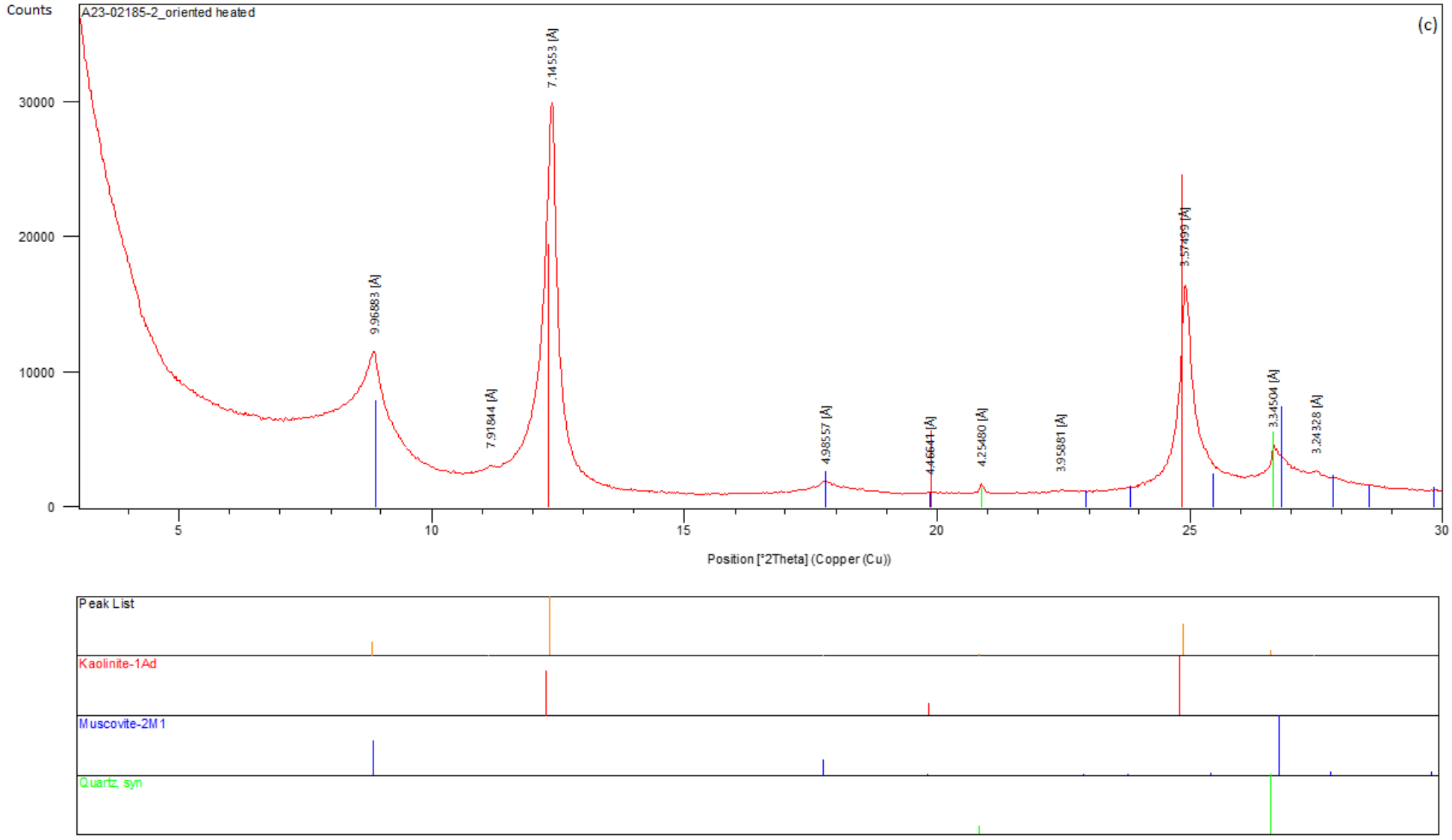
Counts
A23-02185-2_oriented heated
(c)
30000
20000
10000
0
9.96883 [Å]
7.91844 [Å]
7.14553 [Å]
4.98557 [Å]
4.46641 [Å]
4.25480 [Å]
3.95881 [Å]
3.57499 [Å]
3.34504 [Å]
3.24328 [Å]
5
10
15
20
25
30
Position [°2Theta] (Copper (Cu))
Peak List
Kaolinite-1Ad
Muscovite-2M1
Quartz, syn

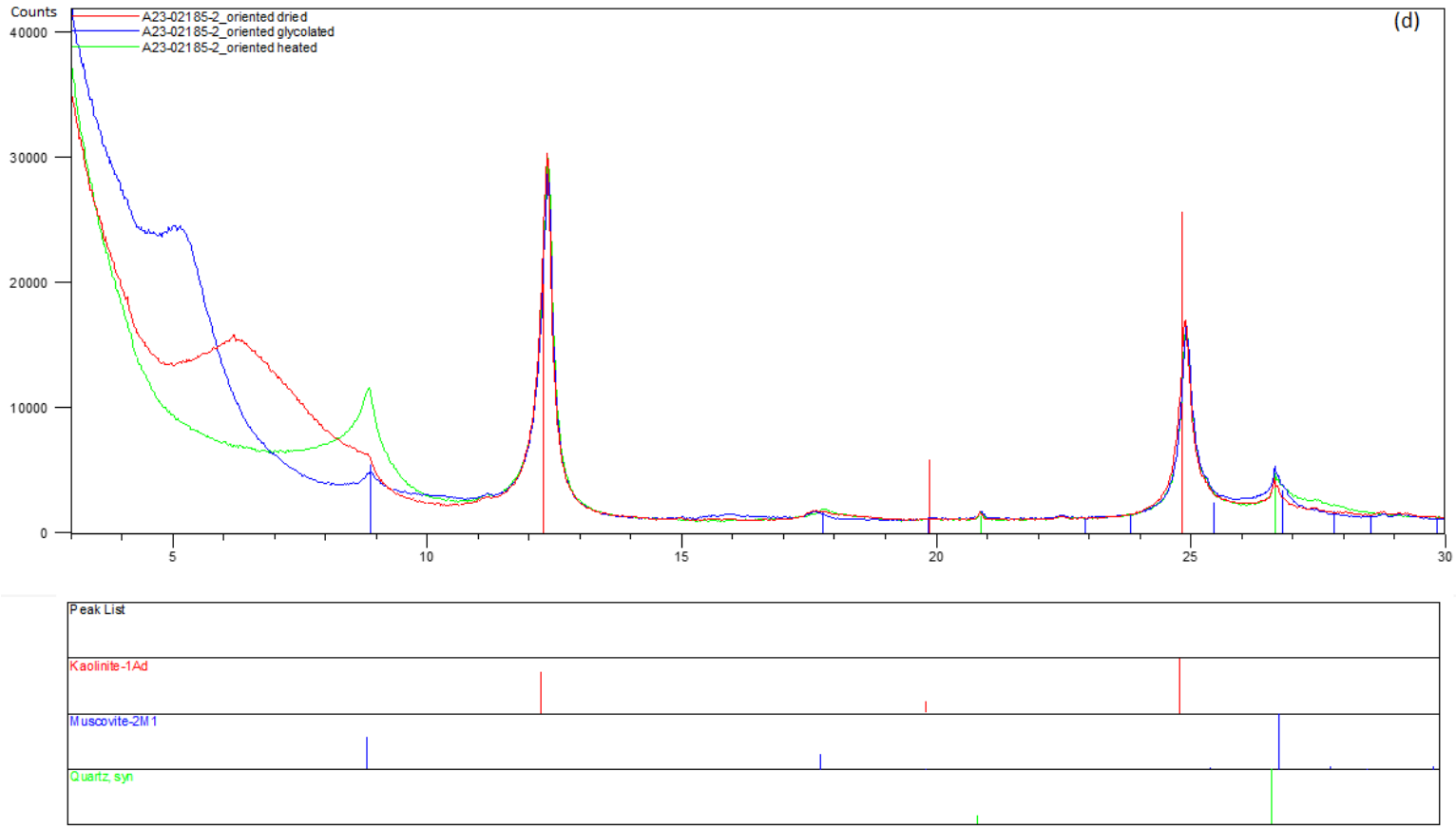

Figure 4.9: Representative XRD patterns of < 2 μm fraction of the Agbada Shales. (a) Oriented dried, (b) ethylene glycol treated (EG) oriented aggregate, (c) oriented heated, and (d) XRD patterns of (a), (b), and (c)

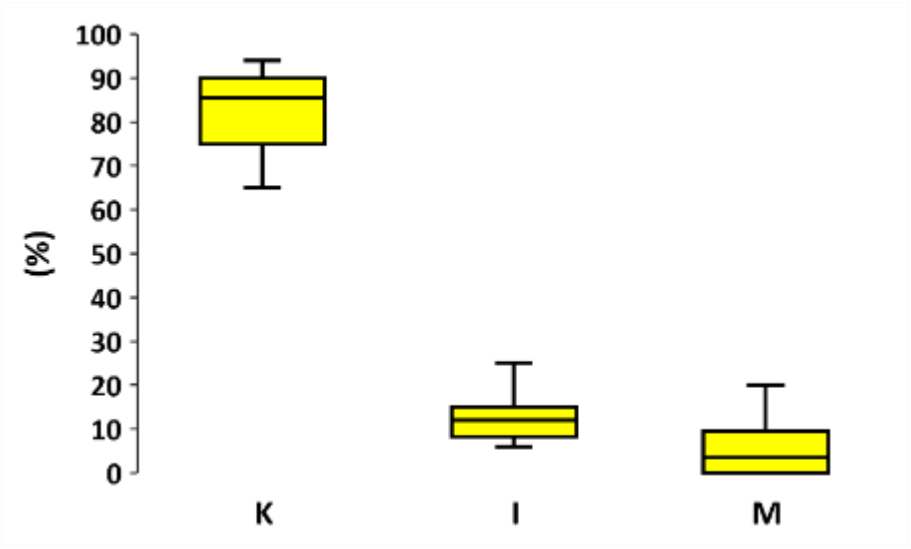

Figure 4.10: Quantitative XRD mineral contents (< 2 µm fraction) presented as a box plot.

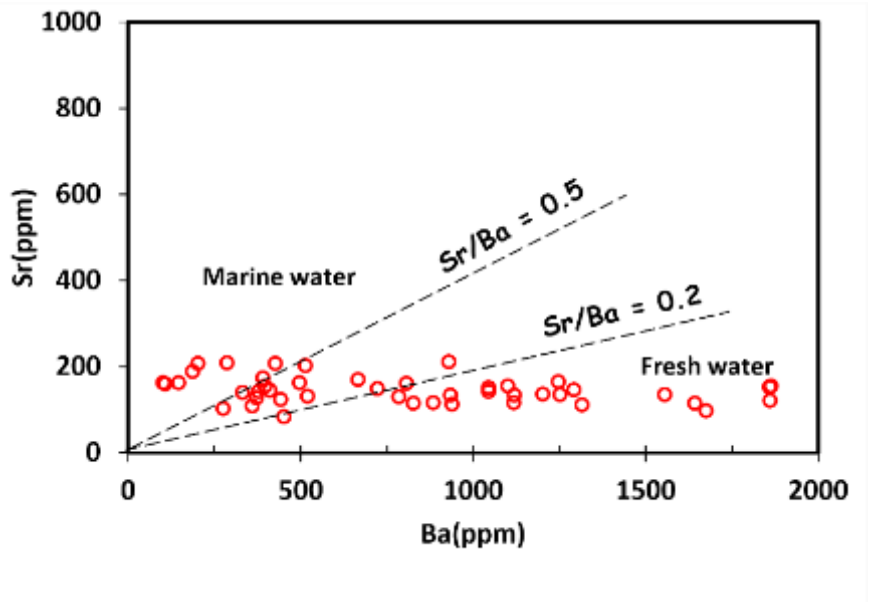

Figure 4.11: Sr vs. Ba qualitative paleosalinity salinity insights of Agbada Formation (Wei and Algeo, 2020). The dashed black lines are used to separate the different fields (Marine, fresh water, and brackish paleodepositional conditions)

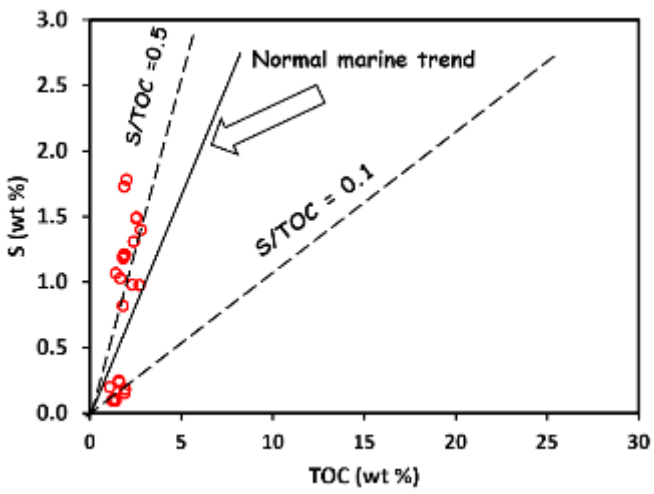

Figure 4.12: Sr vs. TOC qualitative paleosalinity insights of Agbada Formation. Only samples with TOC ≥ 1 were utilized. Thresholds of < 0.1 and > 0.1 depict brackish/marine and freshwater settings respectively. Note that the S/TOC threshold (0.5) for discriminating between the brackish and marine facies boundaries is tentative (Wei and Algeo, 2020). The solid, thick black line represents the normal marine trend (0.36) of Berner and Raiswell (1983).

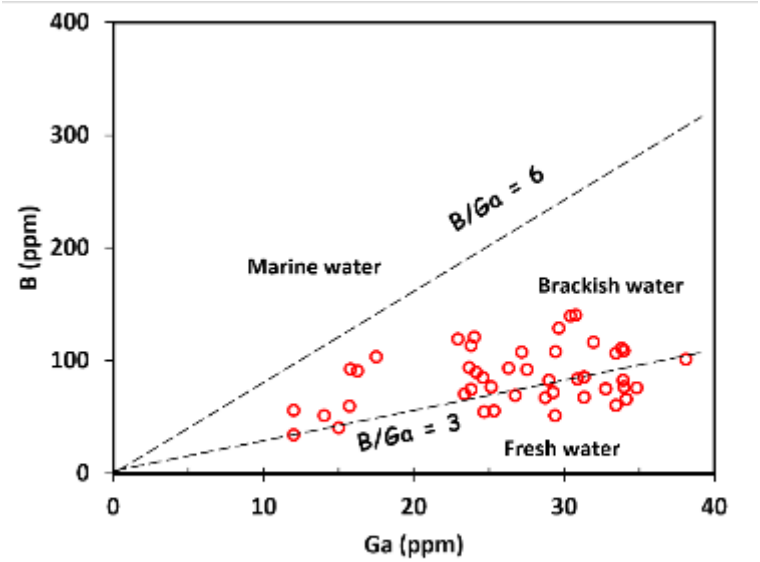

Figure 4.13: B vs. Ga qualitative paleosalinity insights of the Agbada Formation shales. The dashed black lines are used to delineate the different fields (Marine, brackish, and freshwater).

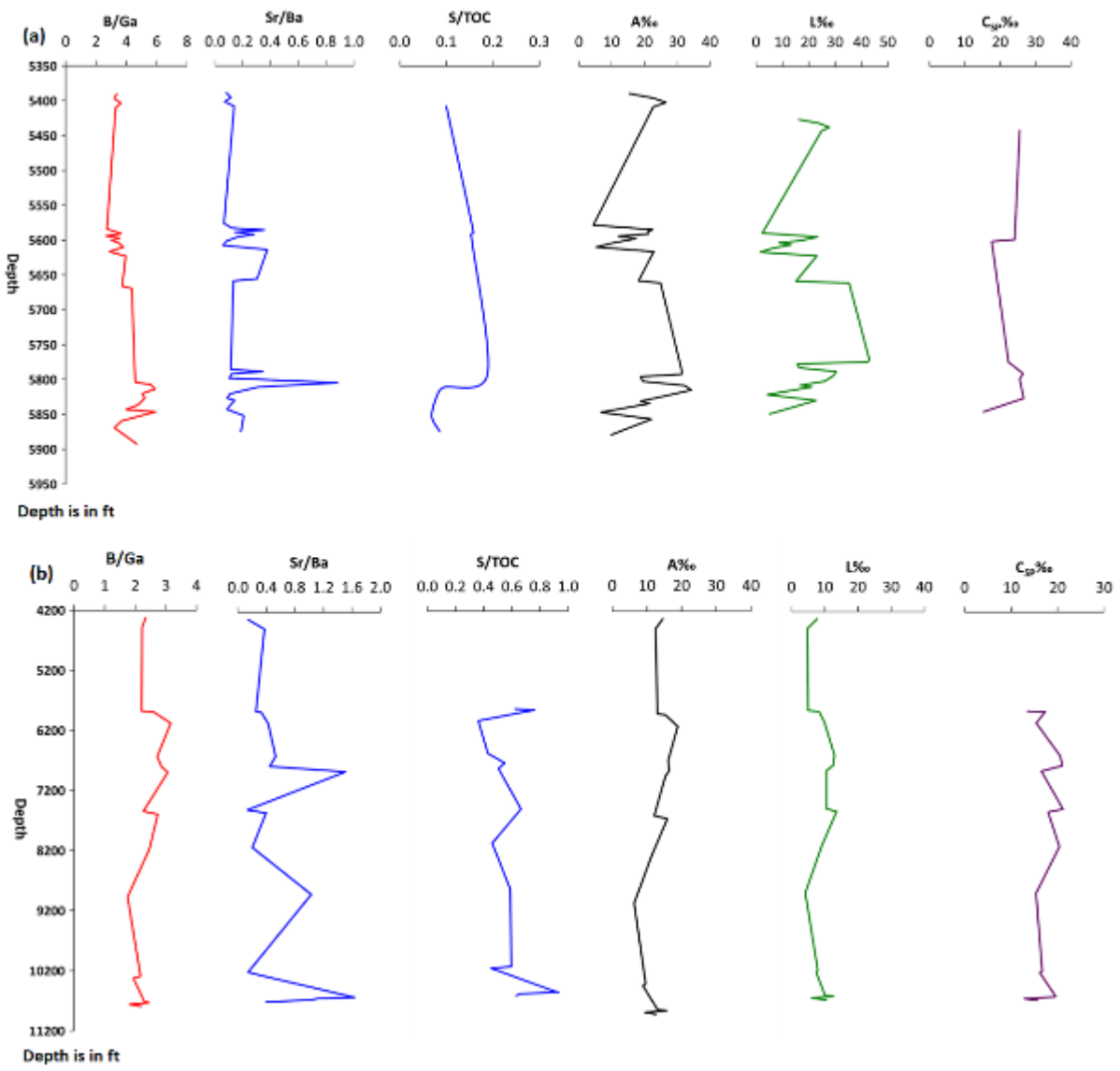

Figure 4.14: Paleosalinity proxies vs. depth (ft) trends for W1 and W2. (a) and (b) illustrates B/Ga, Sr/Ba, S/TOC, Adams Sp (A), Landergren and Carvajal Sp (L), and Couch Sp (C) versus depth for the Agbada shales.

It is noteworthy to mention that a tentative S/TOC threshold (Fig. 4.5) was adopted to discriminate between marine and brackish depositional conditions since the S/TOC paleosalinometric proxy does not effectively separate them, although it might still be possible to distinguish low-salinity brackish water from seawater, but not at salinities reflecting more than half of that of seawater (Berner and Raiswell, 1984). In addition, although overlap may exist for brackish and marine conditions when using established thresholds for Sr/Ba (e.g., Wei and Algeo, 2020), integrating various proxies avoids secondary influences on any single proxy and improves confidence in interpretation. Nevertheless, the Sr/Ba, B/Ga and S/TOC paleosalinometric proxies are qualitative indicators and, therefore, further insight utilizing a quantitative approach (boron-derived paleosalinity proxies) has to be considered to provide a robust evaluation of the paleosalinity.

The use of boron in evaluating paleosalinity is attributed to its linear relationship with salinity, particularly for sediments from marine facies that have significantly higher boron concentrations than those of freshwater systems. This analogous disparity is preserved in clays since clay minerals are capable of adsorbing boron (Illite has the strongest adsorption capacity, montmorillonites and probably chlorites are intermediate, and kaolinites have the least capacity; Couch, 1971) from water and the adsorbed quantity may therefore reflect the salinity of the ancient water system (Goldschmidt and Peters, 1932; Frederickson and Reynolds, 1960; Walker and Price, 1963; Walker, 1968; Couch, 1971). A previous study (Couch, 1971), which utilized boron for paleosalinity reconstruction, has assigned salinities of 20–30‰ to inner-shelf and littoral environments, 30–35‰ to open-marine, and >35‰ to slope environments. In the current investigation, all of the boron-derived paleosalinity proxies: equivalent boron (Fig. 4.15), Adam's (4.4–34.3‰, 17.3 ± 7.3‰), Landergren and Carvajal's (1.6–43.1‰, 15.5 ± 10.2‰) and Couch's (12.8–26.7‰, 19.3 ± 4.1‰) are consistent and reflect strong positive correlations with each other and also pointing to low saline (brackish) settings that contain inputs from

freshwater and little marine influence, which suggest inner-shelf and littoral environments. In addition, although the mean value (3.8‰) for the different methods is small and consistent, it is noteworthy that Couch's boron-derived paleosalinometer is believed to be more reliable and widely applicable because it is dependent on the composition and adsorption capacities of various clay mineral fractions and established data was used to calibrate the Freundlich isotherm adsorption equation. Moreover, paleosalinity curves generated using Couch's method were also supported by faunal evidence (Couch, 1971).

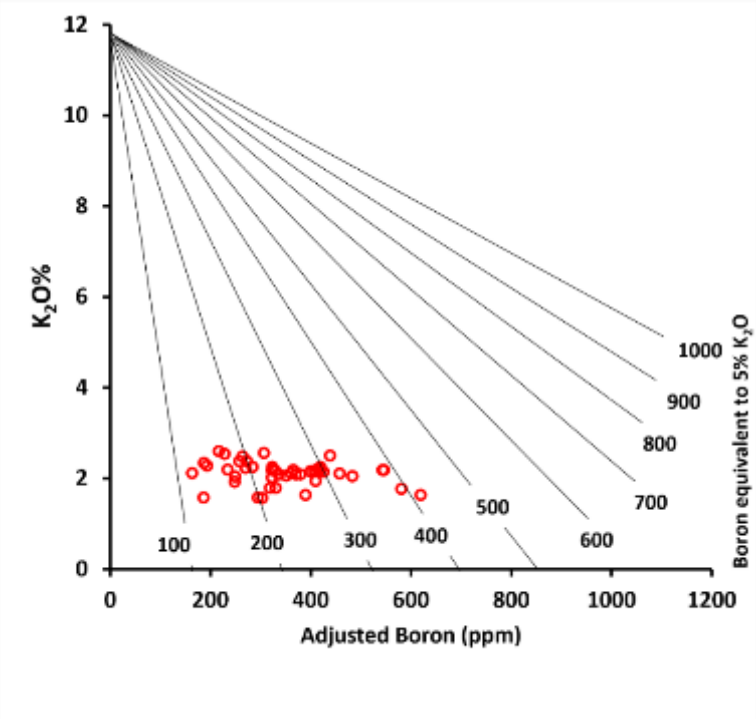

Figure 4.15: Departure curves for computing equivalent boron from adjusted boron concentration (After Walker 1968). Note that equivalent boron values of < 200pm, 200–300 ppm, and 300-400 ppm suggest low salinity water, brackish environment, and normal marine environment (Walker and Price, 1963; Walker, 1968).

The overall signals from boron-derived paleosalinity proxies and elemental ratios (Sr/Ba, B/Ga, and S/TOC) are consistent with the paralic signatures of the Agbada Formation, and characterized by a diverse assemblage of palynomorphs, represented numerously by terrestrially derived pollen and spores with significant marine-derived dinoflagellate cysts and foraminiferal test linings (Bankole et al., 2014). To the best of the authors' knowledge, this investigation presents the first utility of B/Ga, Sr/Ba, and S/TOC for paleosalinity watermass reconstruction in the Agbada Formation, providing an inorganic geochemical perspective with a valuable contribution to the geology of the Niger Delta Basin.

4.6 Conclusions

A multi-proxy investigation utilizing elemental ratios (B/Ga, Sr/Ba, and S/TOC) and boron-derived paleosalinity proxies was conducted to decipher the paleosalinity conditions prevalent in the paralic facies of the Agbada Formation. This is the first study utilizing elemental ratios for paleosalinity reconstruction in the basin.

The paleosalinity proxies consistently suggest brackish water settings with dominant freshwater inputs and little marine influence. The result is consistent with paralic facies of the Agbada Formation and highlights fluvial-to-marine transition that documents areas with marine influence over seasonal and tidal timeframes and zones that experience only freshwater and/or periodic marine influence. We suggest a similar approach would be suitable for paleosalinity water mass reconstruction in other ancient systems, as integrating various proxies is essential and presents a framework for refining perceptions and limiting secondary influences on any single proxy, thereby improving confidence in the interpretation.

References

Adams, T., Haynes, J., Walker C., 1965. Boron in Holocene illites of the Dovey Estuary, Wales, and its relationship to palaeosalinity in cyclothems. Sedimentology, 4, 189–195.

Adereti, O., Feldman, H., Unomah, G., 2012. Key elements of a world class petroleum system: lowstand shelf edge reservoirs in the Southeastern Niger Delta, Nigeria. Nigerian Association of Petroleum Explorationists Bulletin, 24(1), 38–42.

Anomneze, D. O., Okoro, A.U., Ajaegwu, N.E., Akpunonu, E.O., Obiadi, I.I., Ahaneku, C.V., Okeke, G.C., 2020. Description and interpretation of fault-related sedimentation and controls on shelf-edge deltas: implication on sand transportation to the basin floor in parts of Eastern Niger Delta. Journal of Petroleum Exploration and Production Technology, 10, 1367–1388.

Anyiam, U.O., Uzuegbu, E., 2020: 3D seismic attribute-assisted stratigraphic framework and depositional setting characterization of frontier Miocene to Pliocene aged Agbada Formation reservoirs, deep offshore Niger Delta Basin. Marine and Petroleum Geology. 122, 104636.

Avbovbo, A. A., 1978, Tertiary lithostratigraphy of Niger Delta: American Association of Petroleum Geologists Bulletin, 62, 295-300.

Bankole, S.I., Schrank, E., Osterloff, P.L., 2014. Palynostratigraphy, palaeoclimates and palaeodepositional environments of the Miocene aged Agbada Formation in the Niger Delta, Nigeria. J. Afr. Earth Sci. 95, 41–62.

Barakat, A. O., Rullkotter J., 1997. A comparative study of molecular paleosalinity indicators: chromans, tocopherols and C_{20} isoprenoid thiophenes in Miocene Lake sediments (Nordlinger Ries, Southern Germany). Aquat. Geochem. 3(2), 169–190.

Beka, F.T., Oti, M.N., 1995. The distal offshore Niger Delta: frontier prospects of a mature petroleum province. In: Oti, M.N., Postma, G. (Eds.), Geology of Deltas. A.A. Balkema, Rotterdam, pp. 237–241.

Benesh, N.P., Plesch, A., Shaw, J.H.., 2014. Geometry, kinematics, and displacement characteristics of tear-fault systems: an example from the deep-water Niger Delta. AAPG Bull. 98, 465–482.

Berner R. A. and Raiswell R., 1983. Burial of organic carbon and pyrite sulfur in sediments over Phanerozoic time: a new theory. Geochim. Cosmochim. Acta 47(5), 855–862.

Berner R. A. and Raiswell R., 1984. C/S method for distinguishing freshwater from marine sedimentary rocks. Geology 12(6), 365–368.

Berner R. A., Baldwin T. and Holdren, Jr., G. R., 1979. Authigenic iron sulfides as paleosalinity indicators. J. Sediment. Res. 49(4), 1345-1350.

Bilotti, F., Shaw, J.H., 2005. Deep-water Niger Delta fold and thrust belt modeled as a critical-taper wedge. The influence of elevated basal fluid pressure on structural styles. AAPG (Am. Assoc. Pet. Geol.) Bull. 89, 1475–1491.

Bohor, B. F., Gluskoter, H.J., Boron in illite as an indicator of paleosalinity of Illinois coals. Journal of sedimentary petrology, 43(4), 945-956.

Bokanda, E.E., Philip, F., Bisse, S.B., Ashukem, E.N., Belinga, B.C., Bokanda, F.B., Ligbwah, V. B., Chin, T.B., Ekomane, E., 2022. Trace elements geochemistry, total organic carbon, palaeosalinity, and hydrothermal characteristics of the Cretaceous black shale in the Mamfe Basin (West Africa). Solid Earth Sciences, 7, 237–246.

Brockamp, Olaf, 1973. Borfixierung in authigenen und detritischen Tonen. Geochim. et Cosmochim. Acta, 37, 1339-1351.

Buatois L. A., Netto R. G., Ma´ngano M. G., 2010. Ichnology of late Paleozoic postglacial transgressive deposits in Gondwana: Reconstructing salinity conditions in coastal

ecosystems affected by strong meltwater discharge. In Late Paleozoic Glacial Events and Postglacial Transgressions in Gondwana, 468 (eds. O. R. Lo´pez-Gamundı´ and L. A. Buatois). GSA Special Papers, 149–173.

Bukry, D., 1974. Coccoliths as paleosalinity indicators–Evidence from Black Sea. In The Black Sea Geology, Chemistry, and Biology: Tulsa, Oklahoma, American Association of Petroleum Geologists Memoir (eds. E.T. Degens, D.A. Ross) 20. pp.353–363.

Burke, K., 1972, Longshore drift, submarine canyons and submarine fans in development of Niger Delta, AAPG Bulletin, 56, 1975-1983.

Chen, B., Liu, G., Wu, D., Sun, R., 2016. Comparative study on geochemical characterization of the Carboniferous aluminous argillites from the Huainan Coal Basin, China. Turk. J. Earth Sci. 25, 274–287.

Chen, Z., Chen, Z., 1997. Quaternary Stratigraphy and Trace-Element Indices of the Yangtze Delta, Eastern China, with Special Reference to Marine Transgressions. Quaternary Research, 47, 181–191.

Cheng, M., Zhang, Z., Jin, C., Wei, W., Wang, H., Algeo, T.J., Li, C., 2023. Salinity variation and hydrographic dynamics in the early Cambrian Nanhua Basin (South China). Sci. China: Earth Sci. 66, 1674–7313.

Clays and Clay Minerals, Proc. 8th Natl. Conf., Pergamon Press, Oxford, p. 203-213.

Corredor, F., Shaw, J.H., Bilotti, F., 2005. Structural styles in the deep-water fold and thrust belts of the Niger Delta. AAPG (Am. Assoc. Pet. Geol.) Bull. 89 (6), 753–780.

Couch, E. L., Grim, R. E 1968. Boron fixation by illites: Clays and Clay Minerals, 16, 249-256.

Couch, E.L., 1971. Calculation of paleosalinities from boron and clay mineral data. AAPG Bull. 55, 1829–1837.

Damuth, J.E., 1994. Neogene gravity tectonics and depositional processes on the deep Niger Delta continental margin. Mar. Petrol. Geol. 11 (3), 320–346.

De Vos W. and Tarvainen T., 2006. Geochemical Atlas of Europe, Part 2: Interpretation of Geochemical Maps, Additional Tables, Figures, Maps and Related Publications. Geological Survey of Finland, Espoo, Finland, p. 618.

Degens.E. T., Williams, E. G., and Keith, M. L., 1957. Environmental studies of Carboniferous sediments, Part 1: Geochemical criteria for differentiating marine and fresh-water shales: Am. Assoc. Petrol. Geol. Bull., 41, p. 2427-2455.

Dominik, J., and Stanley, D. J., 1993. Boron, beryllium and sulfur in Holocene sediments and peats of the Nile delta, Egypt: Their use as indicators of salinity and climate. Chemical Geology 104, 203–216.

Doust, H., and Omatsola, E., 1990. Niger Delta, in J. D. Edwards and P. A. Santogrossi, eds., Divergent/passive margin basins: AAPG Memoir 48, 201–238.

Ejedawe, J. E., and S. J. L. Coker, 1984. Dynamic interpretation of organic-matter maturation and evolution of oil-generative window: AAPG Bulletin, 68, 1024-1028.

Ejedawe, J.E., Coker, S.J., Lambert-Aikhionbare, D.O., Alofe, K.O and Adoh, F.O., 1984. Evolution of oil-generative window and oil and gas occurrence in Tertiary Niger Delta basin. American Association of Petroleum Geologists Bulletin 68, .1744–1751.

Ekpo, B.O., Essien, N., Neji, P.A., Etsenake, R.O., 2018. Geochemical fingerprinting of western offshore Niger Delta oils. J. Petrol. Sci. Eng. 160, 452–464.

Ekweozor, C. M., and Daukoru, E.M, 1984, Petroleum source bed evaluation of Tertiary Niger Delta--reply: American Association of Petroleum Geologists Bulletin, 68, 390-394.

Ekweozor, C.M., Okogun, J.I., Ekong, D.E.U., Maxwell, J.R., 1979. Preliminary organic geochemical studies of samples from the Niger Delta, Nigeria: part 1, analysis of crude oils for triterpenes. Chemical Geology, 27, 11-28.

Ekweozor, C.M., Okoye, N.V., 1980. Petroleum source-bed evaluation of Tertiary Niger Delta. AAPG Bulletin, 64, 1251-1259.

Evamy, B.D., Haremboure, J., Kamerling, P., Molloy, F.A., Rowlands, P.H., 1978. Hydrocarbon habitat of Tertiary Niger Delta: American AAPG Bulletin, 62,1-39.

Frankl, E.J. and Cordry, E.A., 1967. The Niger Delta oil province recent developments onshore and offshore. 7th World Petroleum Congr., Mexico City Proc. IB, p. 195-209.

Frederickson, A. F., Reynolds, R. C., Jr., 1960. Geochemical method for determining paleosalinity: Clays Clay Miner. 8, 203‑213.

Goldhaber, M. B. and Kaplan, I. R., 1974. The sulfur cycle. In: E. D. Goldberg (Editor), The Sea. Wiley-Interscience, New York, NY, Vol. 5. pp. 569-655.

Goldschmidt, V. M., Peters, C., 1932. Zur Geochemie des Bors. Teil I u II: Akad. Wiss. Gottingen, Nachr., Mat.-Phys. Kl.,402-407, 528-554.

Haack, R.C., Sundararaman, P., and Dahl, J., 1997, Niger Delta petroleum System, *in*, Extended Abstracts, AAPG/ABGP Hedberg Research Symposium, Petroleum Systems of the South Atlantic Margin, November 16-19, 1997, Rio de Janeiro, Brazil.

Haack, R.C., Sundararaman, P., Diedjomahor, J.O., Xiao, H., Gant, N.J., May, E.D., Kelsch, K., 2000. Niger Delta petroleum systems, Nigeria. In: Mello, M.R., Katz, B.J. (Eds.), Petroleum Systems of the South Atlantic Margins, vol. 73. American Association of Petroleum Geologists Memoir, pp. 213–231.

Harder, H., 1961. Einbau von Bor in detritische Ton- minerale: Geochim. et Cosmochim. Acta, v. 21, 284-294

Hasegawa, T., Hibino, T., Hori, S., 2010. Indicator of paleosalinity: Sedimentary sulfur and organic carbon in the Jurassic–Cretaceous Tetori Group, central Japan. Island Arc, 19, 590–604.

He, J., Ding, W., Jiang, Z., Jiu, K., Li, A., Sun, Y., 2017. Mineralogical and chemical distribution of the Es3 L oil shale in the Jiyang Depression, Bohai Bay Basin (E China):

implications for paleoenvironmental reconstruction and organic matter accumulation. Mar. Petrol. Geol. 81, 196–219.

Hofer, G., Wagreich, M., Neuhuber, S., 2013. Geochemistry of fine-grained sediments of the upper Cretaceous to Paleogene Gosau Group (Austria, Slovakia): implications for paleoenvironmental and provenance studies. Geoscience Frontiers 4, 449–468.

Holmden C., Creaser R. A., Muehlenbachs K., 1997. Paleosalinities in ancient brackish water systems determined by 87Sr/86Sr ratios in carbonate fossils: A case study from the Western Canada Sedimentary Basin. Geochim. Cosmochim. Acta 61(10), 2105–2121.

Hosper, J., 1971. The geology of the Niger Delta area, in the geology of the East Atlantic continental margin, Great Britain, Institute of Geological Science. Report 70(16), 121–141.

Ingram B. L., Conrad M. E., Ingle J. C., 1996. Stable isotope and salinity systematics in estuarine waters and carbonates: San Francisco Bay. Geochim. Cosmochim. Acta 60(3), 455–467.

Jaglarz P. and Ucham A., 2010. A hypersaline ichnoassemblage from the Middle Triassic carbonate ramp of the Tatricum domain in the Tatra Mountains, Southern Poland. Palaeogeogr. Palaeoclimatol. Palaeoecol. 292, 71–81.

Jolly, B.A., Lonergan, L., Whittaker, A.C., 2016. Growth history of fault-related folds and interaction with seabed channels in the toe-thrust region of the deep-water Niger Delta. Mar. Petrol. Geol, 70, 58-76.

Krueger, S.W., Grant, N.T., 2011. The growth history of toe thrusts of the Niger Delta and the role of pore pressure. In: McClay, K., Shaw, J., Suppe, J. (Eds.), Thrust Fault- Related Folding: AAPG Memoir, vol. 94, pp. 357–390.

Kulke, H. (1995): Nigeria. In: Kulke, H. (Eds), Regional Petroleum Geology of the World. Part II: Africa, America, Australia and Antarctica, Gebru Borntraeger, Berlin, 143–172.

Lambert-Aikhionbare, D. O., and Ibe, A.C., 1984. Petroleum source-bed evaluation of the Tertiary Niger Delta: discussion: American Association of Petroleum Geologists Bulletin, 68, 387-394.

Landergren, S., 1945. Contribution to the geochemistry of boron. II. The distribution of boron, *in* Some Swedish sediments, rocks, and iron ores; the boron cycle in the upper lithosphere: Arkiv Kemi, Mineralogi och Geologi, Bd. 19, Heft 5, Ano. 26, 31 p.

Landergren, S., 1958. On the distribution of boron in different size classes in marine clay sediments: Geol. Foren. Stockholm Forh., Bd. 80, Heft 1, 492, p. 104-107.

Landergren, S., and Carvajal, M. C. (1969). Geochemistry of boron, II. The relationship between boron concentration in marine clay sediments expressed as an adsorption isotherm. Ark. Kem. Mineral. Geol. 5, 13.

Lehner, P., and De Ruiter, P.A.C., 1977, Structural history of Atlantic Margin of Africa: American Association of Petroleum Geologists Bulletin, 61, 961-981.

Li, Y., Fan, T., Zhang, J., Wei, X., Zhang, J., 2021. Impact of paleoenvironment, organic paleoproductivity, and clastic dilution on the formation of organic-rich shales: a case study about the Ordovician-Silurian black shales, southeastern Chongqing, South China. Arab J Geosci, 8,10225–10239.

Maloney, M., Davies, R., Imber, J., Higgins, S., Kings, S., 2010. New insights into deformation mechanisms in the gravitationally driven Niger Delta deep-water fold and thrust belt. AAPG (Am. Assoc. Pet. Geol.) Bull. 94 (9), 1401–1424.

Matthiessen, J., 1995. Distribution patterns of dinoflagellate cysts and other organic-walled microfossils in recent Norwegian-Greenland Sea sediments. *Marine Micropaleontology*, *24*(3-4), 307-334.

Merki, P., 1972. Structural geology of the Cenozoic Niger Delta. In: Dessauvagie, T.F.J., Whiteman, A.J. (Eds.), African Geology. University of Ibadan Press, Ibadan, Nigeria, pp. 635–644.

Neff J. M., 2002. Barium in the ocean. In Bioaccumulation in Marine Organisms: Effect of Contaminants from Oil Well Produced Water. Elsevier, Amsterdam, pp. 79–88.

Nelson B. W., 1967. Sedimentary phosphate method for estimating paleosalinities. Science 158 (3803), 917–920.

Nwachukwu, J.I., Chukwura, P.I., 1986. Organic matter of Agbada Formation, Niger Delta, Nigeria. AAPG (Am. Assoc. Pet. Geol.) Bull. 70, 48–55.

Nwajide, C.S., 2013. Geology of Nigeria's Sedimentary Basins. CSS Bookshops Limited, Lagos, p. 565.

Obi, I.S., Onuoha, K.M., Dim, C.I.P., 2024. Highlighting relationships between sand thicknesses, reservoir-seal pairs and paleobathymetry from a sequence stratigraphic perspective: An example from Tortonian Serravallian deposits, onshore Niger Delta Basin. Energy Geoscience, 5, 100215. https://doi.org/10.1016/j.engeos.2023.100215.

Ogbe, O.B., Okoro, A.U., Ogagarue, D.O., Osokpor, J., Overare, B., Ocheli, A., Opatola, A.O., Oluwajana, O.A., 2021. Reservoir hydrocarbon prospectivity and productivity evaluations of sands S-600 and S-700 of Fega field, onshore Niger Delta Basin, Nigeria. Journal of African Earth Sciences, 184, 104311.

Osokpor J., Overare, B., 2019. Source Rock Evaluation and Hydrocarbon Potentials in the Northern Depobelt, Niger Delta Basin. Journal of Mining and Geology. 55(1), 17-28.

Osokpor J., Overare, B., 2019. Source Rock Evaluation and Hydrocarbon Potentials in the Northern Depobelt, Niger Delta Basin. Journal of Mining and Geology. 55(1), 17-28.

Osokpor, J, Lucas, F. A., Osokpor, O.J, Overare, B., Izeze., O.E., Avwenagha., E.O., 2015. Palynozonation and lithofacies cycles of Paleogene to Neogene age sediments in PML-1

well, northern Niger Delta Basin. Pacific Journal of Science and Technology, 16, 286 – 297.

Osokpor, J., Lucas, F.A., Osokpor, O.J., Overare, B., Alaminiokuma, G.I., Ogbe, O.B., Daniya, T.S., Avwenagha E.O., 2016. Petroleum potential of Paleogene-Neogene age sediments in well TN-1, western Niger Delta basin. Pacific Journal of Science and Technology 17 (1), 288–300.

Osokpor, J., Ogbe, O.B., 2023. The pattern of organic matter type occurrence and distribution in predicting hydrocarbon source formation: an example from Eocene Niger Delta Basin shale deposits. J. Sediment. Environ. https://doi.org/10.1007/s43217-023-00146-6.

Overare, B., Osokpor, J., Ekeh, P.C., Azmy, K., 2020. Demystifying provenance signatures and paleo-depositional environment of mudrocks in parts of southeastern Nigeria: constraints from geochemistry. J. Afr. Earth Sci. 172, 103954.

Overare., B., Azmy, K., Garzanti, E., Osokpor, J., Ogbe, O.B., Avwenagha, E.O., 2021. Decrypting geochemical signatures in subsurface Niger delta sediments: Implication for provenance, weathering, and paleoenvironmental conditions. Marine and Petroleum Geology, 126, 104879.

Palmer M. R., Spivack A. J. and Edmond J. M., 1987. Temperature and pH controls over isotopic fractionation during adsorption of boron on marine clay. Geochim. Cosmochim. Acta 51(9), 2319–2323.

Pirrus E., 1992. Freshening of the late Vendian basin on the East European Craton. Proc. Estonian Acad. Sci. 41, 115–123.

Potter, P. E., Shimp N. F., Witters J., 1963. Trace elements in marine and fresh-water argillaceous sediments. Geochim. Cosmochim. Acta 27(6), 669–694.

Pyle, K. M., Hendry, K. R., Sherrell, R. M., Meredith, M. P., Venables, H., Lagerstrom, M., Morte-Rodenas, A., 2017. Coastal barium cycling at the West Antarctic Peninsula. Deep Sea Res. Part II 139, 120–131.

Quan, Y., Liu, J., Hao, F., Cai, Z., Xie, Y., 2020. Paleosalinity assessment and its influence on source rock deposition in the western Pearl River Mouth Basin, South China Sea. GSA Bulletin, 132 (7/8),1741–1755.

Reijers, T.J.A., 2011. Stratigraphy and sedimentology of the Niger Delta. Geologos,17 (3) 133–162.

Reijers, T.J.A., Petters, S.W., and Nwajide, C.S., 1997. The Niger Delta Basin, *in* Selley, R.C., ed., African Basins--Sedimentary Basin of the World 3: Amsterdam, Elsevier Science, 151-172. doi.org/10.1016/S1874-5997(97)80010-X

Reinhardt E. G., Stanley D. J. and Patterson R. T., 1998. Strontium isotopic-paleontological method as a high-resolution paleosalinity tool for lagoonal environments. Geology, 26 (11), 1003–1006.

Remírez, M.N., and Algeo, T.J., 2020. Paleosalinity determination in ancient epicontinental seas: A case study of the T-OAE in the Cleveland Basin (UK): Earth-Science Reviews, 201, 103072. https://doi .org/10.1016/ j.earscirev.2019.103072.

Retallack G. J., 2020. Boron paleosalinity proxy for deeply buried Paleozoic and Ediacaran fossils. Palaeogeogr. Palaeoclimatol. Palaeoecol., 109536.

Reynolds, Jr., R. C., 1965. The concentration of boron in Precambrian seas. Geochim. Cosmochim. Acta, 29(1), 1-16.

Shiller A. M. and Frilot D. M., 1996. The geochemistry of gallium relative to aluminium in Californian streams. Geochim. Cosmochim. Acta 60(8), 1323–1328.

Short, K.C., Stauble, A.J., 1967. Outline of geology of Niger Delta, American Association of Petroleum Geologists Bulletin, 51, 761-779.

Song, J., Bao, Z., Zhao, X., Gao, Y., Song, X., Zhu, Y., Deng, J., Liu, W., Wang, Z., Ming, C., Meng, Q., Zhang, L., Mao, S., Zhang, Y., Yu, X., Wei, M., 2018. Sedimentology and geochemistry of Middle–Upper Permian in northwestern Turpan–Hami Basin, China: Implication for depositional environments and petroleum geology. Energy Exploration and Exploitation, 36(4)- 910–941.

Song, Y., Gilleaudeau, G. J., Algeo, T.J., Over, D.J., Lyons, T.W., Anbar, A.D., Xie1, S., 2021. Biomarker evidence of algal-microbial community changes linked to redox and salinity variation, Upper Devonian Chattanooga Shale (Tennessee, USA). GSA Bulletin, 133 (1/2) 409–424.

Spear N., Holland H. D., Garcia-Veıgas J., Lowenstein T. K., Giegengack, R., Peters H., 2014. Analyses of fluid inclusions in Neoproterozoic marine halite provide oldest measurement of seawater chemistry. Geology 42, 103–106.

Spivack, A.J., Palmer, M.R., and Edmond, J.M., 1987, The sedimentary cycle of the boron isotopes. Geochimica et Cosmochimica Acta, 51, 1939–1949.

Stacher, P.,1995. Present understanding of the Niger Delta hydrocarbon habitat, In: Oti, M. N., and Postma, G., eds., Geology of deltas: Rotterdam, A.A. Balkema, 257-267.

Tenthorey, E., Hermann, J., 2004. Composition of fluids during serpentinite breakdown in subduction zones: evidence for limited boron mobility. Geology 32(10), 865–868.

Tourtelot, H. A., L. G. Schultz, and C. Huffman, 1961. Boron in bentonites and shales from the Pierre shale. South Dakota, Wyoming, and Montana: U.S. Geol. Survey Prof. Paper 424C, 288-292.

Tuttle, M.L.W., Charpentier, R.R., Brownfield, M.E., 1999. The Niger Delta Petroleum System: Niger Delta Province, Nigeria, Cameroon, and Equatorial Guinea. USGS Open-file, Africa report 99-50-H.

Van Geel, B., 2001. Non-pollen palynomorphs, *in* Smol, J.P., Birks, H.J.B., Last, W.M., Bradley, R.S., and Alverson, K., eds., Tracking Environmental Change Using Lake Sediments: Terrestrial, Algal, and Siliceous Indicators: Dordrecht, The Netherlands, Springer, p. 99–119.

Walker C. T. and Price N. B., 1963. Departure curves for computing paleosalinity from boron in illites and shales. AAPG Bull. 47(5), 833–841.

Walker C. T., 1968. Evaluation of boron as a paleosalinity indicator and its application to offshore prospects. AAPG Bull. 52(5), 751-766.

Walker, C. T, 1963, Size fractionation applied to geochemical studies in sedimentary rocks: Jour. Sed. Petrology, 33, 694-7.

Walker, C. T., 1962, Separation techniques in sedimentary geochemistry illustrated by studies of boron: Nature; 194, 1073-1074.

Wang, A., Wang, Z., Liu, J., Xu, N., Li., 2021. The Sr/Ba ratio response to salinity in clastic sediments of the Yangtze River Delta, Chemical Geology 559, 119923.

Weber, K.J., 1987. Hydrocarbon distribution patterns in Nigerian growth fault structures controlled by structural style and stratigraphy. J. Petrol. Sci. Eng. 1, 91–104.

Weber, K.J., Daukoru, E.M., 1975. Petroleum Geology of the Niger Delta: Proceedings of the Ninth World Petroleum Congress, vol. 2. Applied Science Publishers, pp. 210–221.

Wei W., Algeo T. J., Lu Y., Lu Y., Liu H., Zhang S., Peng L., Zhang J. and Chen L., 2018. Identifying marine incursions into the Paleogene Bohai Bay Basin lake system in northeastern China. Int. J. Coal Geol. 200, 1–17.

Wei, W., and Algeo, T.J., 2020. Elemental proxies for paleosalinity analysis of ancient shales and mudrocks. Geochimica et Cosmochimica Acta, 287, 341–366.

Wei, W., Lu, Y., Ma, Y., Zhang, J., Song, H., Chen, L., Liu, H., Zhang, S., 2021. Nitrogen isotopes as paleoenvironmental proxies in marginal-marine shales, Bohai Bay Basin, NE China, Sedimentary Geology, 421, 105963.

Wei, W., Yu, W., Algeo, T.J., Herrmann, A.D., Zhou, L., Liu, J., Wang, Q., Du, Y., 2022. Boron proxies record paleosalinity variation in the North American Midcontinent Sea in response to Carboniferous glacio-eustasy. Geology 50, 537–541.

Whiteman, A., 1982. Nigeria: Its Petroleum Geology, Resources and Potential: London, Graham and Trotman, 394 pp.

Wu, Z., Zhao, X., Wang, E., Pu, X., Lash, G., Han, W., Zhang, W., Feng, Y., 2021. Sedimentary environment and organic enrichment mechanisms of lacustrine shale: A case study of the Paleogene Shahejie Formation, Qikou Sag, Bohai Bay Basin, 573, 110404.

Yang, S.Y., Li, C., Cai, J., 2006. Geochemical compositions of core sediments in eastern China: implication for Late Cenozoic palaeoenvironmental changes. Palaeogeogr. Palaeoclimatol. Palaeoecol. 229 (4), 287–302.

Yang, S.Y., Li, C.X., Yang, D.Y., Li, X.S., 2004a. Chemical weathering of the loess deposits in the lower Changjiang Valley, China, and paleoclimatic implications. Quat. Int. 117 (1), 27–34.

Ye, C., Yang, Y., Fang, X., Zhang, W., 2016. Late Eocene clay boron-derived paleosalinity in the Qaidambasin and its implications for regional tectonics and climate. Sedimentary Geology 346, 49–59.

Zeng, S., Wang, J., Fu, X., Chen, W., Feng, X., Wang, D., Song, C., Wang, Z., 2015. Geochemical characteristics, redox conditions, and organic matter accumulation of marine oil shale from the Changliang Mountain area, northern Tibet, China. Mar. Pet. Geol. 64, 203–221.

Zhang, H., Fan, H., Zhang, F., Wen, H., 2023. Paleosalinity of the Nanhua Basin (South China) during the Cambrian Explosion. Palaeogeography, Palaeoclimatology, Palaeoecology, 627, 111716.

Zhang, M.M., Liu, Z.J., Xu, S.Z., Hu, X.F., Sun, P.C., Wang, Y.L., 2014. Analysis for the Paleosalinity and Lake-level Changes of the Oil Shale Measures in the Lucaogou Formation in the Sangonghe Area of Southern Margin, Junggar Basin, Petroleum Science and Technology, 32:16, 1973-1980.

Zhang, X., Li, S., Yan, M., Wang, X., Geng, G., 2020. Early Cretaceous black shale in the Fajiaying Formation (Lingshan Island, East China): Terrestrial record of hothouse climate. Journal of Asian Earth Sciences, 191, 104200.

Zhang, X., Lin, C., Zahid, M.A., Jia, X., Zhang, T., 2017. Paleosalinity and water body type of Eocene Pinghu Formation, Xihu Depression, East China Sea Basin. Journal of Petroleum Science and Engineering, 158, 469–478.

Zuo, X., Li, C., Zhang, J., Ma, G., Chen, P., 2020. Geochemical characteristics and depositional environment of the Shahejie Formation in the Binnan Oilfield, China. Journal of Geophysics Engineering, 17, 539–551.

Appendix 4.1: Elemental compositions and ratios, clay mineral contents (< 2 μm fraction), Total organic carbon (TOC) values, and paleosalinity analysis of the Agbada shales. K-Kaolinite, I-illite, M-Montmorillonite, Csp- Couch's paleosalinity (Couch, 1971), Eb- Equivalent boron (Walker and Price, 1963), Adam's paleosalinity (Adams et al., 1965), L- Paleosalinity of Landergren and Carvajal (Landergren and Carvajal, 1969).

Depth (ft)	Sample	Sr (ppm)	Ba (ppm)	B (ppm)	Ga (ppm)	K_2O (%)	S (%)	K (%)	I (%)	M (%)	TOC (%)	Sr/Ba	B/Ga	S/TOC	CSp (‰)	Eb (ppm)	A (‰)	L (‰)
Well 1																		
5390.4	R1	153	1858	92	28	2.6	-	-	-	-	1.0	0.1	3.4	-	-	230	15.5	16.2
5397.0	R2	147	1291	109	34	2.2	-	-	-	-	1.0	0.1	3.2	-	-	303	22.6	23.7
5403.5	R3	115	1642	116	32	2.0	-	-	-	-	1.0	0.1	3.6	-	-	344	26.6	27.8
5410.1	R4	143	1043	111	34	2.2	0.1	88	12	-	1.2	0.1	3.3	0.1	25.6	305	22.7	24.8
5584.0	R5A	122	1860	41	15	2.1	-	-	-	-		0.1	3.8	-	-	117	4.4	2.4
5590.6	R5	134	1118	108	29	2.2	-	-	-	-	1.2	0.1	3.7	-	-	303	22.5	23.3
5593.8	R5C	146	409	101	38	2.2	-	-	-	-	-	0.4	2.7	-	-	287	21.0	20.1
5597.1	R6	135	933	94	26	1.9	0.2	92	8	-	1.6	0.1	3.6	0.2	24.1	288	21.1	16.7
5600.4	R7	125	441	71	23	2.2	0.2	84	12	4	1.6	0.3	3.0	0.2	17.6	196	12.1	8.7
5603.7	R8	130	784	85	25	2.1	-	-	-	-	0.9	0.2	3.5	-	-	251	17.4	13.5
5610.2	R9	156	1862	60	16	2.0	-	-	-	-	0.6	0.1	3.8	-	-	177	10.3	5.9
5616.5	R9B	98	1674	35	12	1.6	-	-	-	-	-	0.1	6.7	-	-	126	5.3	1.6
5623.0	R9C	143	378	108	27	2.1	-	-	-	-	-	0.4	4.0	-	-	306	22.9	23.1
5666.0	R9D	109	360	90	24	2.1	-	-	-	-	-	0.3	3.7	-	-	259	18.2	15.2
5669.3	R10	117	883	129	30	2.5	-	-	-	-	0.9	0.1	4.4	-	-	327	24.9	35.3
5800.5	R10A	137	1202	141	31	2.2	-	-	-	-	Nd	0.1	4.6	-	-	394	31.5	43.1
5803.8	R11A	128	372	140	30	2.2	-	-	-	-	0.9	0.3	4.6	-	-	392	31.3	42.4
5807.1	R11	113	937	91	16	2.1	0.2	88	10	2	1.1	0.1	5.6	0.19	22.4	265	18.8	15.6
5813.6	R11-B	116	1117	93	16	2.1					Nd	0.1	5.9	-	-	271	19.4	16.4
5820.2	R11-B2	**209**	285	121	24	1.8	-	-	-	-	Nd	0.7	5.0	-	-	402	32.3	30.4
5826.8	R12	**212**	929	119	23	1.6	0.2	84	12	4	1.9	0.2	5.2	0.10	26.5	423	34.3	29.4

5836.6	R13	135	1251	113	24	2.1	0.2	87	13	-	1.9	0.1	4.8	0.08	25.6	328	25.0	26.1
5843.2	R13B	136	1554	94	24	2.2	-	-	-	-	Nd	0.1	4.0	-	-	264	18.7	16.8
5846.5	R13C	116	825	104	17	2.2	-	-	-	-	Nd	0.1	5.9	-	-	293	21.6	21.2
5859.6	R14A	112	1315	52	14	2.3	-	-	-	-	Nd	0.1	3.7	-	-	141	6.7	4.2
5869.4	R14	149	721	107	33	2.2	0.1	92	8	-	1.4	0.2	3.2	0.07	26.7	299	22.2	22.8
5892.4	R15	84	451	56	12	1.9	0.1	86	9	5	1.3	0.2	8.1	0.09	15.4	174	10.0	5.1
Well 2																		
4327	M1	152	1044	67	29	1.8	-	-	-	-	1.3	0.1	2.3	-	-	221	14.6	7.7
4485	M2	103	274	55	25	1.6	-	-	-	-	1.2	0.4	2.2	-	-	200	12.5	4.8
5879	M3	131	520	56	25	1.6	1.0	75	15	10	1.7	0.3	2.2	0.62	13.5	205	13.0	5.0
5894	M3A	163	495	69	27	1.8	1.1	74	7	19	1.4	0.3	2.6	0.76	17.3	229	15.3	8.3
6082	M4	140	330	75	24	1.6	1.0	65	20	15	2.7	0.4	3.2	0.36	15.5	266	18.9	10.0
6640	M5	208	426	84	31	2.2	1.0	88	12	-	2.3	0.5	2.7	0.43	20.6	237	16.1	13.0
6807	M6	174	391	83	29	2.1	1.3	90	10	-	2.4	0.4	2.9	0.55	21.1	241	16.5	12.6
6899	M7	160	106	77	25	2.0	1.4	75	20	5	2.8	1.5	3.1	0.50	16.5	229	15.3	10.6
7545	M8A	166	1247	77	34	2.5	1.2	92	6	2	1.9	0.1	2.3	0.65	21.2	196	12.1	10.6
7596	M8	156	396	86	31	2.3	1.2	65	15	20	1.8	0.4	2.7	0.66	18.0	235	15.9	13.6
8180	M9	162	805	72	29	2.4	0.8	94	6	-	1.8	0.2	2.5	0.46	20.4	190	11.5	9.1
8974	M10	208	202	51	29	2.3	1.5	91	6	3	2.5	1.0	1.8	0.59	15.4	137	6.3	4.2
10293	M11	156	1100	68	31	2.5	1.5	78	11	11	2.5	0.1	2.2	0.60	16.7	171	9.6	7.9
10325	M11-A	171	666	66	34	2.6	0.8	85	15	-	1.8	0.3	1.9	0.45	16.2	163	8.9	7.4
10718	M12	163	100	75	33	2.3	1.8	90	10	-	2.0	1.6	2.3	0.90	19.6	206	13.1	10.1
10733	M12A	164	145	83	34	2.2	1.7	80	12	8	1.9	1.1	2.4	0.93	19.5	233	15.7	12.6
10763	M12B	190	187	61	33	2.2	1.2	70	25	5	1.8	1.0	1.8	0.66	12.8	170	9.5	6.1
10793	M12-B	203	513	76	35	2.4	1.2	65	20	15	1.9	0.4	2.2	0.63	15.7	201	12.6	10.4

Chapter V

5. Conclusions

This last chapter presents a synopsis of the main findings of this study. The current research has evaluated the Agbada Formation, Niger Delta Basin, using a variety of methods to assess petrographic attributes, diagenesis and influence of rare calcite cement on reservoir quality, and the utility of inorganic geochemical imprints for decoding provenance and paleosanity conditions. This has been made possible by accessing both onshore and offshore subsurface datasets in the basin, including well logs, ditch cuttings and cores. The key findings of this research are highlighted in the following paragraphs.

Chapter II The inorganic geochemical composition of sandstones and shales of the Agbada Formation, Niger Delta Basin, were utilized to constrain source-area weathering, provenance and paleo-redox conditions associated with the depositional subenvironment. The results indicate that the sandstones and shales have experienced moderate to intense paleo-weathering in warm/humid paleoclimatic settings, with observed element mobility order (Ca > Na > Sr > K > Mg > Rb), the same for both sandstones and shales. The $\alpha^{Al}E$ values observed are notably lower than those reported for regions affected by intense weathering, such as subequatorial southern Africa. Moreso, the order of element mobility is slightly different from those observed in sediments from central and southern Africa, but these differences may be accounted for by diverse factors, including different parent rocks, winnowing of mica in shallow-marine environments, degree of recycling, or inheritance. Moreover, shales would be expected to display evidence of notably more intense weathering than associated sandstones which, however, is not observed in the Niger Delta, possibly reflecting source-rock inheritance. The insights from various elemental ratios, including LREE-enrichment, flat HREE pattern, and negative Eu anomaly, point to sources of detritus comprising predominantly of felsic rocks with

considerable recycling of post-Archean siliciclastic rocks derived mainly in turn from granitoid basement rocks, older sedimentary basins, and quartzose siliciclastic sediments in the Niger River catchment. Source terrains largely consisting of quartzose siliciclastic sediments are common in the catchment of the modern Niger River, which today flows for a large tract across the southern edge of the Sahara Desert (sub-Saharan western Africa). Evidence from trace elements sensitive to redox conditions and their Enrichment factors (EF) suggest that the investigated Agbada shales were mainly deposited in an environment that was not oxygen-depleted (oxic-suboxic) but with possibly localized and short-term anoxia, leading to the slightly enriched values for U and Mo. The findings of this investigation contribute to the extensive research in the Niger Delta Basin, which has been chiefly dedicated to hydrocarbon exploration in the last half-century and do fill a gap as far as geochemical information is concerned, providing a valuable and honest contribution to the paralic facies, the dominant hydrocarbon-bearing reservoir in the basin.

Chapter III: This chapter examined the diagenetic imprints and the influence of rare calcite cemented intervals on the reservoir quality of Agbada sandstone, highlighting the petrographic characteristics and the diagenetic evolution of the cements and establishing the relationship or connection between diagenetic processes and porosity distribution, and therefore determining the processes that have been more influential in shaping the reservoir quality. The Agbada Formation consists of quartzose and subordinately quartz-rich feldspatho-quartzose sandstones. The deltaic depositional setting and syn-depositional pore waters underwent variable marine influence that promoted the early formation of pyrite. Siderite and subordinate ferroan calcite suggest iron enrichment in pore waters during early diagenesis. The dissolution of framework grains (mainly unstable feldspars) and kaolinite formation are conspicuous events in the sandstone. Ferroan calcite cements also dissolved, representing only a small percentage of the investigated sandstones, being locally present in a few intervals. Despite some evidence of

compaction, it is generally considered low, as indicated by the dominant point contacts between grains, explaining the lack of pressure dissolution and scarcity of quartz overgrowths that are not particularly important in occluding the reservoir quality of the investigated Miocene Agbada Sandstones. Considering the burial depth of the sandstones, the general lack of pervasive cements and minimal compaction are significant features that have contributed to the high porosity. Apart from a few horizons that contain considerable early cementation that stabilized the rock texture and therefore, less compactional control, mechanical compaction has a comparatively more dominant control on porosity loss, as cementation appears to have been less influential in shaping the reservoir quality.

Calcite-cemented zones are not abundant in the Agbada sandstones. The presence of "poikilitic" calcite cement in a network of grains that appear to float coupled with the prevalence of tangential contacts implies that it is an early diagenetic event and filled pores prior to significant mechanical compaction, but the shale normalized REY patterns do not mimic seawater patterns due to possible contributions from clastic or detrital grains and/or incorporation of particulate matter that can preferentially scavenge LREEs from the overlying water column. Calcite cementation, where present, almost completely occluded primary porosity and was sufficient to strengthen the framework against compaction as its role for porosity preservation is optimized. However, new porosity is generated where the dissolution of the early calcite cement was not compensated by new cement formation. Relics of partly/completely dissolved calcite cements and their optical signatures imply that they are part of the same network of poikilitic calcite cement being isolated due to partial dissolution. However, it is not entirely excluded that the cement dissolution produced only small amounts of secondary porosity, particularly with insignificant sources of carbonates (e.g., carbonate rock fragments, marine shells) and minimal calcite cementation. Although the occurrence of calcite cement is generally small, probably discontinuous and unlikely to represent significant barriers to fluid flow with their localized

influence, understanding their locally significant influence may still contribute to building good reservoir models.

The under-compaction and the presence of clay-rich matrix (mainly kaolinite) in the sandstones are envisaged to cause the production of fines and formation damage during reservoir production, but it is not likely to cause much damage to permeability compared to other clays (e.g. smectite) that are far more destructive, especially if a suitable reservoir management and development plan is put in place to minimize permeability loss. Although significant smectite has been reported in parts of the Niger Delta, requiring a cautious approach in the selection of drilling fluid when penetrating the smectite-bearing horizons, the investigated samples do not contain significant smectite and should not pose an issue during production. The findings of this research provide useful insight into exploration activity, appraisal and recovery of the Agbada sandstone reservoir, including horizons where calcite cementation occurs.

Chapter IV: This chapter provides insights into the paleosalinity conditions that are prevalent in the Agbada Formation through evidence deciphered from elemental ratios and boron-derived paleosalinity proxies. This research is motivated by the fact that bulk sediment geochemical proxies (e.g., B/Ga, Sr/Ba, S/TOC) for reconstructing paleosalinity and their general applicability to fine-grained siliciclastic sediments in the Agbada Formation have not been demonstrated. The perceptions from various elemental ratios consistently indicate low saline (brackish settings) conditions that contain significant freshwater inputs and little marine influence. Additional quantitative insights from boron-derived paleosalinity proxies provide the same insights and also point mostly to low saline (brackish) settings linked to inner-shelf and littoral environments. The perceptions from the various paleosalinity proxies are consistent with paralic facies of the Agbada Formation and represent the interplay between freshwater and seawater that are susceptible to lateral and/or vertical salinity gradients, with zones of lower salinities linked to reduced seawater or increased freshwater inputs and zones of greater

seawater inputs reflecting relatively higher salinities. This research contributes to the geology of the Niger Delta, particularly from an inorganic geochemical perspective, highlighting fluvial-to-marine transition by documenting areas where rare marine influence prevails over seasonal and tidal timeframes and zones that experience only freshwater and/or periodic marine influence. The findings of this investigation validate the faunal evidence in the Agbada Formation, consisting of numerously terrestrially derived pollen and spores with significant marine-derived dinoflagellate cysts and foraminiferal test linings. We suggest a similar approach would be suitable for paleosalinity water mass reconstruction in other ancient systems, as integrating various proxies is essential and presents a framework for refining perceptions and limiting secondary influences on any single proxy, thereby improving confidence in the interpretation.